Cyclic, Tethered and Nanoparticulate Silicones for Material Modification

A Dissertation
Presented to
The Academic Faculty

By

Marcus Bernard Foston

In partial Fulfillment
Of the Requirements of the Degree
Doctor of Philosophy in the
School of Polymer, Textile and Fiber Engineering

Georgia Institute of Technology
August 2008

Cyclic, Tethered and Nanoparticulate Silicones for Material Modification

Approved by:

Dr. Haskell W. Beckham, Advisor
School of Polymer, Textile and Fiber Engineering
Georgia Institute of Technology

Dr. Johannes Leisen
School of Polymer, Textile and Fiber Engineering
Georgia Institute of Technology

Dr. Anselm Griffin
School of Polymer, Textile and Fiber Engineering
Georgia Institute of Technology

Dr. Sankar Nair
School of Chemical and Biomolecular Engineering
Georgia Institute of Technology

Dr. Uwe Bunz
School of Chemistry and Biochemistry
Georgia Institute of Technology

Date Approved: July 2, 2008

ACKNOWLEDGEMENTS

Many people have inspired, guided, and helped me during the eight years I spent at Georgia Tech finishing both my undergraduate and graduate work. I would like to thank them all for a great college experience, making receiving this degree from this prestigious institution only more special. I would first like to thank my family.

My very special thanks to the one person whom I owe everything I am today, my mother, Ollie Foston. Her unwavering faith and confidence in my abilities and in me is what has shaped me into the person I am today. Thank you for everything. I also thank my father, Marvin Foston, who extended his thirst for knowledge, inquisitiveness and intelligence to me, while being a source of support. My thanks as well goes out to my late grandfather William Wellons who showed me the true worth of hard work and served as a living personification of strength. I have a large family and would be doing a disservice if I didn't again thank my many aunts, uncles and cousins who have supported me over the years, it really does take a village to raise a child.

Thanks go to my undergraduates, Jacques Walker and Matthew Soicher, for their hard work. I would like to thank the School of Polymer, Fiber and Textile Engineering, especially those members of the administrative staff without whom I would have missed one too many deadlines. I extend many thanks to my current and past research group members, especially Dr. Bryan White, Dr. Philip Watson and Dr. Sunghyun Nam. Also, I am extremely grateful to my doctoral committee for their input, valuable discussions and accessibility.

I thank all my many friends, who have been with me on this eight year journey in particular Jonathan Duarte, Pratik Sau, Gregory Smith and Christopher Gonzales, for the hours spent reviewing grammar, punctuation, spelling and sentence structure on many papers, reports, proposals and this dissertation.

Finally, this dissertation would not have been possible without the expert guidance of my esteemed advisor, Dr. Haskell Beckham. I would like to gratefully and sincerely thank him for his guidance, understanding, and at times patience. I felt as though he took me under his wing and his mentorship was paramount in providing a well rounded experience consistent my long-term life goals. He encouraged me to not only grow as a polymer chemist but also as an independent thinker. Though not my advisor, Dr. Johannes Leisen has spent many, many hours helping understand the complex topics related to NMR, solid-state NMR, MRI and the operation of the NMR spectrometer and research in general, special thanks to you also. His help had more than half my thesis work possible. I'd also like to thank Dr. Miesha Shofner and David Bostwick for their help.

This research was partially funded by the GAANN Award. I extend thanks to Dr. David Collard for doing an excellent job with overseeing and managing the award distribution.

TABLE OF CONTENTS

LIST OF TABLES

LIST OF FIGURES

LIST OF SCHEMES

LIST OF ABBREVIATIONS

$[\eta]$	intrinsic viscosity
$\langle r^2 \rangle$	mean-squared end-to-end distance
°C	degree Celsius
1D	one dimensional
2D	two dimensional
4D	four dimensional
Å	angstrom
amu	atomic mass unit
ATR	attenuated total reflection
BET	Brunauer-Emmett-Teller
BPP-LED	bipolar pulse pair and longitudinal eddy current delay pulse sequence
*c**	overlap concentration
CD	cyclodextrin
CF_3SO_2H	trifluoromethanesulfonic acid or triflic acid
C_i^{RU}	concentration of the repeat units eluting from the column
C_i^{EG}	concentration of the number of labeled end groups
cm	centimeter
CMPG	Carr-Purcell-Meiboom-Gill
CODEX	centerband-only detection of exchange
CP	cross polarization
CRR	cooperative rearranging region
cSt	centistokes
D	diffusion coefficient
D_2O	deuterium oxide
D_{eff}	effective spin diffusion coefficient
Dia	diameter
DLS	dynamic light scattering
DMA	dynamic mechanical analysis
D_{mobile}	spin diffusion coefficient of the rigid polymer
dn/dc	refractive index concentration increment of the polymer analyte
DNA	deoxyribonucleic acid
DOSY	diffusion ordered spectroscopy

D_{rigid}	spin diffusion coefficient of the mobile polymer
DSC	differential scanning calorimetry
DW	dwell time
D_x	represents a molecule with x silicon atoms that have two siloxane bonds and two substituents
eq	equivalents
FAB	fast atom bombardment
f_b	force required to break one bond in the tethered or matrix polymer
FTIR	fourier transform infrared spectroscopy
FWHM	full width at half-maximum
G	gauss
GE	General Electric
g_n	represents the end-to-end cyclization frequency
G_o	fracture energy
GPC	gel permeation chromatography
H^+	proton
HA	hydroxylapatite
HCl	hydrochloric acid
HE	Hahn-echo
Hz	hertz
IPN	interpenetrated network
J	joule
K	degree Kelvin
KBr	potassium bromide
kg	kilogram
kHz	kilohertz
K_n	molar cyclization constant
KOH	potassium hydroxide
KWW	Kohlrausch-Williams-Watts
L	liter
ℓ	path length
$L(PCy_3)Cl_2Ru=CHR$	Grubb's catalyst
LCCC	liquid chromatography at the critical condition
m	meter
M	molar
MALDI-ToF	matrix-assisted laser desorption/ionization time-of-flight
MAS	magic angle spinning
MC	Monte Carlo
meq	milliequivalents

MHz	megahertz
min	minute
mL	milliliiter
mm	millimeter
mM	millimolar
M_n	number average molecular weight
mol	mole
mol %	mole percent
MRI	nuclear magnetic resonance imaging
MS	mass spectrometry
ms	millisecond
mtorr	milliTorr
M_x	represents a molecule with x silicon atoms that have one siloxane bonds and three substituents
N	population size of chain in a simulated chain distribution
N_2	nitrogen gas
N_A	Avogadro's number
Na^+	sodium cation
NaH	sodium hydride
NaI	sodium iodide
N_e	entanglement degree of polymerization
NI	1-naphthyl isocyanate
nm	nanometer
NMR	nuclear magnetic resonance
n_o	refractive index
NPP	*N*-phenyl pyrrolidinium
OH	hydroxyl group
P(r)	probability function weighting the biased number generator
PCy	tricyclohexylphosphine
PDI	polydispersity index
PDMS	poly(dimethyl siloxane)
PEG	poly(ethylene gycol)
PMA	poly(methyl acrylate)
p^n	the extent of reaction for the linear chains in ring-ring and ring-chain equilibria
POE	poly(oxyethylene)
PP	poly(propylene)
ppm	parts per milllion
PS	poly(styrene)
PVAc	poly(vinyl actetate)

PVP	poly(2-vinylpyridine)
Q_x	represents a molecule with x silicon atoms that have four siloxane bonds and no substituents
RAFT	eversible addition–fragmentation chain transfer
R_g	radius of gyration
RH	relative humidity
Rh	hydrodynamic radius
RI	refractive index
RI_{Cal}	refractive index detector calibration constant
ROMP	ring opening metathesis polymerization
RT	retention time
s	second
SAXS	small-angle scattering
SEC	seize exclusion chromatography
SEM	scanning electron microscopy
Tf	triflic
t_{filter}	filter time
T_g	glass transition temperature
TGA	thermogravimetric analysis
THF	tetrahydrofuran
T_m	melting point
t_m	mixing time
T_x	represents a molecule with x silicon atoms that have three siloxane bonds and one substituents
UV	ultraviolet
Vis	visible
vol	volume
vol. %	volume percent
WISE	wide-line separation
wt. %	weight percent
α_x	molar absorptivity of x
μL	microliter
μm	micrometer
μs	microsecond
σ	surface density of tethered chains
σ_{Rn}	symmetry parameter associated with the size of the units that can be formed in a ring opening reaction of Dn
τ_c	critical interparticle matrix thickness
Φ_c	percolation volume fraction

χ	polymer-polymer thermodynamic mixing term
χ_M	electronegativity as determine by Robert Mulliken

SUMMARY

Rarely in most settings does one polymer exhibit all the material requirements for a particular application. In this case product designers use a blend of several materials with the intent of combining advantageous properties while compensating for weaknesses. I have examined three different topological forms of a material modifier. The modifier is silicone and the three topological forms are cyclic, linear tethers and networked siloxane bonds in the form of a nanoparticulate. Often silicones, or siloxanes, are added to a material because of its unique properties that are related to its inorganic or inorganic-organic hybrid character. This dissertation addresses either the synthesis of silicones for material modification or the effect of the adding silicones to a variety of substrates and polymeric systems.

This thesis can be separated into two main parts: (i) synthesis, characterization and purification of cyclic polydimethylsiloxane (PDMS) and PDMS tethers, and (ii) the dynamics of poly(vinyl acetate) (PVAc)/silica nanocomposites with PDMS surface treatments. The first part details the synthetic procedures, analytical techniques and applications of nonlinear PDMS for use in multi-component polymeric systems and as additives for surface modification. The second part describes the application of advanced solid-state NMR techniques to study polymer dynamics and structure. A considerable portion of my thesis includes investigating and detailing the mechanisms by which the dynamics and structure of a polymer matrix are altered by the addition of silica nanoparticles.

The first three chapters include a basic introduction to the history, commercial preparation, special properties, and applications of silicones, while also specifying the motivation behind the use of nonlinear polymer structures to gain unique material and surface properties. Chapters 2 and 3 present research focused on the first topological form, cyclic PDMS. The synthesis of cyclic polymers is very important to the synthesis and subsequent characterization of cyclic containing multi-component materials. Cyclic PDMS is formed via ring-chain depolymerization and bimolecular coupling and the unique issues associated with the formation, purification and analysis of cyclic polymer topologies. The goal of the work described in these chapters was to find a straightforward high-yield route to form large cycles of PDMS in a relatively high purity.

Chapter 4 focuses on the modification of the next topological form, linear polymers as tethers for surface modification and presents a novel concept for surface-modifying compounds; the incorporation of an ionic-reactive functionality into PDMS is presented. The idea being its ionic character will increase affinity for the surface, surface coverage and levelness, while the subsequent reactive fixation will permanently modify the surface to improve retention and fastness. The use of such chemistry has not been applied for surface modification protocols.

Chapters 5, 6 and 7 discuss the characterization of systems with the third topological form incorporated. They include differences in the viscoelastic behavior of PVAc/silica nanocomposites and the neat PVAc matrix, relating those differences to polymer dynamics and structure as determined by several solid-state NMR experiments. The latter two chapters pertain to PVAc/silica nanocomposites with PDMS surface treatments. Specifically, evaluating how polymer dynamics and structure changes

particularly at the interface\interphase with various PDMS surface treatments having different topologies at the surface. Commercially available PDMS surface treated silica nanoparticles and nanoparticle precursors modified to ensure either loops or tethers on the surface were used, and studied in the same analytical fashion as the PVAc/silica nanocomposites in Chapter 5.

I. Cyclic and Tethered Poly(dimethyl siloxane)

CHAPTER 1

Introduction

Material modification is an important academic and commercial exercise for extending the utility of existing material. As opposed to the development of completely new material, modification of an existing one is much more efficient in terms of time and economics. I have examined three different topological forms of a material modifier. The modifier is silicone and the three topological forms are cyclic, linear tethers and networked siloxane bonds in the form of nanoparticulate.

1.1 Polysiloxanes: applications, history, special properties, commercial preps

Polysiloxanes or silicones have been an integral component of industrial and academic research and use for more than fifty years.[1] These are "hybrid" materials, whose chemical structure combines the inorganic properties of silica with that of an organic carbon-based polymer. In some aspects the resulting properties of a polysiloxane are inferior to that of other commodity organic polymers, i.e. the low modulus. However, when compared to those same organic polymers in severe conditions, such as at extreme temperatures, the polysiloxane whose properties remain fairly constant over a large temperature range, in most cases will exhibit much superior characteristics.[1] Silicones also have many physical and chemical properties that are unique, making them the material of choice for many academic, industrial and household applications.

Part of this end-use versatility stems from the many physical forms silicones can take, which vary in structure and morphology from liquid, gel, rubber or hard plastic

despite the operating temperature.[2] In particular, industry has begun to view silicones as an under-used generic class of high-performance material whose uses as fluids, emulsions, compounds, resins and elastomers could be advantageous in fields as varied as electronics to pharmaceuticals.[3] The uses of silicone can be seen in a vast number of applications and varied technologies. The diversity of applications for silicone is directly linked to the materials good thermal stability, electrical insulation, water-repellency, low surface tension and release properties.[3] The aerospace industry uses silicones as thermal protection for the high temperatures produced by aircraft engines.[3] Because silicone rubbers exhibit superior compatibility with human tissue and body fluids they are used extensively in personal care, pharmaceutical and medical device applications. Silicones have extremely good dielectric loss properties under dry conditions and good electrical properties under humid conditions. Hence, silicone is broadly used for high temperature electronic applications requiring low electrical losses, and can be seen in many other applications specific to the semiconductor industry. Their release properties have made silicone coatings or treatments common place as a surface modifier in applications such as release agents, polishes, sealants, adhesives and water-proofing in industries ranging from construction to textiles.[2,4-6 7]

History of Polysiloxanes

Inorganic silicon based chemistry has been investigated for nearly two centuries. In 1824, Berzelius is attributed the discovery of amorphous silica by the reduction of potassium fluorosilicate with potassium metal and later making tetrachlorosilane. The first organo-silicon compound was synthesized by Friedel and Craft in 1863 via reaction

of tetrachlorosilane with diethyl zinc.[5,6] Ladenburg (who worked in Paris with Friedel on organo-silicon compounds) noticed that a dialkoxydialkylsilane he had synthesized, in the presence of dilute acid made an oil that decomposed only at very high temperatures.[5,6] That was considered the first polysiloxane. The major milestone however, happened in the early 1900's when Kipping prepared various silanes using Grignard reagents, and prepared various polysiloxanes by hydrolysis of dichlorodialkylsilanes.[5,6,8]

Properties of Polysiloxanes

Silicones are a class of synthetic polymers whose main backbone consists of repeating units of silicon and oxygen. The name "silicone" was derived from the organic nomenclature, ketone. Kipping in 1904 originally proposed the structure of dimethyl silicone to be an analogous structure to dimethyl ketone.[5,6] This was based on observed similarities with ketones and the fact that in most cases the low molecular weight silicones investigated had one silicon atom, which is four-coordinate, for every one oxygen and two methyl groups much like a ketone whose central carbon atom is also four-coordinate. Even though this conclusion later proved erroneous, the name remained to describe polysiloxanes. The basic repeat unit chemical structure for silicones follows the formula $[R_2SiO]_n$, where R is an organic substituent group. Because of commercial difficulties with large-scale synthesis, these organic groups are typically limited to methyl, ethyl, phenyl, vinyl and their halogenated derivatives. Not only do the length and molecular weight of the silicones affect properties, but the chemical identity of these substituent groups can also be used to alter the final character of the silicone material.[5]

Depending on the chemical structure of the monomer, the synthetic route used and method of processing, silicones can be linear, branched, cyclic or crossed-linked. The monomer of each repeat unit can be described by the number of alkyl groups attached to the silicone atom. A common repeat unit found in linear polysiloxanes contains di-methyl (alkyl) substituted silicon atoms [-Si$(CH_3)_2$O)-] and is denoted by the letter D, indicating the silicon atoms also have two siloxane bonds (O-Si-O). Silicon with one siloxane bond is represented by M, silicon with three siloxane bonds by T and silicon with no substituents and four siloxane bonds by Q. Subscripts are used to describe the number of these silicon atoms in the compound with that particular number of alkyl substituents present.[5] Superscripts can be used to describe systems with non-alkyl substituents, as seen in Figure 1.1.1.

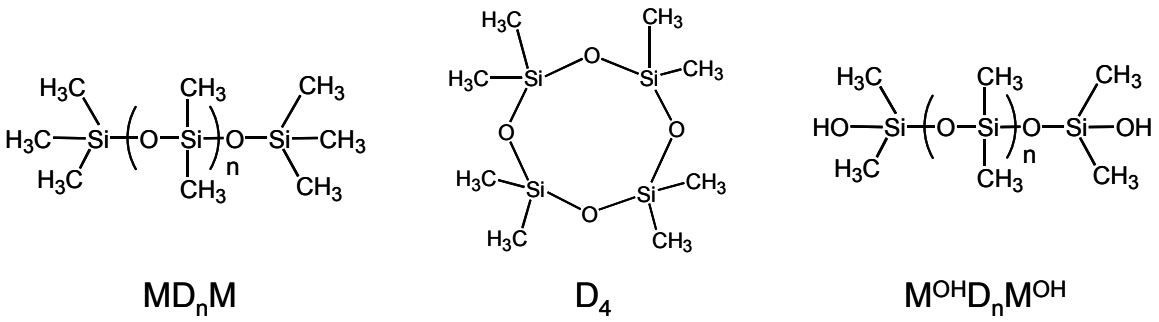

Figure 1.1.1. Examples of silicone nomenclature

The unique properties exhibited by silicones are mainly due to the silicon-oxygen bond. Common properties that define a polysiloxane include odorless, colorless, hydrophobic dielectric material displaying excellent chemical resistant, oxidation resistant, and stable at high and low temperatures.[2,9] The backbones of silicones have an analogous structure to silica, which is well-known for excellent thermal and chemical resistance. Silicon and oxygen also have an electronegativity difference (χ_M^O- χ_M^{Si}) according to Robert Mulliken of 1.19 that induces a degree of polarization that has been

estimated to be twice that of a carbon-oxygen bond whose electronegativity difference (χ_M^O- χ_M^C) is .55.[10] The induced dipole moments along the backbone shields the hydrocarbon substituents from chemical attack, which is evident as polysiloxanes are resistant to oxidative degradation up to temperatures around 200 °C, and can withstand temperatures around 350 °C in an inert atmosphere.[3] Even above 350 °C in an inert atmosphere, the polysiloxane degrades by thermal depolymerization of the siloxane bonds, where 100 % weight loss is achieved at ~ 600 °C.[11] However, the dipole effect does not extend far into the hydrocarbon substituent, and heat stability is therefore lost as the hydrocarbon group size is increased. The same dipole moments that impart good thermal and chemical resistance make the silicon-oxygen bond fairly susceptible to cleavage by acids and bases through nucleophilic attack.[3]

Heat stability of silicone extends beyond high degradation temperatures. It is well documented that the viscosity of polysiloxanes remains fairly constant over a very large temperature range, which is a result of the silicon-oxygen bond.[3] As temperatures rise the polysiloxane chain will begin to expand and uncoil, exposing more of the polymeric chain. The additionally exposed polymeric repeat units increases the silicon-oxygen bonds cumulative ability to exert intermolecular attractive forces via the induced dipole moments. This increase in attractive force essentially counteracts any change in viscosity due to addition of thermal energy.

The bond angle for the backbone of a polysiloxane is between 140-160°, which is considerably larger than the bond angles of a carbon-carbon-carbon or carbon-oxygen-carbon bond that assumes a typical tetrahedral value of ~110°. This large bond angle, the fact the silicon-oxygen bond length is 1.64 Å as opposed to 1.53 Å for a carbon-carbon

bond, along with the space filling hydrocarbon substituents, which are rigidly fixed to the backbone, cause the polysiloxane chain to occupy more volume. Not only does the excluded volume increase relative to carbon-based polymer backbones but also the polysiloxane polymeric chain becomes fairly flexible readily going through its linear 180° conformation. An increased excluded volume, equilibrium chain flexibility (related to T_m) and dynamic chain flexibility (related to T_g) creates irregular chain conformations and reduces the molecules ability to pack efficiently restricting intermolecular attractions. As a consequence, properties such as viscosity, temperature coefficients, surface tension and freezing points are low. Linear silicones do not exhibit thermoplastic characteristics for this reason, and typically have to be highly branched or cross-linked to get any reasonable mechanical properties.[3]

For every repeat unit there are two hydrocarbon substituents. This high density of hydrocarbons along the backbone imparts the molecule's hydrophobic and low surface energy characteristics. As the temperature is increased, this effect is intensified because the polymeric chain expands and uncoils exposing more of the substituents to the surface or substrate.

Preparation of Polysiloxanes

Commercial polysiloxanes can be made using one of two different schemes. Both schemes convert silica into organo-silicon compounds that are then in turn polymerized. Scheme 1.1.1 illustrates how silicon dioxide is converted into elemental silicon in an electrochemical furnace at very high temperatures, which approach ~ 1500 °C. The elemental silicon is reacted with methyl chloride yielding a mixture of

methylchlorosilanes. The crude product is separated via distillation and polymerized in the presence of water to yield hydrochloric acid and a distribution of linear $M^{OH}D_nM^{OH}$ and cyclic $D_{4,5,6}$ products. However, this method is not preferred because: (1) the high energy costs of converting silicon dioxide to elemental silicon and (2) the various methylchlorosilane products differ in boiling points by only a few degrees Celsius making distillation difficult and only effective if done in several steps.

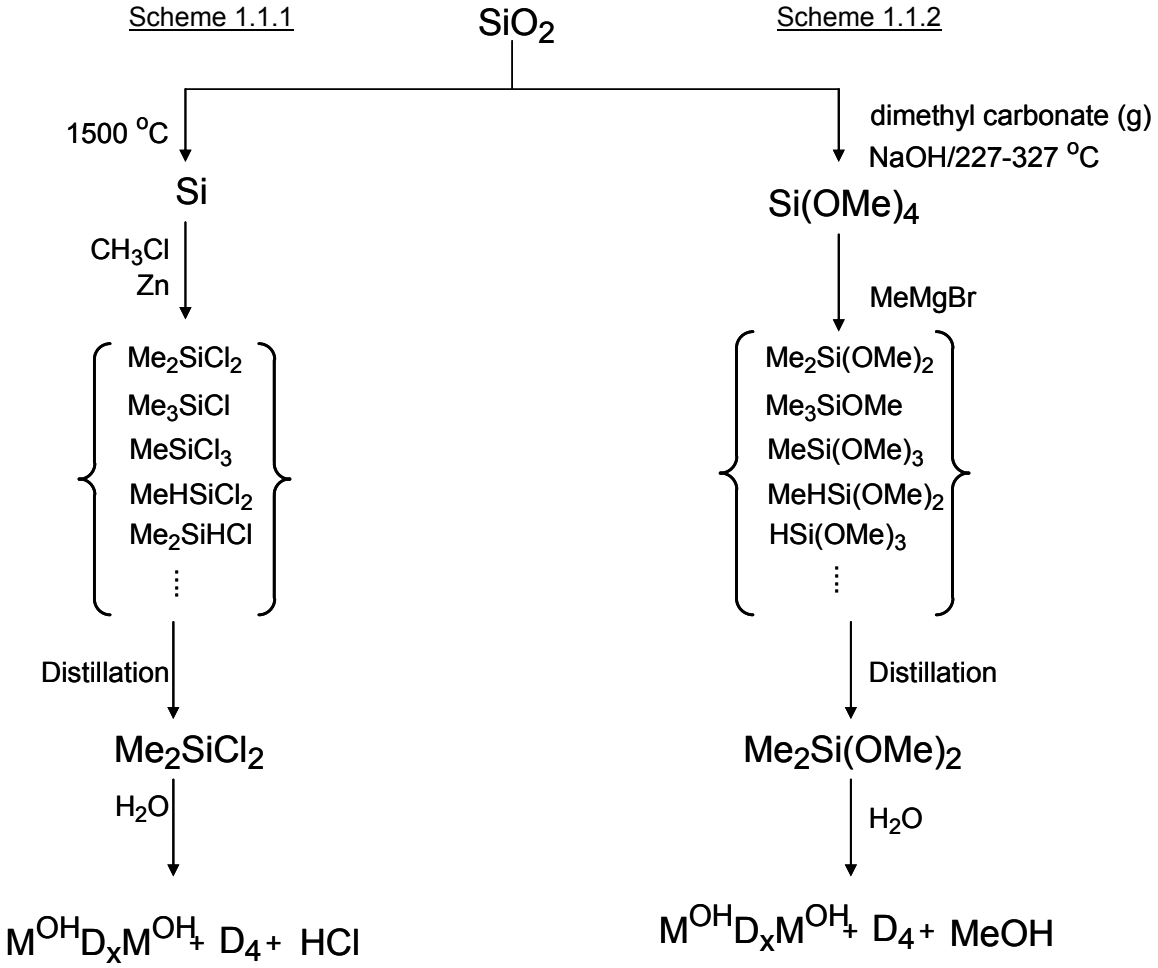

Scheme 1.1.1 and 1.1.2. Industrial production of silicones[6,8]

The more commonly used synthetic route is shown in Scheme 1.1.2.[6] The procedure was pioneered by GE in 1940 and is referred to as the direct process. Energy is conserved as the reduction of silicon in silicon dioxide to elemental silicon is avoided.

Amorphous silica is subjected to gaseous dimethyl carbonate at 500-600 K in the presence of an alkaline metal hydroxide. This converts nearly all the silica to tetra-alkoxysilane, which then using a procedure with Grignard reagents could produce dialkoxydialkylsilane. The dialkoxydialkylsilane, much like the methylchlorosilane produced in Scheme 1.1.1, must be separated by distillation. However the alkoxy groups make the boiling points of the different compounds in the residue further apart than those of the methylchlorosilane crude product, and subsequently the distillation much easier and suitable for industrial applications. The polymerization is then carried out in the presence of water to yield alcohol and a distribution of linear $M^{OH}D_nM^{OH}$ and cyclic $D_{4,5,6}$ products.[8]

Hydrolytic polymerization of dialkoxydialkylsilane or dichlorodialkysilane typically produces cyclic and linear oligomers that have chain lengths too short for any real applications. Therefore, acid or base catalyzed ring-opening polymerization of small cyclic polysiloxanes is used to form larger linear chains. An acid or base, acting as initiator and catalyst, is introduced to the small cyclic polysiloxanes causing ring-chain equilibration and some chain extension. At equilibrium, this reaction will produce a mixture of cyclic material plus a distribution of linear material. The relative amount of each cyclic oligomer produced will change depending on temperature, solvent and the chemical identity of the hydrocarbon substituent. The distribution of cycles formed match a relationship between the log of K_n and n, where K_n is the molar cyclization constant characterizing the stability of a cycle with n repeat units. The small cyclic material can easily be removed by vacuum distillation, leaving a stable hydroxyl-terminated polysiloxane.[12] The reaction can be forced to produce mostly linear product

by adding an end capping agent such as [$Me_3SiOSiMe_3$] (MM). This will reduce the average molecular weight. However, control over the average molecular weight can be achieved by manipulating the ratio of cyclic polysiloxane oligomers and end capping agents.[8]

1.2 Why Cyclic Polymers, Why Tethered Polymers?

Cyclic or ring polymers, sometimes referred to as macrocycles, are molecules containing monomeric units much like a typical linear polymer but arranged in a cyclic topology, having no end groups. Cyclic structures have been well studied in conventional organic chemistry, as early researchers worked on strained cyclic hydrocarbons.[13] It was soon discovered that much larger unstrained rings could be prepared.[13] However, it is well accepted that the topic of cyclic polymers did not become popularized until the late 1950's when some of the first electron micrographs were obtained showing the existence of circular DNA in bacterial chromosomes.[13-15] Numerous antibiotics, alkaloids, peptides, and lipids are other examples of large ring structures found in nature. The structure on the left in Figure 1.2.1 is the alkaloid manzamine A it is isolated from the sea sponges found in the waters of the Okinawa Sea, near Japan, exhibiting significant antileukemic and antimicrobial activity.[16] Whereas the structure on the right is amphotericin B, an intravenous antifungal drug originally isolated in 1955 from bacteria found in the soil along the Orinoco delta in Tembladora, Venezuela.[17]

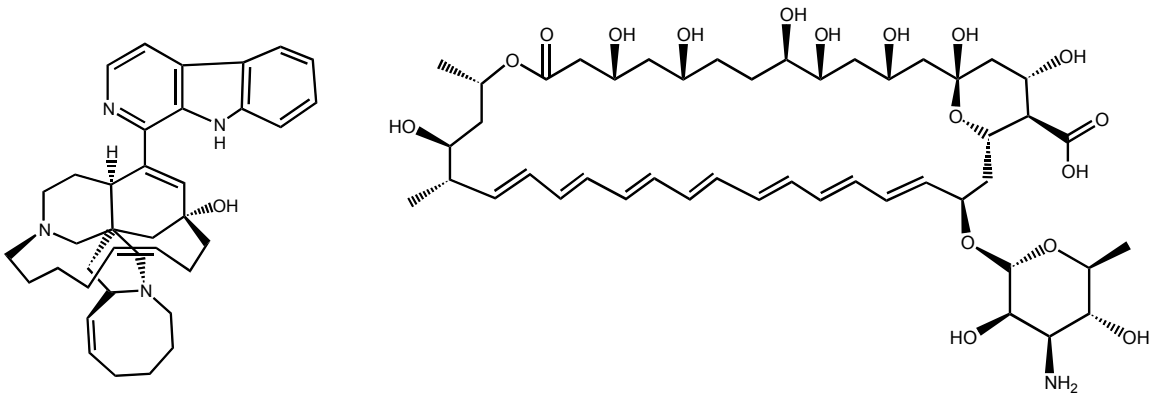

Figure 1.2.1. Examples of cyclic natural products.

The development of synthetic polymers and step-growth polymerization not only produced the first synthetic linear polyamides and polyesters but also a number of large polymeric cyclic molecules.[15] Soon after some work went into the production of large cyclic polymers, particularly the production of rings and linear material in the ring-chain equilibrium of PDMS.[12] Though ironically, typically these cyclic polymers have been seen as unwanted by-products.

The lack of end groups and topological restraints make macrocycles exhibit considerably different properties from their linear counterparts. It has been shown that in melt blends of cyclic and linear PDMS and POE there is an unexpectedly large increase in viscosity and decrease in diffusion coefficient.[15,18-21] This has been attributed to threading of the cyclic and linear material. In general when the molecular weight increases for linear polymer the glass transition temperature also increases, but cyclic PDMS has a negative slope in plots of the T_g against molar mass.[15,20,22]

This brings up the question to why make cyclic polymers at all. Over the past decade or so, studies of cyclic polymers have seen a renewed interest.[15] Particularly, in some academic circles, this can be attributed to the importance of cyclic polymers to the development of multi-component polymeric materials. These materials are typically very

difficult to generate and require large amounts of highly pure large ring polymer feed stocks.

Cyclic Polymers in Multi-Component Polymeric Materials

As investigations into applications for novel topologies and multi-component polymeric materials progress, there is a growing need for innovation in the area of topological copolymers. Therefore as part of the work focused on the synthesis of chemically heterogeneous topological copolymers the need for more efficient methods of synthesizing macrocycles has arisen. As represented in Figure 1.2.2, multi-component polymeric materials can be divided into tree basic categories: blends, covalently linked copolymers and "topological copolymers". The latter category consists of structures where the various chemically distinct components are physically linked or intertwined.[23]

Multi-component polymeric materials in general are an approach to achieve enhanced properties in a polymer. The different components of the material's structure, which have different chemical structure, can combine to produce a material with properties tailored for a specific application. Topological copolymers utilize a topologically induced physical linkage between the components of the structure that does not allow macrophase segregation or leaching as in polymer blends. Also, the structure does not require any particular synthetic route to form chemical linkages as in covalently linked copolymers.

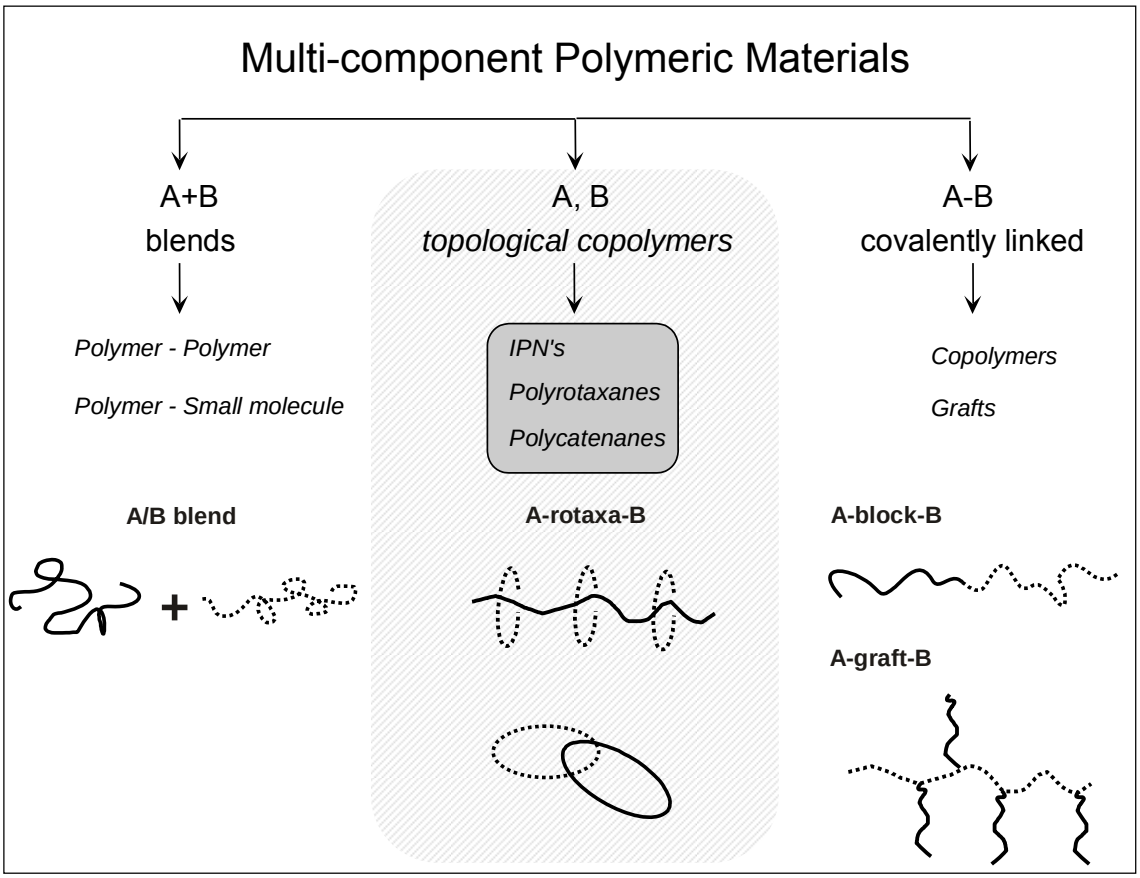

Figure 1.2.2. Multi-component polymeric materials [24]

Three of the most cited topological copolymers are interpenetrated networks (IPN), poly(rotaxane)s and poly(catenane)s. An interpenetrated polymer network is defined as the combination of at least two network forming monomers which do not covalently bond to one another, and as the network forms they become topologically locked and intertwine within one another producing a highly stable, dense material. Much like single-component networks when exposed to solvents an IPN swells but does not dissolve and it creep and flow properties are suppressed making processing them nearly impossible. However, much is known about the properties of IPN and even some are commercialized in products ranging from false teeth to ion-exchange resins, high

impact plastics, adhesives, and vibration damping materials.[25] Mark et al. conducted experiments studying theoretical models for the topological trapping or threading for cyclic polymers which resulted in synthesizing network structures very similar to IPNs. However, in this case the only component is crosslinked and the cyclic topology of the other component forms the topologically locked structure.[26,27]

On the other hand, relatively little is known about poly(rotaxane)s and poly(catenane)s. This is mainly due to the difficulty of synthesizing these structures particularly poly(catenane)s.[28] Catenated poly(styrene) and poly(2-vinylpyridine) was prepared by end-to-end coupling of a PVP dianionic lithium salt with 1,4-bis(bromomethyl benzene) in THF in the presence of PS macrocycles. However, after purification there was only ~ .5 % catenated yield, and if you consider the yield for the preparation of the cyclic PS the overall yield of the reaction is so small, acquiring enough material to investigate material properties would be difficult.[29,30]

Our group has concentrated on the synthesis of poly(rotaxane)s. Rotaxanated polymers are linear polymer chains that have been threaded through cyclic molecules. More specifically, poly(*pseudo*rotaxane)s lack bulky end groups to prevent the cyclic molecules from dethreading, while true poly(rotaxane)s possess the bulky end or blocking groups, either as end-capped or in-chain capped poly(rotaxane)s, as illustrated in Figure 1.2.3.[15,28,31] The efficient and high yield synthesis of various macrocycles and linear polymers terminated with blocking groups is the first step in determining the potential of rotaxanated structures.

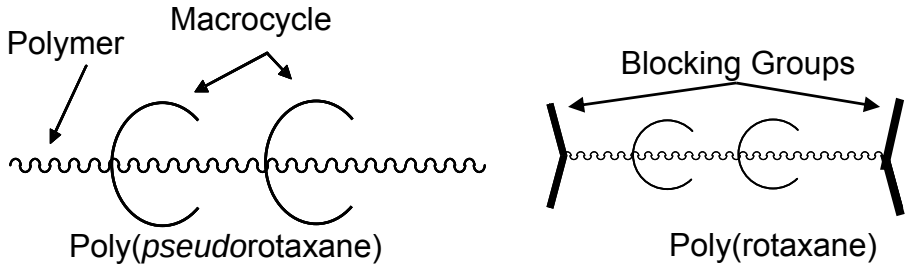

Figure 1.2.3. The poly(*pseudo*rotaxane) is composed of a main chain and threaded cycles whereas the poly(rotaxane) also includes bulky end groups to prevent the cyclic molecules from dethreading.[32]

Future applications for these poly(rotaxane)s include: surface modification, a type of processable interpenetrated network, blend compatibilization, polymer property enhancement, triggerable macromolecular switching devices, insulation for conducting polymer, and biomedical applications. The choice of macrocycle and its concentration on the main chain in a poly(rotaxane)s can be used to adjust the linear polymer's behavior altering: (1) solubility characteristics, (2) phase behavior, (3) melt behavior, and (4) solution viscosities.[33]

Initial synthetic work has been mostly academic for various reasons such as low yields and inability to get cycles to thread the linear polymer. Current efforts have focused on six generic methods of synthesis for main-chain poly(rotaxane)s. (1) A template driven method directs the mixing of the cyclic and linear components.[34,35] (2) An *in-situ* method is where the linear main chain or in-chain stoppered main chain which (a copolymer having the blocking groups incorporated into the repeat unit of the polymer main chain) is polymerized in the presence of the cyclic component.[34,35] During the polymerization process for the *in-situ* method, the threaded cyclic components have no driving force for threading. (3) As an alternative to the *in-situ* method, the polymer can

be threaded by mixing the linear and cyclic component in solution producing a poly(*pseudo*rotaxane). The poly(*pseudo*rotaxane) can then be capped with endgroups producing a poly(rotaxane).[34,35] (4) Another option is to use precapped linear main polymer chains or in-chain stoppered main chains, and perform macrocycle clipping. Macrocycle clipping is the formation of the cyclic component in the presence of the main chain.[34,35] (5) Complementary to macrocycle clipping is macrocycle slipping, where the macrocycle is slipped over the end groups on to the poly(rotaxane). This is generally demonstrated in rotaxanes instead of poly(rotaxane)s. (6) The final approach relies on linear main chains that can be reversibly disassembled, where the cyclic components are incorporated during polymer reassembly.[33,36] However, all the above approaches require large amounts of highly pure large ring polymers feed stocks and a high degree of control over cyclization.

One of the more cited examples of producing a poly(rotaxane) utilized the formation of a poly(*pseudo*rotaxane) from α-cyclodextrin (α-CD) and POE. Then by capping the linear chains with end groups a poly(rotaxane) was prepared.[36,37] In this case, the interior of an α-CD in an aqueous environment is attracted to the hydrophobic ethylene repeat units on the POE. This along with hydrogen bonding between threaded α-CD causes directed threading. The formation of this inclusion complex is an enthalpic process where threading is promoted by self-assembly.[38] Another example of utilizing thermodynamic interactions to promote threading is the threading of crown ethers onto a polyurethane chain. Threading in this case is directed by hydrogen bonding between the crown ethers and amino groups.[39,40]

In contrast, the other less effective method of synthesis for poly(rotaxane)s, in-situ polymerization, lacks a driving force for threading. In these cases, the cycles can be viewed as solvent. Hence the threading is statistical and governed by entropic forces. Factors such as macrocycle concentration, macrocycle size, polymer rigidity, and temperature can be used to influence the probability of threading; however, statistical threading usually results in low threading amounts.[28] There are only a few examples of the formation of poly(rotaxane)s by in-situ polymerization, and one such example is the formation of poly(styrene-*rotaxa*-crown ethers).[28,41] Free radical polymerization of styrene in the presence of crown ethers utilizing initiators modified with bulky end groups and a co-solvent of toluene produced a poly(styrene) with altered physical properties despite low amounts of threaded cyclic material.[28,41]

Though repetitive to state explicitly, to this date three issues have limited the extensive synthesis and potential applications of poly(rotaxanated) materials: (1) insufficient feed stock of cyclic polymers (2) low threading ratios, which is the ratio of cyclic material to linear material, and (3) handling the varied synthetic requirements for the production, synthesis and rotaxanation of cyclic and linear moieties, which obviously change depending on the chemical structure of the cyclic and linear material.

Synthesis of Macrocycles

A heterogeneous poly(rotaxane) has linear and cyclic components that are chemically different structures. The macrocycle in this structure becomes an essential element, where its size and ability to intimately mix with the linear backbone determines threading ratios. In macrocycle threading the spatial requirements of the cyclic

component cavity in relation to the size of the end groups and the linear backbone is crucial to successful and effective threading. Therefore a high degree of control must be exercised over the cyclization step which has typically been achieved using a linear difunctional polymer in dilute solution to avoid chain extension[42] as seen in Figure 1.2.4.

Although many reactions, including polycondensation reactions lead to ring closure, in practice formation of cyclic polymers can be difficult due to unfavorable entropic effects and steric effects. Early work started by Ruggli, Ziegler, and others showed high-dilution conditions are critical to macrocyclization reactions.[42] A strategy to avoid some of the entropic penalty involved in cyclization is the use of linear precursors and pre-organization of those linear structures. Figure 1.2.4 shows two simplistic synthetic strategies for macrocycle assembly: (1) bimolecular coupling, where two components using complementary end group functionality form two identical bonds, via a ring-closing acetylenic coupling reaction, olefin metathesis, condensation, etc. and (2) unimolecular coupling, where a single linear precursor has the appropriate complementary end group functionality to couple, forming one bond within the cycle.

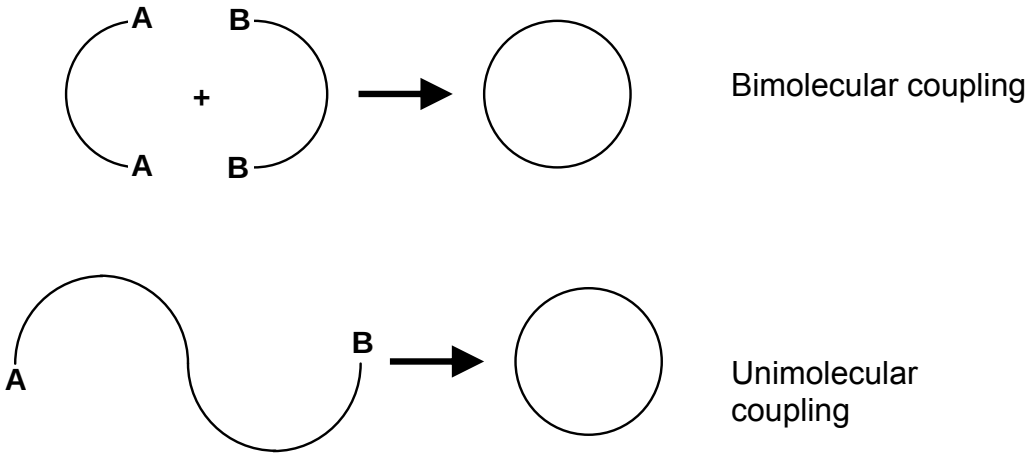

Figure 1.2.4. Cyclization schemes for a difunctional polymer.[43]

As mentioned before, poly(rotaxane)s useful in copolymer applications are heterogeneous in nature, consequently during the rotaxanation step the linear and cyclic materials tend to phase separate. This appears to be one of the major limiting factors in attaining high threading ratios. Using a common co-solvent, pressure, and making structures such as tadpoles or hybrid macrocycles, seen in Figure 1.2.5, have been proposed to increase threading ratios by manipulating the compatibility of the linear and cyclic species. This is done in tadpoles or hybrid macrocycles by incorporating segments identical to those of the linear polymer. Moreover, the tadpole topology can cause association of ordered supramolecular structures in solution, therefore could also be used to template the formation of poly(rotaxane)s and poly(catenane)s circumventing the entropic penalty of the structure formation.[43]

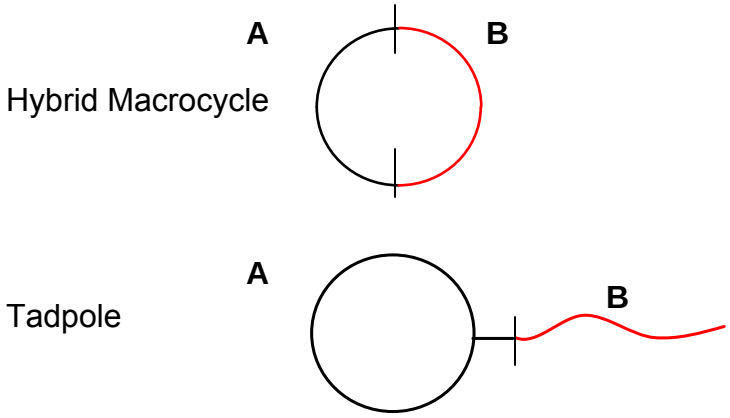

Figure 1.2.5. Hybrid macrocycles and tadpole architectures to be used in multi-component polymeric materials.[43]

Generating cyclic polymers from ring closure of linear precursors require dilute solution conditions which not only waste solvent but effectively prevent large scale production of the cyclic material. Also, the more traditional methods of macrocyclic

synthesis are vulnerable to side reaction and require an additional method to isolate the cycles from the unreacted linear precursors. As opposed to ring formation by either ring-chain equilibration or ring closure of end-functionalized linear precursors under conditions of high dilution, a third method of ring expansion by bond insertion has been explored by Bielawski and Grubbs in accordance with their work on olefin metathesis.[44,45]

In the ring opening metathesis polymerization of moderately strained cyclic polymers, a cyclic variation of the ruthenium complex $L(PCy_3)Cl_2Ru=CHR$, typically referred to as a Grubb's catalyst, remains attached to the chain end of the growing polymer, which is forming through ROMP of a cycloalkene "monomer". As seen in Figure 1.2.6, after the available monomer is polymerized, which provides control over molecular weight, the ruthenium complex facilitates ring closure via intramolecular chain transfer to yield a cyclic polymer. This process can be done in the bulk producing high quantities of high molecular weight cyclic material.[44,45]

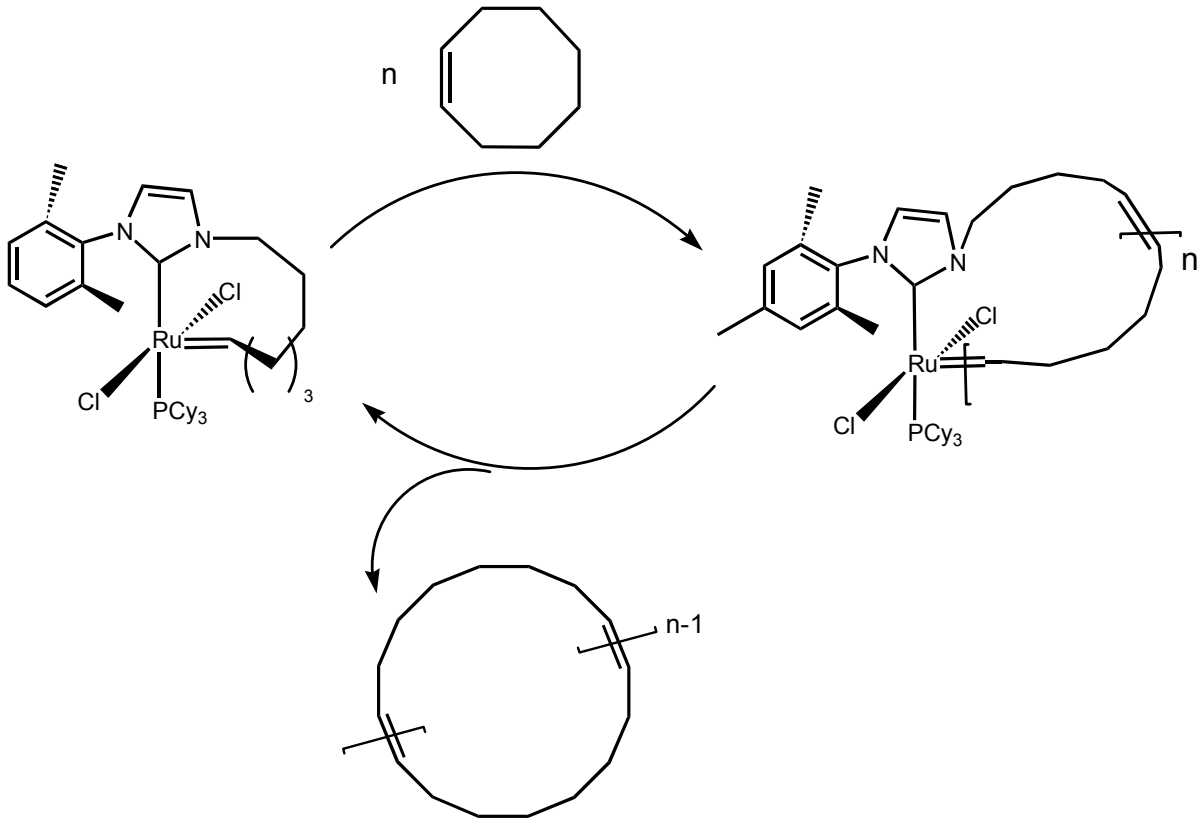

Figure 1.2.6. The synthesis of a cyclic polyoctenamer from *cis*-cyclooctene using ROMP and a cyclic derivation of the Grubb's ruthenium complex catalysts, which results from the intramolecular chain transfer of a transition complex containing both the catalyst and forming macrocycle.[44,45]

Tethered Polymer Chains as Surface or Interface Modifiers

Typically tethered polymer chains refer to oligomers either covalently or non-covalently "grafted from" or "grafted to" solid supports or interfaces, tailoring surface and adhesion properties or compatibilizing interfaces. Tethering is accomplished by immersing a surface in a solution of either, monomer where generation of active sites at the surface can lead to the initiation of a graft polymerization or end-functionalized polymer that can react with the appropriate functionality on the surface.[46-48]

Surface or interface modifications of materials can be achieved by modification of a material via either physisorbed, chemisorbed or covalently attached moieties, as seen in Figure 1.2.7. In some cases a diblock system is utilized. One block favors the solvent, while the other solvophobic block is driven toward surface, anchoring the chain to the surface.[48] A modifying layer that is too thick could affect the bulk characteristics; however, if too thin the layer is susceptible to erosion and less likely to provide the desire effect. Sometimes, because of differences in the material properties of the surface layer and the bulk material, delaminating can be a problem. This problem can be addressed by many methods such as: the use of compatibilizers at the interface, surface interpenetration, or more commonly fixation of a surface modifying/interface compatibilizing moiety through covalent or secondary forces, i.e. tethering.

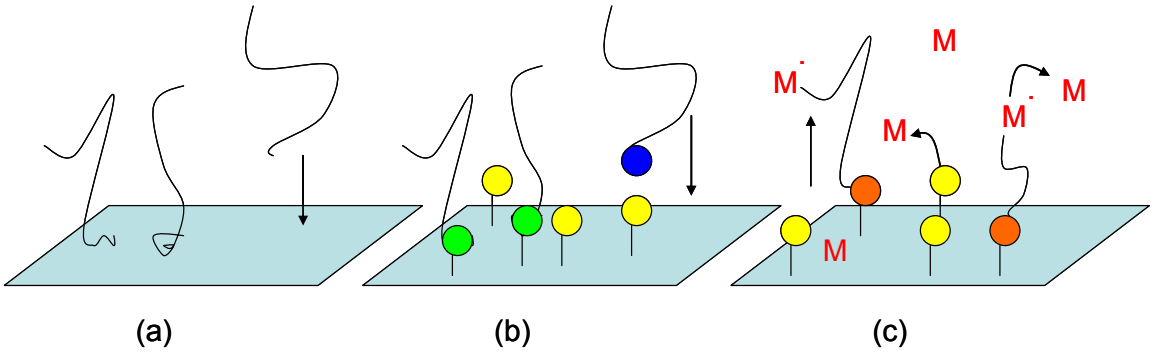

Figure 1.2.7. Schematic depicting tethered polymer chains to a surface (a) physisorbed or chemisorbed, (b) "grafting to" a surface by end-functionalized oligomers and (c) "grafting from" a surface from anchored active reactive centers.

Historically high-end applications for industries such as the medical industry have driven many of the developments in surface modifications. Thins coating of polymers can alter surface wettability and roughness.[48,49] Self-assembled monolayers of short polyethylene oligomers on silica surfaces with -OH and -PEG headgroups inhibited

protein adsorption. This follows a well observed phenomenon where non-ionic hydrophilic surface chemistry resists protein adsorption,[50] most likely due to the high surface energy mismatch between those surface groups and the fairly hydrophobic nature of a large complex proteins.[50,51]

Polymer brushes consist of a dense packing of polymer chains attached to a surface at one end of the polymer chain. Theoretical treatments to study polymer brushes have been around since the late 1970 when work by de Gennes and Alexander popularized the topic.[48] Polymer brushes are used to alter different surface properties such as: chemical or charge terminality on a surface, formation of "smart" surfaces, which responds to external stimuli, wetting control, adsorption of molecules, flocculation control of nanoparticles, etc.[49,52,53]

Polymer Chains in Multi-Component Polymeric Materials

By definition a polymer brush is considered a tethered structure because it is being anchored onto a surface. However, end-functionalized oligomers that can be inserted in a large supramolecular structure can also be considered as a tethered polymer. I view the synthesis of the some of the more complex non linear topologies seen in Figure 1.2.8 as somewhat analogous to the functionalization of a polymer system with macromonomers. A macromonomer is an oligomeric species that has end groups attached that can be polymerized. By using chemically different macromonomers the versatility of these systems producing various architectures and compositions increases.

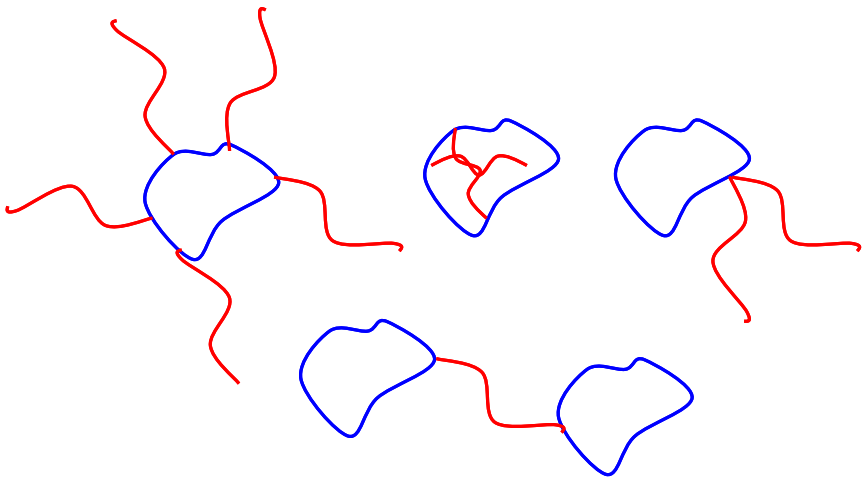

Figure 1.2.8. Complex non-linear topologies to be used in multi-component polymeric materials

1.3 References

1. Mowrer, N. *Polysiloxanes*; Ameron International Performance Coatings and Finishes: 2003; pp 1-11.

2. McGregor, R., *Silicones and Their Uses*. McGraw-Hill Book Co., Inc: New York, 1954.

3. Mark, J.; *Acc. Chem. Res.* **2004**, *37*, 946-953.

4. Ames, J.; *J. Sci. Instr.* **1958**, *35*, 1-8.

5. Colas, A.; Curtis J., Silicone Biomaterials: History and Chemistry & Medical Application of Silicones. In *Biomaterials Science: An Introduction to Materials in Medicine* 2nd Edition ed.; Ratner, B., Ed. Elsevier, Inc.: pp 80-86, 698-707.

7. Ames, J.; *Journal of Scientific Instruments* **1958**, *35*, 1-8.

8. Lewis, L. *Sand to Silicones*; GE Global Research: 2002; pp 1-13.

9. Mowrer, N. *Polysiloxanes*; Ameron International: 2003; pp 1-11.

10. Shriver, D.; Atkins, P., *Inorganic Chemistry*. Fourth Edition ed.; W. H. Freeman and Company: New York, 2006.

11. Clarson, S.; Semlyen, J.; *Polymer* **1986**, *27*, 91.

12. Suter, U.; Mutter, M. Flory, P.; *J. Am. Chem. Soc.* **1976**, *98*, (19), 5740.

13. Kleinschmidt, A.; Burton, A.; Sinsheimer, R.; *Science* **1963**, *142*, (3594), 961.

14. Freifelder, D.; Kleinschmidt, A.; Sinsheimer, R.; *Science* **1964**, *146*, (3641), 254-255.

15. Semlyen, J, *Cyclic Polymers*. Elsevier: New York, 1986.

16. Sakai, R.; Higa, T.; *J. Am. Chem. Soc.* **1986**, *108*, 6404-6405.

17. Lemke, A.; Kiderlen, A.; Kayser, O.; *Appl. Microbiol. Biotechnol.* **2005**, *68*, 151-162.

18. Cosgrove, T.; Griffiths, P.; Semlyen, J.; *Polymer* **1996**, *9*, 1535-1545.

19. Nam, Sunghyun. Dynamics of Cyclic and Linear Poly(oxyethylene), and Threading Conformation in their Blends. Doctor of Philosophy Georgia Institute of Technology, Atlanta, 2006.

20. Semlyen, J.; Wood, B; Hodge, P.; *Polymers for Advanced Technologies* **1993**, *5*, 473-478.

21. Orrah, D; Semlyen, J.; *Polymer* **1988**, *29*, 1455-1458.

22. Alberty, K.; Hogen-Esch, T; Carlotti, S.; *Macromol. Chem. Phys.* **2005**, *206*, 1035.

23. Batten, S.; *Cryst. Eng. Comm.* **2001**, *18*, 1-7.

24. Nagapudi, K. Structure, morphology and dynamics of crown ether-based polyrotaxanes Phd, Georgia Institute of Technology, Atlanta, 1999.

25. Sperling, L.; Mishra, V.; *polymers for Advanced Technologies* **1995**, *7*, 197-208.

26. Mark, J.; *Macromolecules* **1987**, *20*, 2368-2374.

27. Huang, W.; Frisch, H.; Hua, Y.; Semylen, J.; *J. Polym. Sci., Part A: Polym. Chem* **1990**, *28*, 1807-1812.

28. Gibson, H.; Bheda, M.; Enge, P.; *Prog. Polym. Sci.* **1994**, *19*, 843-945.

29. Gan, Y.; Dong, D.; Hogen-Esch, T.; *Macromolecules* **1995**, *28*, 363-385.

30. Gan, Y.; Dong, D.; Hogen-Esch, T.; *Macromolecules* **2002**, *35*, 6799-6803.

31. Semlyen, J, *Large Ring Molecules*. Wiley: New York, 1996.

32. White, B. Rotaxanated Polymers: I. Synthesis and Purification of Cyclic Polydimethylsiloxane II. Synthesis of Poly[(octene-pseudorotaxa-(α-cyclodextrin)]. Doctoral Thesis, Georgia Institute of Technology, Atlanta, 2004.

33. Tuncel, D.; Steinke, J.; *Macromolecules* **2004**, *37*, 288-302.

34. Gibson, H. W.; Engen, P. T.; Shen, Y.; Sze, J.; Lim, C.; Bheda, M.; Wu, C.; *Makromol. Chem., Macromol. Symp.* **1992**, *54-55*, 519.

35. Gibson, H.; Engen, P.; Lee, S.; *Polymer* **1999**, *40*, 1823.

36. Zhao, T.; Beckham, H.; *Macromolecules* **2003**, *36*, 9859-9865.

37. Okada, M.; Harada, A.; *Org. Letters* **2004**, *6*, 361-364.

38. Harada, A.; Kamachi, M.; *Macromolecules* **1990**, *23*, 2821.

39. Nagapudi, K.; Hunt, J.; Shepherd, C.; Baker, J.; Beckham, H.; *Macromol. Chem. Phys.* **1999**, *200*, 2541.

40. Nagapudi, K.; Leisen, J.; Beckham, H.; Gibson, H.; *Macromolecules* **1999**, *32*, 3025.

42. Deffieux, A.; *Macromolecules* **1996**, *29*, 8776-8782.

43. Watson, W. Hybrid Macrocycles for Supramolecular Assemblies. Doctoral Thesis, Georgia Institute of Technology, Atlanta, 2005.

44. Bielawski, C.; Benitez, D.; Grubbs, R.; *Science* **2002**, *297*, 2041.

45. Bielawski, C.; Benitez, D.; Grubbs, R.; *J. Am. Chem. Soc.* **2003**, *125*, 8424-8425.

46. Boyes, S.; Granville, A.; Baum, M.; Akgun, B.; Mirous, B; Brittain, W.; *Surface Science* **2004**, *570*, (1-2), 1-12.

47. Brittain, W.; Mink, S.; *J. Polym. Sci. Part A: Polym. Chem.* **2007**, *45*, 3505.

48. Currie, E.; Norde, W.; Stuart, M.; *Advances in Colloid and Interface Science* **2003** *100 –102,* 205–265.

49. Zhao, B.; Brittain, W.; *Prog. Polym. Sci.* **2000**, *25*, 677–710.

50. Faucheux, N.; Schweiss, R.; Lützow, K.; Werner, C.; Groth, T.; *Biomaterials* **2004**, *25*, (14), 2721-2730.

51. Ratner, B.; *Journal of Molecular Recognition* **1996**, *9*, 617-625.

52. Tezuka, Y.; *Macromol. Symp.* **2003**, *192*, 217-226.

53. Nath, N.; *Adv. Mater,* **2002**, *14*, 17.

CHAPTER 2

High-yield Synthesis of Cyclic Poly(dimethyl siloxane) from Kinetically Controlled Depolymerization of Linear Precursors

2.1 Abstract

Cyclic poly(dimethylsiloxane) (PDMS) can be prepared from commercially available linear α,ω-dihydroxy-PDMS using base-catalyzed unimolecular ring closure. Cyclization was confirmed by GPC, FTIR, MALDI-ToF MS and NMR spectroscopy. Purification of the cyclic PDMS was achieved by removing linear byproducts using an ion-exchange resin. The analytical results and the cyclization simulations, which follow a kinetic Monte Carlo method, show that the cyclic product formed is actually a result of kinetically controlled cyclodepolymerization. Though kinetically controlled cyclodepolymerization results in the formation of small thermodynamically favored cycles the analytical results show that large- to medium-sized PDMS cycles (n>12) can be kinetically trapped in yields approaching 70% of the total amount of cycles whereas cyclization by ring-chain equilibration of small ring oligomers leads to no more than 13% large- to medium-sized PDMS cycles (n>6). Cyclodepolymerization of the linear precursor resulted in a polydisperse cyclic product with a reduced number-average molecular weight, where the yield of any one large cycle is relatively small.

2.2 Introduction

As early as the 1940's researchers such as Wilcock and Scott had been studying the equilibrium molecular weight distributions of poly(siloxane) systems.[1-4] They soon realized that not only linear and branched topologies existed in the equilibrate but also cyclic material was present. Through careful fractional distillations, the composition of the mixture of linear and cyclic components in the equilibrate, up to ~ D_6 cycles, was analyzed.[4] The equilibrium constants were determined for material with 4, 5 and 6 repeat units and seemed to indicate that the cyclic material consisted of stable unstrained rings. The formation of these rings were attributed to a reversible reaction that produced and consumed ring and linear chains and is represented by the ring closure/ring opening equilibration in the bottom left portion of Figure 2.1.

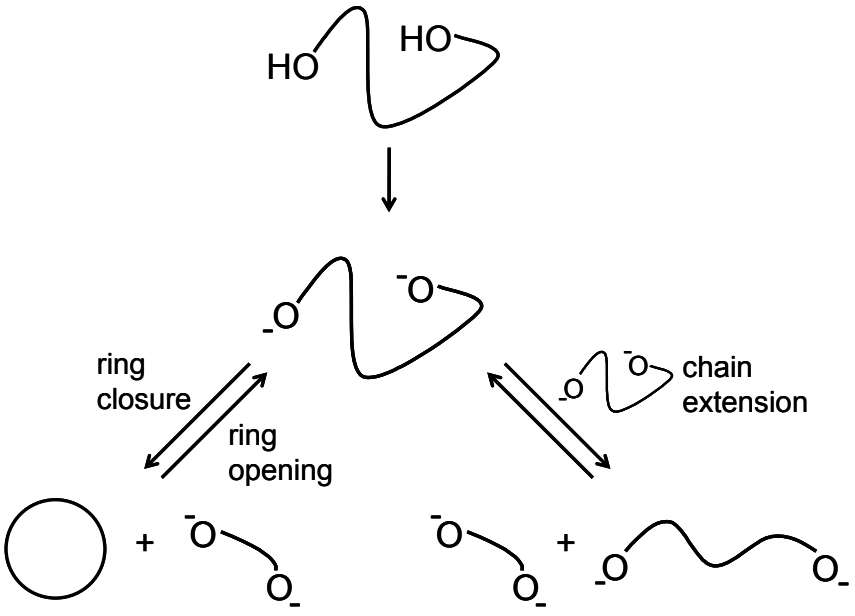

Figure 2.1. Deprotonation of α,ω-dihydroxy-PDMS yields silanolate chain ends that initiate ring-chain equilibration through ring closure, ring opening and chain extension. Dilute-solution conditions promote the intramolecular process of ring closure, and concentrated conditions encourage chain extension. Counter ions are not shown.

This ring-chain equilibration can also be depicted in a more traditional chemical equilibrium expression:

$$D_y \leftrightarrow D_{y-n} + MD_{n-2}M \qquad \text{Eq. 2.1}$$

The molar cyclization equilibrium constant, K_n which describes the stability of a cycle with n-units, D_n is then given by[1-7]:

$$K_n = \frac{[D_{y-n}][MD_{n-2}M]}{[D_y]} = \frac{[MD_{n-2}M]}{p^n} \qquad \text{Eq. 2.2}$$

Using Flory's statistical mechanical description of the most probable distribution of linear chains resulting from chain-chain equilibration, the cyclization equilibrium expression can be simplified, where p^n is the extent of reaction for the linear material, a measurable quantity.[5-7]

With advancements in analytical and separation techniques such as vacuum distillation, solvent fractionation, gas and liquid chromatography, and gel permeation chromatography, subsequent investigations of larger PDMS rings were accomplished. Supported by the collected work of Carmicheal et al., who extended the analysis of the PDMS equilibrate to D_{25}, Brown and Slusarczuk were able to prepare cyclic PDMS up to 250 repeat units in milligram quantities.[8-10] By heating octamethylcyclotetrasiloxane (D_4) and/or decamethylcyclopentasiloxane (D_5) neat or in the presence of toluene with traces of a base catalyst, potassium hydroxide, preparation of PDMS equilibrate was achieved. The resulting cyclic and linear molecular weight distributions were used to calculate the molar cyclization constants for D_4-D_{250} by using a modified form of Eq 2.2[6]:

$$K_n = [D_n]_{equil}\left(\frac{\overline{P}_w - 1}{\overline{P}_w + 1}\right)^{-n} \qquad \text{Eq. 2.3}$$

where P_w is the weight-average degree of polymerization for the linear component in the equilibrate.[6]

Brown and Slusarczuk were then able to construct a log-log plot, as seen in Figure 2.2, that describes the molar cyclization constant as a function of ring size during ring-chain equilibration. The plot shows a negative slope with a global stability maximum at D_4, local minimum at D_{12}, and local maximum at D_{15}, where the region after the local maximum shows a shallower slope than that after the global stability maximum, which corresponds to a slope of ~ - 2.86 over the range D_{20}-D_{200} (typical of thermodynamically controlled systems).

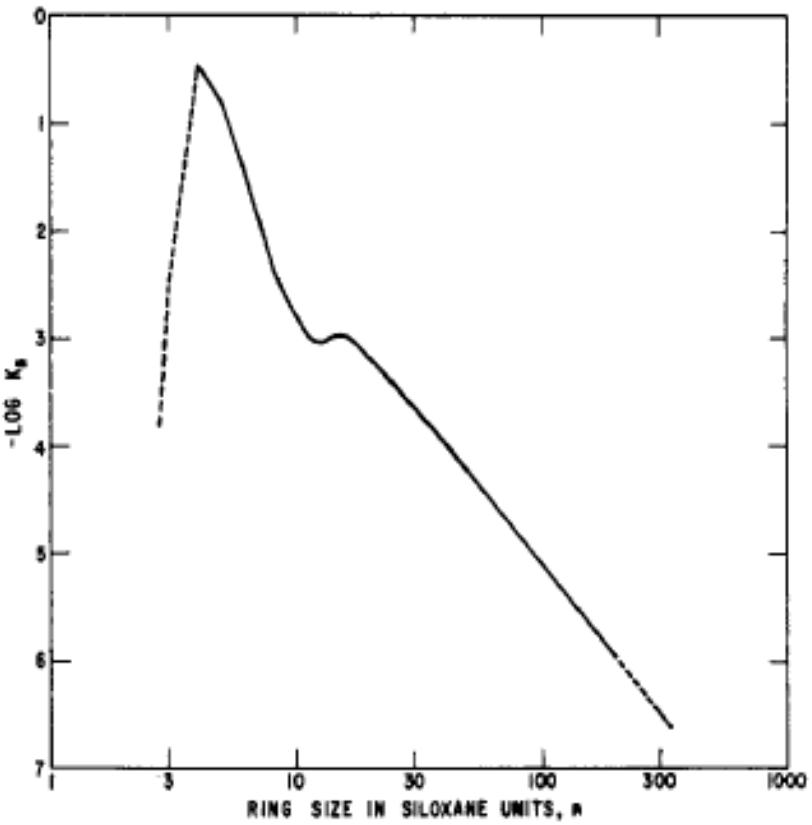

Figure 2.2. The stability of PDMS cycles during ring-chain equilibration is described by the molar cyclization constant, K_n, which is dependent on the number of siloxane repeat units, n. The equilibrate was formed by heating octamethylcyclotetrasiloxane with KOH in toluene at 110 °C. [Reprinted with permission from Brown, J. F.; Slusarczuk, G. M. *J. Am. Chem. Soc.* **1965**, 87, 931. Copyright © 1965 American Chemical Society.]

The most important result from their work was the realization that this reaction route produces an equilibrate composed mostly of cyclic material, $[(CH_3)_2SiO]_x$, agreeing with equilibrium constants as predicted by Jacobson-Stockmayer cyclization theory.[11] Jacobson and Stockmayer developed a theoretical expression for the molar cyclization equilibrium constant based upon Gaussian chain statistics describing the random-coil conformation of linear polymers in solution or melt. Their cyclization theory related end-to-end ring closure to the size of the corresponding linear polymer chain, specifically to the probability of the mean-squared sum of the bond vectors equaling zero. This probability function is defined by the mean-squared end-to-end distance, $\langle r^2 \rangle$, a relationship which again was used to generate an equation for the molar cyclization constants, K_n:

$$K_n = \frac{\left(\frac{3}{2\pi \langle r^2 \rangle_n} \right)^{3/2}}{N_A \sigma_{Rn}} \qquad \text{Eq. 2.4}$$

where N_A is Avogadro's number and σ_{Rn} is a symmetry parameter associated with the size of the units that can be formed in a ring opening reaction of D_n.[2,3]

Exhaustive purification schemes of the product mixtures formed via ring-chain equilibration using fractionation and preparative gel permeation chromatography have been successful for isolating narrow fractions of cyclic PDMS up to molecular weights of 50 kg/mol (~ 1300 ring atoms). However, yields for any given cycle size are rather limited. This is because the decreased concentration of a given cyclic PDMS in such equilibrium mixtures is directly related to the probability that its ends will meet as governed by its statistical conformations or its molar cyclization constant. For example, Dodgson and Semlyen reported that the base-catalyzed equilibration of $[(CH_3)_2SiO]_4$ and $[(CH_3)_2SiO]_5$

oligomers in toluene took several days and resulted in approximately 13% yield for all (n>6) large cyclic siloxanes.[20]

PDMS has been prepared traditionally not only by base- but also acid-catalyzed ring-chain equilibration of $[(CH_3)_2SiO]_x$ (x = 3, 4 or 5) in the bulk or in solution. Cationic polymerization of D_3 cycles was carried out in methylene chloride or in heptane in the presence of a "super" protonic acid (CF_3SO_2H).[12,13] The authors not only proposed a mechanism by which PDMS is cationically polymerized but also showed after enough time the reaction will proceed to the same equilibrate seen in base-catalyzed systems and predicted by Jacobson-Stockmayer cyclization theory.

Equilibrate formation is not the only route to produce cyclic PDMS. In a study detailing the high temperature thermal behavior of linear PDMS, it was found at 350 °C PDMS depolymerized into a mixture of cyclic and linear material.[14] Chromatographic analysis showed the cyclic product formed was a mixture of ring sizes in which the ring concentration of a given size decreases in a mostly continuous fashion with increasing molecular weight. Also, it was determined that the depolymerization mechanism was consistent with the acid activation of silanol end groups catalyzed by the either the surfaces of the reaction vessel or ionic impurities, and not due to bond interchange reactions. Similarly, a mixture of cyclic PDMS with ring sizes from 6 to 20 was generated using an acidic Zeolite-type fixed bed catalyst at temperatures from 500 to 700 °C.[15] The unifying characteristic for all the above reaction routes to cyclic PDMS utilize a depolymerization process to access the cyclic topology.

Another route to macrocycle formation is reaction preformed under pseudo-dilution conditions.[2,3,21,22] In general with increasing dilution, the generation of cycles is favored at

the expense of chain formation. Particularly with the development of techniques such as MALDI-ToF MS to monitor more complex reactions, kinetically controlled step-growth polymerization has become a technique to produce cyclic polymers.[16] Cyclic oligomer formation from ring-chain equilibration as seen in Figure 2.1 is not restricted to polysiloxanes. Any polymer that can be polymerized via ring-opening polymerization or step-growth polymerization in which the terminal end of a polymer acts as a reactive center that can also react with equal propensity with either the cyclic monomer or the polymer (linear or cyclic) backbone itself will perform backbiting. Essentially, the end groups and repeat unit of the polymer are the reactants.[16-19] Therefore, in these types of systems, by controlling the reaction mixture concentration and time/temperature profile ring polymers in fairly high yield and purity can be kinetically trapped.

High-yield synthesis of cyclic PDMS may be achieved by ring closure of end-functionalized linear PDMS using a complementary difunctional coupling agent in dilute solution. This end-coupling in dilute-solution route was demonstrated on commercially available α,ω-dihydroxy-PDMS (M_n ~ 1.5 kg/mol), which was converted to cyclic PDMS in 77% yield.[21,22] This published method begins with deprotonation of the α,ω-dihydroxy-PDMS precursor with sodium hydride followed by stirring overnight or until all solid particulates had dissolved. Following addition of a dichlorodimethylsilane coupling agent, the reaction was allowed to proceed for another 24 hours before quenching with an anion-exchange resin to remove any remaining charged linear species. The product was washed with water to remove salts and vacuum distilled to remove low-molecular-weight byproducts. The cyclic architecture of the PDMS product was proven by MALDI-ToF MS, GPC, FTIR and NMR spectroscopy. For the purposes of this account, the important point of this

procedure to note is that α,ω-dihydroxy-PDMS is deprotonated in dilute solution (below the overlap concentration, c^*) for hours before the coupling agent is added.

In the analysis of the depolymerization the molar mass of the linear precursors is fundamental. (Also, in Chapter 3 to avoid side reactions and maximize yield, stoichiometric balance between reactants, particularly in bimolecular coupling is important.) Applying completely different methods, similar molecular weight results were only found within 2 significant figures, making it difficult to assign a stoichiometric molecular weight. Examples of this type of inconsistently for PDMS is found in the literature,[23] an in the interest of moving forward the molecular weights used were a compromise between manufacturer suggested masses and the mass determined by various analytical techniques. Initially, molecular weights were determined by GPC in toluene using a universal calibration curve based on six narrow polystyrene standards; attempts were made to verify these values using MALDI-ToF spectrometry and NMR for the smaller material and using static light scattering for the largest linear precursor, as seen in Appendix A, Table A.1. After a linear polymer is converted into a cyclic one there should be a characteristic increase in retention time for the cyclic polymer that is only due to the smaller hydrodynamic volume of a cycle. This shift can be related to the change in Mark-Houwink constants[24] and therefore can be theoretically determined for any particular linear precursor.

When larger linear precursors were used exposed to a NaH/THF solution and followed by the addition of a dichlorodimethylsilane coupling agent, the resulting cyclic PDMS was the same size. This is revealed in Figure 2.3 as the GPC chromatograms of three different linear PDMS precursors (1.5, 4.2, and 6.0 kg/mol) resulted in cyclic PDMS with identical GPC chromatograms. While the cyclic PDMS prepared from the 1.5 kg/mol linear

precursor has the retention time shift in the direction expected as a result of the coupling reaction shown in Figure 2.3, the shift had a magnitude too large to be due solely to cyclization and the cyclic PDMS products prepared from the larger precursors were much smaller than expected. These data suggest that some base-catalyzed equilibration occurs during this reaction procedure, as depicted in Figure 2.1, leading to the "chewing up" or depolymerization of some of the PDMS.

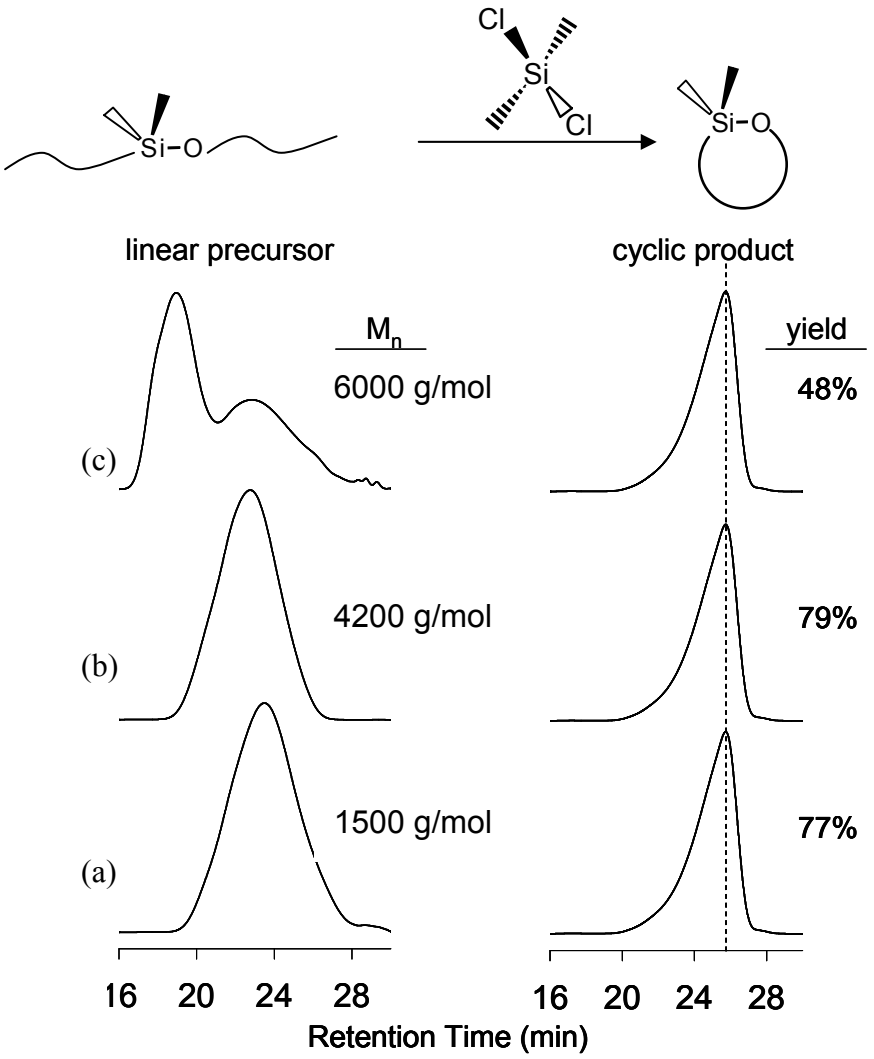

Figure 2.3. End-coupling dilute-solution route to cyclic PDMS. GPC traces for linear (on left) and cyclic (on right) PDMS from three different molecular weights of α,ω-dihydroxy-PDMS: (a) M_n ~ 1.5 kg/mol, (b) M_n ~ 4.2 kg/mol, and (c) M_n ~ 6 kg/mol. When the deprotonation step is allowed to proceed overnight, the product cyclic PDMS is the same size.

For a deprotonated α,ω-dihydroxy-PDMS chain in dilute solution, the reaction mixture which is dominated by intramolecular interaction leads to ring closure. Thus, cyclic PDMS could appear by either coupling of chain ends according to the scheme at the top of Figure 2.3, or by ring closure according to Figure 2.1. For the 1.5 kg/mol α,ω-dihydroxy-PDMS [Figure 2.3 (a)], the cyclic PDMS product has the same structure and molecular weight regardless of the reaction path. The question naturally arose as to whether the coupling agent was being incorporated into the cyclic PDMS as proposed in the scheme shown in Figure 2.3. Since the coupling agent was unlabelled dichlorodimethylsilane and the linear precursor was polydisperse, it was not straightforward to determine spectroscopically whether the coupling agent was being incorporated.

In this chapter, it is shown that the coupling agent does become incorporated into the cyclic PDMS, but not quantitatively. Base-catalyzed equilibration occurs as well, the first step of which is backbiting by the anionically charged ends of the deprotonated α,ω-dihydroxy-PDMS precursor to give rings. In fact, we show that this first ring-closure step (see Figure 2.1) is sufficiently fast to use this procedure as an effective high-yield route to large cyclic PDMS with molecular weights governed by the size of the linear precursor and the amount of time the PDMS precursor mixture is allowed to react.

2.3 Experimental Section

2.3.1 Materials

All reagents were used as received. α,ω-Dihydroxy-PDMS (DMS-S15: M_n ~ 1.5 kg/mol, 45-85 cSt, c^* = 548 g/L; DMS-S21: M_n ~ 4.2 kg/mol, 90-120 cSt, c^* = 233 g/L;

DMS-S27: M_n ~ 18 kg/mol, 700-800, cSt, c^* = 69 g/L; DMS-S35: M_n ~ 35 kg/mol, 5,000 cSt, c^* = 40 g/L) from Gelest and (bimodal, M_n ~ 6 kg/mol, 900-1,100 cSt, c^* = 173 g/L) from Sigma-Aldrich. [$c^* = 1/[\eta]$ and M_n were a comprise between manufacturer suggest molecular weight and molecular weight as determined from GPC, NMR and LS.] Hydrochloric acid (reagent grade, 37%), sodium hydride (dry, 95%), dichlorodimethylsilane (99%), 1-naphthyl isocyanate (98%), tetrahydrofuran (anhydrous, 99.9%), methanol, hexane and toluene (HPLC grade, 99.8%) were purchased from Sigma-Aldrich. 1,4-Bis(dimethylchlorosilyl)benzene (95%) was purchased from Silar Laboratories. Macroporous anionic-exchange resin AG MP-1M (1 meq/mL, 0.7 g/mL, 100-200 mesh, chloride form) was purchased from Bio-Rad Laboratories and dried under vacuum prior to use.

2.3.2 Instrumentation

Samples for gel permeation chromatography (GPC) were prepared in a 1 wt. % solution of toluene and filtered through a 0.45-μm nylon filter, with an eventual injection volume of 100 μL. GPC was conducted in toluene (1 mL/min) at 303 K on three Waters Styragel columns (5-μm beads: HR 1, HR 3, HR 4) or (5-μm beads: HR .5, HR 1, HR 3) that were connected to a Waters 2690 separations module and Waters 2410 refractive index detector. The latter column set was used to gain better resolution for smaller oligomers between 0-30 kg/mol. Number-average molecular weights were determined by integration of the selected peaks using a third-order polynomial universal calibration curve computed from six narrow polystyrene standards (HR 1, 3 and 4: 215, 72.2, 30.3, 13.1, 3.76, 1.26 kg/mol or HR .5, 1 and 3: 30.3, 28.6, 13.1, 3.76, 2.85, 1.26 kg/mol) in toluene along with the following

Mark-Houwink constants: k = 0.0075 ml/g and a = 0.75 for polystyrene in toluene[39]; k = 0.0042 [(ml/g)(mol/g)^a] and a = 0.77 for cyclic PDMS in toluene[24]; k = 0.0042 [(ml/g)(mol/g)^a] and a = 0.83 for linear PDMS in toluene[24].

MALDI-ToF mass spectrometry was carried out on an ABI Voyager-DE PRO Biospectrometry Workstation operated in reflectron mode with dithranol serving as the matrix (used to observe M_n less than 5,000 amu) or a Micromass TofSpec 2E operated in linear mode with α-cyanohydroxycinnamic acid. NaI or ambient sodium ions were used for ionization. Most modern MALDI-TOF mass spectrometers are capable of operating in either linear or reflectron modes. In linear mode the laser and detector are arranged in a linear orientation to one another, where maximum mass resolution observed is ~ 600 (mass resolution is a dimensionless ratio of the mass of a peak to its width) up to ~100,000 amu. In reflectron mode a ion reflector is located at the end of the flight tube helping resolve ions whose kinetic flight energy is similar, where maximum mass resolution observed is ~ 3400 up to ~5,000 amu.[30,32,40] IsoPro 3.0 was used to simulate isotopic distribution of peak assignments.

^{1}H, ^{13}C and ^{29}Si NMR spectra were measured on a Bruker AMX 400 or DRX 500 in chloroform-*d*. ^{1}H and DOSY NMR spectra were collected with a Bruker DRX 500 in chloroform-*d*. The DOSY experiments were conducted using the bipolar pulse pair and longitudinal eddy current delay (BPP-LED) pulse sequence.[25] Field gradient calibration was accomplished using the self-diffusion coefficient of pure water at 25 °C (2.299 * 10^{-9} m^2s^{-1}). The gradients were applied for 2 ms and the diffusion time was 80 ms. Gradient settling times were 500 μs and the eddy current elimination duration was 5 ms. Homospoil gradients were applied for 1 ms during diffusion and eddy current settling durations. The gradients

were incremented 16 times from 1.7 G/cm to 63.0 G/cm. A total of 128 free induction decays containing 8K complex data points were collected at each gradient. The recycle delay was 10 s and 8 dummy scans were applied before the first data were collected.

2.3.3. Synthesis

Glassware was dried at 120 °C overnight. Round-bottom flasks with stir bars were sealed with rubber septa and cooled while evacuating and then backfilling with dry N_2.

Base-catalyzed unimolecular ring closure of α,ω-dihydroxy-PDMS

In a 250-mL flask with magnetic stir bar under positive nitrogen pressure, a septum was removed and sodium hydride (2.1 eq based on the M_n of the PDMS) was transferred into the flask using a spatula. The flask was then evacuated and THF (200 mL) was charged by cannula. After allowing a minimum amount of time for the sodium hydride to fully suspend and dissolve (typically ~ 5 min), α,ω-dihydroxy-PDMS (~ 7.5-10 g/L) was added with a syringe, and the mixture was stirred. It is important to note that the concentration of PDMS in the reaction flask is below the overlap concentration (c^*=1/[η]). Aliquots were extracted at various times after injecting the PDMS. The aliquot was quenched with 2.5 eq (based on the M_n of the PDMS) of 1-naphthyl isocyanate (topologically-resovled GPC experiments), excess of .1M HCl in methanol (methanol-quenched experiments) or excess of AG MP-1M anion-exchange resin (resin-quenched experiments). All procedures the mixture was filtered using vacuum filtration and solvent was removed by rotary evaporation, and the crude material was dissolved in hexane, washed with distilled water (× 2) to remove salts, and dried

over magnesium sulfate. The mixture was filtered and the solvent removed by rotary evaporation.

2.3.4 Reagents and Products

Linear α,ω-Dihydroxy-PDMS

^{1}H NMR (CDCl3): δ -.02-.40 (m, CH_3SiCH_3), 2.53 (s, HOSi). ^{29}Si NMR ($CDCl_3$): δ -10.7(s, HOSi), -20.5, -21.41, -22.02 (m, CH_3SiCH_3). ^{13}C NMR ($CDCl_3$): δ .88-.42, .082 (m, CH_3SiCH_3). IR: broad, 3100-3700 cm^{-1}, sharp, 790 cm^{-1}.

Cyclic PDMS

^{1}H NMR (CDCl3): δ -.02-.40 (m, CH_3SiCH_3). ^{29}Si NMR ($CDCl_3$): δ -22.02 (m, CH_3SiCH_3). IR: sharp, 790 cm^{-1}.

Linear α,ω- Naphthalen-1-yl-carbamic Acid Endgroups

^{1}H NMR (CDCl3): δ -.02-.40 (m, CH_3SiCH_3), 8.01-7.32 (7H, m, Naphthyl Endgroup).

2.4 Results and Discussion

To assess whether the coupling agent was being incorporated into the cyclic PDMS, the ring closure procedure was carried out on 1.5 kg/mol α,ω-dihydroxy-PDMS using 1,4-bis(dimethylchlorosilyl)benzene as the coupling agent. Assuming only ring closure at the coupling agent, integration of the chemical shifts for the phenyl protons in the coupling agent and the methyl protons along the backbone of the PDMS in a standard ^{1}H NMR spectrum of the washed and distilled product indicated ~ 40% of the coupling agent was incorporated into the resulting cyclic PDMS. Attachment of the coupling agent to the PDMS was confirmed with ^{1}H DOSY NMR which revealed the same self-diffusion coefficient (-9.9 m^2/s) for the

main signals due to cyclic PDMS and for those due to the bis(dimethylsilyl)benzene coupling agent. The unincorporated coupling agent appeared with a diffusion coefficient of -9.2 m^2/s, and can be seen in Appendix A, Figure A.12.

Standard 1D ^1H NMR was used with DOSY NMR to prove that the coupling agent was incorporated into the linear precursor. Incorporation of chemical moieties into larger oligomeric, polymeric or supramolecular structures can be difficult to prove by standard 1D NMR alone since the atoms involved in the linkage are present in such low concentrations and their spectral signatures can be complex with difficult to resolve data due to overlapping, convoluted resonances. We have found in these cases that DOSY NMR is particularly useful since all of the NMR-active nuclei in the attached moiety may be used to determine whether it is attached to the larger substrate compound.[25,26] If cyclization occurs by incorporation of the coupling agent as proposed in the reaction scheme of Figure 2.3, the DOSY spectrum should show all chemical shifts at the same diffusion coefficient. We routinely use this analytical method to verify the incorporation of small molecule moieties into polymeric systems, in particular to study the cyclization of larger linear precursors with complementary bifunctional coupling agents.

Since some of the product does not include the coupling agent, and all of the product is cyclic PDMS, then some of the cyclic product must result from the ring-chain equilibration scheme of Figure 2.1. A time-resolved study was performed using gel permeation chromatography (GPC) to track the formation of cyclic PDMS and general evolution of the product mixture upon deprotonation of α,ω-dihydroxy-PDMS in dilute solution. Figure 2.4 shows the GPC traces of the resin-quenched product mixture at 5 min, 1 hour and 3 hours after addition of 1.5 kg/mol or at 15 min and 25 min after addition of 18 kg/mol linear

precursor to a NaH/THF solution. If the distribution of the cyclic product of the 18 kg/mol linear precursor is pure or mostly pure cycles then generation of large cycles is possible and happens in a much higher relative yield than ever reported before. In general, the products from both molecular weights exhibit an increase in retention time as a function of time after addition, which is due to a reduction in hydrodynamic volume caused by (a) cyclization, or (b) a reduction in molecular weight, or (c) both. As before, to make any substantial conclusion about whether cyclization occurs, these GPC data were complemented with MALDI-ToF, FTIR and NMR spectra.

For the low-molecular-weight precursor (1.5 kg/mol), FTIR and NMR data (in Appendix A) indicate a complete disappearance of silanol end groups at just 5 minutes. This is consistent with a MALDI-ToF mass spectrum of the same sample that shows a distribution of peaks which are separated and evenly divisible by 74 amu (after subtraction of the ionizing species), the mass of the PDMS repeat unit. Lastly, the gravimetric yield of the purified cyclic product collected at 5 min was ~ 78%. Though direct confirmation of topology is impossible, the combined results above indicate a fairly high yield of pure cyclic material. Thus, cyclic PDMS was prepared rapidly in high yield by this base-catalyzed unimolecular ring closure of deprotonated 1.5 kg/mol α,ω-dihydroxy-PDMS in dilute solution and purified with an ion-exchange resin.

The rapid formation of cycles should not be surprising considering that cyclization requires only one of the chain ends of the linear precursor to find its own backbone. This is consistent with the reported timescales of cyclization dynamics from fluorescence studies of intramolecular excimer formation in linear PDMS end-labeled with pyrene groups. For a PDMS chain with M_n = 6.6 kg/mol, the mean cyclization rate constant is ~ 10^6 s^{-1}.[27-29] This

generally increases with decreasing molecular weight and is also higher for chain-end cyclization with interior parts of the same chain. This latter point is important as it is expected the deprotonated PDMS chain ends backbite at interior points of the same chain to produce cycles that are smaller than those that would be prepared by end-to-end coupling. The slight broadening of the GPC peak for the 1.5 kg/mol sample at 5 min reflects the consequent change in the molecular weight distribution. As the reaction proceeds beyond 5 min, the GPC peak continues to broaden and becomes increasingly multimodal, signifying progression of the reactions shown in Figure 2.1 and a general reduction in the average molecular weight of the product. After 3 hours, the main GPC peak for the product derived from the 1.5 kg/mol precursor appears at ~ 26 min, and persists as the main peak even after an 18-hour equilibration period (see Figure 2.3 and 2.4). This retention time corresponds to a ring size of ~ 15 repeat units (~ 1.1 kg/mol), which is an apparently preferred size in this size range as a plot of the molar cyclization constants versus PDMS ring size reveals a local "stability maximum" at D_{15}.

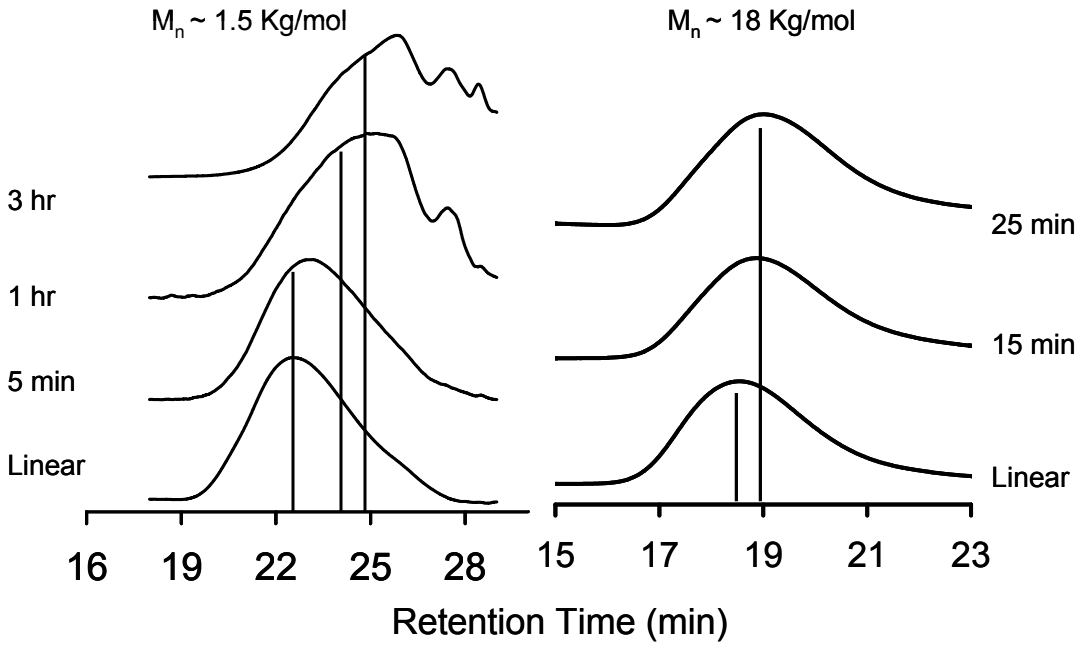

Figure 2.4. GPC traces of α,ω-dihydroxy-PDMS and the product following its deprotonation in dilute solution and quenching with an ion exchange resin to remove charged linear species. The molecular weights at top refer to the linear precursor: M_n ~ 1.5 kg/mol (45-85 cSt) and M_n ~ 18 kg/mol (700-800 cSt). The times refer to the times after addition of the linear precursor to a NaH/THF solution.

MALDI-ToF is a particularly important analytical tool for monitoring the cyclization of larger linear precursors as the reduced concentration of end groups makes it difficult to monitor their disappearance with NMR or FTIR spectroscopy.[30] Also, MALDI-ToF (assuming the spectra can be quantified) is the only common technique that can not only track the changes in molecular weight but also the population of topologies in that molecular weight distribution. This makes it an indispensable tool when trying to understand the kinetics of cyclization. Kricheldorf et al. reported the role of cyclization in kinetically controlled polycondensations involving the polymerization of difunctional monomers under dilute solution conditions. Aided by self-dilution as monomer is consumed during polymerization, high yield of high molecular weight cyclics is promoted at high percent conversion.[16] Montaudo looked at lactide ring-opening polymerization, showing with MALDI-ToF cyclic products in the low-molecular-weight fraction, indicating that ester exchange occurs by intramolecular backbiting reactions (transesterification/ring-chain equilibration).[19] They determined the average degree of polymerization versus percent conversion to cyclic product by using MALDI-ToF for a variety of polymers such as polyesters, polycarbonates, poly(ether sulfone)s and poly(ether ketone)s. Both authors make the point that the original theories of step-growth polymerization formulated by Carothers and Flory severely underestimate the population of cyclic material in polycondensation products, mainly because techniques were not available to readily detect their formation.

Although this is true, the usefulness of MALDI-ToF in this study is rather limited because, MALDI-ToF can under-represent the average molecular weight particularly for polydisperse polymeric systems.[31,32] There is no evidence showing molecular weight discrimination during ionization; instead, this under-representation of the molecular weight is due to an instrumental effect. Basically in a highly polydisperse system the ionized material reaches the detector as a continuous stream with the matrix and low-molecular-weight oligomers having the shortest time of flight eventually causing detector saturation. This skews the molecular weight distribution seen in the spectra towards the low-molecular-weight oligomers and increases the noise especially in the higher-molecular-weight portion of the spectra. The majority of the tested samples in this study have a PDI > 2. Performing fractionation or SEC is a possible route to using MALDI-ToF to probe higher molecular weights; however this was not done here. In addition, for reasons not quite clear, the MALDI ionization process seemed at times to be very inefficient on some of the PDMS samples producing only noise in the spectra even at low molecular weights. The same structural components that impart the excellent stability observed for PDMS also most likely make the soft ionization techniques used in MALDI and FAB difficult. Therefore, only a few MALDI-ToF data sets were ever obtained above ~ 4,000 amu for any of the molecular weights or topologies. Also, mass discrimination effects were never quantified.

In the full spectrum of Figure 2.5, two overlapping polydisperse distributions are observed for the resin-quenched product trapped at 25 min after deprotonation of the 18 kg/mol α,ω-dihydroxy-PDMS. The main peaks in each distribution are separated by 74 amu, the mass of the PDMS repeat unit. The major distribution, which includes the peaks marked (a) and (b) in Figure 2.5, is due to the sodium-cationized cyclic PDMS. The minor

distribution includes the peak marked (c) and is due to sodium-cationized linear PDMS. The minor component peaks, which are rather masked by the noise of the spectra, are due to linear PDMS having a low relative intensity that increases with molecular weight until the intensity of both linear and cyclic material match above 5000 amu. The peaks in the minor component distribution represent linear material of the same number of repeat units as the cycles and therefore are shifted by 18 amu, the increase expected due to the end groups of the linear species. The presence of this minor distribution and the fact that its relative intensity increases with molecular weight suggest the resin may have decreasing effectiveness, as the molecular weight of the charged linear by-product increases. However, as stated previous, quantitative interpretation of a MALDI spectrum is difficult and inconclusive. (Appendix A, Figure A.21-A.22 includes a MALDI-ToF of the methanol quenched 1.5 and 35 kg/mol cyclic product, both spectra obtained in reflectron mode.)

Because MALDI-ToF is utilized in a very similar fashion throughout this dissertation, it seems necessary to comment on the procedure used to perform peak assignments. Starting with the mass at the peak maximum for the signal of interest, the molar mass of the end groups and any probable cationizing agents were subtracted, leaving only the mass of the PDMS. This value was divided by the molar mass of a repeat unit of PDMS, then the value closest to an integer was used to determine the identity of the cationizing agent, the chain topology (whether end groups are present) and the number of PDMS repeat units corresponding to that peak. Part of what made this analysis difficult was the presence of ionic contamination, leading to the cationization of the same species by multiple agents. Even after attempting to remove any ambient salt content with repeated washings and dialysis tubing, some of the MALDI spectra would show peaks cationized by protons,

potassium and sodium. This could possibly cause confusion during analysis as peaks from different cationizing material, topologies and/or molecular weights could overlap. The inset in Figure 2.5 shows a zoomed view of an unresolved isotope multiplet of the sodium cationized cyclic PDMS at 4833 amu. The x-markers represent the simulated isotopic distribution of linear H^+/PDMS with 65 repeat units, where o-markers and □-markers represent the simulated isotopic distribution of cyclic Na^+/PDMS and linear Na^+/PDMS with 65 repeat units. The results of the simulated isotopic distribution confirm the peak at 4833 amu belongs to cyclic Na^+/PDMS. The combined molecular weight summation analysis and isotopic simulation was performed on all MALDI signals of interest to determine and verify peak assignments. (A similar process of peak assignments was performed on methanol-quenched product which was conducted above the overlap concentration, trapped at 5 min after deprotonation of 35 kg/mol α,ω-dihydroxy-PDMS. Again this spectrum was obtained in reflectron mode because the linear mode spectra only showed noise. The increased resolution shows a resolved isotopic multiplet, making the correlation between the simulated and real isotopic distributions very dramatic and worth mentioning/viewing.)

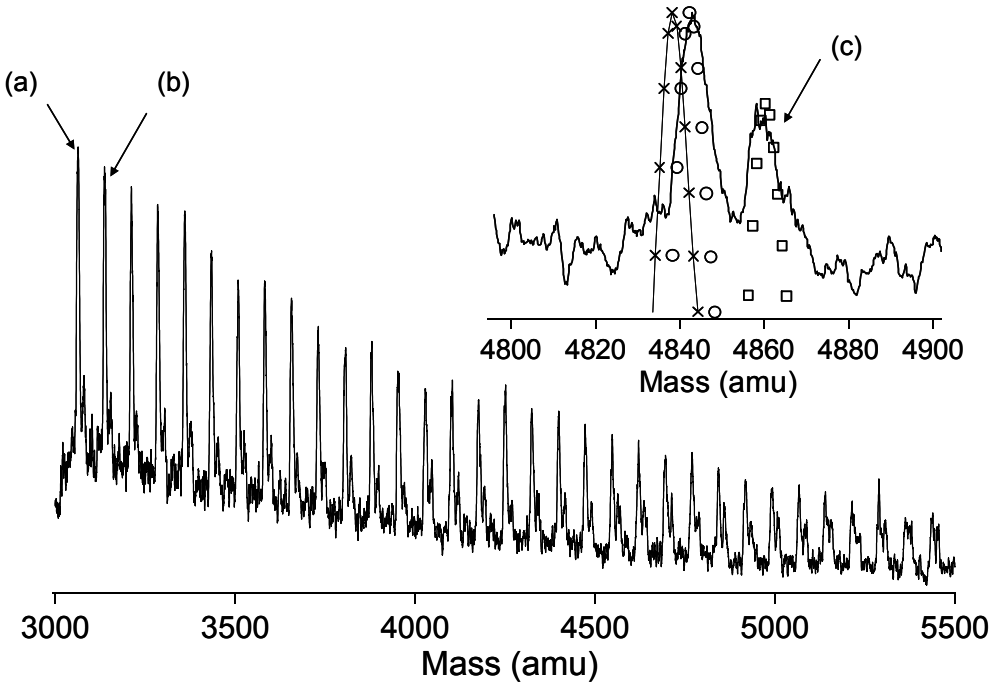

Figure 2.5. MALDI-ToF spectrum of the resin-quenched product trapped at 25 min after deprotonation of α,ω-dihydroxy-PDMS (M_n ~18 kg/mol, 700-800 cSt), obtained in linear mode. (a) 3138 amu = Na^+/cyclic PDMS of 42 repeat units, (b) 3211 amu = Na^+/cyclic PDMS of 43 repeat units and (c) 4851 amu = Na^+/linear PDMS of 65 repeat units. The inset is a zoomed view of the isotope multiplets from the sodium-cationized cyclic PDMS at 3138 amu. The (x) represent the simulated isotopic distribution of linear H^+/PDMS, where (o) represents the simulated isotopic distribution of cyclic Na^+/PDMS and (□) represents the simulated isotopic distribution of linear Na^+/PDMS.

At this point, the 1.5 kg/mol α,ω-dihydroxy-PDMS precursor has been shown explicitly to produce cyclic PDMS in high yield. However, two questions still remain unanswered so far: (1) exactly how are the cycles formed from linear precursors in this intramolecular backbiting process and (2) whether or not we are actually making large cycles from the larger precursors in high yield. The second question is directly related to the fact we have no way via spectroscopy or any other technique so far to ensure the quantity or purity of the cyclic product over 4,000 amu (the only good quality linear mode spectrum of a cyclic product is seen in Figure 2.5). Though it has been shown that the ion-exchange resin

is effective at removing linear byproducts for the 1.5 kg/mol precursor, Figure 2.5 suggests this may not be true for the larger linear material. The first question on the other hand goes to more fundamental issues, and both questions are important to understand this ring-forming process.

To understand how cycles are formed from linear oligomers we again looked at the well documented work reported by Brown and Slusarczuk, where the stability of PDMS cycles during ring-chain equilibration was determined and described by the a molar cyclization constant, K_n, which is dependent on the number of siloxane repeat units. A log-log plot of the molar cyclization constants versus PDMS ring size shows a primarily negative slope as ring size increases. This suggests there is a considerable thermodynamic driving force to form smaller cycles versus large cycles, and that the formation of large cycles is unlikely. However, Brown studied the ring-chain/chain–extension equilibration process of undiluted material from D_4 and D_5 cyclic material, and though the driving forces are the same, the reaction path and subsequent kinetics studied in this chapter are very different. By lowering the reaction concentration below the overlap concentration and using a sufficiently large precursor, we can manipulate the ring-chain equilibrium system to promote intramolecular processes and kinetically trap large cycles. In principle, with detailed knowledge of the intramolecular behavior of a PDMS chain, information about the time evolution of both the molecular weight and topology can be simulated.

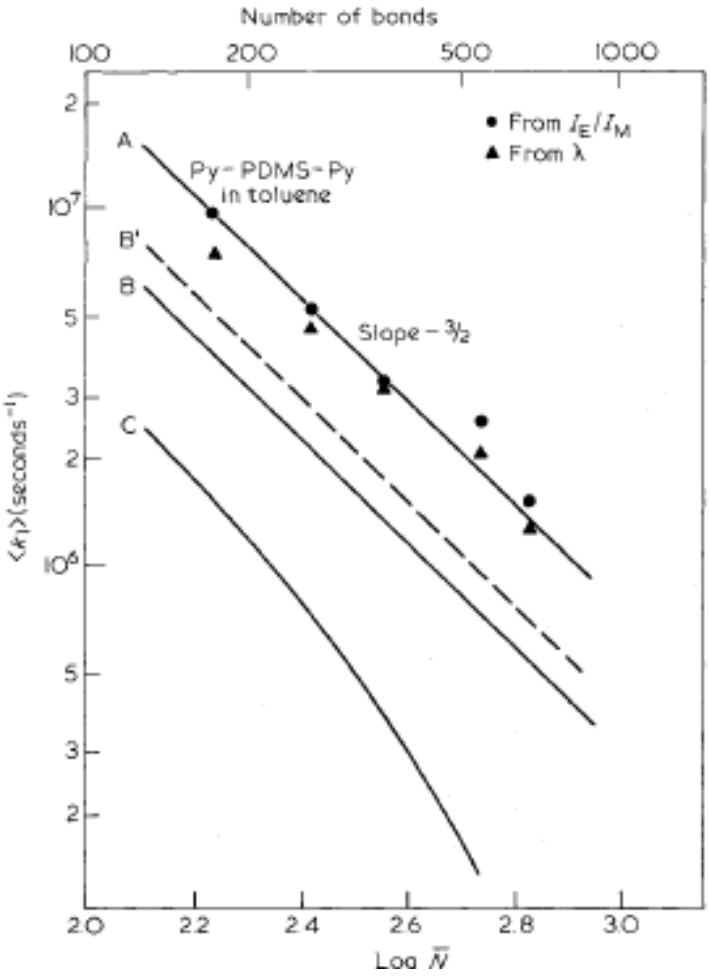

Figure 2.6. The log end-to-end cyclization frequency or rate (sec^{-1}) of a chain with n units is proportional to the log of the ring size formed. These is data from fluorescence decay of (A) PDMS in toluene at 22 °C with an experimental slope of -1.255, (B) PS in cyclohexane at 34.5 °C with an experimental slope of -1.52, (B') is data from B corrected to 22 °C and the viscosity of toluene, and (C) PS in toluene at 22 °C. [Reprinted with permission from Svirskaya, P; Winnik, M. *Polymer.* **1983**, 24, 319. Copyright © 1983 Published by Elsevier Ltd.]

Based on mean end-to-end cyclization rate data from the same fluorescence studies of intramolecular excimer formation in linear PDMS end-labeled with pyrene groups mentioned previously, an expression relating the number of PDMS repeat units and the cyclization rate is reported in Eq. 2.5:

$$\log\langle g_n \rangle = -1.25\log(n) + 9.54 \qquad \text{Eq. 2.5}$$

where g_n represents the end-to-end cyclization frequency or rate (sec^{-1}) of a chain with n units and is from data in Figure 2.6 (-1.25 is the slope of the log end-to-end cyclization frequency versus the log of the ring size).

A Monte Carlo (MC) simulation is a method of iteratively evaluating a model using sets of randomly generated values as inputs to the model parameters. This type of simulation is often used to solve models which are complex, nonlinear, or involve several undetermined parameters. A kinetic MC simulation is intended to determine the time evolution of the parameters in a model. In this case the deprotonated silanol end groups can react with any repeat unit along its chain, and to simplify the system for the kinetic MC simulation we just regard intramolecular interactions and consider only one end group of a chain backbiting as a cyclization event. Basically the simulation creates a distribution of linear chains of N population size by applying a Gaussian molecular weight distribution based on a user-defined number-average molecular weight and PDI as given in these expressions:

$$\sigma = M_n * (PDI - 1)^{1/2} \qquad \text{Eq. 2.6}$$

and

$$N_i = \frac{1}{\sigma\sqrt{2\pi}} * \exp\left(-\left[\frac{(i * 74 + 18) - M_n}{2\sigma} \right]^2 \right) \qquad \text{Eq. 2.7}$$

where N_i equals the number of chains in the distribution of i repeat units. A weighted random number generator is used, where the frequency of generating a number, r, more specifically producing a cycle with r units from a chain with n repeat units follows the function, $\delta(r)$. A probability function, P(r) can also be defined, in which the function describes the probability of producing a cycle with r units from a chain with n repeat units where the integral of the probability function is one. Using P(r), the simulation can

determine where along the backbone of a linear chain (with n repeat units) to backbite, which depends on the ratio of the end-to-end cyclization frequency or rate constants between D_n and D_r, as described in Eq. 2.8,

$$\delta(r) = \frac{g_r}{g_n}, \text{ n and } r \geq 4 \qquad \text{Eq. 2.8}$$

and

$$\frac{\delta(r)}{\int_4^n \delta(n)dn} = P(r) \qquad \text{Eq. 2.9}$$

The simulation then can perform a single cyclization event or iteration for the entire population of linear chains (see Appendix A, Programs A.1-A.3 for the Matlab code). The program keeps track of the resulting linear and cyclic distribution; therefore, it is possible to perform multiple cyclization iterations, approximating the kinetic behavior of base-catalyzed depolymerization of PDMS oligomers during ring-chain equilibration in dilute solution. The program produces simulated cyclic distributions in which the x-axis represents the molecular weight of the cyclic species and the y-axis reflects either N_i, the number of cyclic molecules or N_iM_i, the number of repeat units in the cyclic molecules of that molecular weight as illustrated in Figure 2.7.

Eq. 2.10 can be used to convert number-average molecular weight, M_n, to hydrodynamic volume, V_H, where K and α are Mark-Houwink constants for linear PDMS in the case of the precursor and for cyclic PDMS in the case of the cyclic product.[24] The theoretical retention time (RT) shifts or the difference in the RT for the linear precursor and cyclic product were then calculated by solving the cubic in Eq. 2.11 for the simulated linear precursor and cyclic product M_n:

$$V_H = KM_n^{(1+\alpha)} \quad \text{Eq. 2.10}$$

and

$$\log(V_H) = a_1 + a_2(RT) + a_3(RT)^2 + a_4(RT)^3 \quad \text{Eq. 2.11}$$

where a_1, a_2, a_3 and a_4 are constants used in the third-order polynomial of the actual universal calibration curve used to determine molecular weight on the GPC.

Winnik's work on cyclization kinetics describes cyclization as a diffusion-controlled intramolecular rate process (as opposed to rate kinetics dominated by transition states and activation energies). The cyclization rate of a linear chain is strongly affected by the short-time behavior of its segmental motion. Therefore the cyclization rate is dependent on three factors: (1) solvent viscosity, (2) chain stiffness and (3) chain hydrodynamic volume,[27,28] and the slope of the cyclization rate versus number of repeat units is determined by how those factors scale with molecular weight. This provides a route, though not investigated in this chapter to modify the slope of the end-to-end cyclization rate versus molecular weight by adjusting the temperature and/or solvent quality. This can be observed in Figure 2.6, as the second derivative of the PS in toluene curve (C) is clearly non-zero unlike the (corrected to 22 °C and the viscosity of toluene) PS in cyclohexane curve (B'). Approximately at the point where the curve C turns downward there is an order of magnitude crossover in hydrodynamic volume for PS in toluene versus cyclohexane. Large PS chains are much larger in toluene than in cyclohexane, which accounts for the relative increase in the cyclization frequency slope and consequently cyclization frequency of the large PS chains in cyclohexane.

Table 2.1. Simulation of the cyclization of linear PDMS with M_n ~ 15 kg/mol and a PDI ~ 1.3 (simulating the 18 kg/mol precursor) done over multiple cyclization iterations, N = 28,000 chains. The table list simulated results of the molecular weight and % yield for cyclic material.

	Linear		Cyclic				
Cyclization Iterations	M_n (g/mol)	PDI	M_n (g/mol)	PDI	%Yield [i]	%Yield n>12	Theoretical RT Shift (min)
1	11400	1.37	3000	2.52	18	17	-
2	9600	1.48	2800	2.54	32	30	-
3	8000	1.60	2700	2.53	46	42	-
5	5700	1.83	2400	2.56	65	59	2.14
10	2500	2.68	2200	2.60	88	79	2.22
20	400	2.75	2000	2.63	94	83	2.25
50	-	-	2000	2.63	94	83	-

Table 2.1 lists the results of cyclization iterations for linear and cyclic material and the percent cyclic yield of a simulated reaction of the 18 kg/mol precursor. Using the number-average molecular weight of the linear precursor and the resulting simulated cyclic material, the theoretical GPC retention time shift was calculated by applying the same universal GPC calibration curve used to determine the molecular weights of the precursors. Therefore, the theoretical retention time shift should not only account for the reduction in molecular weight during ring-chain equilibration as described in Table 2.1, but also the reduction in hydrodynamic volume due to cyclization. Also, note the percent yields for large threadable rings are much higher than the cited yields given by Dodgson and Semlyen on the base-catalyzed equilibration of $[(CH_3)_2SiO]_4$ and $[(CH_3)_2SiO]_5$ oligomers in toluene.

[i] Theoretical yield based on recoverable material after drying in vacuum at 100 mtorr, cyclic n>5 and linear n>6.

Simulations on other precursors were also performed and are depicted in Appendix A, Figures A.23-A.25.

GPC data of the 18 kg/mol precursor and resin-quenched cyclic product at 2 min of the same precursor showed an experimental retention time shift of 2.13 min, matching well within some small error of the theoretical retention time shifts in Table 2.1. Also, the experimental gravimetric yield of the resin-quenched cyclic product at 2 min of the 18 kg/mol precursor was ~ 87%, again matching the results of the simulation.

The experimental data not only validates the simulation but also its close agreement with the simulated results indicate that the cyclic material is produced as prescribed by Eq. 2.5. Also, through this an idea of how large cycles are made can be developed. Though the formation of smaller cycles is favored, the amount of material extracted from the linear feed source is comparatively small. Conversely, though the tendency to form larger cycles is smaller, the impact on the cyclic distribution is much more weighted, essentially as long as the larger cycles form above some minimum rate threshold there will be a considerable amount of the overall quantity of repeat units from the linear feed stock in the cyclic distribution represented by medium to large cycles (n>12). Unfortunately, as a consequence the distribution of cyclic material will be fairly broad, making isolation of any given large ring size or narrow fraction of large ring sizes challenging.

Figure 2.7 (a) and (b) display the effect of linear precursor molecular weight and relative cyclization rate on the cyclic product resulting from backbiting of PDMS. As illustrated in Figure 2.7 (a), the general shape of the resulting cyclic populations are similar no matter the molecular weight of the precursor, essentially the relative amount of any particular ring size is constant. This makes sense considering the slope of cyclization rate

does not depend on the linear precursor. The only difference is the relative amount of repeat-unit feed stock. Viewed as a mass balance, larger precursors have a higher concentration not only of repeat units but also repeat units that can be depolymerized into large cycles (e.g. $MD_{10}M$ can not form D_{20} by intramolecular processes only). Therefore, depolymerization of large precursors can produce a greater number of large cycles, as ascribed by the cyclization rate slope. This is what makes the overall gravimetric cyclic yield and number-average molecular weight increase. More interestingly, Figure 2.7 (b) shows the cyclic product distributions with different cyclization rate constant slopes. As the slope approaches zero the distribution flattens and the relative amount of large cycles increases. Again by manipulating the system to reduce this slope one could increase the relative amount of large cycles generated.

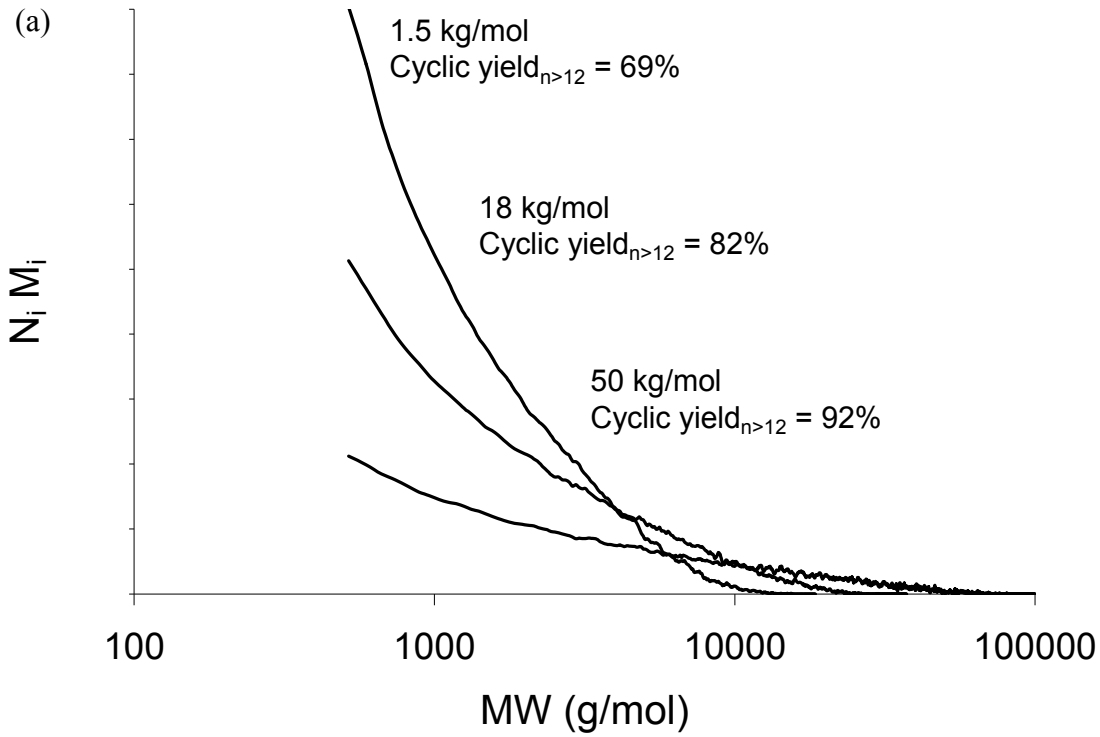

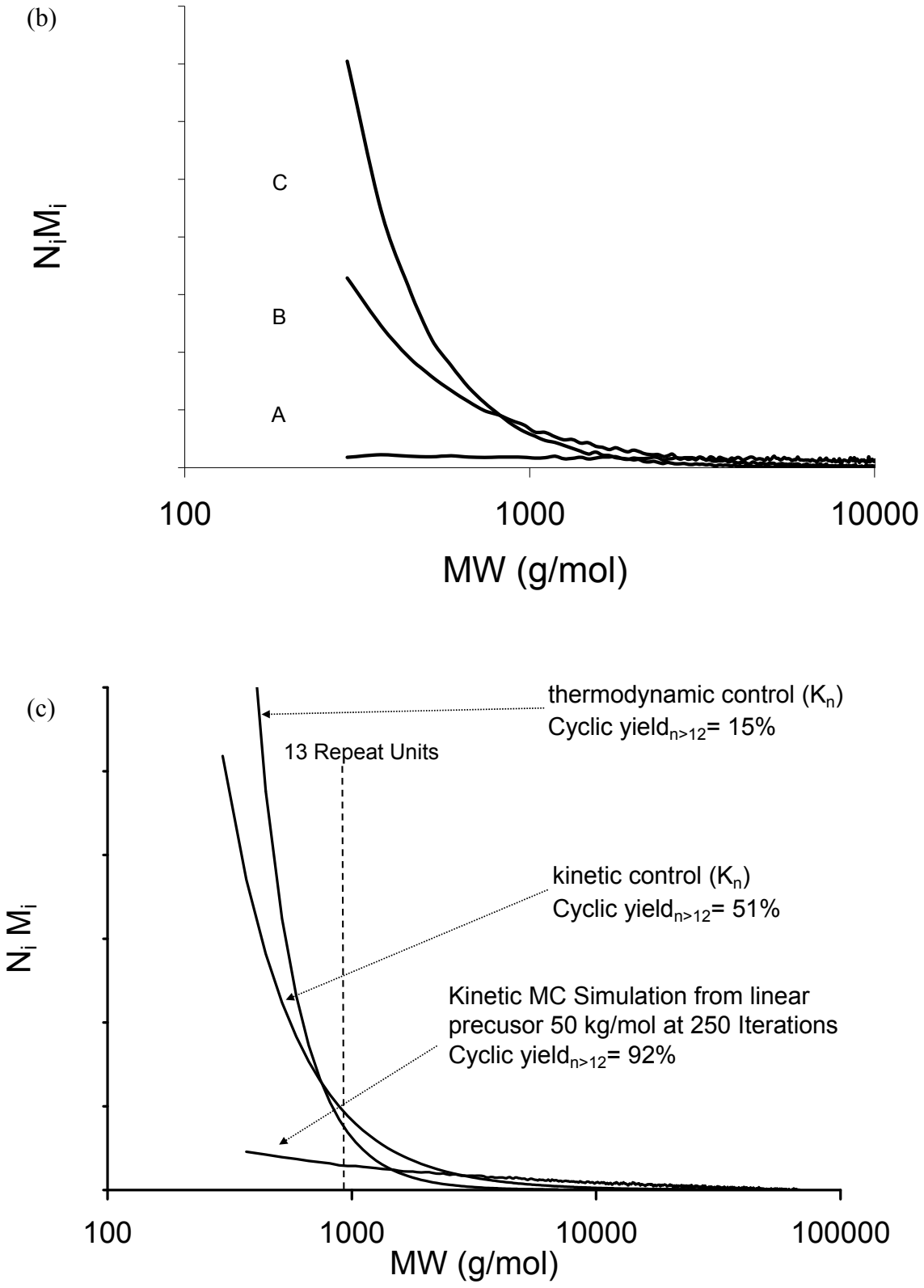

Figure 2.7. Simulated cyclic distributions of cyclic product from linear precursors: (a) after 250 cyclization iterations of material based the 1.5

kg/mol, 18 kg/mol, and 50 kg/mol, (b) after 3 cyclization iterations of 18 kg/mol with different cyclization rate constant slopes, where slope/slope$_{PDMS}$ = (A) .02, (B) 1.26 and (C) 2.38 and (c) based on K_n determined from theoretical values determined for thermodynamic and kinetically controlled ring-chain equilibration. [slope$_{PDMS}$ = -1.25] All curves in Figure 2.7 were normalized by the area of the N_iM_i curve.

Ring-chain equilibration and polycondensation reactions are considered either kinetically or thermodynamically controlled. In a thermodynamically controlled system, the equilibrium reactions which produce a linear and cyclic product distribution are defined by the energetic minimum of the system at any percent conversion. The system discussed in the introduction, studied by Brown and Slusarczuk, is the quintessential example of a thermodynamically controlled ring-chain equilibration. Experimentally it was found that log of K_n scales with the number of repeat units to the -2.86 power.[8] Jacobson and Stockmayer calculated theoretical values for thermodynamically controlled K_n based upon Gaussian chain statistics and determined a characteristic relationship, where log K_n scales with the number of repeat units to the -2.5 power.[2,3,33,34] In kinetically controlled systems (in most cases intended to produce cyclic polymer) the reaction conditions are such that the equilibrium reactions are absent and the product formed does not represent the energetic minimum of the system but rather reflects the rate of the various possible reactions in the system. Ignoring thermodynamic interactions within the chains (long-range intramolecular interactions) others have calculated the log of K_n scales with the number of repeat units to the -1.5 power for kinetically controlled polymerization.[33,34] Figure 2.7 (c) shows the simulated cyclic product distribution for depolymerization of a 50 kg/mol PDMS precursor and theoretical equilibrium cyclic product distributions generated from calculated K_n values based upon the characteristic exponents describing a kinetically or thermodynamically controlled system.

The plot clearly shows depolymerization of PDMS provides the route to large cyclic material with the highest yield.

Even with the simulated molecular weight and topological results, there still is a considerable need for a method capable of tracking the ring-chain mixture of large precursors. All of the analytical methods described above suffer from some limitations with respect to sensitivity and/or usefulness. Other than topology the primary difference between cyclic and linear polymers is the presence of end groups; however, the end group concentration is particularly low for larger precursors. It is fairly common in multidimensional NMR experiments for a portion of the molecule to be selectively labeled to resolve overlapping signals in a NMR spectrum. Trichloroacetyl isocyanate has been used for *in-situ* derivatization of protic polymer end groups. The protic end groups are converted to imidic functionalities resulting in a proton signal at ~ 7.5-11 ppm.[35] For the purposes of this study, the labeling moiety should react with the end group fairly easily and quantitatively, and would not only be used to resolve the end group signal by changing the chemical shift but also to amplify the signal by using a group that contains multiple protons. Though this solution may provide information about percent cyclic yield, it still can not prodive information about the molecular weight distribution of the cyclic or linear material. However, there are several other references that describe labeling polymers with chromophores that yield fluorescent, radioactive or ultraviolet (UV) activity, which can be tracked with various chromatographic detectors.[36-38]

This method has been applied in our present work on cyclic PDMS. Instead of quenching the terminal silanolate groups in the reaction mixture with the ion-exchange resin or methanol, 1-naphthyl isocyanate (NI) is used as outlined in Scheme 2.1. This makes the

linear material UV active (molar absorptivity, $\alpha_{PDMS} \approx 0 << \alpha_{NI}$), and using a UV-Vis and refractive index (RI) detector in series on a GPC we developed a fairly effective method to track the molecular weight and topology of the ring-chain mixture for large precursors.

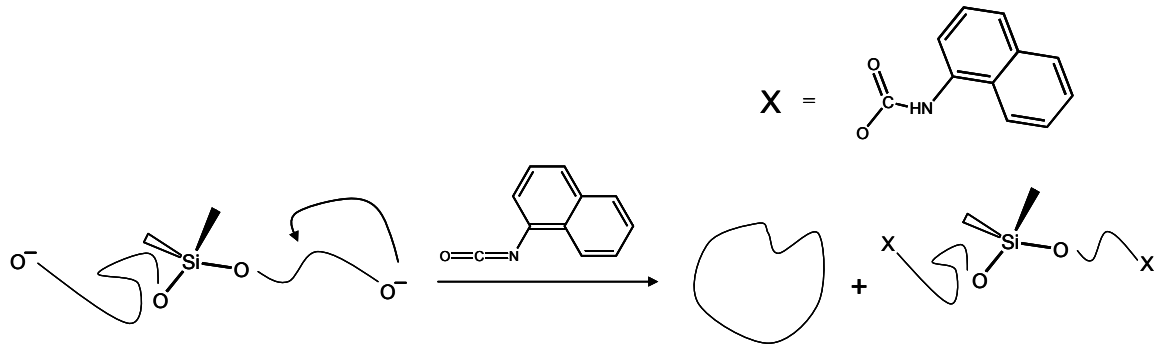

Scheme 2.1. Ring-chain equilibration of a linear PDMS precursor followed by quenching with 1-naphthyl isocyanate.

Let us first consider the empirical relationships that relate the for a RI detector:

$$I_{i\_RI} = \frac{RI_{Cal}}{n_o} * \frac{dn}{dc} * C_i^{RU} = k_{RI} * N_{i_{L+C}} * M_{i_{L+C}} \qquad \text{Eq. 2.12}$$

The resulting intensity described by Eq. 2.12 represents the signal from the molecular weight distributions of both the cyclic and linear material, where I_{i_RI} is the resulting intensity from the RI detector at retention time i, C_i^{RU}= concentration of the repeat units from cyclic and linear material in g/vol eluting from the column at time i, RI_{Cal} is the detector calibration constant, n_o is the refractive index of the pure solvent and dn/dc represents the refractive index increment of the polymer analyte. The equation can then be simplified by integrating the above constants and the volume term in the concentration into a single constant, k_{RI}. The resulting mass of analyte (repeat units) observed by the detector is divided into the number of chains and cycles N_{iL+C} and their molecular weight M_{iL+C}. Again, let us first consider the empirical relationships that relate the for a UV-Vis detector:

$$I_{i\_UV} = \alpha * \ell * C_i^{EG} = k_{UV} * N_{i_L} \qquad \text{Eq. 2.13}$$

On the other hand, Eq. 2.13 represents the signal from the molecular weight distributions of only linear material, where I_{i_UV} is the resulting intensity from the UV-Vis detector at retention time I, C_i^{EG} = concentration of the number of labeled end groups in mol/vol, ℓ represents the path length and α is the molar absorptivity of the NI end group. This equation also can be simplified by combining the α, ℓ and the volume term into a constant, denoted by k_{UV}. This leaves a term corresponding to moles of end groups, which is easily converted to N_{i_L}, the number of linear chains. Once the number and molecular weight of the linear and combined populations versus retention time can be determined, a simple calculation for percent cyclic yield is possible. (The full calculation can be found in Appendix A.) Even more powerful, once the increase in hydrodynamic volume due to the labeled end groups is quantified, subtracting the UV and RI chromatographs can provide a route to deconvolute the cyclic and linear molecular weight distributions (this can not be done by any other technique other than MALDI, which has its limitations as discussed previously).

Using NMR of a 1.5 kg/mol cyclic product mixture, the ratio of labeled end groups to repeat units of PDMS was determined for the mixture of PDMS cycles and linear chains terminated with the naphthalene end groups (NMR is very effective tool to analyze low-molecular-weight precursor cyclic products). This same mixture was run using the dual detector (RI and UV-Vis) GPC setup. The observed integrated intensities from both detectors and the percent of cycles as determined by NMR were used to calculate a

calibration to relate the intensities of the two detectors, solving for k_{RI} and k_{UV}. The 18 kg/mol precursor naphthyl isocyanate-quenched product at 2 min was run using the dual detector GPC setup. It was then determined that the reaction product of a naphthyl isocyanate-quenched 18 kg/mol precursor at 2 min was at least 71% cyclic yield, which is within a ± 20% deviation of the percent cyclic yield from both resin-quenched experiments (87% gravimetric yield) and the simulations (83% cyclic yield by simulation). Figure 2.8 shows the UV signal of the linear precursor, which was subtracted from the overall integration of the quenched linear by-product as seen in Figure 2.8, and determined to be negligible.

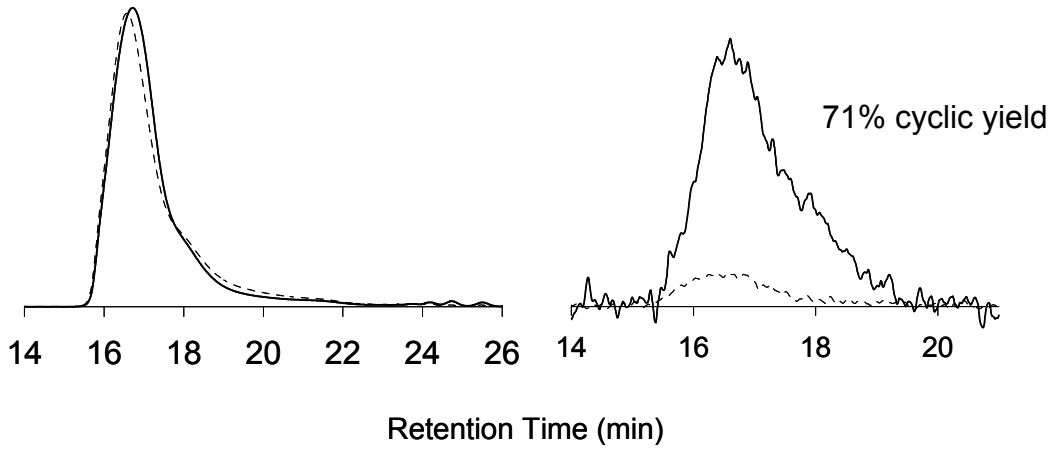

Figure 2.8. Ring-chain equilibration of 18 kg/mol, quenched with an excess 1-naphthyl isocyanate in dilute-solution route to cyclic PDMS. GPC traces for linear precursor (dotted lines) and cyclic product (solid lines), where the refractive index signal (on the left) and UV absorption signal (on the right) are shown.

2.5 Conclusions

Cyclic PDMS has been prepared by kinetically controlled cyclodepolymerization of linear α,ω-dihydroxy-PDMS in dilute solution. This is a base-catalyzed depolymerization of PDMS into cyclic products. In this kinetically controlled cyclodepolymerization route, cyclization competes with ring opening and some minor chain extension. A coupling agent is not needed to generate ring structures. Using a kinetic Monte Carlo simulation, the sequence of events leading to cyclic product was determined. As part of the investigation into how the linear material is consumed and cyclic material is formed, a novel method of analyzing GPC data to determine the cyclic and linear distributions of a mixture of topologies was developed. Ultimately it was determined that large cycles could be made; however as a consequence of the depolymerization the relative amount of large cycles never changes. The cyclic product will always be a large distribution of ring sizes and isolating any particular fraction of rings will again require exhaustive effort. But when compared to the relative percent yields extracted from equilibrates formed by polymerizing D_4, yields of larger rings is much higher when cycles are generated from depolymerization of linear precursors. If the goal is to generate a large fraction of ring ($n \geq 12$), for example for threading, the kinetically controlled cyclodepolymerization of larger linear precursors may be the method of choice.

2.6 References

1. Scott, D.; *J. Am. Chem. Soc.* **1946**, *68*, 2294.
2. Semlyen, J., *Cyclic Polymers*. Elsevier: New York, 1986.
3. Semlyen, J., *Large Ring Molecules*. Wiley: New York, 1996.
4. Wilcock, D.; *J. Am. Chem. Soc.* **1946**, *68*, (4), 691-696.

5. Flory, P., *Principles of Polymer Chemistry*. Cornell University Press: Ithaca, New York, 1953.

6. Flory, P.; Semlyen, J.; *J. Am. Chem. Soc.* **1966**, *1*, 8814.

7. Carothers, W.; *J. Am. Chem. Soc.* **1929**, *31*, 2548.

8. Brown, J.; Slusarczuk, G.; *J. Am. Chem. Soc.* **1965**, *87*, 931.

9. Carmichael, J.; Gordon, D.; Isackman, F.; *J. Phys. Chem.* **1967**, *71*, 2011.

10. Carmichael, J.; Winger, R.; *J. Polym. Sci.: Part A, Gen. Pap.* **1965**, *3*, 971-984.

11. Jacobson, H.; Stockmayer, W.; *J. Chem. Phys.* **1950**, *18*, 1600.

12. Wilczek, L.; Chojnowski, J.; *Makromol. Chem. 184, 77-90 (1983)* **1983**, *184*, 77-90.

13. Wilczek, L.; Chojnowski, J.; *Makromol. Chem.* **1986**, *181*, 39-51.

14. Clarson, S.; Semlyen, J.; *Polymer* **1986**, *27*, 91.

15. Crivello, J.; Lee, J.; *Chemistry of Materials* **1989**, *1*, (4), 445-451.

16. Kricheldorf, H.; Schwarz, G.; *Macromol. Rapid Commun.* **2003**, *24*, (5/6), 359-381.

17. Kricheldorf, H.; Bohme, S.; Schwarz, G.; *Macromolecules* **2001**, *34*, 8879-8885.

18. Kricheldorf, H.; Rabenstein, M.; Schmidt, M.; *Macromolecules* **2001**, *34*, 713-722.

19. Montaudo, G.; Montaudo, M.; Wisniewski, M.; *Macromolecules* **1996**, *29*, 6461-6465.

20. Dodgson, K.; Sympson, D.; Semlyen, J.; *Polymer* **1978**, *19*, 1285.

21. White, B. Rotaxanated Polymers: I. Synthesis and Purification of Cyclic Polydimethylsiloxane II. Synthesis of Poly[(octene-pseudorotaxa-(α-cyclodextrin)]. Doctoral Thesis, Georgia Institute of Technology, Atlanta, 2004.

22. White, B.; Watson, W.; Beckham, H.; *Macromolecules* **2002**, *35*, 5345-5348.

23. Gotz, H.; Maschke, U.; Ewen, B.; *Macromol. Chem. Phys.* **2000**, *201*, (12), 1311-1316.

24. Dodgson, K.; Semlyen, J.; *Polymer* **1977**, *18*, 1265.

25. Zhao, T. NMR Pulse Sequence Development and Studies of Threaded Macromolecules. Doctoral Thesis, Atlanta, 2004.

26. Zhao, T.; Beckham, H.; *Macromolecules* **2003**, *36*, 9859-9865.

27. Winnik, M.; *Ace. Chem. Res.* **1985**, *18*, 73-79.

28. Winnik, M.; Redpath, T.; *Macromolecules* **1980**, *13*, 328-335.

29. Svirskaya, P.; Danhelka, J.; Winnik, M.; *Polymer* **1983**, *24*, 319.

30. Montaudo, G.; Montaudo, M.; Samperi, F.; *Prog. Polym. Sci.* **2006**, *31*, 277-357.

31. Axelsson, J.; Scrivener, E.; Derrick, P.; *Macromolecules* **1996**, *29*, 8875-8882.

32. McEwen, C.; Jackson, C.; Larsen, B.; *International Journal of Mass Spectrometry and Ion Processes* **1997**, *160*, 387-394.

33. Chojnowski, J.; *Journal of Inorganic and Organometallic Polymers* **1991**, *1*, (3), 29-54.

34. Chojnowski, J.; Kowalski, J.; *Makromol. Chem.* **1997**, *178*, 1351-1366.

35. Postma, A.; Davis, T.; O'Shea, M.; *Polymer* **2006**, *47*, 1899-1911.

36. Caldkrara, F.; Hruska, Z.; Winnik, M.; *Makromol. Chem.* **1993**, *194*, 1411-1420.

37. DeAngelis, P.; *Analytical Biochemistry* **2000**, *284*, 167-169.

38. Goodman, C.; Roof, A.; Weigley, M.; *J. Polym. Sci.: Part A, Polym. Chem.* **2005**, *43*, (12), 2657-2665.

39. Oth, J., Desreux, V.; *Bull. Soc. Chim. Belges* **1954**, *63*, 285.

40. Liu, X.; Maziarz, E.; Lai, Y.; *International Journal of Mass Spectrometry* **2004**, *238*, 227-233.

CHAPTER 3

Preparation of Cyclic Poly(dimethylsiloxane) via Bimolecular Dehydrocoupling of Telechelic α,ω-Linear Precursors

3.1 Abstract

Cyclic poly(dimethylsiloxane) (PDMS) was prepared from commercially available telechelic linear α,ω-dihydroxy-PDMS in a platinum catalyzed bimolecular dehydrocoupling ring-closing reaction with a telechelic linear α,ω-dihydrido-PDMS. As opposed to the cyclic product formed during ring-chain equilibration of a linear precursor, we have gained control over the spread and center of the final molecular weight distribution of the cyclic product. This is clearly reflected in the number average molecular weight and PDI data generated from GPC of the cyclic products resulting from kinetically controlled ring-chain depolymerization and dehydrocoupling ring-closure of the 18 kg/mol α,ω-dihydroxy-PDMS linear precursor (PDI ~ 2.6). The M_n and PDI of the cyclic product for the dehydrocoupling ring-closure is approximately the same as the linear precursor, whereas the M_n for the cyclic product resulting from ring-chain depolymerization decreases by more than half and the PDI increases to approximately 4.5. Purification of the cyclic PDMS was achieved by removing linear byproducts by inclusion complexation with γ-cyclodextrin (CD), although I also found that γ-CD is not effective at sequestering linear PDMS chains over ~ 5 kg/mol. All yields of pure cyclic PDMS were greater than 60 %.

3.2. Introduction

The synthesis of large ring polymers is currently of great interest as mentioned in previous chapters. Cyclic polymers in general are been synthesized using one of three methods[1,2]; however, these methods have major limitations, mainly: restriction to low molar masses and a failure of most methods to effectively separate the linear by-product. These limitations can be overcome by a method involving kinetically trapping the ring polymers resulting from ring-chain equilibration of a linear α,ω-hydroxy-PDMS in dilute solution and purifying the crude product with an ion-exchange resin.[3,4] Dilute solution conditions are critical to ring closure because the condition promotes intramolecular processes.[1,2]

In the previous chapter, I employed a cyclization scheme following Jacobson-Stockmayer predictions where base-catalyzed nucleophilic attack between silanolate end groups on linear PDMS with the repeat units along the backbone causes cyclization.[1,2,5] This process is referred to as ring-chain equilibration, which is a fairly predictable process, but as it turns out also difficult to control because of the speed of the reaction, lack of adjustable reaction parameters and the overwhelming thermodynamic potential to form small cycles. However it was determined that it was possible to form large rings and get high cyclic yields, although as a consequence of the depolymerization of the linear precursors during ring-chain equilibration the relative amount of any large ring size in the distribution is small. The cyclic product will always be a large distribution of ring sizes and isolating any particular fraction of rings will require exhaustive effort. However if your goal is to have a minimal ring size, i.e. for threading, the percent yields can be quite high. For example, kinetically controlled depolymerization of ~ 18 kg/mol

linear PDMS precursor can lead to a cyclic product containing upwards to 80 % threadable cycles (n>12).

Deprotonation of α,ω-dihydroxy-PDMS leads to silanolate chain ends that can backbite at different positions along the chain to give rings of various sizes. Adding a large excess of dichloro-coupling agent to the reaction mixture can mitigate this broadening of the molecular weight distribution. To avoid backbiting altogether, the silanolate intermediates must be avoided. An alternative to cyclization via ring-chain equilibration is cyclization by either ring expansion by bond insertion or ring closure of end-functionalized linear precursors under conditions of high dilution.[1,2,6] The main advantage being the synthesis of extremely high and/or narrow molecular weight distributions. In this chapter I report the novel synthesis of cyclic PDMS according to Scheme 3.1. This scheme seems advantageous because unlike cycles formed during ring-chain equilibration the molecular weight distribution of the linear precursor is preserved. In fact, we show that ring-closure via a Pt-catalyzed dehydrocoupling of linear α,ω-dihydroxy-PDMS and α,ω-dihydrido-PDMS is a valuable high-yield route to cyclic PDMS where the molecular weight distribution of the cyclic product indicates the presence of large cycles with a PDI similar to the linear precursor.

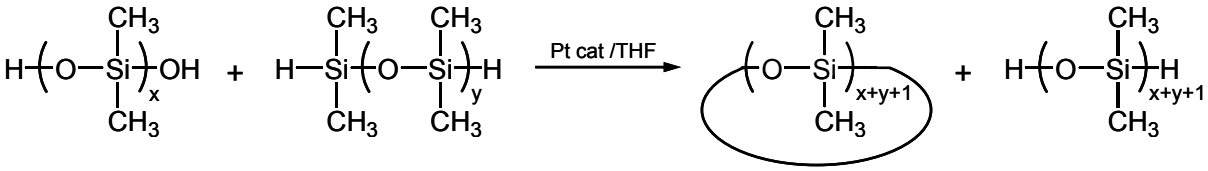

Scheme 3.1. Pt-catalyzed dehydrocoupling of linear α,ω-dihydroxy-PDMS and α,ω-dihydrido-PDMS in dilute solution leads to cyclic PDMS.

Various cyclic polystyrenes architectures (i.e. cycles and cycles with branches) were prepared using a combination of living anionic polymerization and coupling via small molecule difunctional agents. There are a series of studies that primarily focus on telechelic dihalogeno- or diethylenic compounds that utilize the dianionic ends of a living polystyrene chain.[7-10] Not only cyclic polystyrenes but also poly(2-vinylpyridine)s, polydienes, and other various copolymers have been prepared by this method.[11,12]

However, in step-growth material that performs ring-chain equilibration, like PDMS, the use of a coupling agent to cause ring closure at the end groups of a linear precursor will only lead to a minor component of the cyclic product. To avoid the silanolate intermediates and ring-chain equilibration altogether, I then decided to attempt cyclization through a non-nucleophilic coupling reaction. Organic chemistry is ripe with a catalog of non-nucleophilic coupling reactions. Ring closure by ester, amide, C-C bond or C=C bond formation could be achieved by a number of activating or coupling agents. Although, the complementary terminal groups necessary for many of these reactions are not commonly found end groups requiring additional modification to the linear precursor, particularly in the case of commercially purchased material. In many of these reactions a catalyst is needed, often toxic, that requires additional effort to remove.

With the development of ruthenium-based olefin metathesis catalysts, interest in the synthesis of medium and large rings using ring-closing olefin metathesis has grown within this decade. This C=C bond formation route has been shown to be highly efficient at producing large rings in high yield and purity with an astonishing tolerance for a variety of functional groups.[13] Another commonly cited macrocyclic coupling reaction is

based on the Glaser or Hay coupling. A variety of small unsaturated macrocycles were prepared using copper(II) salt oxidization in methanolic pyridine.[14]

Another consequence of avoiding the formation of silanolate end groups during cyclization is the ionic exchange resin is no longer an effective route to remove linear by-product. Traditionally purification schemes, though tedious and time consuming, using fractionation and preparative gel permeation chromatography have been used for isolating narrow fractions of cyclic polymers. More recently, liquid chromatography at the critical condition (LCCC) has been used in successful fractionation of cyclic polystyrenes from their linear counterparts. This is done by adjusting the temperature, solvent and stationary phase so that a critical condition is formed, where analyte retention on the stationary phase not only depends on entropic size exclusion as in traditional GPC but also enthalpic interactions with the linear polymer end groups.[7,15-17] In practice however factors such as low molecular weights, large polydispersities, and different end group functionality make preparative LCCC difficult.

There are numerous examples of using cyclodextrins to separate, sequester and purify small molecules based on structural characteristics like branching or topology.[18] Cyclodextrin (CD) is part of a family of cyclic oligosaccharides. The Greek letter assigned as a prefix indicates the number of glucose residues in the ring, which produce a rigid well-defined cavity. In the case of α-CD there are six glucose residues making a cavity size of ~ 4.5 Å, while the β and γ forms have 7 and 8 residues and form cavity sizes of ~ 7.0 and 8.5 Å, respectively.[19] The structure seen in Figure 3.1, produces what could be considered a truncated cone where the two ends of the structure are not identical. One end is wider and bears the secondary C_2 and C_3 hydroxyl groups, while

the narrower end contains the primary C_6 hydroxyl group. The ring structure of CDs results in a hydrophobic interior cavity, which promotes linear chain threading. This enthalpic directed threading is also referred to as the formation of polymeric inclusion complexes, in which one host component (CD) forms a cavity or channel in which another chemical species (polymeric chain) is located. There are no covalent bonds between the guest and host components; however, secondary bonding such as hydrogen bonding and polar-apolar interactions cause attraction and spontaneous threading, enclosing the guest molecule.[19-21]

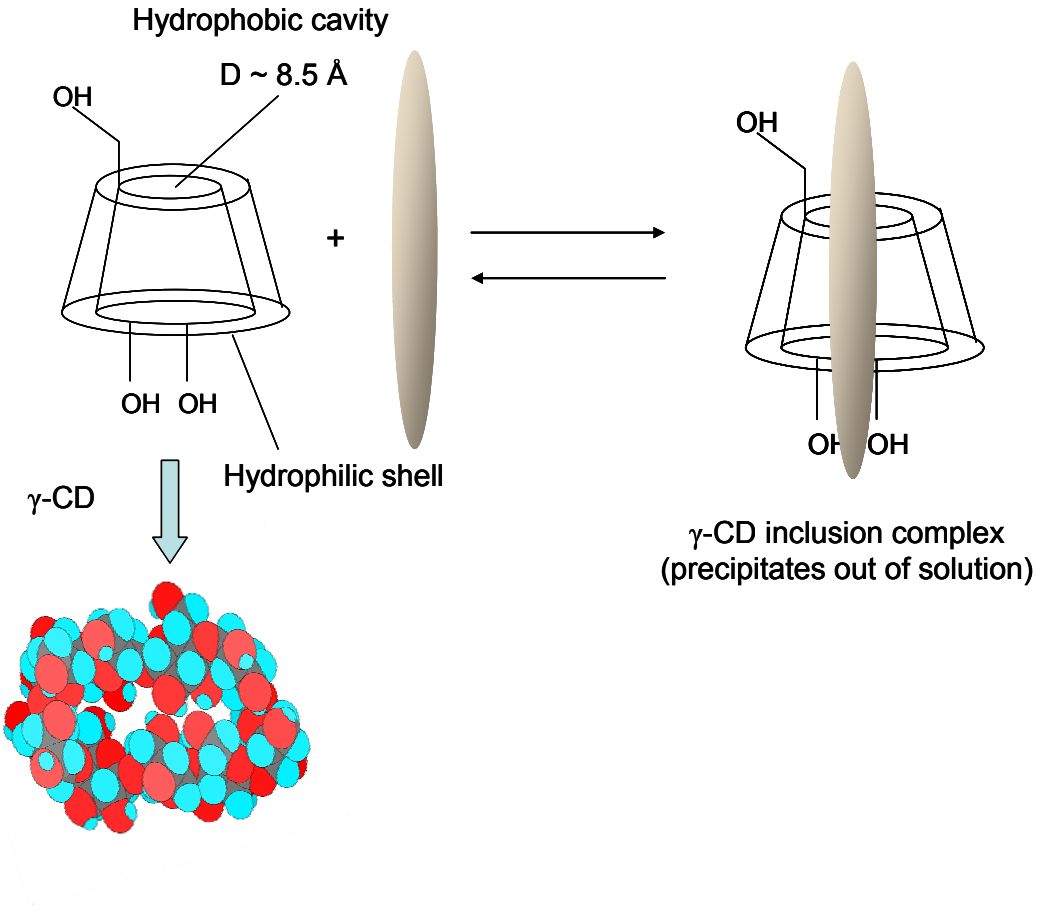

Figure 3.1. The truncated cone structure of gamma cyclodextrin along with a schematic illustrating inclusion complexation and how an inclusion could be used to sequester linear topologies.

In work detailing the structural features of γ-CD inclusion complexes, Porbeni et al. concluded that the process of γ-CD inclusion complex formation sequestered a large portion of the linear chains in a mixture of linear and cyclic material and therefore could be a method to separate cyclic PDMS oligomeric by-product.[18,22,23] One of the most significant advantages in considering CD as a potential route to purify cyclic polymer is the wealth of knowledge on cyclodextrin chemistry and the physics of inclusion complexes.[18,22,23] It has been shown that CD will form inclusion complexes with almost all commodity hydrophilic and hydrophobic polymers, with the only constraint being whether the guest polymer has the appropriate chain length and cross-sectional area to thread the cavity of the CD. Previous work done showed cyclic POE prepared from linear precursors was in actual fact purified by inclusion complexation and precipitation of linear byproducts using α-CD.[20,21,24]

I considered several coupling reactions that involved both unimolecular and bimolecular processes. Part of our interest in polysiloxanes is their great commercial importance, therefore the coupling reaction to be used would involve a commodity siloxane such as α,ω-dihydroxy-PDMS. Group VIII catalytic dehydrocoupling of hydrosilanes with hydroxyl-containing compounds have been widely used; however much of the work involves O-silylation of carbinols. Most mechanistic studies on dehydrocoupling of hydrosilanes suggest transition metal activation of Si-H bonds, either through oxidative addition or formation of an σ-complex, making the silicon atom susceptible to attack by the alcohol.[25] As shown in Figure 3.2, the generation of the activated complex with an alcohol is followed by reductive elimination causing formation

of a Si-O bond which is accompanied by elimination of a hydrogen molecule, hence the moniker dehydrocoupling.[25]

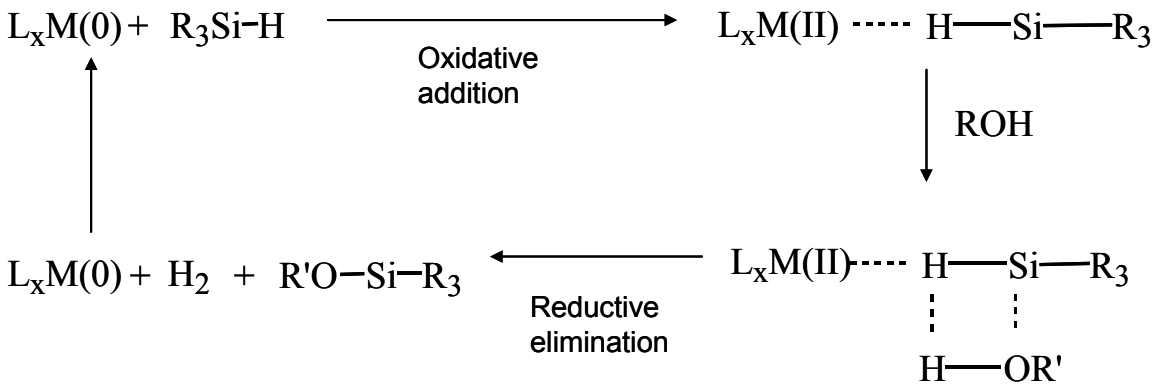

Figure 3.2. Proposed reaction mechanism for the dehydrocoupling of hydrosilanes.[25]

Nickel, ruthenium, rhodium, palladium and platinum complexes have widespread application to this type of silyation coupling reactions. There is recent work by Zhang reporting the dehydrocoupling polymerization of poly(silphenylene siloxane) by bis-silanes and disilanols catalyzed by rhodium complexes. In this work I decided to use a hexachloroplatinic acid (H_2PtCl_6), also know as Speier's catalyst**,** as our group VIII catalyst, mainly because of my familiarity with the compound and the relative ease by which it can be removed from organic products (by precipitation).[25-29]

3.3 Experimental Section

3.3.1 Materials

All reagents were used as received. α,ω-Dihydroxy-PDMS (DMS-S15: M_n ~ 1.5 kg/mol, 45-85 cSt, c^* = 548 g/L; DMS-S27: M_n ~ 18 kg/mol, 700-800 cSt, c^* = 69 g/L) and α,ω-dihydrido-PDMS (M_n ~ .73 kg/mol, 2-3 cSt) were purchased from Gelest.

Hydrogen hexachloroplatinate(IV) hexahydrate (≥ 37.50% as Pt), methanol (99%), tetrahydrofuran (anhydrous, 99.9%), and toluene (HPLC grade, 99.8%) were purchased from Aldrich. γ-Cyclodextrin (γ-CD; Wacker) was used as received.

3.3.2 Instrumentation

Samples for gel permeation chromatography (GPC) were prepared and conducted as in Chapter 2. MALDI-ToF mass spectrometry was carried out as in Chapter 2. ^{1}H, ^{13}C and ^{29}Si NMR spectra were measured on a Bruker AMX 400 or DRX 500 in chloroform-*d*.

3.3.3 Synthesis

Glassware was dried at 120 °C overnight. Round-bottom flasks with stir bars were sealed with rubber septa and cooled while evacuating and then backfilling with dry N_2.

Ring-closing Dehydrocoupling of α,ω-dihydroxy-PDMS with linear α,ω-dihydrido-PDMS.

In a 250-mL flask with magnetic stir bar and condenser under positive nitrogen pressure, a septum was removed and vacuum dried hydrogen hexachloroplatinate(IV) hexahydrate (1 mM) was transferred to the flask using a spatula. The flask was then evacuated and THF (200 mL) was charged by cannula. After allowing a minimum amount of time for the platinum catalyst to fully dissolve (typically ~ 5 min), α,ω-dihydroxy-PDMS (1.2 eq based on the M_n of α,ω-dihydroxy-PDMS) and α,ω-dihydrido-PDMS (1 eq based on the M_n of α,ω-dihydrido-PDMS) were added with syringes (combined [PDMS] ~ 7.5-10 g/L), and the mixture was stirred. It is important to note that the concentration of PDMS in the reaction flask is below the overlap concentration

(c^*=1/[η]). The solution was refluxed and stirred for another 18 hours. The solvent was removed by rotary evaporation, and the crude material was dissolved in toluene, washed with distilled water (× 2) to remove salts, and dried over magnesium sulfate. The mixture was filtered removing the magnesium sulfate and catalyst with a vacuum filter and the solvent removed by rotary evaporation afforded (1.9 g, 98%). ^{1}H NMR ($CDCl_3$): δ -.02-.10 (m, CH_3SiCH_3), 2.3 (s, HOSi). ^{29}Si NMR ($CDCl_3$): δ -21.40 (b, $HOSi(CH_3)_2$), -22.7 (b, CH_3SiCH_3). ^{13}C NMR ($CDCl_3$): δ .733 (m, CH_3SiCH_3). IR: Si-OH stretch, broad, 3550-3700 cm^{-1}, Si-H stretch, sharp, 2120 cm^{-1}, Si-O-Si stretch, broad, 790 cm^{-1}.

Purification of cyclic PDMS by inclusion complexation of linear byproducts with γ-CD.

A saturated solution of γ-CD in distilled water (5 mL, 0.04 g/mL) was prepared and 50 mg of crude product, containing both cyclic and linear PDMS (assuming approximately 25% of the crude product is linear) was added at room temperature. The mixture was supersonically agitated for about 90 min and allowed to stand overnight at room temperature. The cloudy suspension was then separated by centrifugation in which the uncomplexed γ-CD and complexed linear PDMS collected at the bottom of the centrifuge tube.[14] The cyclic PDMS was decanted from the top of the mixture. The purification procedure above was repeated 3 times. Then dissolved in toluene, washed with distilled water (× 2) to remove γ-CD, and dried over magnesium sulfate. The mixture was filtered and the solvent removed by rotary evaporation afforded (60%).

3.3.4 Reagents and Products

Linear α,ω-dihydrido-PDMS

^{1}H NMR (CDCl3): δ .04-.08, .16-.18 (m, CH_3SiCH_3), 4.76 (m, HSi). ^{29}Si NMR ($CDCl_3$): δ -7.93, (s, HSi), -20.33 (b, $HSi(CH_3)_2$), -22.75 (b, CH_3SiCH_3). ^{13}C NMR ($CDCl_3$): δ .653 (m, $HSi(CH_3)_2$), .427, .330 (m, CH_3SiCH_3). IR: Si-H stretch, sharp, 2120 cm^{-1}, Si-O-Si stretch, broad, 790 cm^{-1}.

Linear α,ω-dihydroxy-PDMS

^{1}H NMR (CDCl3): δ -.02-.40 (m, CH_3SiCH_3), 2.53 (s, HOSi). ^{29}Si NMR ($CDCl_3$): δ -10.7 (s, HOSi), -20.5, -21.41(b, $HOSi(CH_3)_2$), -22.02 (b, CH_3SiCH_3). ^{13}C NMR ($CDCl_3$): δ .88-.42, .082 (m, CH_3SiCH_3). IR: Si-OH stretch, broad, 3100-3700 cm^{-1}, Si-O-Si stretch, broad, 790 cm^{-1}.

3.4 Discussion and Results

Platinum-catalyzed bimolecular dehydrocoupling of telechelic linear α,ω-dihydroxy-PDMS with α,ω-dihydrido-PDMS in dilute solution (see Scheme 3.1) was performed, the cyclic product purified by inclusion complexation of the linear material with γ-CD and then was followed typically by GPC as shown in Figure 3.3.

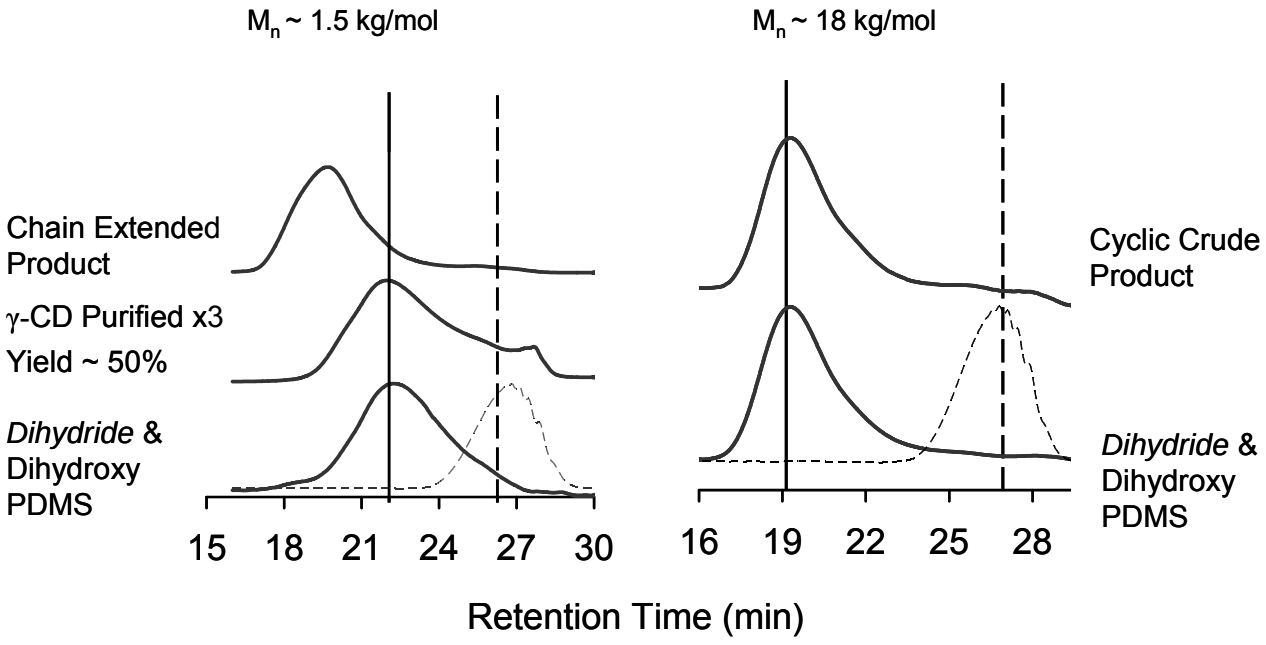

Figure 3.3. GPC traces of the dehydrocoupling of α,ω-dihydroxy-PDMS (M_n ~ 1.5 kg/mol, 45-48 cSt), α,ω-dihydrido-PDMS (M_n ~ .73 kg/mol, 2-3 cSt), chain extended, and γ–cyclodextrin purified cyclic PDMS products (on the left). GPC traces of the dehydrocoupling of α,ω-dihydroxy-PDMS (M_n ~ 18 kg/mol, 700-800 cSt), α,ω-dihydrido-PDMS (M_n ~ .73 kg/mol, 2-3 cSt), crude cyclic and resin purified cyclic PDMS products (on the right).

Unlike unimolecular coupling (which always results in a reduction of hydrodynamic volume), in bimolecular coupling one may sometimes expect a shift to shorter retention times (or a larger hydrodynamic volume) since the hydrodynamic volume of the cycle is not only altered by a topological change but also a combination of the volumes of the two linear precursors. The GPC trace in Figure 3.3 of the γ–cyclodextrin-purified cyclic PDMS product from the 1.5 kg/mol dihydroxy-PDMS precursor showed a slight decrease in retention times from 22.2 to 21.9 min. Using the Mark-Houwink constants for cyclic and linear PDMS, the appropriate calibration curve and a similar procedure as in Chapter 2 the observed retention time shift corresponds to a

theoretical molecular weight increase of ~ 2 kg/mol. Though this is greater than the listed molecular weight of .73 kg/mol for the dihydrido-PDMS, but it is well within the commonly associated error of GPC analysis (which can be considerable large for results corresponding to the high or low ends of the calibration curve). Also, the GPC trace for the γ–cyclodextrin-purified cyclic PDMS appears to have a shoulder or small tailing component persisting until the retention time of the dihydrido-PDMS precursor, indicating that product may not be pure. Nevertheless, the NMR and IR spectra indicate a pure product. In the previous chapter I was concerned with NMR and FTIR spectroscopy as technique to monitor the cyclization of larger linear precursors as the reduced concentration of end groups may have made it difficult to monitor their disappearance. This seems to be direct evidence that below some concentration threshold NMR will not confirm the presence of linear material through end group chemical shifts. To mitigate this effect higher concentrations of the PDMS in *d*-chloroform were made, though at nearly ~ 75 % by volume, the 18.0 kg/mol dihydroxy-PDMS precursor and its cyclic products showed no conclusive results.

In general, with the disappearance of end groups, the products formed from the reaction in Scheme 3.1 could only result from: (a) cyclization, (b) chain extension, or (c) both. So, to show further proof of cyclization another reaction between linear α,ω-dihydroxy-PDMS and α,ω-dihydrido-PDMS was conducted at a concentration ~ 8 times more concentrated than that involved in the cyclization reaction. Following Carothers's equation which assumes only chain extension, a percent conversion of 60 % results in a

degree of polymerization* of ~ 3, yet the GPC data of the γ–cyclodextrin-purified cyclic PDMS product in Figure 3.3 shows almost no shift in retention time from that of the starting dihydroxy-PDMS precursor. NMR end group analysis on the chain-extended product showed a 57 % conversion, and as can be seen in Figure 3.3 produced a drastic increase in the molecular weight.

Figure 3.4 shows the MALDI-ToF spectra of the γ–cyclodextrin purified product resulting from the dehydrocoupling of the linear precursors. A series of signals separated by 74 amu are seen in Figure 3.4, indicating that only cyclic PDMS is present in the γ–cyclodextrin purified product. The gravimetric yield for the γ–cyclodextrin purified product was ~ 50 % signifying that at most half the crude product is comprised of unreacted linear material. In spite of the gravimetric yield, the dehydrocoupling most likely is more efficient than that (based on NMR and IR of crude products), since an appreciable amount of both linear and cyclic material can be lost during the repeated purification steps. Also, a spectrum of crude product showed no linear material with any hydride end groups. This suggest that once a dihydrido functionalized oligomer reacts with a dihydroxy functionalized oligomer the resulting species is a short-lived intermediate that rapidly cyclizes rather than remain in solution or further react with other linear material.

* Degree of polymerization in this case considers the linear precursor as the monomer; therefore, a product with a DP of ~3 should be 3 times the molecular weight of the precursor.

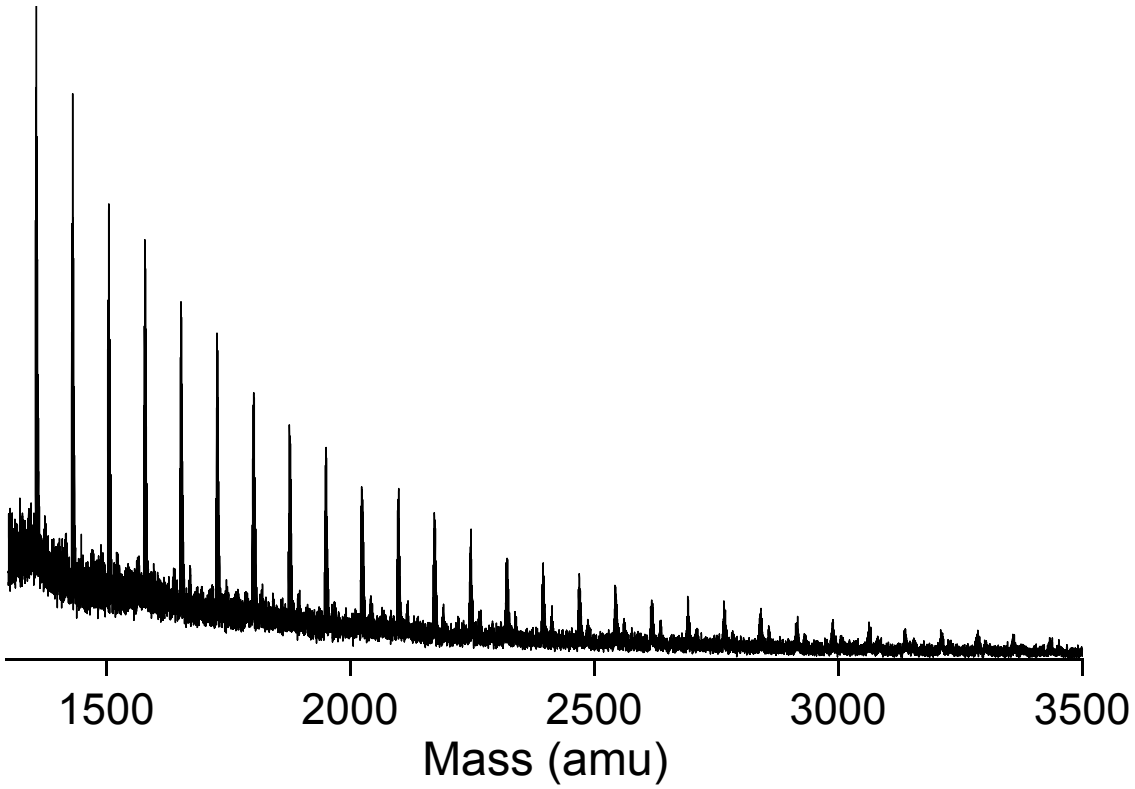

Figure 3.4. MALDI-ToF spectrum of the γ–cyclodextrin purified cyclic product resulting from the dehydrocoupling of α,ω-dihydroxy-PDMS (M_n ~ 1.5 kg/mol, 45-48 cSt), α,ω-dihydrido-PDMS (M_n ~ .73 kg/mol, 2-3 cSt). Each peak is separated by 74 amu the repeat unit molecular weight of PDMS and represents a sodium-cationized cyclic.

The NMR spectra shown in Figure 3.5 and Figure 3.6 show the chemical functionality in the linear dihydroxy- and dihydrido-PDMS. The NMR spectrum of both linear starting materials contained a major peak at ~ .08 ppm due to methyl groups on internal silicones. The shorter linear precursors show an additional peak adjacent to the

major peak at ~ .08 ppm shifted downfield to ~ .16 ppm, which can be attributed to methyl groups on internal silicones near the end groups. A downfield peak appears at ~ 2.5 ppm due to the silanol end groups on the dihydroxy-PDMS and at ~ 4.7 ppm for the silane end groups on the dihydrido-PDMS. Note in the NMR spectra the cyclic crude product and purified product there is a complete disappearance of the hydroxyl and hydride groups from the reaction mixture. The inset is a zoomed view clearly showing the area where the chemical shifts of the end groups exist. The disappearance of end groups suggests that either chain extension or cyclization occurred.

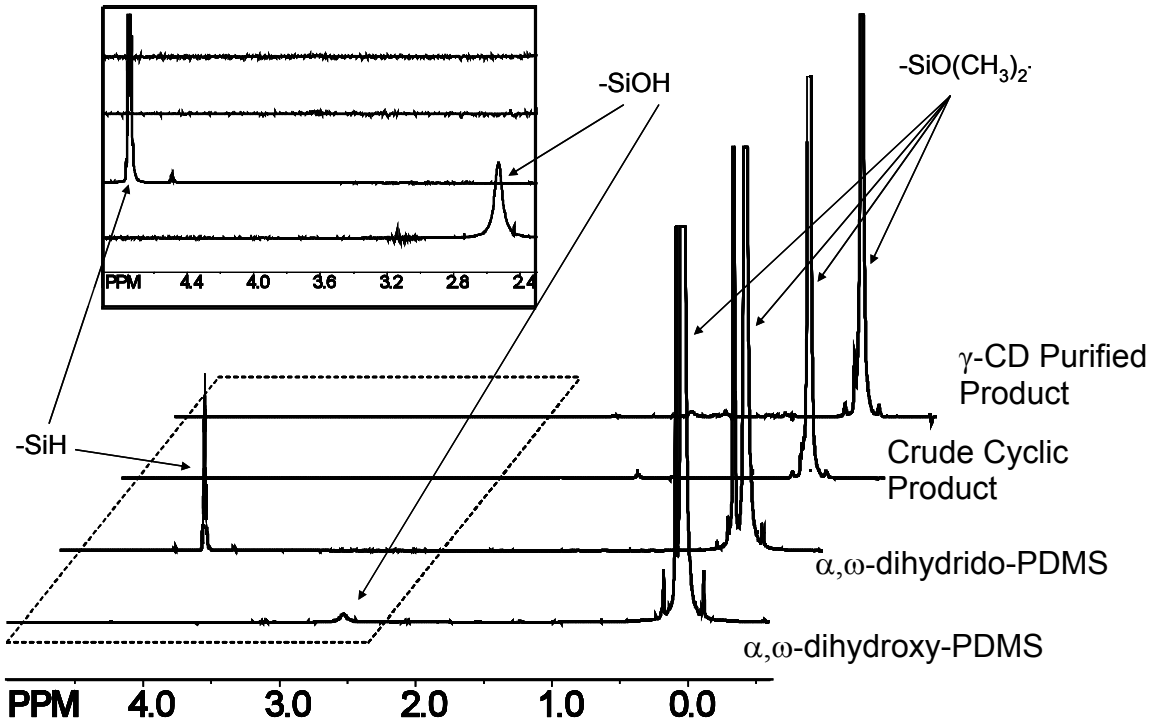

Figure 3.5. ^{1}H NMR spectrum of linear α,ω-dihydroxy-PDMS, linear α,ω-dihydrido-PDMS, γ–cyclodextrin purified cyclic product and crude product, which is a mixture linear and cycles, resulting from the dehydrocoupling of α,ω-dihydroxy-PDMS (M_n ~ 1.5 kg/mol, 45-48 cSt), α,ω-dihydrido-PDMS (M_n ~ .73 kg/mol, 2-3 cSt). The inset is a zoomed vertical stack of the NMR spectra from 4.8 to 2.3 ppm.

Figure 3.6 shows the ^{29}Si NMR spectrum of the both linear starting materials and the γ–cyclodextrin-purified cyclic product. ^{29}Si NMR is another spectroscopic technique used here to determine the existence of end groups, being particularly useful in studying systems with changing silicon groups, however because of the nuclei's aggravatingly long T_1 relaxation and low relative sensitivity it is not as simple or valuable as ^{1}H NMR (in most cases). Even so, all spectra contained a major peak at ~ 22 ppm due to D group silicon atoms on internal silicones. Figure 3.6 clearly confirms disappearance the peak at ~ 10.7 ppm due silicon on the silanol end groups of the dihydroxy-PDMS and at ~ -7.9 ppm for the silane end groups on the dihydrido-PDMS.

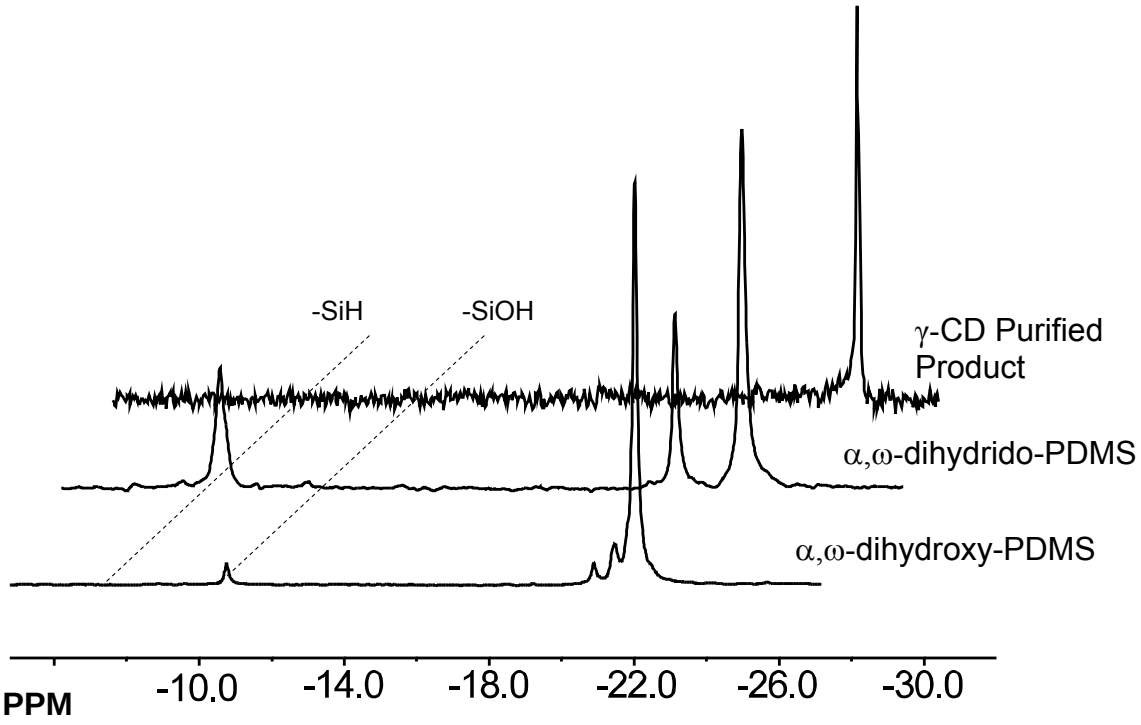

Figure 3.6. ^{29}Si NMR spectrum of linear α,ω-dihydroxy-PDMS, linear α,ω-dihydrido-PDMS, γ–cyclodextrin-purified cyclic product, resulting from the dehydrocoupling of α,ω-dihydroxy-PDMS (M_n ~ 1.5 kg/mol, 45-48 cSt), α,ω-dihydrido-PDMS (M_n ~ .73 kg/mol, 2-3 cSt).

In Figure 3.7 the IR spectrum of the linear dihydroxy-PDMS revealed a broad –OH peak for hydrogen-bonded material from 3120 to 3470 cm^{-1} and sharper series of peaks out towards ~ 3700 cm^{-1} representing isolated hydroxyl groups, was not present in the purified product. A sharp characteristic adsorption band for the silane end group is at 2120 cm^{-1}, which also does not appear in the cyclodextrin-purified cyclic PDMS product. This not only indicates cyclization happens but also shows the effectiveness of the CD purification scheme. The adsorption bands for the hydrogen-bonded silanol group disappears in the crude product, however the spectra indicate a small amount of free hydroxyl and silane groups still are present. The residual linear precursor and chain-extended product in the crude product could be attributed to inefficient catalytic activity or more likely due to some stoichmetric imbalance from inaccurate molecular weight information and/or the polydispersed nature of both precursors. Infrared spectroscopy should provide a considerably higher sensitivity compared to NMR[30] however at some point (for large precursors and high cyclic yields) a detection threshold will be reached and the IR data will show a similar trend with respect to end group appearance as seen in the NMR data.

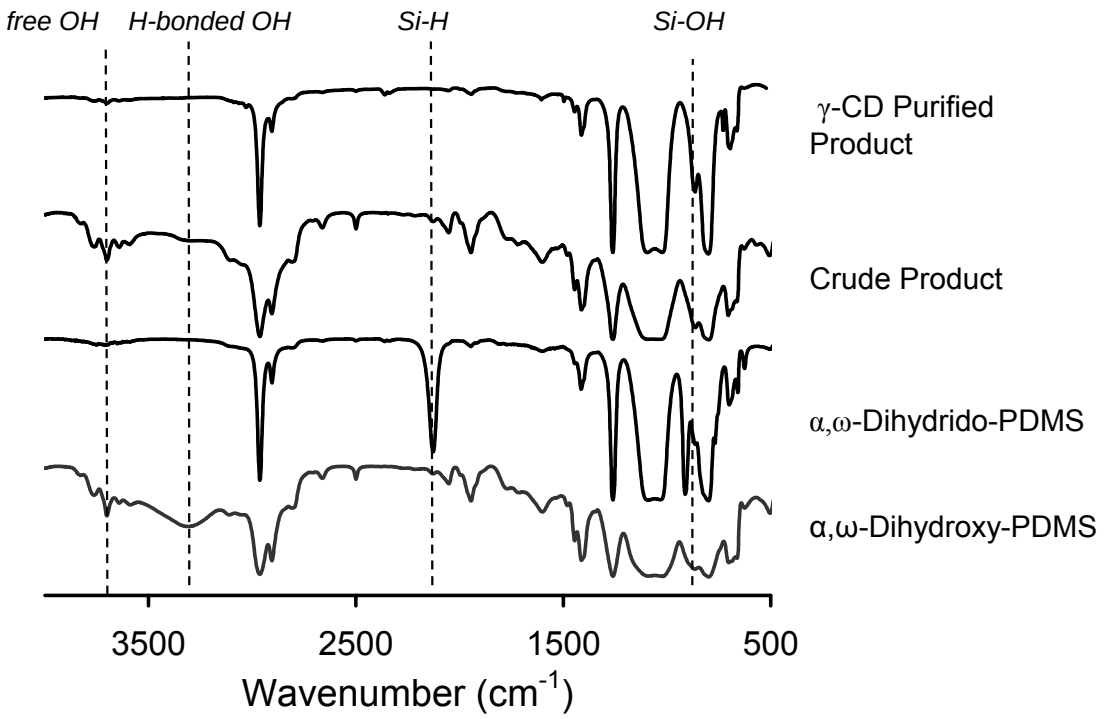

Figure 3.7. IR spectrum of the linear α,ω-dihydroxy-PDMS, (M_n ~ 1.5 kg/mol, 45-48 cSt), α,ω-dihydroxy-PDMS (M_n ~ .73 kg/mol, 2-3 cSt), crude and γ–cyclodextrin-purified cyclic PDMS products, showing the disappearance of the silanol group over the range of 3100-3700 cm^{-1} and silane group at 2120 cm^{-1}.

Purification of the linear byproduct from the cyclic material is also an important step in the cyclization procedure. In the previous chapter this was achieved by utilizing the chemical difference in the linear and cyclic topologies. An anionic ion-exchange resin is added to the reaction mixture, pulling the deprotonated linear species out of solution. Deprotonation however, leads to ring-chain equilibration therefore making that purification procedure in the dehydrocoupling reaction counter-productive.

Cyclodextrins have also been used to separate linear and cyclic topologies. The interior of a γ-CD in an aqueous environment is attracted to the hydrophobic dimethylsiloxane repeat units on the PDMS. This inclusion complex can not form on

cyclic material and is insoluble in water making it ideal for a means of separation.[18,20,24] Figure 3.8 shows the effectiveness of the CD purification method for smaller linear precursors. The crude cyclic product shows a small IR signal for the hydride end groups and free silanol groups, notice these peaks disappears completely in the γ–cyclodextrin purified cyclic PDMS product.

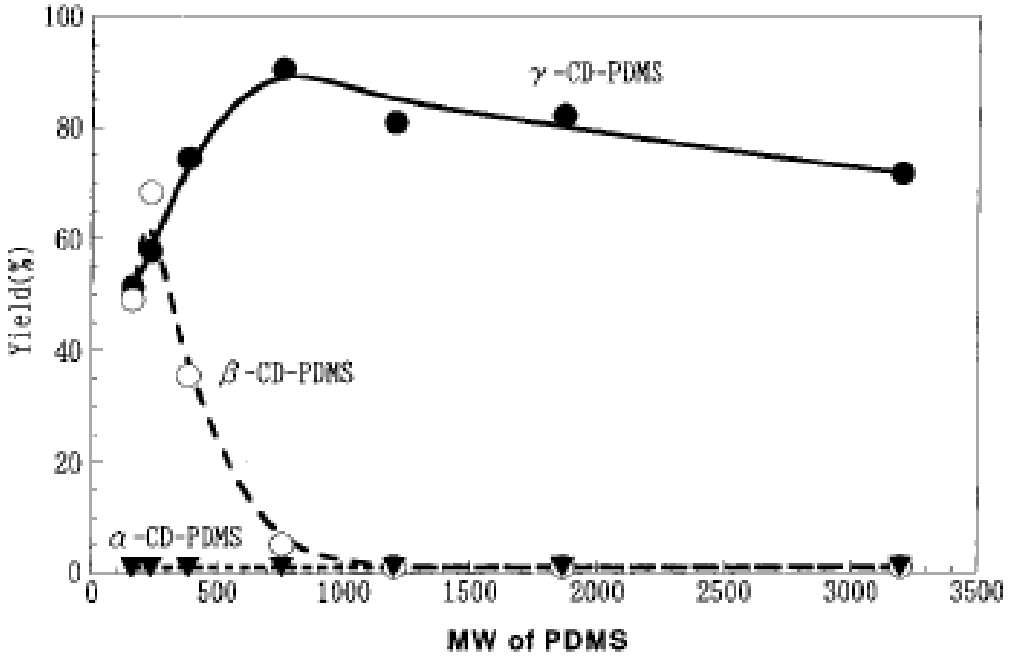

Figure 3.8. Yields of CD-PDMS complexes as a function of the molecular weight of PDMS. [Reprinted with permission from Okumura, H.; Kawaguchi, Y.; Harada, A. *Macromolecules*, **2001**, 34, 6338-6343 Copyright © 1965 American Chemical Society.]

As seen in Figure 3.3 the molecular weight of the γ-CD purified product more resembles the distribution of the dihydroxy precursor (repeated purification would increase the distribution's similarity to the linear precursor), which is what would be expected for bimolecular coupling where one component, the dihydrido-PDMS precursor is much smaller that the other component, the dihydroxy-PDMS precursor. Harada et al. looked at inclusion complexes formed with either γ-CD, β-CD, or α-CD and PDMS of a

variety of molecular weights. Steric hindrance due to the dimethylsiloxane groups along the main chain of PDMS prevented complex formation with α-CD. However, it was determined that the cavity in γ-CD and β-CD was large enough to contain PDMS.[18,23] Figure 3.7 shows the yields of the complexes as a function of the molecular weight of PDMS. γ-CD complexation yields increase reaching a maximum at .76 kg/mol or about 10 repeat units. The plot then shows yield decrease with increasing molecular weight of the PDMS. And though the data only includes small oligomers up to 32.0 kg/mol, I believe it's reasonable to postulate that at some molecular weight the complexation yield of γ-CD with PDMS will show a decrease similar to the β-CD complexation data. Therefore, since the yield of the inclusion complexes between PDMS and γ-CD is a function of the molecular weight of PDMS, this limits the effectiveness of the method as the linear precursor molecular weight increases.

The majority of the Pt-catalyst is removed simply by filtration of the re-dissolved crude product in toulene; this was confirmed gravimetrically. However, it is quite obvious by the faint black color the PDMS assumes that all the catalyst is not removed. However no further attempts to purify the product were made.

A major contention made in this chapter pertains to the fact dehydrocoupling is a means to facilitate more control over the cyclization reactions without any additional end group modification to commodity siloxanes. Figure 3.9 shows the GPC traces from 18 kg/mol linear α,ω-dihydroxy-PDMS and the cyclic products resulting from ring-chain depolymeriation and dehydrocoupling with α,ω-dihydrido-PDMS. The product formed by ring-chain equilibration not only has a drastically shifted peak maximum, indicating a considerable overall molecular weight reduction. But also shows a much broader peak

reflecting its increased PDI and spread of the molecular weight distribution. Whereas the GPC trace of the cyclic product formed via dehydrocoupling closely matches that of the linear precursor in center and spread.

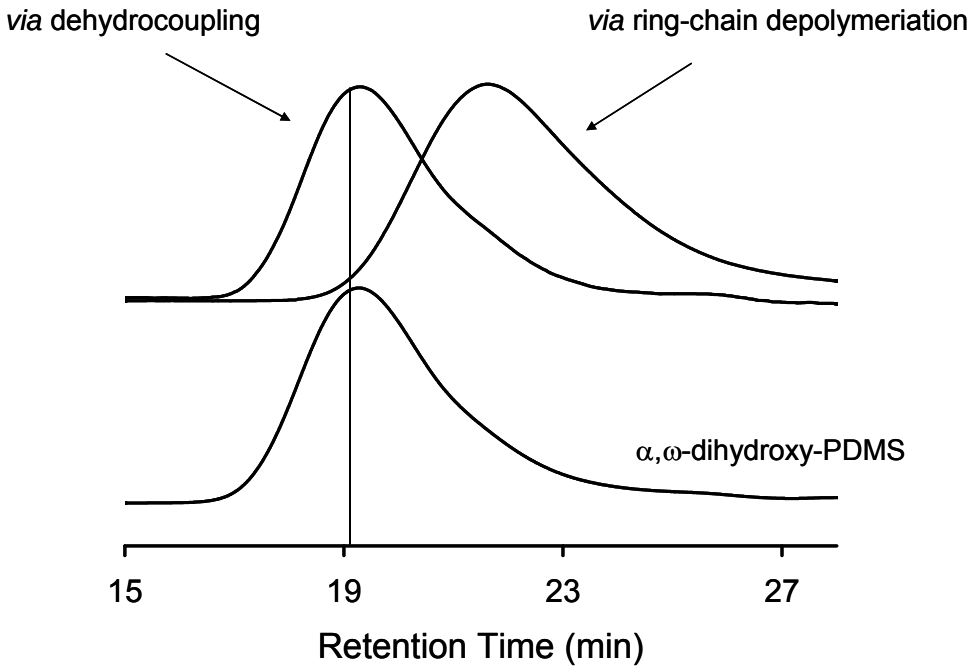

Figure 3.9. GPC traces of the linear α,ω-dihydroxy-PDMS (M_n ~ 18 kg/mol, 700-800 cSt) and the cyclic products resulting from ring-chain depolymeriation and dehydrocoupling with α,ω-dihydrido-PDMS (M_n ~ .73 kg/mol, 2-3 cSt).

3.5 Conclusions

Dehydrocoupling facilitates more control over the cyclization reactions, and therefore provides a greater potential to manipulate the molecular weight distribution of the cyclic product simply by changing the molecular weight of the linear precursor. Particularly interesting and useful is the comparison of the cyclic crude product with that of the chain extended product. The only difference in the reaction was the concentration of PDMS in solution. However, the GPC trace in Figure 3.3 clearly shows that the

molecular weight of the chain extended product is ~ 3 times that of the cyclic crude product, supporting the conclusion that mostly intramolecular processes and cyclization did occur. The use of γ-CD was found to be an effective method of separating cyclic and linear PDMS under ~ 5 kg/mol, which is related to the yield of the inclusion complex at that molecular weight. The use of a base then addition of an anionic resin was investigated as an alternative method of separating cyclic and linear PDMS over 10 kg/mol. However a large reduction in the molecular weight was observed, which is related to how fast the PDMS enters the ring-chain equilibration, and proved not to be a viable method of separation. As a final comment, though the use a group VIII organometallic/metallic catalyst to facilitate dehydrocoupling is not novel, I still believe this study along with similar work is important to future applications of poly(siloxane)s in a variety of areas. This seems to be even more true particularly considering the commodity nature of poly(siloxane)s and proliferation in the use of silica, which both present silanol terminality.

3.6 References

1. Semlyen, J., *Cyclic Polymers*. Elsevier: New York, 1986.

2. Semlyen, J., *Large Ring Molecules*. Wiley: New York, 1996.

3. White, B. Rotaxanated Polymers: I. Synthesis and Purification of Cyclic Polydimethylsiloxane II. Synthesis of Poly[(octene-pseudorotaxa-(α-cyclodextrin)]. Doctoral Thesis, Georgia Institute of Technology, Atlanta, 2004.

4. White, B.; Watson, W.; Beckham, H.; *Macromolecules* **2002**, *35*, 5345-5348.

5. Flory, P.; Semlyen, J.; *J. Am. Chem. Soc.* **1966**, *1*, 8814.

6. Winnik, M.; *Ace. Chem. Res.* **1985**, *18* 73-79.

7. Cho, D.; Park, S.; Chang, T.; *Macromolecules* **2001**, *34*, 7570-7572.

8. Lepoittevin, B.; Dourges, M.; Cramail, H.; *Macromolecules* **2000,** *33,* , 8218-8224.

9. Geiser, D.; Hocker, H.; *Macromolecules* **1980**, *13*, 653-656.

10. Lepoittevin, B.; Hemery, P.; *Polym, Adv. Technol.* **2002**, *13*, 771-776.

11. Boutillier, J.; *European Polymer Journal* **2002**, *38*, 243-250.

12. Gan, Y.; Dong, D.; Hogen-Esch, T.; *Macromolecules* **1995**, *28*, 383-385.

13. Lee, C.; Grubbs, R.; *J. Org. Chem.* **2001**, *66*, 7155-7158.

14. Diedrich, F.; *Angew. Chem. Int. Ed.* **2000**, *39*, 2632.

15. Lee, H.; Lee, H.; Chang, T.; *Macromolecules* **2000**, *33*, 8119-8121.

16. Takano, A.; Yuuki Kushida, Y.; Matsushita, Y.; *Macromolecules* **2007**, *40*, 679-681.

17. Mengerink, Y.; Peters, R.; Cramers, C.; *Journal of Chromatography A* **2001**, *914*, 131-145.

18. Porbeni, F.; Edeski, E.; Tonelli, A.; *Polymer* **2001**, *42*, 6907-6912.

19. Szejtli, J.; *Chem. Rev.* **1998**, *98*, 1743-1753.

20. Singla, S. Topological Effects on Properties of Multicompontent Polymer Systems. Phd Thesis, Georgia Institute of Technology, Atlanta, 2004.

21. Okumura, Y.; Ito, K.; Hayakawa, R.; *Polym. Adv. Technol.* **2000**, *11*, 815-819.

22. Okumura, H.; Okada, M.; Harada, A.; *Macromolecules* **2000** *33* 4297-4298.

23. Okumura, H.; Kawaguchi, Y.; Akira Harada, A.; *Macromolecules* **2001**, *34* 6338-6343.

24. Singla, S.; Zhao, T.; Beckham, H.; *Macromolecules* **2003**, *36*, 6945-6948.

25. Lukevics, E.; Dzintara, M.; *Journal of Organometallic Chemistry,* **1985**, *295* 265-315.

26. Li, Y.; Kawakami, Y.; *Macromolecules* **1999**, *32*, 3540-3542.

27. Zhang, C.; Laine, R.; *J. Am. Chem. Soc.* **2000**, *122*, 6979-6988.

28. Corey, J.; *Advances in Silicon Chemistry* **1991**, *1*, 327-387.

29. Zhang, R.; Mark, J.; Pinhas, A.; *Macromolecules* **2000**, *33*, 3508-3510.

30. Servaty, R.; Schiller, J.; Arnold, K.; *Bioorganic Chemistry* **1998**, *26*, 33–43.

31. Oth, J., Desreux, V.; *Bull. Soc. Chim. Belges* **1954**, *63*, 285.

32. Dodgson, K.; Semlyen, J.; *Polymer* **1977**, *18*, 1265.

33. Montaudo, G.; Montaudo, M.; Samperi, F.; *Prog. Polym. Sci.* **2006**, *31*, 277-357.

CHAPTER 4

Ionic Self-Assembly and Covalent Fixation of Ionic-Reactive Silicones on Cellulosic Substrates

4.1 Abstract

Surface modification was investigated by application of quaternary *N*-phenyl pyrrolidinium mono-terminated polydimethylsiloxane (PDMS) oligomers with an intended but not limited to specific end-use as a textile finish to be used as a water repellent or fabric hand softener. The method of surface modification by formation of permanent polymer brushes on a solid substrate via adsorption of end-functionalized polymers from solution demonstrates the use of a novel ionic-reactive end group with the intended purposes of increased surface coverage and levelness. The ionic-reactive end-functionalized polymer upon application will adsorb and bind to a complex substrate because of complementary electrostatic charges. Subsequent heating will convert those ionic bonds to covalent bonds, and permanently fix the polymer to the substrate. Functionalized PDMS oligomers were prepared from commercially available monocarbinol-terminated PDMS oligomers and *N*-phenyl pyrrolidine. NMR spectroscopy and MALDI-ToF spectrometry show the major product is quaternary phenyl pyrrolidinium oligomers with gravimetric yields of ~ 95 %, while GPC shows no appreciable change of the molecular weight distribution. Covalent fixation and surface characteristics of treated cotton fabric, microcellulose granules and cellophane films was determined using FTIR.

4.2. Introduction

Since its inception, the textile industry has relied on the treatment (primarily wet processing) of fiber and fiber blends in a fabric to facilitate construction and optimize appearance and performance. In particular dyes and finishes have been used to give textiles specific visual, mechanical and functional properties. Chemical finishes have been used on a wide variety of materials to impart anti-static, hydrophilic/hydrophobic, soil-repellent properties, as only a few examples.[1]

However, as the industry has matured modern concerns about the environment have overlapped with the direction of developing textile products and processes. General public sentiment and recent more stringent legislation of ecotoxicological considerations related to issues such as safely storing, applying and disposal of finishing and dying chemicals have pushed changes in the nature of chemicals and processing methods used.[2,3] This could be done by either reducing the amount of chemicals used or using more environmentally harmless materials. As a consequence, the former route to more ecofriendly practices will increase the added value of a textile product by minimizing the amount of chemical finish, water and energy required during production as compared to traditional treatment methods.

Traditional finishes are used to modify surface properties in a finished product. In textiles, surface properties of a fiber can determine gloss, water-repellency, dye affinity, adhesion, and stain resistance.[4,5] There has been little work done on reactive or ionic finishes. The majority of industry use finishes that rely on concentration gradients and secondary forces to promote exhaustion, adsorption, binding and fastness. This binding is fairly weak because no covalent bond is formed making most finishes non-permanent.

Also, there is no thermodynamic driving force for exhaustion so adsorption requires large excesses of finish during application increasing the cost and waste associated with these type processes. Yigor et al. attempted to modify the surface of polyamide-6 by melt blending the nylon with organofunctionally terminated PDMS oligomers. During blending, the functional group on the PDMS reacts with the amide group on the nylon, resulting in blends that showed permanently silicone-rich surfaces.[6] However in this instance the bulk material is modified also and melt blending with reactive oligomers will only work for certain thermoplastics, making this modifying method less attractive.

Reactive dying or finishing is one of the more popular techniques to permanently modify cellulosic, wool and nylon fibers. The reactive material utilizes a chromophore which is attached to a reactive group that will covalently link with the appropriate chemical moiety on the polymeric backbone or chain end at the surface of the substrate. During wet processing depending on the chemical structure of the substrate, alkaline conditions and elevated temperatures are required to facilitate reaction of the reactive group. Typical reaction condition for reactive finishes have two major consequences: (1) cotton substrates alone can build up negative surface charges in water and the resulting electrostatic barrier can repel dyes or ionic finishes and retard exhaustion, and (2) the fixation can also produce dead material that require additional washing to remove. Because of this, typical reactive dye exhaustion and fixation levels for cotton fibers are poor, about 50 to 80 % fixation.[2] To overcome this, large amounts of salt are added to the dye liquor and dying is performed at elevated temperatures over an extended amount of time. Other than offsetting the zeta potential of the substrate, salt is added to reduce the solubility of the dye once it has diffused into the substrate, increasing dye retention.

Traditional reactive dye recipes require 30-100 g/L of salt, and in many cases is released in the plant's effluent.[2,3,7] Though the toxicity for many plants, animals and fish are low for these types of electrolytes, the sheer enormous use of them around the world in the textile industry makes it a major concern.

An older member in the class of finishes and dyes employs ionic moieties to promote exhaustion. Ionic dyeing or finishing forms ionic bonds therefore fastness compared to reactive systems is lower. The non-permanent nature of ionic bonds allow dye or finish molecules to shuffle along the surface, self-assembling, and reaching some equilibrium. Again salt is often used to manipulate ionic repulsion and the zeta potential of the surface.

A simple yet novel route to improve upon an age-old technology would be to combine the advantageous attributes of both reactive and ionic finishing. The idea being, ionic assembly will form a monolayer with a higher surface coverage, exhaustion and retention more homogeneous than any purely non-reactive or reactive system. The substrate could then be removed from the solution containing the ionic-reactive moiety, maximizing the effectiveness of the surface modification and minimizing waste. I see the use of this powerful chemistry as an effective method for surface modification, particularly on complex surfaces where no thermodynamic driving force exist to promote adsorption or retention of the modifying moiety.

Though I have chosen to focus on the intended end-use for ionic-reactive surface modifying moieties as textile finishes or dyes, they are also part of a larger class of materials, called polymer brushes. Polymer brushes can be used to alter different surface properties such as: chemical or charge terminality on a surface, wetting control,

adsorption of molecules, flocculation control of nanoparticles, etc.[8-12] Polymer brushes are among a large list of macromolecular structures used to change the surface properties of a substrate.[13] A common motivation for surface modification with a polymer brush is to make a surface more hydrophobic or hydrophilic, which can be readily conducted by chemical coupling reactions.

Kishida et al. grafted poly(ethylene glycol) (PEG) chains to cellulose haemodialysis membranes to improve blood compatibility. Grafting was achieved by derivation of mono-terminated carboxy-PEG with carbodiimide in toluene to create the anhydride form of PEG. Esterification between PEG and the hydroxyl groups on the membrane surface followed the addition of dimethylaminopyridine to the PEG anhydride in the presence of a cellulosic substrate. The immobilized polymer formed a polymer brush structure that increased the contact angle, indicating more hydrophobic surface character, which seemed to hinder the direct contact of plasma proteins with the membrane surface. More interestingly, when a free carboxyl group was the terminal functionality of the PEG tethers, protein adsorption and platelet adhesion are accelerated.[14]

Another example of tethering polymer chains to a substrate to modify its surface properties can be found in the field of polymer composites which has grown over the years, as there has been a considerable need to improve mechanical properties of existing polymeric systems. Typically reinforcing filler is added to a polymeric matrix to dissipate and distribute forces over the entire part. This increases properties like tensile and impact strength. However, to generate these improved mechanical properties the filler must be well dispersed and have good adhesion at the interface. One interesting

approach to improve adhesion in cellulose fiber-reinforced polypropylene, which for enthalpic reasons has a poor adhesion at the interface, is to graft compatibilizing agents to the surface of the fibers. Specifically, polypropylene chains with 6 % maleic anhydride were used, and it was observed with dynamic mechanical measurements and tensile testing that the grafted polymer brushes increased stress dissipation.[15]

Using polymer brushes, which refers to an assembly of tethered polymer chains, maximizes surface coverage by utilizing the dense packing usually associated with them. In the absence of external fields or confining geometry, chains in a polymer brush adopt stretched configurations. This is because the polymer chains are so crowded that they are forced to extend away from the surface of the substrate to avoid overlapping.[13] The particular system discussed in this paper can be classified as "grafted to" polymer brushes and their ionic-reactive character makes them even more attractive to use on substrates with complex cross-sections. Determined by Monte Carlo simulation, in typical surface modification by polymer adsorption and polymer brush formation (by ionic or secondary forces) the kinetics are diffusion controlled, where adsorption and the subsequent fixation is dominated and controlled by the diffusion of the modifying moiety in solution.[16-19] On the other hand, reactive oligomers used to form polymer brushes rely on the same secondary forces to promote end group adsorption and fixation, however the fixation becomes permanent due to the covalent linkage. The kinetics of this grafting process has been shown to be more complex, and ultimately dominated by the reaction rates of the end group with the substrate.[20]

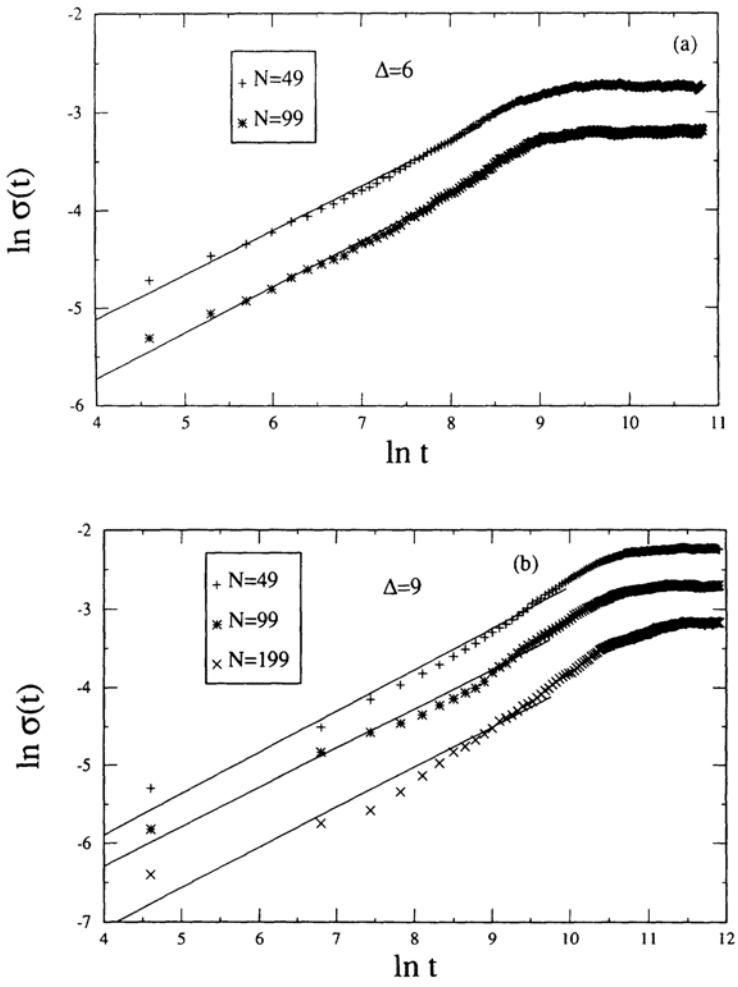

Figure 4.1. Log-log plot of Monte-Carlo simulations of polymer chain adsorption, where σ(t) is the number of chains per unit area and Δ is an an enthalpic parameter describing the energy gained by adsorbing the end group of the polymer to the substrate (a) Δ=6 and N=49 and 99 (b) Δ=9 and N=49, 99 and 199. All straight lines fit a slope ~ ½. [Reprinted with permission from Zajac, R. *Physical Review E.* **1994**, 49, 3071. Copyright © 1994 American Physical Society.]

The number of chains adsorbed on the surface per unit area of substrate, σ(t), as a function of time, *t*, is said to initially fit Eq. 1 which describes a diffusion-controlled process:

$$\log[\sigma(t)] = \log[C] + \frac{1}{2}\log[t] \qquad \text{Eq. 4.1}$$

The constant C is proportional to $D^{1/2}$, where D is the diffusion constant (inversely proportional to chain length), and to an enthalpic parameter, Δ, describing the energy gained by adsorbing the end group of the polymer to the substrate. The simulation work was supported by surface force balance measurements on mica substrates as polystyrene chains terminated with zwitterionic groups adsorbed from a good solvent. It was found that PS chains bearing three zwitterionic groups show a higher surface coverage than the chains bearing only one zwitterionic group.[19] However, Eq. 1 can only describe the initial stage of the growth or the diffusion-limited regime, since it does not include saturation at one monolayer.[17] At some point the kinetics of adsorption will monotonically decrease and level off to some saturation point because of the reduction of available sites on the substrate and the adsorbed layer screening. Basically the entropic penalty to adsorption becomes so high no more chains will adhere to the surface. This kinetic regime is referred to as penetration-limited regime because penetration of chains through the maturing brush is the rate limiting step.[18] As seen in Figure 4.1, the saturation point is then controlled by the length of the chains (inversely proportional) and the Δ parameter (proportional).

Ionic-reactive moieties separate the adsorption and permanent fixation processes, making the polymer brush formation a diffusion controlled mechanism. Therefore adsorption is still controlled as described above however the Δ is much higher than any purely reactive moiety because of ionic interactions.[19] Increasing Δ will result in a larger C for Eq. 1, increasing the amount of polymer adsorption, as described in chains per unit area, at any given time after t=0 including the final saturation level. Because of the non-permanency of the ionic attraction between the chains and the substrate, the saturation

point is actually an equilibrium point, where chains on the surface and chains in solution exchange.[17] In this case the saturation or equilibrium point depends on another parameter describing the packing of the chains on the surface. There is some configuration of chains that will minimize the entropic penalty to dense polymer adsorption. As the chains randomly adsorb onto the surface the packing is also random and maybe inefficient. However, because the ionic-reactive material is in equilibrium, the system spontaneously finds the most efficient packing, increasing the number of chains fixed on the surface compared to purely reactive material.

One solution to improve the affinity of any type of surface treatment to a substrate is to modify the surface charge via chemical processes to induce ionic attraction and bonding. Hauser investigated the use of 2,3-epoxypropyltrimethylammonium chloride to render the surface of cotton cationic and alter its dyeing behavior. Cationization of the surface is achieved via *in-situ* formation of oxiranylalkyl-ammonium chloride by a base, while the base also creates alkoxide ions on the surface of the cellulose. Under these conditions the *in-situ* formed epoxy will ring open giving rise to an ether linkage between the substrate and the modifying alkyl ammonium, leaving the ammonium group attached at the surface. It was then found that this surface showed excellent anionic dye yields and color fastness properties without the use of electrolytes, fixation agents or subsequent washings.[21]

Based on this work researchers began to use cationic cotton substrates produced by exposure to 2,3-epoxypropyltrimethylammonium chloride to perform layer-by-layer deposition of complementary charged polyelectrolytes.[22] The authors recognize functional textiles such as safety and protective clothing, sporting apparel and selective

filtration systems require tailoring selectivity, diffusivity, permeability and chemical, frictional and thermal resistivity. Manipulation of these properties will almost always require a level, permanent, robust surface modification. The layer-by-layer deposition technique could then provide a route to surface modify complex and unique structures with a variety of moieties in a controlled manner. It was found that multiple alternating nanolayers of polyelectrolytes could be formed with a high degree of control on the surface of a cationic cotton fiber.[22,23] However, layer-by-layer deposition only utilizes ionic bonding between polyelectrolytes, whose formulations are far from common place, raising the issue of permanency and usefulness. Also, there may be some applications in which formation of multilayers is advantageous, however in most arenas the ideal surface modification would involve the formation of a densely packed monolayer, much like the polymer brushes formed from tethering of a mono-functional polymer.[22]

Since the early 1990's Tezuka et al. has utilized an interesting chemistry to form unique topologically complex macromolecular structures in high yield and purity from macromolecular "building blocks" containing suitable reactive end groups.[24-29] Specifically their work centers around the use of moderately strained cyclic onium cation groups, seen in Figure 4.2, and soft nucleophiles such as carboxylates.[26] The macromolecular "building blocks" functionalized with the appropriate complementary end group will first self-assemble in solution due to ionic bonding. Upon heating the nucleophile will cause the quantitative and selective ring-opening reaction of the cyclic onium groups.

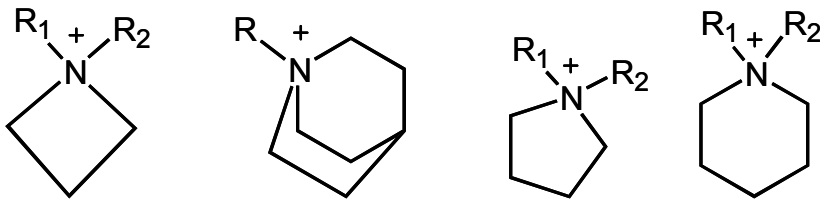

Figure 4.2. Cyclic onium cations.

Scheme 4.1 shows three reactions that are possible when cyclic onium salts are exposed to strong nucleophiles (e.g. alkoxide or carboxylate) and heated. All three of the reactions are in competition and their individual rate constants govern the major product. The chemical identity of both the nucleophile and cyclic onium groups and the temperature at which the ring-opening is carried out is important as it affects the propensity of the cyclic onium groups to perform Hoffmann elimination or substituent removal.[26] Therefore, it is important then to determine how experimental conditions affect each reaction pathway, with the goal of maximizing ring opening, which is the route that leads to surface modification. Substituent removal is caused by nucleophilic attack on the *exo*-*N*-substituent labeled R_1 in Scheme 4.1, producing a cyclic tertiary amine while eliminating an ether or ester. This would seemingly require the α-carbon on the R_1 substituent to be sterically accessible and somewhat electrophilic.[26] Following this, Tezuka replaced *N*-methyl pyrrolidinium with *N*-phenyl pyrrolidinium as the reactive group on his macromolecular "building blocks". There was a noticeable suppression in substituent removal, which was attributed to crowding in the nucleophilic transition state that attack on the *exo*-*N*-phenyl group would allow. In addition, an aniline derivative group is a much better leaving group than an alkylamino group in nucleophilic

substitution reactions, promoting attack at a location on the reactive group (*endo*-methylene within the cyclic onium) that leads to ring-opening.[30-33]

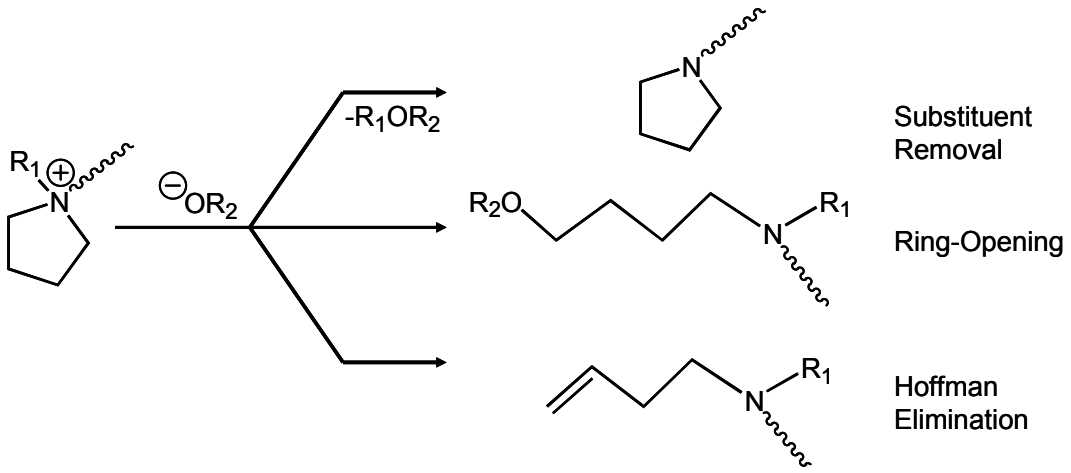

Scheme 4.1. Three reactions are prossible when cyclic onium groupss are exposed to a nucleophile and heated. Note that the nucleophile (-OR_2) is only incorporated via ring-opening pathway.

Hofmann elimination requires proton abstraction by the nucleophile in the β-position from either the *endo*-cyclic or *exo*-cyclic methylene units. This however requires aggressive conditions of both highly elevated temperatures and hard nucleophiles. The *N*-phenyl group in NPP was also shown to cause an inhibitory effect on elimination.[26]

Ring-opening is facilitated by attack on the *endo*-methylene within the cyclic onium producing an amino ether or ester group. The driving force for this ring opening is the ring strain, based on this I found 5-memebered ring to be best suited for application as an ionic-reactive moiety. The smaller 4-membered groups have sufficient strain to cause ring opening at temperatures close to room temperature.[30] However, the larger 6-membered rings require higher temperatures to cause reaction both because of reduced ring strain and steric effects due to the equatorial positions of the substituent resulting in

the lowering of the selectivity of the ring-opening reaction over substituent removal or Hofmann elimination.[31]

The goal of this work is to demonstrate the feasibility of ionic-reactive groups for attaching chemicals to surfaces. More specifically, the goal is to synthesize a mono-terminated electrolytic polymer that will utilize self-organization on the surface of materials with unique and complex cross-sections and chemical heterogeneity to achieve: (1) a more homogeneous coverage, (2) increased affinity, exhaustion and fastness, and (3) minimize the amounts of finishing or dyeing material, water and/or energy used during application while also reducing the amount of finishing or dyeing material wasted, decreasing effluents.

4.3 Experimental Section

4.3.1 Materials

All reagents were used as received. Monocarbinol-terminated PDMS (M_n ~ 5.5 kg/mol, 100 cst) was purchased from Gelest. Sodium hydroxide (97%), hydrochloric acid (37%), Poly(4-vinylpyridine) 2 % cross-linked with divinylbenzene, 2 % Cross-linked with divinylbenzene aminomethyl polystyrene 200-400 mesh with an extent of amino labeling: 1.0-2.0 mmol/g loading, Trifluoromethanesulfonic anhydride (99%), methanol (99%), dichloromethane (anhydrous, 99.9%), chloroform, (anhydrous, 99.9%), tetrahydrofuran (anhydrous, 99.9% and HPLC grade, 99.8%) and hexane (HPLC grade, 99.8%) were purchased from Aldrich. *N*-phenyl pyrrolidine (98%) was purchased from Alfa Aesar.

4.3.2 Instrumentation

^{1}H were measured on a Bruker AMX 400 spectrometer in chloroform-*d*. ^{1}H and DOSY NMR spectra were collected with a Bruker DRX 500 in chloroform-*d* as in Chapter 2. Samples for gel permeation chromatography (GPC) were prepared and conducted as in Chapter 2. MALDI-ToF mass spectrometry was carried out as in Chapter 2. ATR-FTIR spectra were obtained using a Bruker Vector 22 spectrometer at room temperature. The optical bench included a PIKE MIRacle™ ATR sampling accessory with a horizontally oriented, single reflection ZnSe ATR crystal.

4.3.3 Synthesis

Glassware was dried at 120 °C overnight. Round-bottom flasks with stir bars were sealed with rubber septa and cooled while evacuating and then backfilling with dry N_2.

Triflation of Monocarbinol-terminated PDMS.

50-mL 2-neck flask with magnetic stir bar, was fitted with a rubber septum and goose-neck under positive nitrogen pressure, the septum was removed and poly(4-vinylpyridine) 2 % cross-linked with divinylbenzene, that had been dried overnight under vacuum at 40 °C (2.0 g, 17 mmol based on the molar mass of vinylpyridine, 2.10 eq) was transferred into the flask. The flask was then evacuated and dichloromethane (10 mL) was charged by cannula. The flask was then backfilled with dry nitrogen gas and left under positive nitrogen pressure. After allowing a minimum amount of time for the solid reagents to fully suspend (typically ~ 2 min), trifluoromethanesulfonic anhydride (2.9 g, 12 mmol, 1.5 eq) then monocarbinol-terminated PDMS (8.0 mmol, 1 eq based on the M_n of the PDMS) were added with syringes as pure components and the mixture was stirred. The solution was stirred for 4 hours after which the solvent was stripped off

under vacuum using a liquid nitrogen trap. The crude product was re-dissolved in 10 ml of hexane or toluene. That mixture was filtered and the liquid filtrate washed with a saturated aqueous solution of sodium bicarbonate (x2). The solution of material in hexane or toluene was dried over magnesium sulfate. The mixture was filtered and the solvent removed by rotary evaporation and further dried under vacuum at 100 mtorr overnight which afforded a clear viscous liquid (yield 100%). ^{1}H NMR ($CDCl_3$): δppm 4.60 (2H, t, TfO-C*H*$_2$-$CH_2OC_3H_6Si$-), 3.72 (2H, t, $TfOCH_2$-C*H*$_2$-OC_3H_6Si-), 3.44 (2H, t, $TfOCH_2CH_2O$-C*H*$_2$-C_2H_4Si-), 2.70 (2H, m, $TfOCH_2CH_2OCH_2$-C*H*$_2$-CH_2Si-), 1.53 (4H, m, -$SiCH_2$-C_2H_4-CH_3), .78 (3H, t, -SiC_3H_6-C*H*$_3$), .44 (4H, t, $TfOC_2H_4OC_2H_4$-C*H*$_2$-$(C_2H_6SiO)_x$-C*H*$_2$-C_3H_7), -.21-.09 (s, -(C_2*H*$_6$SiO)$_x$-). IR: sharp, S=O stretching ~1410 cm^{-1}; sharp, Si-O stretching ~790 cm^{-1}.

Synthesis of N-Phenyl pyrrolidinium functionalized PDMS.

50-mL 2-neck flask was fitted with a condenser, 10-mL powder addition funnel, and goose-neck in series, rubber septum and magnetic stir bar. The flask was evacuated and anhydrous chloroform (10 mL) was charged by cannula. The flask was then backfilled with dry nitrogen gas and left under positive nitrogen pressure. 2% Cross-linked (aminomethyl)polystyrene was added to the powder funnel under positive nitrogen pressure. *N*-phenyl pyrrolidine (1.28 g, 5.0 mmol, 1.2 eq) and mono-triflic terminated PDMS (4 mmol, 1 eq based on the M_n of the PDMS) were added to the flask with syringes as pure components. The flask was brought to reflux and stirred for 24 hrs before adding another aliquot of *N*-phenyl pyrrolidine (1.28 g, 5.0 mmol, 1.2 eq) with a syringe as a pure component. The mixture was allowed to reflux for another 24 hrs before adding the (aminomethyl)polystyrene to the flask via the powder addition funnel.

Once cooled to room temperature, the mixture was filtered using vacuum filtration and the solvent was removed using rotary evaporation. The crude product was further dried under vacuum. Residual NPP was removed vacuum distillation at 120 °C and 100 mtorr overnight which afforded a waxy orange-yellowish solid (yield 96%). ^{1}H NMR ($CDCl_3$): δppm 7.70 (1H, t, NPP; Ar-*para*), 7.60 (2H, d, NPP; Ar-*meta*), 7.54 (2H, d, NPP; Ar-*ortho*), 4.60-4.36 (2H, NPP-C*H*$_2$-$CH_2OC_3H_6Si$-), 4.20-4.00 (4H, NPP; -C*H*$_2$-N-C*H*$_2$-C_2H_4), 3.31 (2H, t, NPP-CH_2-C*H*$_2$-OC_3H_6Si-), 3.19 (2H, t, NPP-CH_2-C*H*$_2$-OC_3H_6Si-), 2.39 (2H, NPP; -$CH_2NC_2H_4$-C*H*$_2$-), 2.14 (2H, NPP; -CH_2NCH_2-C*H*$_2$-CH_2-), 1.53 (4H, m, -$SiCH_2$-C_2H_4-CH_3), .78 (3H, t, -SiC_3H_6-C*H*$_3$), .53 (2H, t, NPP-$C_2H_4OC_2H_4$-C*H*$_2$-Si-), .44 (2H, t, -Si-C*H*$_2$-C_3H_7), -.21-.09 (s, -(C_2H_6SiO)$_x$-). IR: broad, amine N-CH_2 stretching ~2820-2960 cm^{-1}; sharp, phenyl C=C stretching ~1600 cm^{-1}; sharp, Si-O stretching ~790 cm^{-1}.

Application of N-Phenyl pyrrolidinium functionalized PDMS to Cellulose Samples.

Either microcellulose granules or cellophane (.5 g) was placed in a beaker with 50 ml of .3 M solution of NaOH for 15 min. The sample was then washed by constant agitation in THF for 1 min, and then transferred to a beaker with 25 ml of 5 wt. % of NPP-PDMS or monocarbinol-PDMS in THF for 15 min. The samples were then placed in an oven at 75-80 °C for 10 min. The samples are then rinsed with .1 M solution of HCl and distilled water. The samples were then washed with fresh THF in a Soxhlet extractor for 2 hrs. ATR-FTIR: broad, OH stretching ~3630-3015 cm^{-1}; medium, amine N-CH_2 stretching ~2955 cm^{-1}; sharp, Si-O-CH_3 stretching ~1260 cm^{-1}; sharp, Si-O stretching ~790 cm^{-1}.

4.3.4 Reagents and Products

N-Phenyl pyrrolidine

^{1}H NMR ($CDCl_3$): δppm 7.29 (1H, t, Ar-*para*), 6.82 (2H, d, Ar-*meta*), 6.69 (2H, d, Ar-*ortho*), 3.19 (4H, t, -C*H*$_2$-), 2.12 (4H, t, -C*H*$_2$-). IR: broad, amine CH_2 stretching ~2820-2960 cm^{-1}; sharp, phenyl C=C stretching ~1605 cm^{-1}; sharp, aromatic N-C stretching ~1360 cm^{-1}.

Monocarbinol-terminated PDMS

^{1}H NMR ($CDCl_3$): δppm 3.65 (2H, t, HOC*H*$_2$-$CH_2OC_3H_6$Si-), 3.45 (2H, t, $HOCH_2$-C*H*$_2$-OC_3H_6Si-), 3.35 (2H, t, $HOCH_2CH_2O$-C*H*$_2$-C_2H_4Si-), 2.10 (1H, s, *H*-$OC_2H_4OC_3H_6$Si-), 1.53 (4H, m, $SiCH_2$-C_2H_4-CH_3), .78 (3H, t, -SiC_3H_6-C*H*$_3$), .44 (4H, t, $HOC_2H_4OC_2H_4$-C*H*$_2$-$(C_2H_6SiO)_x$-C*H*$_2$-C_3H_7), -.21-.09 (s, -(C_2H_6SiO)$_x$-). IR: broad, free and hydrogen bonded OH stretching ~3200-3800 cm^{-1}; sharp, Si-O-CH_3 stretching ~1260 cm^{-1}; sharp, Si-O stretching ~790 cm^{-1}.

4.4 Results and Discussion

Before performing chemical surface modification of the cellulose materials the ionic-reactive moiety must first be added to the modifying material, which in the case is monocarbinol-terminated PDMS. The general scheme in Scheme 4.2 replaces the carbinol group with a good leaving group then via nucleophilic substitution adds the ionic-reactive moiety. The choice of cyclic onium salt for an ionic-reactive group is fairly important. Considering factors such as tendency of the ionic-reactive group to perform elimination or substituent removal upon covalent fixation, typical processing temperatures, cost and availability, we began work on the use of *N*-phenyl pyrrolidine

(NPP). Aromatic tertiary amines can be poor nucleophiles because of steric and electronic reasons.

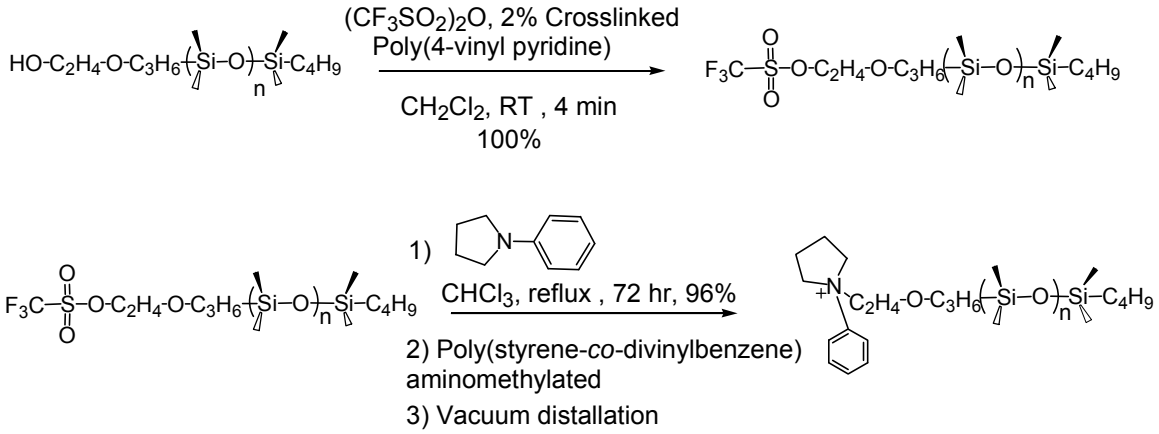

Scheme 4.2. Nucleophilic substitution of a monocarbinol–terminated PDMS that has been modified with triflic anhydride to produce a mono-*N*-phenyl pyrrolidinium functionalized PDMS.

The observed retention times in the GPC traces indicate that the molecular weight of the monocarbinol-terminated PDMS was M_n ~ 5.5 kg/mol, and PDI ~ 1.2. This corresponds to ~ 60 repeat units of dimethylsiloxy groups, which is roughly 90 mol % of the chain. The monocarbinol-terminated PDMS precursor used, is terminated on one end by a butyl group and a on the other end by hydroxyethoxypropyl group.

Diblock copolymer brushes prepared via sequential surface-initiated RAFT polymerization showed contact angle measurement results similar to that of polymer brushes comprised of a homopolymer of the outer layer. They observed this even when the outer layer was less than 40 % of the total thickness of the tethered layer.[34] I initially anticipated that the end-terminated butyl group and the small nature of the precursors used could alter the intended modifying properties of the PDMS. Based on end-to-end distance calculations the butyl group only occupies ~ 4 % of the total thickness of the tethered layer and therefore not likely to dominate the surface coverage unless a tightly

packed structure is formed at the surface. I then concluded a sufficiently large precursor was chosen, containing a high enough percentage of dimethylsiloxy units to dominate the surface characteristics and resolve this matter.

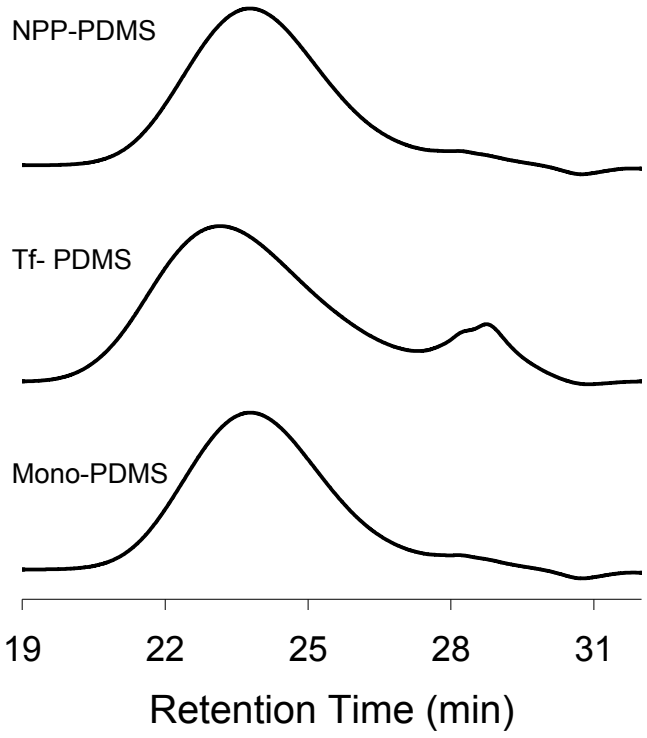

Figure 4.3. GPC traces of the monocarbinol terminated PDMS, triflic and NPP-modified products.

Triflic anhydride is a particularly strong electrophile, useful for introducing trifluoromethanesulfonic leaving groups that are typically used for nucleophilic inactivated systems. Reactions of an alcohol with an acid anhydride produce an acid, in this case triflic acid, considered a "super" acid. By adding crosslinked poly(4-vinyl pyridine) it acts as an acid solid support scavenger, protecting the PDMS from acid-catalyzed chain-chain and ring-chain equilibration. The reaction was monitored by GPC, which demonstrated a slight broadening and shift in retention times from 23.8 min to 23.2

min, corresponding to ~ .7 kg/mol increase in M_n (there is a theoretical ~.15 kg/mol increase in M_n) for the triflic PDMS product as seen in Figure 4.3. The shift to a shorter retention time corresponds to an increase in hydrodynamic volume presumably due to the change in end group. A smaller shoulder peak forms in the GPC trace of the triflic PDMS product and because of its high retention time is attributed to some small molecule impurity, whether that originates as a result of the reaction or from the GPC sample preparation. As the end group is converted to NPP the hydrodynamic volume decreases and the retention time for the purified NPP-functionalized PDMS increases to 23.7 min. This indicates the acid scavenger worked as intended and no depolymerization, cyclization, or major unintended side reactions were present in either step of the end group modification. All reactions proceeds in quantitative yields at room temperature, and complete conversion was confirmed by complete disappearance of the carbinol proton in ^{1}H NMR spectroscopy, as seen in Figure 4.4.

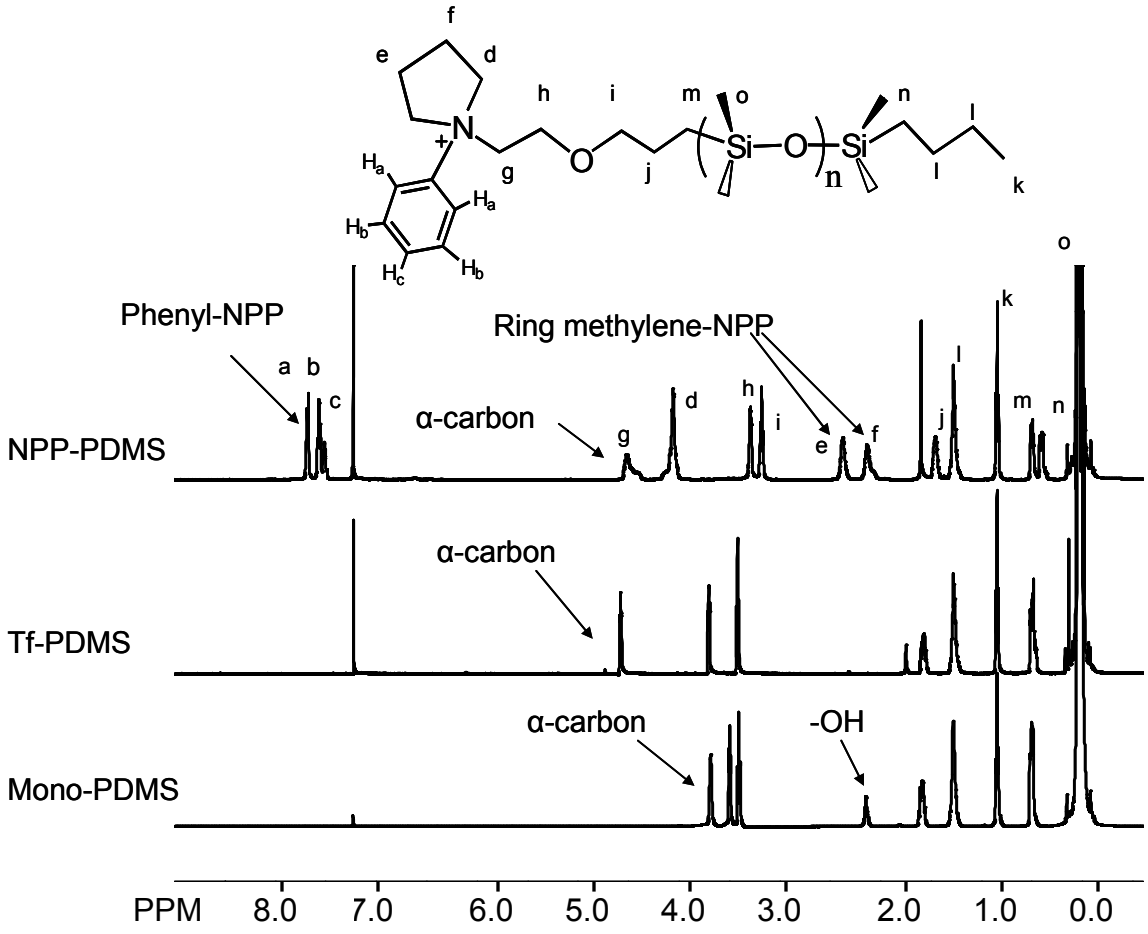

Figure 4.4. ^{1}H spectra of the monocarbinol-terminated PDMS, triflic and NPP modified products. Note the α carbon proton resonance changes, the disappearance of the hydroxyl resonance and the appearance of aromatic and methylene protons belonging to NPP.

Even with the use of the trifluoromethanesulfonyl leaving groups, to get high enough yields to make this useful in a potential industrial application the subsequent reaction of the triflic-terminated PDMS with NPP required refluxing in chloroform for ~ 3 days. A crosslinked polystyrene aminomethylated resin was used as a reagent scavenger to remove any unreacted triflic-terminated PDMS. ^{1}H NMR of the final product, shown in Figure 4.4, indicated a pure product. The chemical shift of the protons on the α carbon to the hydroxyl group show a shift from 4.6 to 4.2 ppm, which was

expected as the positively charged NPP group withdraws less electron density than the trifluoromethanesulfonyl group shifting protons in close proximity upfield.

Incorporation of chemical moieties into larger oligomeric, polymeric or supramolecular structures can be difficult to prove by standard 1D NMR alone since the atoms involved in the linkage are present in such low concentrations their spectral signatures are subsequently of very low intensity. Also, the ^{1}H NMR spectrum of the NPP-terminated PDMS is rather crowded and there is considerable line broadening due to its polymeric nature which typically integrates poorly and is difficult to resolve. We have found in these cases that diffusion-ordered NMR spectroscopy (DOSY) is particularly useful since all of the NMR-active nuclei in the attached moiety may be used to determine whether it is attached to the larger substrate compound. To explicitly ascertain whether the NPP group was being truly being incorporated onto the PDMS chain, ^{1}H DOSY was measured, and is shown in Figure 4.5 (a). The 2D spectrum revealed the same self-diffusion coefficient (-8.15 m^2/s) for the signals due to the methyl protons in the backbone of PDMS at ~ .05 ppm and for those due to the phenyl group in the quaternary amine at ppm > 7, indicating both chemical units belong to the same structure. As further proof in Figure 4.5 (b), an additional 2D DOSY spectrum was obtained for a mixture of *N*-phenyl pyrrolidine and monocarbinol terminated PDMS in chloroform-*d*. The spectrum clearly shows the unreacted NPP and PDMS have different self-diffusion coefficients. Note the chemical shift resulting from the *para*-aromatic protons on NPP overlap the signal from chloroform, causing an averaging of the two diffusion coefficients.

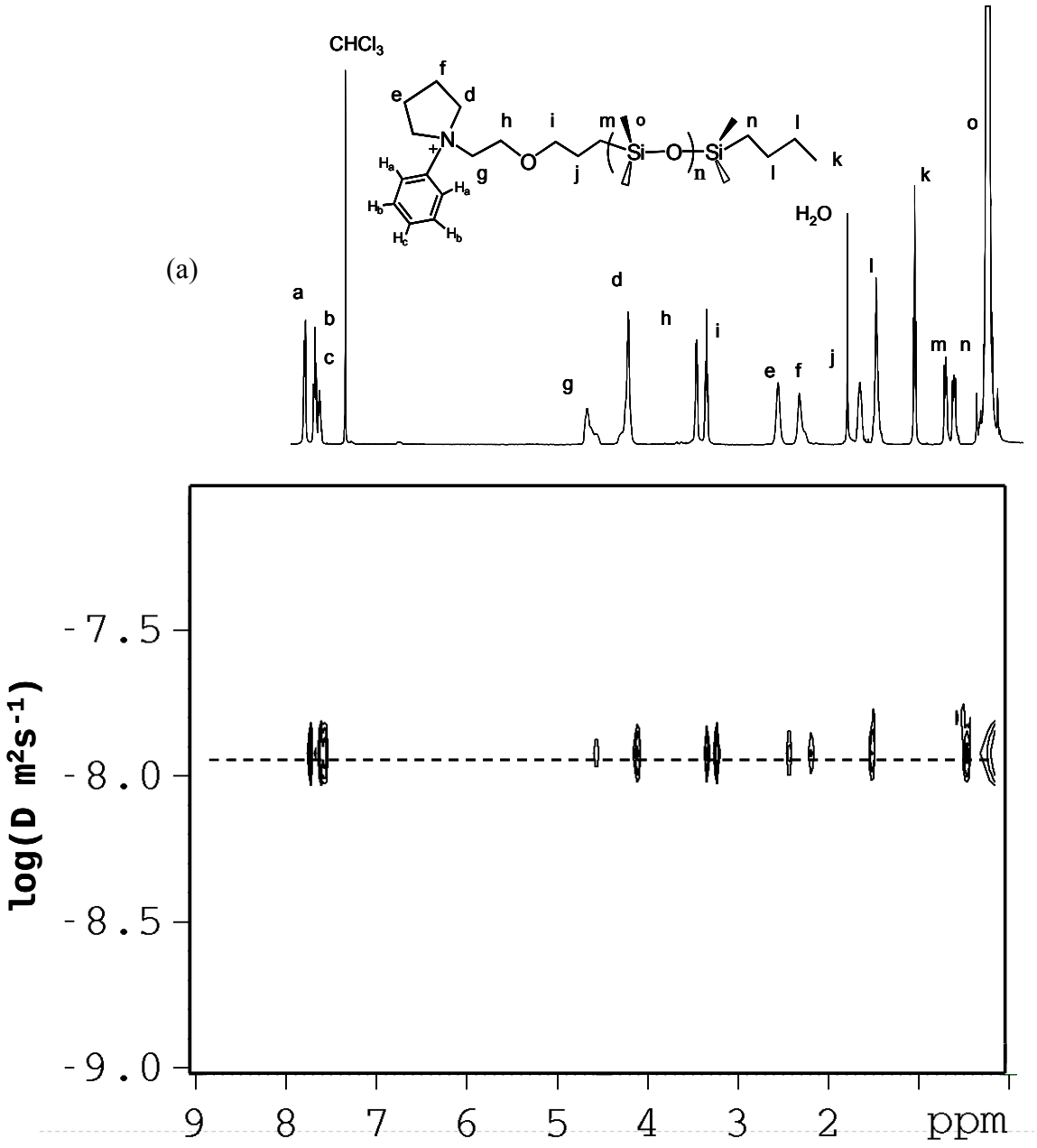
(a)
CHCl3
H2O
a
b
c
d
e
f
g
h
i
j
k
l
m
n
o
-7.5
-8.0
-8.5
-9.0
log(D m2s-1)
9
8
7
6
5
4
3
2
ppm

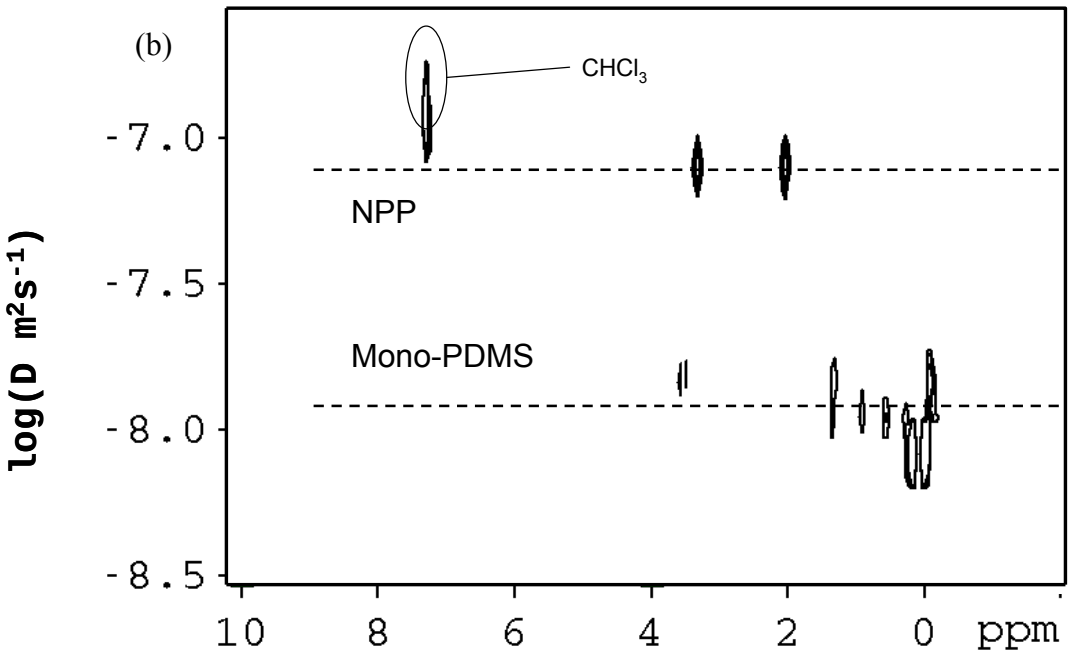

Figure 4.5. ^{1}H DOSY NMR spectrum of (a) mono-*N*-phenyl pyrrolidinium functionalized PDMS and (b) a mixture of *N*-phenyl pyrrolidine and monocarbinol terminated PDMS. Note the chemical shift resulting from the *para*-aromatic protons on NPP overlap the signal from chloroform, causing an averaging of the two diffusion coefficients.

The full MALDI-TOF spectra from which the regions of Figure 4.6 (c) are selected contain the characteristic envelope of peaks representative of a polydisperse synthetic polymer and are seen in Figure 4.6 (a) and (b). The MALDI-TOF spectrum in Figure 4.6 (a) is actually two overlapping distributions, each having peaks separated by 74 amu corresponding to the molar mass of a dimethylsiloxy repeat unit. After peak assignment analysis the major distribution is attributed to the NPP-functionalized PDMS and the other from unreacted triflic-PDMS. The sample was an early functionalization attempt in which the product formed was only subjected to 24 hours of reflux in methylene chloride, leading to only ~ 60 % conversion (by MALDI). The MALDI-TOF spectrum in Figure 4.6 (b) is of a purified product formed after 74 hours of refluxing

triflic-PDMS with NPP in chloroform and the addition of (aminomethyl) polystyrene to the refluxing mixture at 48 hours to remove residual triflic-PDMS, with a gravimetric yield of ~ 96 %. After modification of the synthetic procedure (changing the reaction solvent to chloroform, increasing the reaction time to 48 hours and adding an additional equivalent of NPP after 24 hours) most if not all the triflic-PDMS is probably consumed. However because there are no other simple post-reaction methods to remove residual triflic-PDMS, addition of the aminomethyl polystyrene resin was left in the synthetic procedure to ensure product purity.

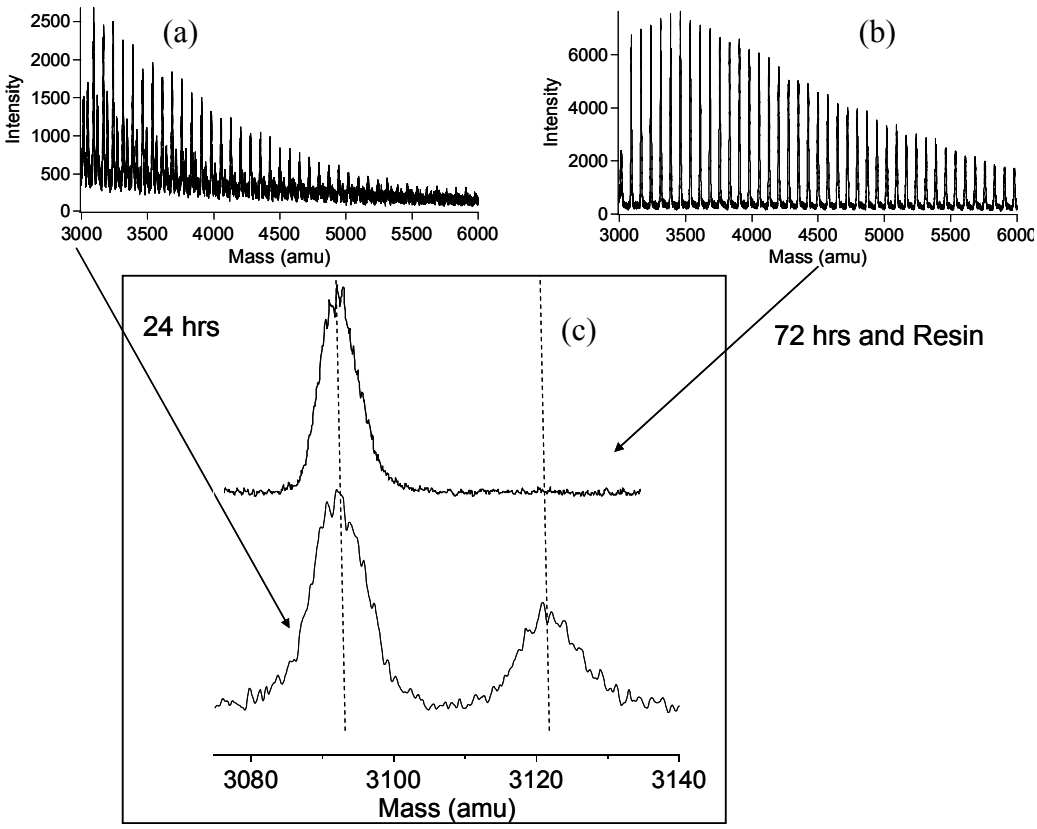

Figure 4.6. (a) MALDI-ToF spectrum of crude product formed after 24 hr of refluxing triflic-PDMS and NPP. (b) MALDI-ToF spectrum of purified product formed after 74 hr of refluxing triflic-PDMS and NPP and addition of aminomethyl polystyrene to remove residual triflic-PDMS. (c) Enlarged and stacked spectra of the purified product (top) and crude product (bottom). Peak to the left: 3092 amu = NPP-PDMS of 37 repeat units. Peak to the right: Triflic-PDMS.

Figure 4.7 shows the FTIR spectrum of the monocarbinol, triflic and NPP-terminated PDMS. IR data in this case are not only useful in proving the exchange of end groups, but also provide critical information about existence and position of adsorption bands for characteristic functional groups which can be used for later analysis of the covalent fixation of the ionic-reactive PDMS onto a cellulosic substrate. The IR spectrum of monocarbinol-terminated PDMS shows two peaks of interest: a broad peak from 3120 to 3770 cm^{-1} representing water, free and hydrogen-bonded hydroxyl end

groups, and a strong absorption band at ~ 790 cm^{-1} representing the stretching mode of the siloxane backbone. The broad hydroxyl peak disappears in the IR spectra of the triflic-terminated PDMS leaving a series of smaller sharper peaks >3400 cm^{-1} mostly likely due to water and isolated hydroxyl groups. The appearance of a peak at ~ 1410 cm^{-1} in the IR spectra of the triflic-terminated PDMS due to a sulfonyl group (S=0 streching) and at ~ 1600 cm^{-1} in the IR spectra of the NPP-terminated PDMS due to C=C stretching in the phenyl group of NPP are both strong indicators the end group structure changed as intended. Lastly, an adsorption band at ~ 2820-2960 cm^{-1} (amine CH_2 stretching), which is typically associated with quaternary amines, developed in the IR spectra of the NPP-terminated PDMS.

.

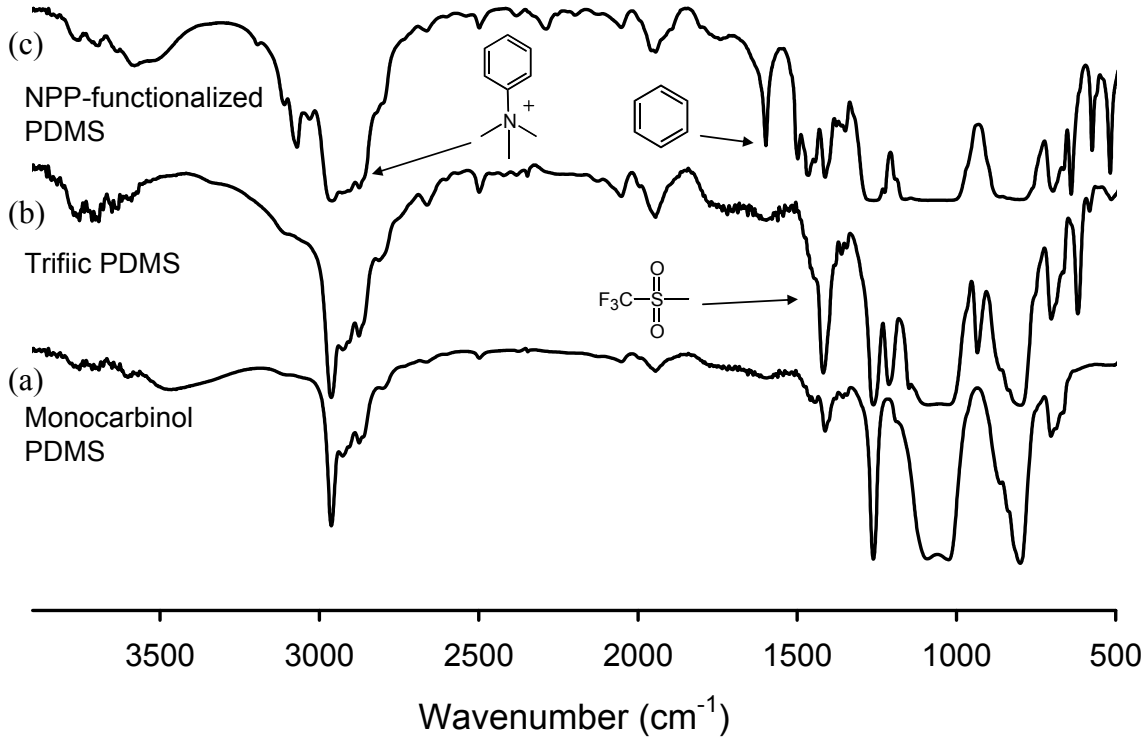

Figure 4.7. FTIR spectra of (a) monocarbinol, (b) triflic and (c) *N*-phenyl pyrrolidinium-functionalized PDMS (liquid on KBr plate).

The aim of the next part of my work was to determine whether the ionic polymer covalently fixes to a cellulosic substrate. To activate the self-assembly process the cellulose was placed in aqueous solution of sodium hydroxide (following a batch processing method) most likely deprotonating the majority of hydroxyl groups on the cellulose backbone near the surface of the film. After exposure to a solution of *N*-phenyl pyrrolidinium functionalized PDMS the cellulose was modified, as seen in Scheme 4.3, by heating in an oven to 80°C, a compromise between the optimal temperature for ring opening of the quaternary ionic-reactive group and the temperature at which surface browning seemingly occurred.

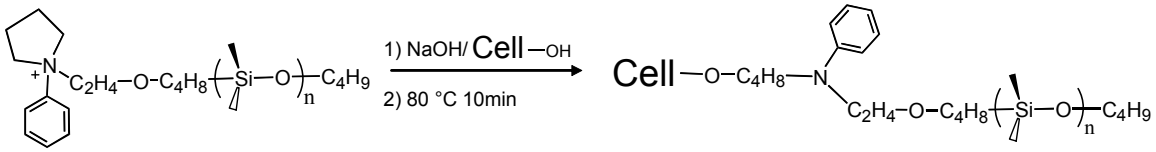

Scheme 4.3. Ring opening of moderately strained quaternary reactive groups with an alkoxide group on the surface of a cellulosic substrate.

A solution of NPP-PDMS was recovered from the batch process and analyzed to determine whether exposure to the deprotonated alkoxide groups on the cellulose or any residual sodium hydroxide had created dead material. NMR showed no major impurity formation and indicated that the solution could be re-used with no loss in reactivity. As further proof of the stability of the quaternary ionic-reactive group, .5 mL of a .3 M NaOH solution in D_2O/THF (80:20) was mixed with a 1 mL 12 wt. % solution of NPP-PDMS in chloroform-*d*. The structure of the NPP-PDMS was monitored by NMR over

48 hours showing no change in the chemical shift for the protons in the pyrrolidinium ring as shown in Figure 4.8.

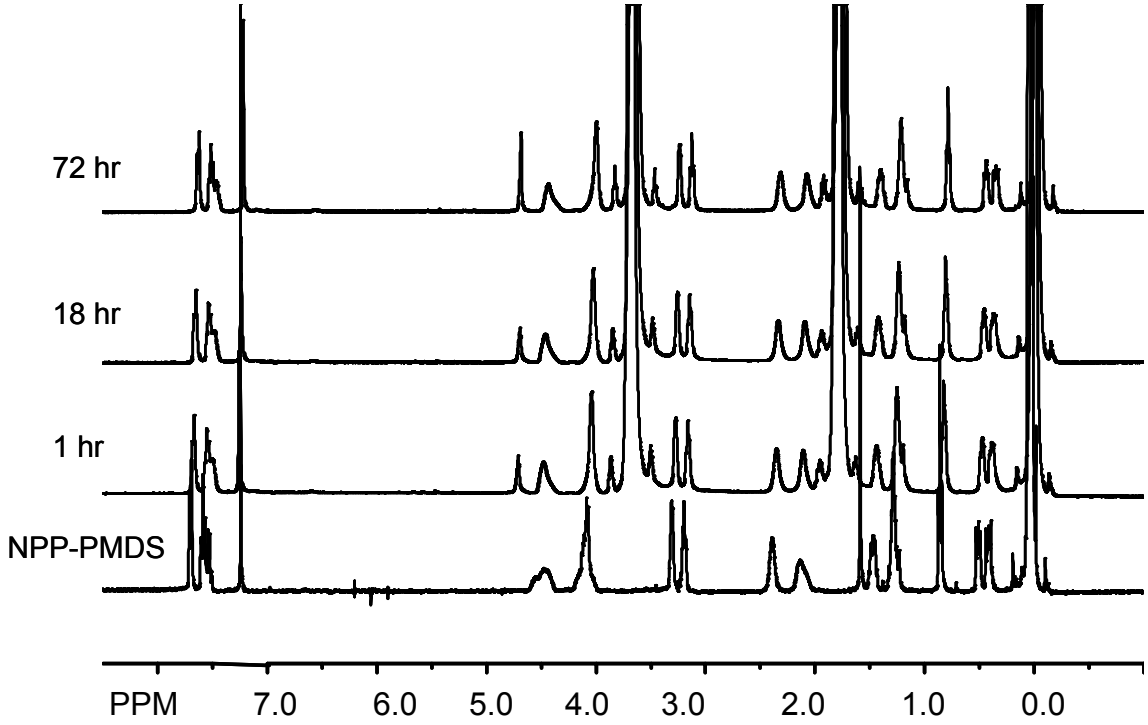

Figure 4.8. ^{1}H spectra of the NPP-terminated PDMS exposure to NaOH solution in D_2O/THF (80:20) in chloroform-*d* as a function of time in hours. Note the α carbon proton resonance at 4.6 ppm, the appearance of aromatic and methylene protons belonging to NPP does not change.

To evaluate the ionic self-assembly and ion-exchange capabilities of the NPP-PDMS, an experiment was conducted in which microcellulose granules were exposed to the NPP-functionalized PDMS without heating to cause covalent fixation. As shown in Figure 4.9, two samples, both having been treated with NPP-functionalized PDMS were made. However one sample was washed in a Soxhlet extractor for 2 hours with THF to remove the adsorbed and ionically bounded material. Figure 4.9 (c) show the disappearance of the characteristic absorption bands around 790 cm^{-1} and 1260 cm^{-1} that correspond to the presence of PDMS on the surface of the microcellulose granules after

washing. Initially, I thought I could use microcellulose granules to quantitatively evaluate surface modification. As evident in the FTIR spectra in Figure 4.9, this was successful to study the ionic self-assembly process; however, the use of particles ~ 20 μm in diameter did not provide enough surface area to show unambiguous changes in spectral intensity for the fixed and washed material. Therefore, from this point on cellophane and ATR-FTIR became the primary substrate and method used repeatedly, to investigate the application of the ionic-reactive finish. Though with this evidence alone verifying ionic assembly (versus adsorption) is difficult, the results still indicate that no reaction happen without heating, and serves to dispel earlier concerns that the strong nucleophile of the alkoxide could trigger unwanted reactions at room temperature.

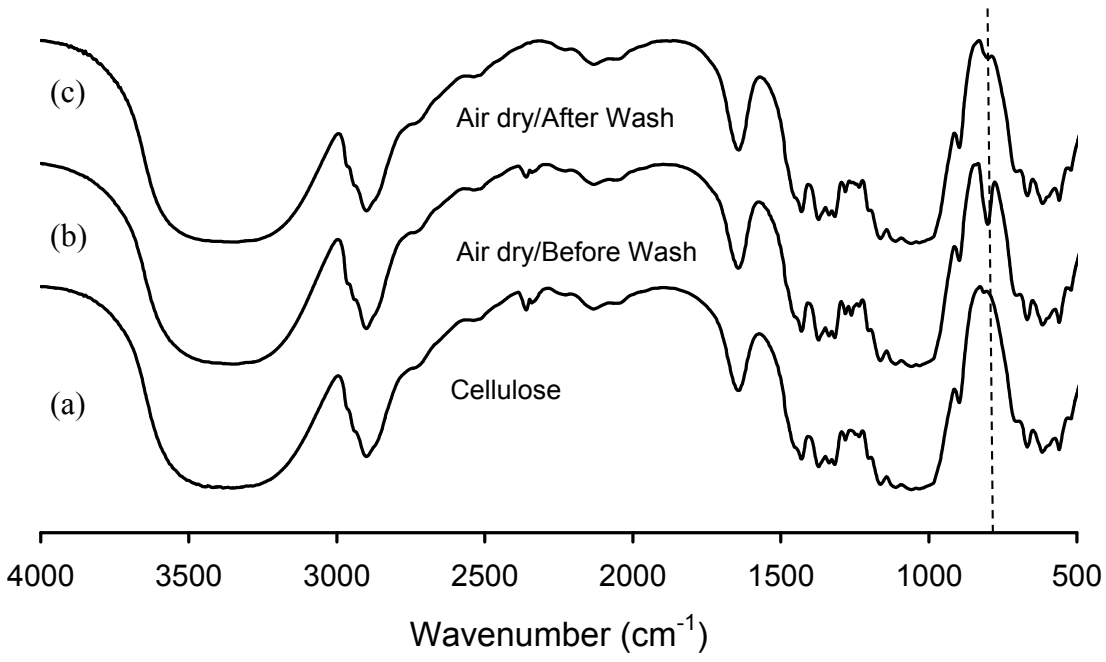

Figure 4.9. FTIR spectra of (a) untreated microcellulose granules, (b) microcellulose granules exposed to functionalized PDMS and air dried and (c) microcellulose granules exposed to functionalized PDMS, air dried and washed in a Soxhlet extractor for 2 hr with THF (15 wt. % in KBr pellet).

A typical ATR-FTIR spectrum of NPP-PDMS modified cellophane is shown in Figure 4.10 (c). The absorption bands around 790 cm^{-1} and 1260 cm^{-1} confirmed the presence of PDMS on the surface of the cellophane. This signal however could be resulting from adsorbed PDMS on the surface of the film that had not been removed by the washing procedure. As a control, cellophane was treated similarly to the sample seen in Figure 4.10 (c); however, monocarbinol-terminated PDMS was used. The control sample seen in the IR spectra in Figure 4.10 (b) is cellophane with only adsorbed PDMS. The spectral changes in Figure 4.9 (b) and (c) indicate that the washing procedure is sufficient to remove adsorbed material; therefore the PDMS in the NPP-PDMS modified cellophane is covalently linked to the surface. Further proof of covalent fixation is a peak at ~ 2955 cm^{-1} that show the formation of the amine linkage resulting from ring-opening of the cyclic onium group.

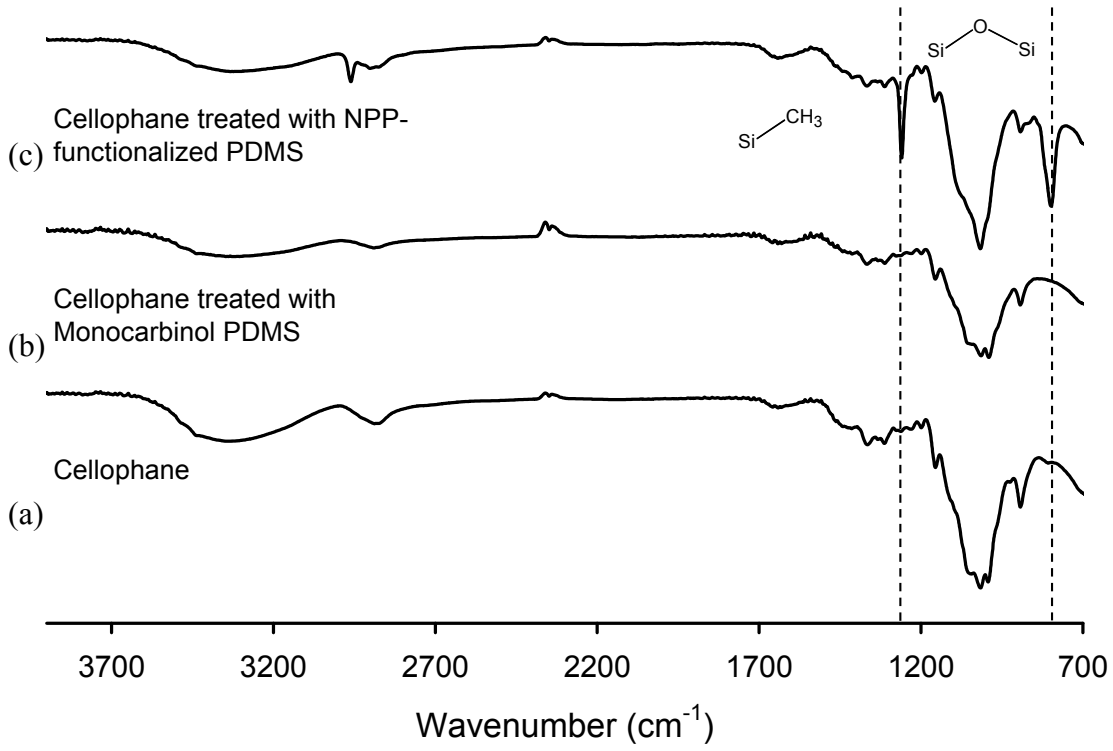

Figure 4.10. ATR-FTIR spectra of (a) untreated cellophane, (b) cellophane with adsorbed PDMS on the surface that was washed in a Soxhlet extractor for 2 hr with THF and (c) cellophane treated with *N*-phenyl pyrrolidinium functionalized PDMS, heated to 80°C to facilitate fixation and washed in a Soxhlet extractor for 2 hr with THF.

I attempted to experimentally verify surface coverage by conducting contact angle measurements on the surface modified cellophane. I chose not to report those data and use it as evidence of surface-modification because the cellophane film during application and fixation of the ionic-reactive finish shrinks causing the formation of a highly rough surface, producing inconsistent results. However upon removal of all outliers the contact angle data seems to at least suggest the surface is silicone rich.

Another key result omitted from this chapter is a study of the exhaustion of the reactive-ionic PDMS versus the control unmodified monocarbinol-terminated PDMS.

This could have been done by evaluating the decrease in NMR signal of a properly formulated application bath, however; time limitation prevented me from performing this experiment.

4.5 Conclusions

Reactive PDMS oligomers were prepared from commercially available monocarbinol-terminated PDMS oligomers and *N*-phenyl pyrrolidine via a triflic intermediate. NMR and MALDI-ToF suggest high yield and purity of the NPP product after exposure to aminomethyl polystyrene resin.

Surface modification of cellulosic substrates has been demonstrated through application of ionic-reactive telechelic PDMS oligomers. FTIR-ATR of microcellulose and cellophane films with adsorbed PDMS on the surface and cellophane films treated with n-phenyl pyrrolidinium functionalized PDMS before and after washing in THF indicate that ionic association of polymer chains at the surface is followed by covalent fixation upon heating.

4.6 References

9. Nath, N., *Adv. Mater,* **2002,** 14, 17.

10. Currie, E.; Norde, W.; Stuart, M., *Advances in Colloid and Interface Science* **2003** 100 –102 205–265.

11. Zhao, B.; Brittain, W., *Prog. Polym. Sci.* **2000,** 25, 677–710.

12. Ratner, B., *Journal of Molecular Recognition* **1996,** 9, 617-625

13. Brittain, W.; Mink, S., *J. Polym. Sci. Part A: Polym. Chem.* **2007,** 45, 3505.

14. Kishida, A.; Mishima, K.; Konishi, H.; Ikada, Y., *Biomaterials* **1992,** 13, (2), 113-120.

15. Felix, J.; Gatenholm, P., *Journal of Applied Polymer Science* **1991,** 42, 609-620.

16. Zajac, R., *Physical review. E* **1995,** 52, (6), 6536 -6549.

17. Zajac, R., *Physical review. E* **1994,** 49, (4), 3096.

18. Smith, G.; Zhang, Y.; Bedrov, D.; Dadmun, M.; Huang, Z., *Langmuir* **2006,** 22, 664-675.

19. Titmuss, S.; Briscoe, W.; Klein, J., *Journal of Chemical Physics* **2004,** 121, (22), 11408 -11419.

20. Huang, Z.; Ji, H.; Mays, J.; Dadmun, M, *Macromolecules* **2008,** 41, 1009-1018.

21. Hauser, P.; Tabba, A., *Color. Technol.* **2001,** 117, 282-288.

22. Hyde, K.; Rusa, M.; Hinestroza, J., *Nanotechnology* **2005,** 16 S422–S428.

23. Hsieh, M.; Farris, R.; McCarthy, T., *Macromolecules* **1997,** 30, 8453-8458.

24. Tezuka, Y.; Hayashi, S., *Macromolecules* **1995,** 28, 3038.

25. Tezuka, Y.; Iwase, T.; Shiomi, T., *Macromolecules* **1997,** 30, 5220-5226.

26. Tezuka, Y.; Oike, H., *Macromol. Rapid Commun.* **2001,** 22, 1017-1029.

27. Tezuka, Y.; Shida, T.; Shiomi, T.; Imai, K.; Goethals, E., *Macromolecules* **1993,** 26, 575-580.

28. Oike, H.; Mouri, T.; Tezuka, Y., *Macromolecules* **1999,** 32, 4819-4825.

29. Oike, H.; Mouri, T.; Tezuka, Y., *Macromolecules* **2001,** 34, 6592-6600.

30. Ceriche, G.; Luchetti, L., *Tetrahedron* **1993,** 49, (46), 10733-10738.

31. Cerichelli, G.; Illuminati, G.; Lillocci, C., *J. Org. Chem.* **1980,** 45 3952-3957.

32. Cospito, G.; Illuminati, G.; Lillocci, C.; Petride, H., *J. Org. Chem.* **1981,** 46 2944-2947.

33. Illuminati, G.; Lillocci, C., *J. Org. Chem.* **1977** 42, (13), 2201.

34. Boyes, S.; Granville, A.; Baum, M.; Akgun, B.; Mirous, B; Brittain, W., *Surface Science* **2004,** 570, (1-2), 1-12.

II. Dynamics of Poly(vinyl acetate)/Silica Nanocomposites with Poly(dimethyl siloxane) Surface Treatments

CHAPTER 5

Dynamics of Poly(vinyl acetate)/Silica Nanocomposites

5.1 Abstract

Chain dynamics in poly(vinyl acetate)/silica nanocomposites with particular interest at the matrix/filler interface were examined with solid-state NMR. Nanocomposites containing 12.5 vol. % filler were studied with ^{1}H T_2 relaxation measurements, 2D ^{13}C exchange and ^{1}H spin diffusion experiments. T_2 relaxation data, which can be used to describe chain molecular motion, was measured at temperatures between 45 and 130 °C and found to be non-exponential in nature. They were analyzed using a Kohlrausch-Williams-Watts function, commonly associated with a spatially heterogeneous distribution of correlation times. At 90 °C, which is approximately 45 °C above the calorimetric T_g, the sample containing the silica nano-fillers had a wider distribution of T_2 relaxation times with a shorter characteristic T_2 relaxation time. 2D exchange experiments were conducted at 55 °C to monitor motions of the side-group carbonyl in the 1 – 10 kHz range. 2D data were recorded for a series of mixing times and a correlation function for carbonyl-group re-orientation was extracted. This analysis revealed a broad distribution of correlation times for both the nanocomposite and the pure poly(vinyl acetate); however, while both materials are characterized by the same average correlation time, the nanocomposite exhibits a wider distribution of correlation times. The spin diffusion experiment verified the presence of different regions of chain mobility in the filled sample, where the "mobile" region has an effective diameter of ~ 27 nm.

The data from all these NMR experiments indicate the chains located in the nanocomposite have on average slower dynamics compared with those in the neat sample. The spin diffusion data in particular imply this is related to restricted chain dynamics near the nano-filler or at the interface/interphase. This physical interpretation of the polymer structure along with previous work done on this nanocomposite system seemingly supports the argument that this effect on the chains near the nano-filler extends throughout the bulk sample.

5.2 Introduction

Since the early 1980's when the term "nanocomposite" was coined, nanoscale inorganic fillers were added to thermoplastic and thermoset polymeric material to form composites.[1] The addition of these nano-fillers considerably improves properties of the matrix polymer including tensile strength, heat distortion temperature, and modulus when compared to neat systems or composites prepared with micro-sized particles.[2-5] A large area of continued interest lies with the synthesis, characteristics and applications of nanocomposites, which are defined by the particle size of the dispersed phase (diameter $\leq$ 100 nm).[6] It is widely accepted that the enhanced performance seen in these nanocomposite systems are related to the high surface-to-volume ratio of a nanoparticle. However, at this nano-scale a consensus about the mechanisms of reinforcement, polymer structure and dynamics of the polymeric matrix particularly near the filler-matrix interface has yet to be developed.

Most of the improved mechanical properties in these nano-filled polymer systems can be directly correlated with a dramatic increase in shear and dynamic modulus.[7-9]

These materials not only display elastic reinforcement but also have demonstrated non-linear dynamic mechanical properties, very similar to the viscoelastic behavior of filled cross-linked or amorphous elastomers, rarely seen in most other types of polymer systems. Specifically poly(vinyl acetate) (PVAc)/silica nanocomposites above the glass transition temperature have been shown to have a higher storage and loss modulus than neat PVAc.[10-12]

Also, in the study above as the strain amplitude was increased the dynamic storage modulus decreased in a non-linear fashion for the nano-filled PVAc samples.[10-12] The authors compare this phenomenon to the similar viscoelastic behavior seen in rubbers filled with carbon black and refer to it as the Payne effect. A. R. Payne, first noted the stress-strain behavior of rubbers with varying strain amplitude. Rubber compounds, particularly ones filled with carbon black, demonstrated a dependence of the elastic modulus on the strain amplitude. At small strain amplitudes, an increase in strain amplitude corresponds to a decrease in elastic modulus. However, when the strain amplitudes became sufficiently large the elastic modulus rapidly drops in a non-linear manner to a lower limit.[13]

The effect of filler volume fraction, filler surface chemistry and filler size has been studied in many composite systems. Elastic reinforcement in microcomposites has been described by several theories, particularly based on mechanical percolation and agglomeration. Agglomeration relies on weak particle agglomerate formation. In high enough concentrations and particularly in hydrophobic environments, silica fillers have been observed performing particle floccuation that can lead to the formation of interparticle networks primarily because of hydrogen bonding at the hydroxyl groups on

the silica surfaces.[4,14-16] Excluding the formation of macroscopic domains, the interparticle networks create a microstructure for filler networking. Upon deformation, particle-particle slippage or friction as particles contact one another and reorientate act as a damping mechanism absorbing energy, causing subsequently an increase in the elastic reinforcement.

Though not probed in this study the observed non-linear dynamic mechanical properties and the subsequent modulus recovery when strain amplitudes are returned to low levels must also be accounted for in any proposed theory describing the elastic reinforcement in these systems. Weak arguments pertaining to filler-matrix and particle-particle bonding and de-bonding at high strain amplitudes could be made to explain the non-linear dynamic mechanical phenomena. However these theories are difficult to substantiate experimentally, because there exist very few techniques that can directly and selectively probe the interfacial interactions of the matrix and/or the filler-matrix interface particularly during a shear event.

On the other hand according to percolation theory, filler particles are randomly dispersed in a polymer matrix and reinforcement is mainly attributed to non-specific filler-matrix interactions.[8] Essentially, during a stressing event on a polymer composite, stress concentrations in regions near the filler-matrix interface cause a plane strain/plane stress transition leading to shear yielding or irreversible shear deformation of the polymer matrix in the very localized domains. Those stress concentration regions can be considered as a "shell" around the particle with some volume defining the thickness of interparticle matrix ligaments. If the volume in-between the particles is less than or equal to the volume formed by the "shell", then a percolation threshold is reached, a percolation

pathway is formed and the shear yielding process can propagate over the entire matrix in the deformation zone. Beyond this percolation threshold or critical thickness of interparticle matrix ligament values this shear yielding process becomes an efficient energy absorbing mechanism causing a significant and abrupt increase in elastic reinforcement.[8]

The original work detailing mechanical percolation by Wu was done on nylon modified by the addition of elastomeric particles. When the percolation concentration of rubber particles in the nylon matrix was reached the composite system showed a sudden transition (the primary characteristic defining percolation) from brittle to tough behavior.[8,17] Mathematically the critical interparticle matrix thickness, ε_c, was described by:

$$\varepsilon_c = d\left[\gamma\left(\frac{\pi}{6\phi_c}\right)^{\frac{1}{3}} - 1\right] \qquad \text{Eq. 5.1}$$

where is the *d* represents the particle diameter, Φ_c the percolation volume fraction and β is a geometric constant that depends on the packing of the particles ($\gamma = 1.0$ for a cubic lattice geometry). Routinely, references can be found contributing elastic reinforcement in polymer nanocomposites solely to percolation at volume fractions as low as 1-3 %.[18-21] Though the observed additional reinforcement is real, for the reinforcement to be due only to percolation at a filler volume fraction as low as 1 % and particle diameter of 27 nm, the interparticle matrix thickness would have to be ~ 90 nm, as calculated by Eq. 5.1. This seems highly unlikely considering the formation of an interface/interphase is a localized phenomenon, with a length scale typically characterized by the matrix's radius of gyration.[22,23] The calculated critical interparticle matrix thickness of 90 nm would

then correspond to more than 10 times the R_g of most polymers with a molecular weight under 100 kg/mol. Therefore, mechanical percolation as described earlier as the major or sole mechanism for reinforcement in the hypothetical nanocomposite system above is unlikely. Also more importantly, in no way does percolation explain the observed Payne effect (non-linear dynamic behavior).

The PVAc/silica nanocomposites investigated in this study show additional dynamic mechanical properties that can not be straightforwardly or exclusively explained by classical micromechanical descriptions, percolation or particle agglomeration. S. S. Sternstein et al. have shown in previous dynamic mechanical studies on the same PVAc/silica nanocomposite system, that observed reinforcement is much higher than can be calculated using a mixing analysis, such as predicted by the Guth-Gold theory (in which the change in elastic modulus scales as an polynomial of the filler fraction).[12,24 25] In this case, the fact that the filler fraction is much lower than in other similar microcomposite materials and the Payne effect is observed again make the established mechanical percolation in the matrix unlikely or minor.[12]

In the initial papers by S. S. Sternstein et al., mainly based on SEM data, particle network formation was completely rejected as a mechanism for elastic reinforcement and the observed Payne effect.[11,12] However, subsequent small-angle scattering (SAXS) experiments carried out on the PVAc/silica nanocomposite indicate considerable silica particle aggregation. They found the aggregates formed in a hierarchical structure where the smallest aggregates of silica particles were on the order of ~ 40 nm (particle diameter ~ 27 nm). The second level or next largest clustering of silica particle in the PVAc matrix showed polydispersed aggregates similar to mass-fractal objects while even larger

agglomerates were detected forming in the third level. As the concentration of particle in the composite was increased, the number, size and size polydispersity of the aggregates increased. By studying these systems as a function of filler fraction and filler surface chemistry (changing the propensity of aggregate formation) it was determined that not only increased aggregate size but also size polydispersity of the aggregate decreases polymer reinforcement.[26] The authors then suggested that particularly at lower filler fractions a combination of filler aggregation and filler-matrix interactions lead to reinforcement. Though they also content that aggregation can not explain the identical dynamic mechanical behavior of filled samples when subjected to different amounts of static strain offset or prestretching (considering the particle aggregate microstructure and subsequent response to dynamic stress should change upon stretching). The dynamics of these systems are clearly very complicated with many open questions.

Many of the same experimental conclusions and results by Sternstein were also seen by Kalfus in PVAc/hydroxylapatite (HA) nanocomposite systems.[23] The similar nature of the PVAc/HA and PVAc/silica systems with respect to surface chemistry and filler-matrix interactions make Kalfus' conclusions even more relevant. Which support the conclusions to be made in this chapter and what will be referred to as the additional "entanglement" model for the description of the viscoelastic response of a composite system. In this case, they also found increased elastic reinforcement compared to the neat PVAc and non-linear dynamic mechanical properties. However, unlike Sternstein's study their work centered on elastic modulus recovery. After subjecting the PVAc/HA nanocomposite to high strain amplitude dynamic stress, the time it took to recover the original storage modulus was deemed the storage modulus recovery time. Using the

reptation model, commonly associated with the chain dynamics in a polymer melt, and an idealized structure of an adsorbed chain, a theoretical treatment was constructed describing the viscoelastic response of the immobilized adsorbed chains at the filler-matrix interface and in the interphase. It was found that the storage modulus recovery time was solely dependent on the chain dynamics of the interphase instead of filler or particle network rearrangement.[22,23]

Using dynamic rheological experiments the silica filler was found to significantly affect both energy dissipation and elastic reinforcement within the PVAc matrix, resulting in an unexpected conclusion where the nano-filler restricted chain mobility not only in the local domains surrounding the nano-filler but also modifying the more global polymer matrix dynamics.[10-12] In the above mentioned studies on the PVAc/nano-silica system Sternstein then proposed a third mechanism for reinforcement, where enthalpic and topological filler-matrix interactions act as additional "entanglements" in the polymer matrix causing both short- and long-range effects in the motion of the matrix polymer chains, which is precisely the type of dynamics that can be probed by NMR.[27-32] The nature of this proposed mechanism could account for some of the discrepancies in the literature pertaining to percolation in nanocomposites. When enough filler is added to the matrix these far-field effects in the motion of the matrix polymer chains could dominate the matrix, producing a percolation-like condition. In the low concentration range studied here the silica nanoparticles will primarily only form interfacial bonds with the polymer matrix. This interfacial interaction is amplified in nanocomposites since the total surface area of the particles is very large. Therefore, the filler-matrix interface and interphase dynamics greatly affects the overall dynamics of the bulk material.[33]

Supporting the proposed third mechanism are studies on how the energetics of filler-matrix adhesion effects the rheological properties of silica-filled composites.[34,35] Suggesting that particle size, filler fraction, and surface chemistry affect the size of the filler-matrix interphase and the friction experienced between that and the bulk polymer matrix. Although the authors do not attribute this "friction" to chain entanglements and mention nothing of affecting the global dynamics of the matrix, the work provides insight to how important this interfacial bonding is to the local and bulk dynamics. Furthermore, the same studies suggest that the work of adhesion (W_a) determined by dynamic viscosity is not only material dependent but also a function of testing conditions. If testing amplitude and frequency affects impact the W_a value, then perhaps similar affects are included in the release mechanism of bond chains from the filler surface and interphase at high dynamic loading. This release mechanism could be used to explain the non-linear reduction in dynamic storage modulus with increasing strain amplitude.

More relevant work in the field of NMR by Blum et al. indicates the presence heterogeneous segmental mobility by deuterium line-shapes in a deuterated sample of poly(methyl acrylate) (PMA) adsorbed on silica particles.[29-31] It was concluded that chains near the surface of the silica show a wide distribution of mobilities that are slower than the motion of the chain observed in the bulk and at the polymer-air interface. The distribution of mobilities at the surface of the silica was then attributed to structures such as adsorbed loops, free tails and tethered chain segments.[29] Similar deuterium NMR studies were conducted by the same investigators on deuterated sample of PMA adsorbed on silica particles where an overlayer of PMA was subsequently adsorbed to study polymers chain "sandwiched" between a silica surface and a polymer layer. In this case,

it was found the polymer overlayer further reduced the dynamics of the bound polymer at the surface of silica.[29-31] These conclusions on the polymer dynamics near the silica-polymer and polymer-overlayer interface are seemingly supported by studies conducted on the T_g of thin films cast on silica supports.[36,37] The major implication of these conclusions show NMR as an effective method to investigate the chain dynamics in a composite system. However, more importantly now there is evidence describing how a polymer chain whose chemical structure is very similar to PVAc behaves on the surface of a silica particle, establishing a probable mechanism by-which entanglements could form. This information along with additional NMR studies can be used to build a more extensive model of the morphology of the interface and bulk matrix chains in PVAc/silica nanocomposites.

In this chapter, chain dynamics in PVAc/silica nanocomposites were examined with solid-state NMR above the T_g as though it was a filled elastomer in which additional reinforcement is achieved by modifying the entanglement density. Also, dynamic mechanical measurements were performed and all data were analyzed using the proposed structure of the filled samples in Figure 5.. The goals being two-fold: (1) through a series of solid-state NMR experiments to gain insight into the mechanism by which fumed silica nano-fillers affect polymer structure and dynamics for reinforcement of nanocomposites. (2) Then to use the data from both techniques to establish a mechanism and describe a physical interpretation by which reinforcement is achieved in a PVAc/silica nanocomposite. Nanocomposites containing 12.5 vol. % nano-filler were studied with ^1H T_2 relaxation measurements, ^1H spin diffusion and 2D ^{13}C exchange experiments.

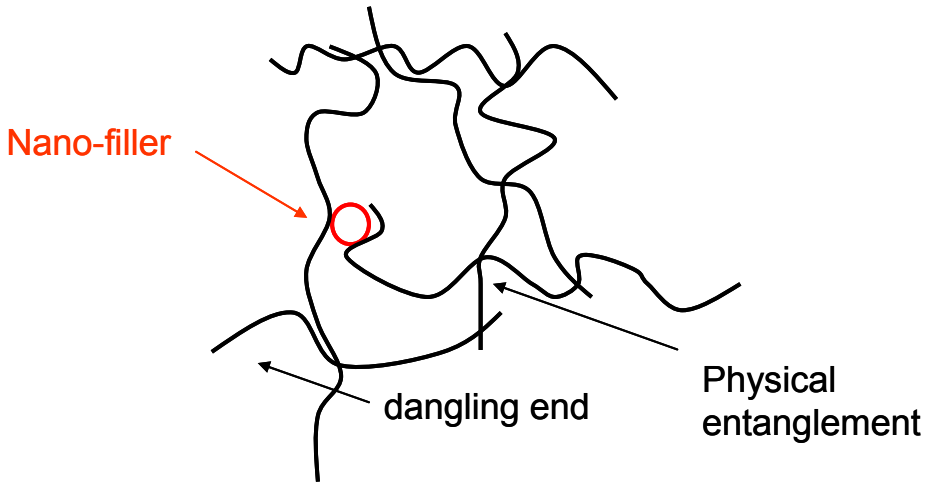

Figure 5.1. Schematic of the filled system

5.3 Experimental Section

5.3.1 Materials

Amorphous PVAc (purchased from Aldrich) with a weight-average molecular weight of 83 kg/mol was used. The sample showed a T_g of ~ 42 °C measure by DSC. The polymer was obtained from Aldrich. The silica nano-filler was MP-5 fumed silica which was obtained from Cabot. Two samples were prepared: one sample of neat PVAc, the other contained 12 % by weight of fumed silica with a specific surface area of approximately 200 m^2/g. The silica was used as received and possessed a non-surface-modified functionality presumably of hydroxyl groups.

5.3.2 Instrumentation

Differential scanning calorimetry was performed on a Seiko Instruments DSC 220C under nitrogen purge on samples weighing 10 – 15 mg sealed in aluminum pans heated at a rate of 10 °C/min. Thermogravimetric thermograms were performed on a

Seiko Instruments TG/DTA 320 under nitrogen purge on samples weighing 10 – 15 mg in aluminum or platinum pans heated at a rate of 10 °C/min.

Dynamic light scattering in acetone was conducted with a Wyatt Technologies DAWN EOS light scattering detector equipped with a quasielastic light scattering autocorrelator.

Solid-State NMR Measurements

NMR samples were prepared by loading both the neat and filled PVAc into 7-mm cylindrical ceramic MAS rotors. Repetitive steps of packing sample and heating the rotor were conducted to fully compress and load the maximum amount of sample. All solid-state NMR measurements were carried out on a Bruker DSX-300 spectrometer in a Bruker double-resonance MAS probehead at spinning speeds of 5 kHz. 32 scans were collected for ^{1}H T_2 measurements. ^{1}H T_2 experiments were measured at temperatures between 45-130°C with a Hahn spin-echo sequence[58] as seen in Figure 5.7 (a) for temperatures below 60 °C and a Carr-Purcell-Meiboom-Gill[59] sequence as seen in Figure 5.7 (b) for temperatures above 60 °C to minimize line-broadening due to increased thermally driven diffusive chain motions that amplify the B_o inhomogeneities. Both sequences used recycle delays of 5 s, ^{1}H 90 ° pulse lengths of 5 μs, ^{1}H 180 ° pulse lengths of 10 μs. The echo times (τ) for the HE sequence were varied exponentially where τ = 20-5000 μs. The echo times (τ) for the HE sequence were varied exponentially where D = 50 μs and *n* = 2-400 . For ^{13}C two-dimensional exchange spectra, standard cross-polarization (CP) pulse techniques were used with ^{1}H 90 ° pulse lengths of 5 μs and a contact pulse length of 3000 μs. The evolution time t_1 increment was 2 * dwell time (DW=7.01 μs) and the mixing time t_m was set at 1, 10, 20, or 100 ms as seen in Figure

5.12.[48] Number of scans ranged from 32-128, depending on the mixing time and had recycle delays of 5 s. For ^{1}H spin diffusion, a 300 μs Goldman-Shen filter was used to select to mobile region of the polymer matrix and magnetization was then allowed to diffuse over mixing times of t_m= 1-1000 ms as seen in Figure 5.18 (b).[49] The temperature in the probe is based on the variation of the ^{207}Pb spectrum of a sample of lead nitrate and is calibrated relative to literature data on its isotropic shift.[60]

T_1^H affects were eliminated by repeating the experiment with a 3 μs Goldman-Shen filter, and normalizing the intensity by $I_{300\ \mu s}(t_m)/\ I_{3\ \mu s}(t_m)$.[49] 1 k scans were collected for ^{1}H spin diffusion NMR measurements with recycle delays of 5 s. In spin diffusion experiments the reduction of intensity versus mixing time provides information about magnetization exchange rate between mobile and rigid regions, T_1^H relaxation during the mixing time can bias these results. Since any experiment of the same mixing time experiences the same T_1^H relaxation the ratio between intensities from an experiment with a 300 μs filter and a 3 μs filter was taken to eliminate T_1^H effects in the spin diffusion data while retaining the spin diffusion character. As a consequence no good data could be obtained at long mixing times. Most of the signal is lost due to the filter and even more attenuation occurs during the mixing time, so at long mixing times the ratio was a result of two intensities with a relatively large uncertainty. Essentially, the resulting ratio has twice the relative error and becomes extremely unreliable data points, at times appearing random with respect to the spin diffusion curve.

Two-dimensional wide-line separation (2D WISE) spectra were collected with a contact time of 100 μs and a recycle delay of 10s. 128 t_1 increments of 4 μs were

measured for spectral widths of 125 kHz in the ^{1}H dimension. The number of scans collected was 512.

5.4 Result and Discussion

5.4.1 Dynamic Light Scattering

Dynamic light scattering was preformed on the silica nanoparticle with the intention of characterizing the filler size and aggregative behavior. The particle size distribution of the silica nanoparticles from DLS after dispersion and sonication in acetone is in good agreement with the results obtained by Sternstein from the size distribution analysis of SAXS data. The major particle radius distribution, seen in Figure 5.1 for the silica nanoparticles, ranges from 49 to 306 nm with a peak maximum at 105 nm (SAXS data for the 2.5 vol. % silica/PVAc composite suggests the radius for smallest of particle cluster in the matrix to be 100 nm). There are two other peaks, one representing a single particle with a mean radius of 14.2 nm (or a particle diameter of 28.4 nm), which matches data belonging to the first level of particle cluster hierarchy and the manufacturer quoted particle diameter of 18 and 27 nm respectively.[b] The second peak corresponds to larger aggregates with a hydrodynamic radius around 12200 nm. Therefore, by comparison with published SAXS data it is reasonable to assume the particle size distribution seen in Figure 5.1 somewhat reflects the nature of aggregation and the particle dispersion within the nanocomposite also.

[b] The silica nano-filler used was the MP-5 fumed silica with no surface treatment obtained from Cabot. The manufacture list the specific surface area obtained from nitrogen adsorption and BET analysis as 200 m^2/g, which corresponds to a particle diameter of ~27 nm.

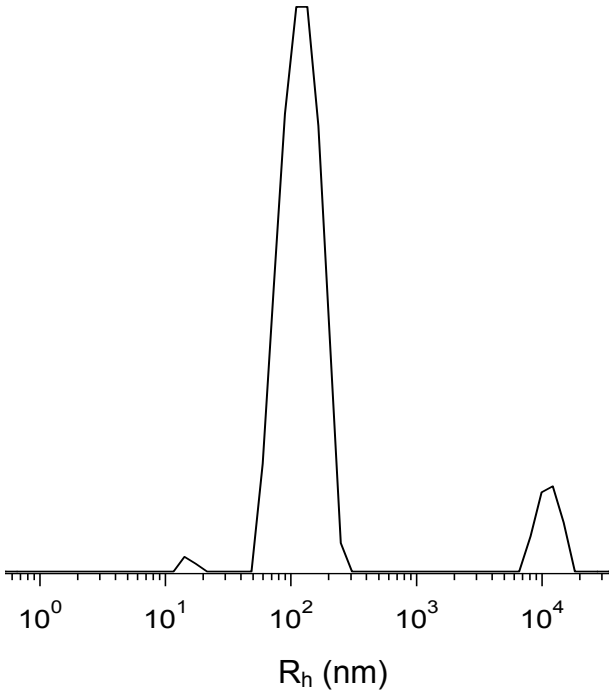

Figure 5.2. Hydrodynamic radius distribution of silica nanoparticles and their aggregates after dispersion and sonication in dilute acetone solution at 25 °C from dynamic light scattering.

5.4.2 Thermal Analysis

Figure 5.3 shows the DSC thermograms for neat PVAc and the filled PVAc nanocomposite in an inert N_2 atmosphere. No melting endotherms were present which was expected as the PVAc is completely amorphous. The glass transition temperatures observed showed a slightly higher T_g for the nanocomposite, and is ~ 2 °C higher than the T_g for the neat sample which displayed a T_g at 42 °C. 42 °C will serve as a benchmark temperature at which the dynamics and any differences in the dynamics of the systems increase, and therefore most of the NMR experiments will be run above that temperature. Though the increase in transition temperature is small and just inside the typical variability we report for the instrument (± 2 °C), repeated heating cycles indicate the difference statistically significant. This suggests some change in the mobility of the

bulk sample due to the addition of the nanoparticles. This effect is more dramatic in rheological measurements collected by Sternstein; however this is what this chapter will attempt to probe.

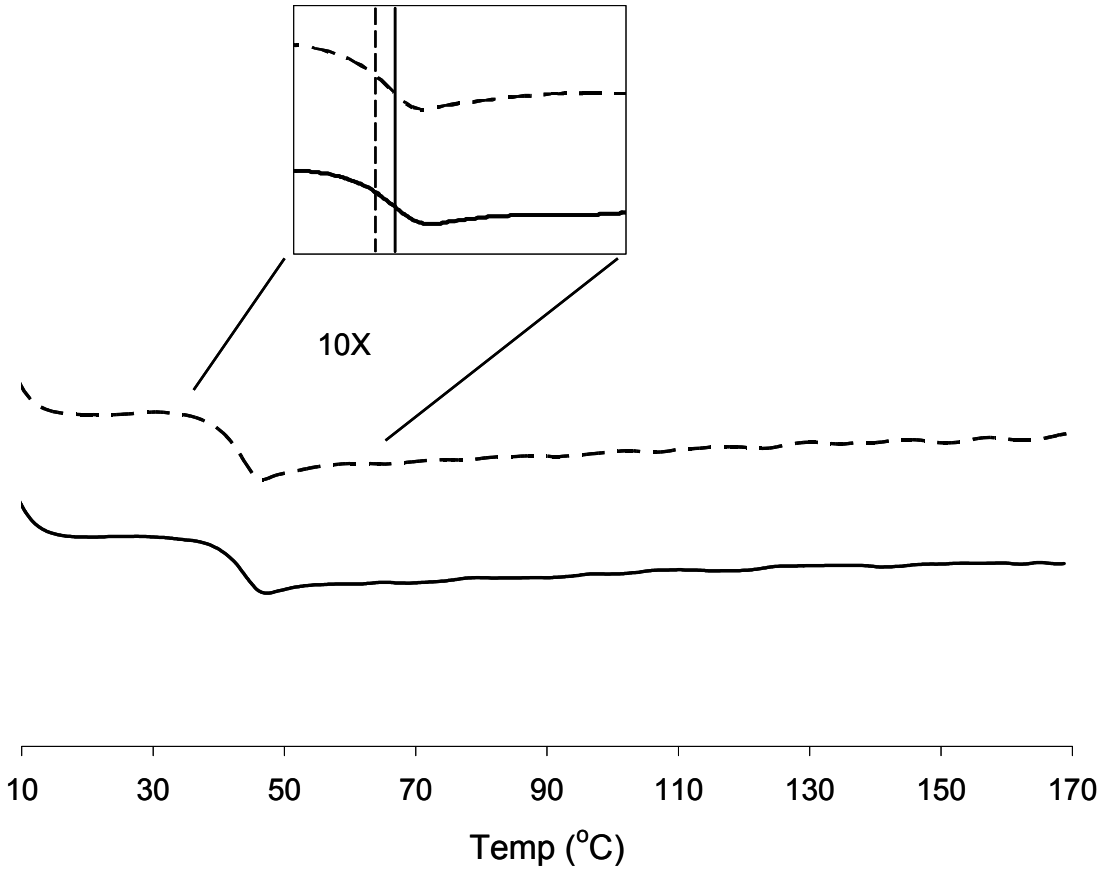

Figure 5.3. DSC thermograms (second heating, 10°C/min) for neat PVAc (dotted line) and 12.5 % vol. PVAc/silica nanocomposite (solid line) in an inert N_2 atmosphere.

5.4.3 ^{1}H Spectra and Bloch Decay Experiments

NMR techniques have been successfully used to investigate the dynamics of polymers in the bulk and at the interface of a composite system for many years.[28] The first approach used here is based on ^{1}H NMR Bloch decays which can give information

about the overall chain mobility of the system characterized by the lineshape and linewidth. As shown in Figure 5., we expect the dynamics of the polymer matrix in the composite at temperatures above the T_g to be somewhat analogous to a cross-linked or filled elastomeric system. Much like a cross-linked structure the dynamics will be dominated by mobile free (chains between junctions) or dangling chains and by the rigid nanoparticle attached or entangled chains. Broad line-widths result from intramolecular dipolar interactions and anisotropic motion which typically characterize rigid polymer chains. On the other hand, mobile polymeric chain segments that can perform fully isotropic rotational and translational motion produce narrow linewidths. Figure 5.4 (a), (b), and (c) shows ^1H spectra for neat PVAc and filled PVAc with 12.5 vol. % of silica particles at various temperatures (Figure 5.4 (c) overlays the neat and filled PVAc spectra for comparison in a stacked fashion for 4 temperatures to show lineshape/width differences). The spectra in Figure 5.4 are fairly symmetric lineshapes, which at first glance could be described by simple Gaussian, Lorentzian or some combination of these functions. The spectrum for the neat sample at room temperature is the superposition of the at least two but what appears as the convolution of multiple peaks, having the broad peak components dominate the overall lineshape. As the temperature is increased the peak becomes narrower as the narrow component begins to dominate the lineshape. The spectra of the filled sample follow a similar trend as temperature is increased. However, the spectrum at room temperature shows a much lower relative intensity for the narrow component. And by comparing the lineshape/width of the neat and filled sample as a function of temperature it becomes clear the progression to a completely narrow lineshape/width requires much more energy to initiate than the neat sample. This

suggests that there is some mechanism in the filled sample that significantly increases the portion of rigid chains at low temperatures and that same mechanism retards chain mobility with respect to the neat sample as the temperature is increased.

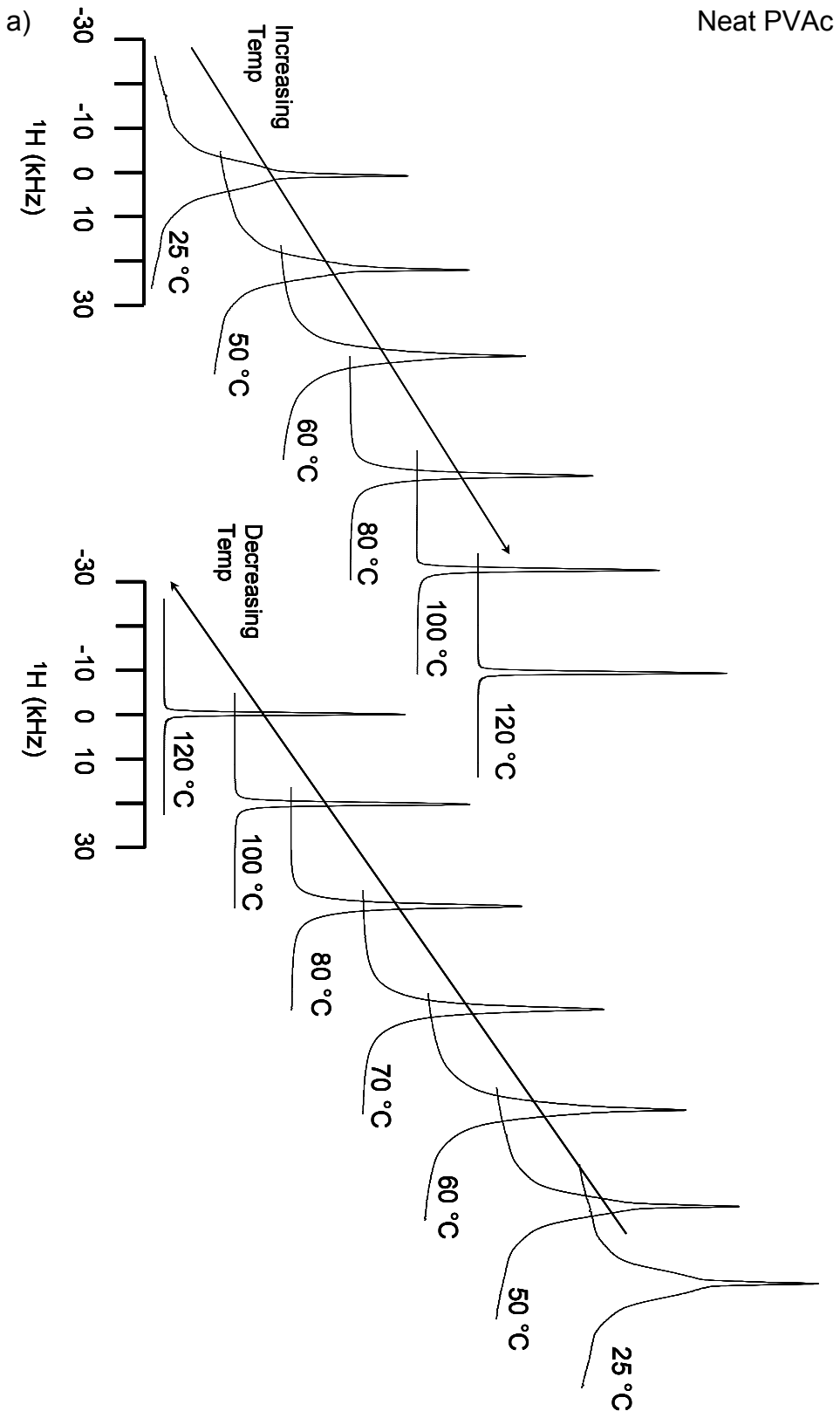
a)
Neat PVAc
Increasing Temp
Decreasing Temp
25 °C
50 °C
60 °C
80 °C
100 °C
120 °C
70 °C
-30 -10 0 10 30
1H (kHz)

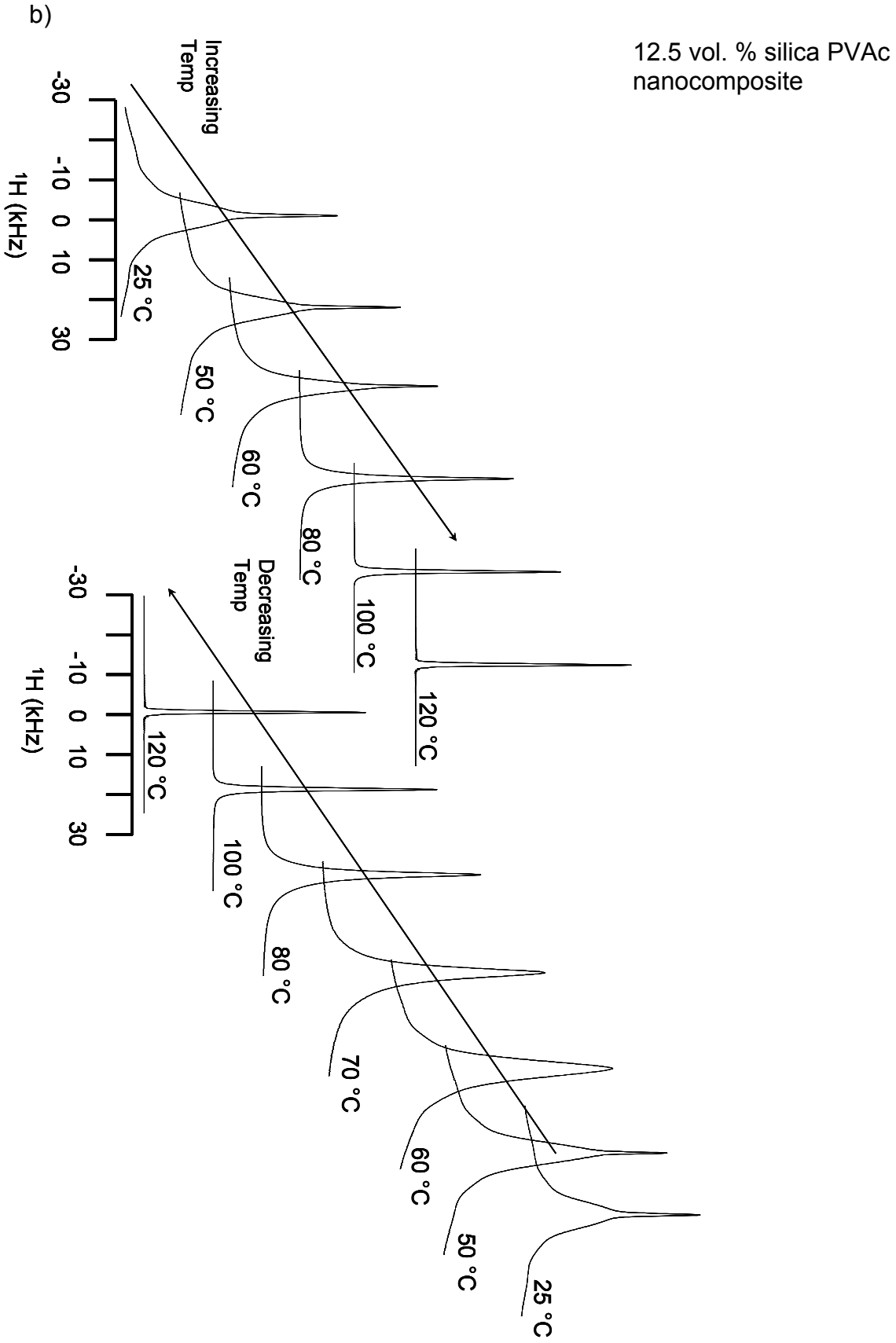
b)
12.5 vol. % silica PVAc nanocomposite
Increasing Temp
Decreasing Temp
^{1}H (kHz)
-30
-10
0
10
30
25 °C
50 °C
60 °C
80 °C
100 °C
120 °C
70 °C

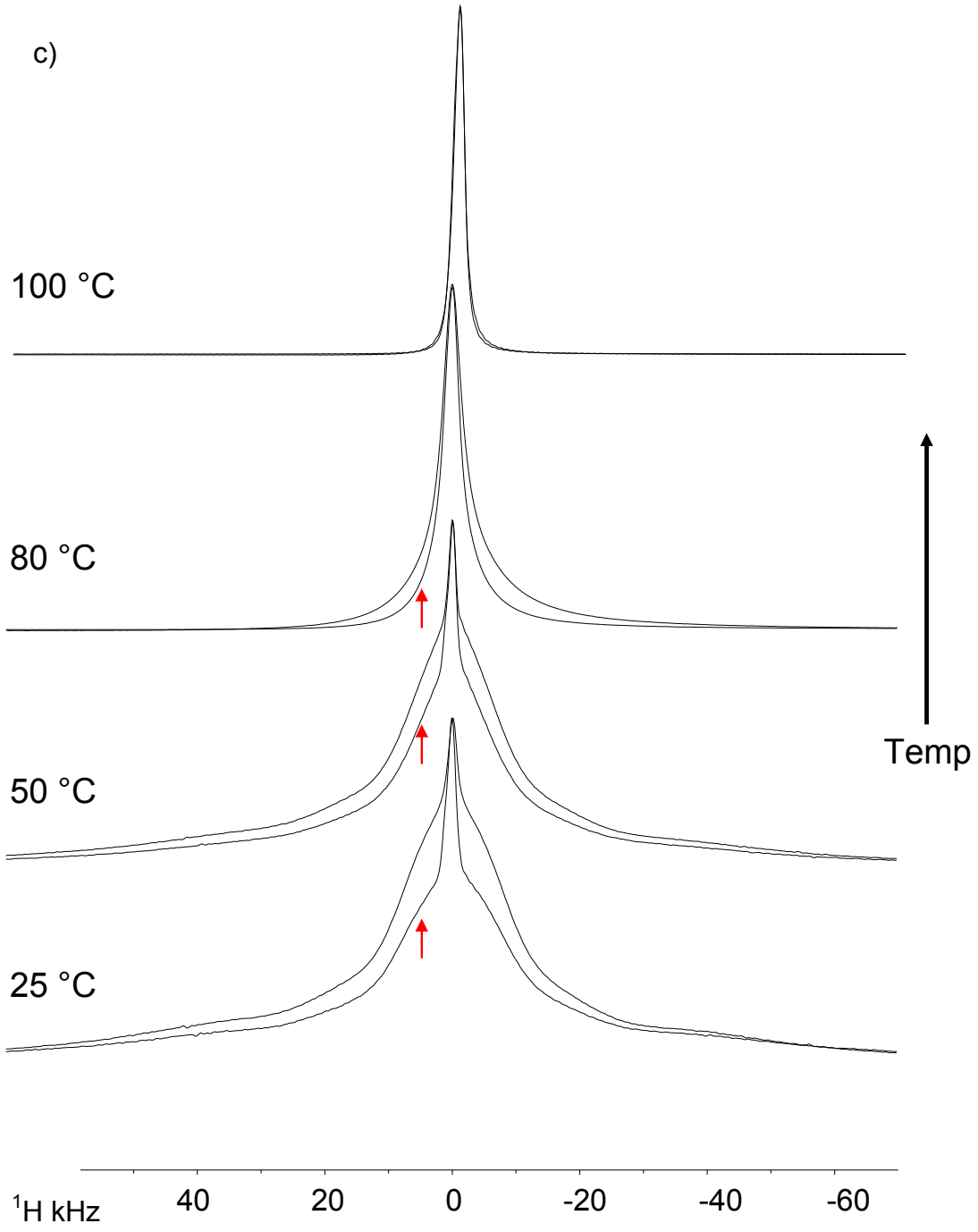

Figure 5.4. ^{1}H spectra for (a) neat PVAc and (b) PVAc filled with 12.5 vol. % of silica particles at various temperatures. (c) Stacked spectra of the neat PVAc (denoted by a red arrow) and the PVAc filled with 12.5 vol. % of silica particles.

The presence of a narrow component in the spectra at room temperature was initially a concern. At temperatures below T_g, we would not expect to observe a component mobile enough to generate this feature in the lineshape. To verify the validity of these results a series of Bloch decays were taken. Both neat and filled samples were dried in a vacuum oven above T_g to remove any water or any residual solvent, although, thermal analysis indicated that adsorbed moisture or residual solvent content were not present. Bloch decays were taken in a decreasing then increasing stepwise fashion from 130 °C to room temperature 3 times. Consistent results verified the initially obtained lineshapes and the analysis above. The question then arose what was the origin of this narrow component in the neat sample at such low temperatures.

2D heteronuclear wide-line separation (WISE) NMR can be used to probe the molecular dynamics of individual chemical groups in the repeat structure of a polymer. In 2D WISE experiments ^{13}C chemical resolution is correlated to ^{1}H chemical resolution via a 2D plot. Basically for every ^{13}C resonance, a WISE experiment will show the corresponding proton lineshape, which can be used to determine the mobility of the protons associated with the carbon corresponding to a particular ^{13}C resonance.

Using the spectrum obtained from a 1D ^{13}C CP MAS sequence shown in Figure 5.5 (c), peak assignments for the PVAc were made. The signals around 170–185, 60–85, 35–60 and 10–35 ppm are assigned to the carbonyl, methine, methylene and methyl carbons, respectively.[38,39] The 2D WISE spectrum in Figure 5.5 (a) and (b) show the resonance attributed to the methyl group with a linewidth of ~ 27 kHz which is slightly broader lineshape than the methylene and methine group signal, indicating slower site-specific dynamics most likely due to hindered rotation resulting from carbonyl

interactions. The more important observation is that all the signals in the 2D WISE spectrum show some intensity corresponding to the same narrow component seen in the ^{1}H Bloch decay of the neat sample at room temperature. This suggests that in some way all the protons in the repeat unit contribute to the narrow component, and that the narrow component in the lineshape is not site-specific. Based upon that conclusion, it occurred that smaller oligomeric "sol"-like polymer chains most likely contribute significantly to the lineshapes, and at room temperature the relative intensity and mobility difference between this "sol" component and the larger polymer chains are sufficient enough to impart what appears to be a two component lineshape. The filler in the nanocomposite reduces the mobility of various portions of the matrix chain mobility distribution in such a way as to mitigate this effect at room temperature by producing a smaller ratio of mobile chains.

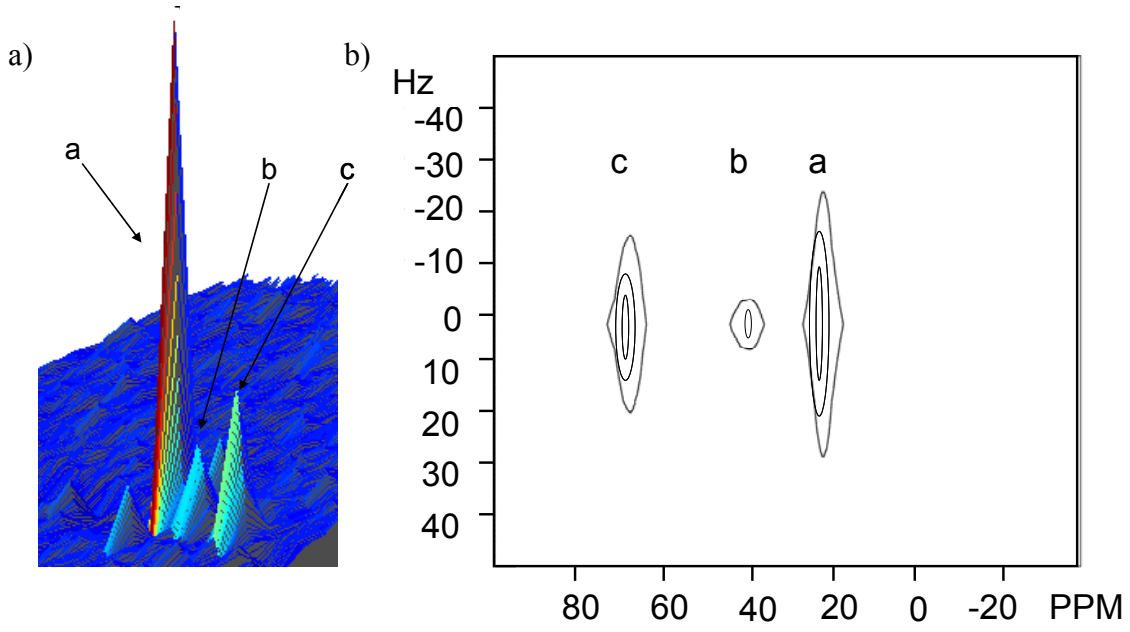

c)

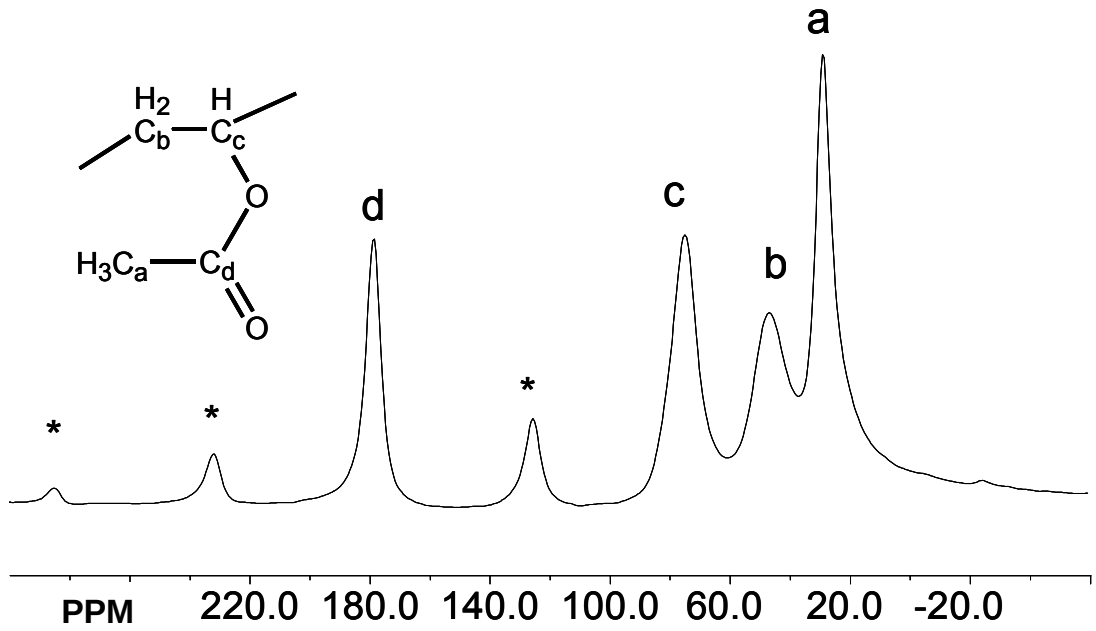

Figure 5.5. (a) Shaded surface plot and (b) contour plot of a 2D WISE NMR spectra of neat PVAc at room temperature with no mixing time and contact time of 100 μs. (c) 13C CP MAS spectrum for neat PVAc with a contact time of 1 ms at spinning 5 kHz and room temperature (* = spinning side bands).

5.4.4 Spin-Spin Relaxation Experiments

In order to further elucidate the nature of the different polymer mobility observed in the nanocomposite material, a T_2 experiment was conducted. A T_2 experiment or spin-spin relaxation probes how fast the nucleus loses transverse magnetization. A characteristic parameter for this process is called the spin-spin relaxation time T_2. *I(t)*, a measurable quantity and common notation for the independent parameter in equations modeling T_2 relaxation, describing the magnetization detected as a function of echo time *t*. The T_2 can be used to describe molecular motion and decays as a function of local inhomogeneities in the magnetic field mainly due to perturbation by nuclei through space or dipolar interactions. The basic T_2 experiment uses an excitation pulse to invert the

population of nuclear spins, aligning them in the z-direction of Figure 5.6. As the spins relax onto the x-y plane they also precess around the z-axis. As they precess around the z-axis, their x-y plane projections loss coherency because each nuclei will experience slightly different surroundings. This loss of coherency is T_2 relaxation. This is measured by allowing a delay between excitation and acquisition. The echo time is varied and the magnetization detected is *I(t)* .

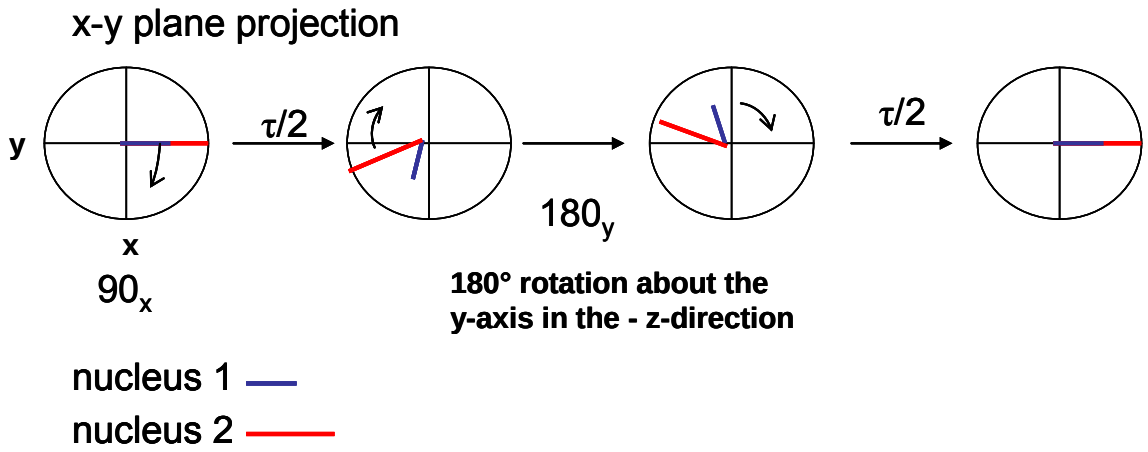

Figure 5.6. Dephasing in the x-y plane of two nuclei with a 180° refocusing pulse.[c]

Typical T_2 decay constants for solids and liquids range between 3-30 μs and 30-300 ms, respectively, while "soft" material such as polymers have T_2 decays of .1-3 ms.[28] Refocusing with a 180° pulse is used to eliminate dephasing due to other factors such as electron shielding (chemical shift), perturbation by nuclei through bonding electrons (*J*-coupling) and magnetic field inhomogeneity.[27,40] Rigid or slow moving material effectively experience stronger dipolar interactions, causing short echo times to be dominated by the behavior of the rigid attached or entangled chains. The longer

[c] **www.chem.queensu.ca/FACILITIES/NMR/nmr/webcourse/t2.htm**

relaxation is mainly due to faster motion of the mobile free or dangling chains because of averaging of the dipolar interactions.[27,40]

Hahn-echo (HE) and Carr-Purcell-Meiboom-Gill (CPMG) Sequences

The actual sequences used to probe the spin-spin relaxation were the Hahn-echo (HE) and Carr-Purcell-Meiboom-Gill (CPMG) sequences, seen in Figure 5.7. As stated previously, the decay measured in T_2 experiments can be related to dephasing due to local inhomogeneities in the magnetic field from several sources. The HE sequence attempts to eliminate all factors causing dephasing other than dipolar coupling by application of one 180° inversion pulse after τ/2 time. Essentially after exicitation and during the τ/2 time before the 180° pulse dephasing happens because of chemical shift, J-coupling and magnetic field inhomogeneity.

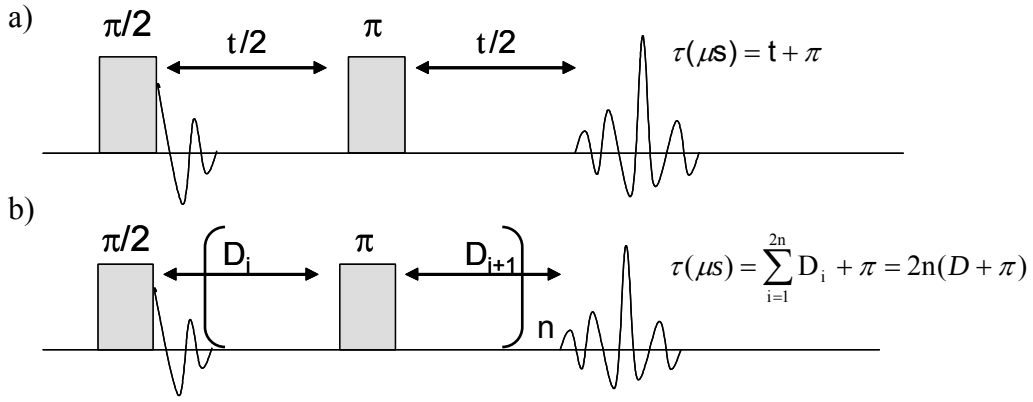

Figure 5.7. Pulse sequences for the measurement of molecular motion and dynamics in poly(vinyl acetate)/silica nanocomposites. π/2 and π denote 90° and 180° rf-pulses, respectively. Echo time (τ) follows the equations in the figure and is the time between excitation and acquisition. (a) Hahn spin–echo experiment used to measure relaxation of traverse ^{1}H magnetization. The first rf-pulse flips the magnetization into the XY plane and the second inverts the magnetization before obtaining the echo. (b)

The Carr-Purcell-Meiboom-Gill sequence is derived from the Hahn spin-echo sequence and also measures relaxation of traverse ^{1}H magnetization. Multiple 180° rf-pulses are used to further correct for dephasing due to magnetic field inhomogeneity.

As illustrated in Figure 5.6, if two nuclei with different chemical shifts precess during the first $\tau/2$ time, the difference in chemical shift will cause each nucleus to precess at a different rate causing dephasing. After the application of a 180° pulse and spin inversion occurs, the nuclei will precess by the same amount during the period between the inversion pulse and acquisition as during the period between the excitation and the inversion pulse because the identity and the chemical shifts of the nuclei have not been changed, eliminating the effects on dephasing due to different chemical shift. This refocusing pulse works similarly for J-coupling and magnetic field inhomogeneity.[27]

The CMPG sequence is a modified HE sequence. Instead of using one 180° pulse and allowing $\tau/2$ time between excitation, refocusing and acquisition, the CMPG utilizes a train of n 180° pulses, allowing τ/n time between pulses and having an echo time = $n(\tau+180°)$.[27] This sequence was designed for materials that display increased diffusion without exhibiting isotopic tumbling such as polymers near T_m. The use of one refocusing pulse assumes that the nuclei will precess by the same amount before and after the inversion pulse. However increased diffusion causes molecules to move within the magnetic field. Therefore the magnetic field inhomogeneity experienced during the first $\tau/2$ time will be different from the magnetic field inhomogeneity experienced during the second $\tau/2$ time. To counter this, multiple refocusing pulses with a shorter period in-between refocusing is used.

The magnetization tip angle resulting from a radio frequency pulse is related to the power and duration of the pulse. At typical power levels, a 180° pulse will last about 10 μs. In a CMPG experiment, the first data point taken in a T_2 decay curve corresponds to $n = 2$, where the echo time is $2(\tau+10)$ μs. If τ is too short the sequence continuously irradiates and simply heats the sample and if τ is too long the sequence misses data points at short echo times. Thus, the CMPG sequence is most effective to use on material with longer T_2 times.

Kohlrausch-Williams-Watts (KWW) Model

If the assumption made earlier from Figure 5. is correct, *I(t)* should have two components. The first component is due to mobile regions which show longer relaxations, fully isotropic rotational motion, narrow linewidths and correspond to a simple exponential function. The other component exhibits short echo times, large intermolecular dipolar interactions resulting in line-broadening and typically corresponds to a Gaussian approximation. T_2 relaxation data measured at temperatures between 45 and 130 °C were found to be non-exponential and also not Gaussian in nature. They were analyzed using a Kohlrausch-Williams-Watts function, commonly associated with a spatially heterogeneous distribution of relaxation times, which is typical in completely amorphous polymeric samples and is modeled by the function[41]:

$$I(t) = I_O \exp\left[\left(\frac{-t}{T_2}\right)^{\beta}\right] + \text{offset} \qquad \text{Eq. 5.2}$$

The molecules in a glass-forming material are said to move cooperatively, and form cooperative rearranging regions (CRRs) that are related to the length scale of spatial heterogeneity.[42-44] The non-exponential relaxation nature of polymers above the glass

transition temperature is associated with the superposition of multiple relaxation processes that have different rates, leading to the wide distribution of relaxation times.

The KWW model, as seen in Eq. 5.2, is a stretched-exponential equation that describes a stretched exponential function or a sum of exponential decays, assuming the population of relaxers fits a distribution. It describes many relaxation processes in materials such as muscle, bone, dielectrics, polymers, and glasses,[41] and can be used to fit T_2 data obtained from both a Hahn-echo or CMPG experiment. The characteristic T_2 value or relaxation time represents the center of that distribution and β is the spread of the distribution. β ranges from 0 to 1, where 1 is a single exponential function and 0 is an infinitely spread distribution. Ideally the limit of a T_2 decay curve with respect to echo time upon complete T_2 relaxation should be zero. However, an offset parameter is often added to T_2 decay models to account for incomplete intensity attenuation or DC offset (corresponds to a small direct current or constant voltage being added to the entire signal shifting the data slightly in the vertical direction). The offset is an additional fitting parameter used to help optimize the fit of a model and can account for deviations from the model or even baseline effects. However, particularly at higher temperature, it was noted that this offset itself seemed to be dependent on echo time and fit an exponential decay, so the T_2 decay data were analyzed both with a constant offset and an exponential offset.[d] Figure 5.8 shows typical spin-echo decay curves for the neat and filled samples. The curves clearly illustrate the stretched exponential character of the decay.

[d] An exponential offset will alter Eq. 5.2: $I(t) = I_O \exp\left[\left(\frac{-t}{T_2}\right)^{\beta}\right] + I_{offset} \exp\left(\frac{-t}{T_{offset}}\right)$

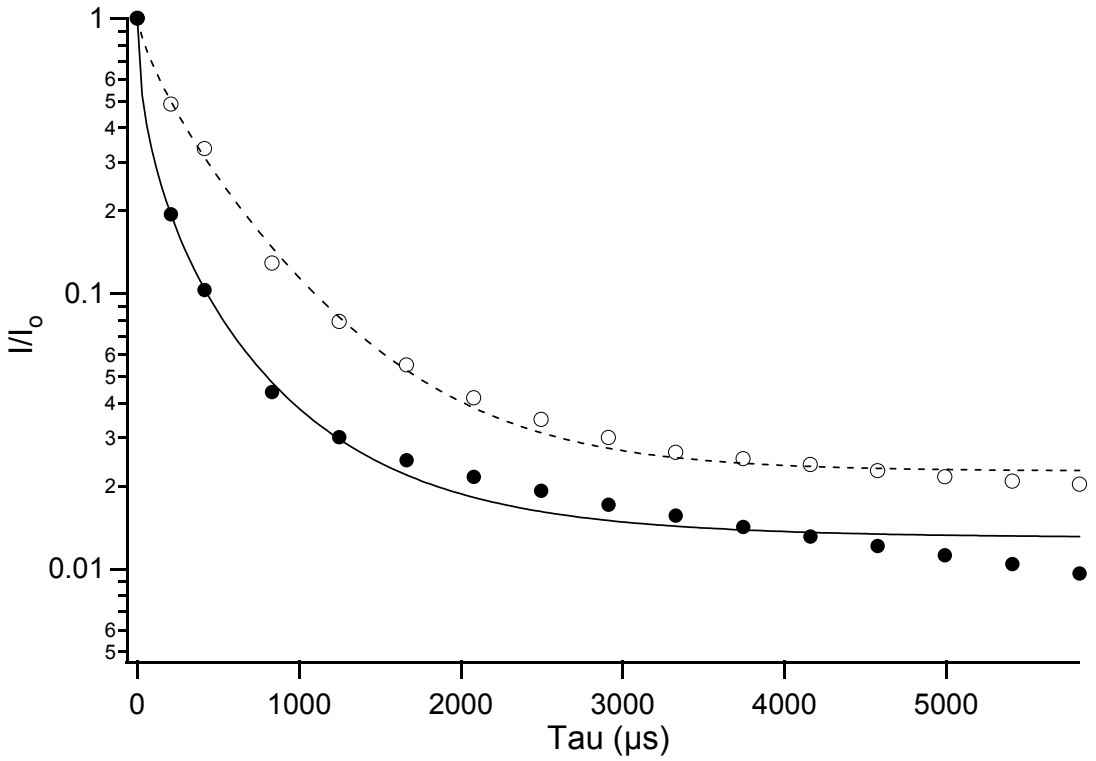

Figure 5.8. Plot of spin-echo decay at 80 °C obtained using the KWW model with the constant offset and CMPG sequence. 12.5 vol. % filled (●) Neat PVAc (○).

Carr-Purcell-Meiboom-Gill with a Constant Offset (CPMG) Data

Figure 5.9 (a) and (b) show how the T_2 and β values change as the temperature increases using the KWW model with the constant offset and CPMG sequence, providing information of how the relaxation and subsequent molecular motion changes for both neat and filled samples. At temperatures approximately 45 °C above T_g, the sample containing the silica nano-fillers had a wider distribution of correlation times with a shorter characteristic T_2 relaxation time. The T_2 data show that from 50 °C to near 90 °C the characteristic relaxation time is < 10 μs for both the neat and filled sample. The fact that, for our two samples, no significant difference in relaxation time can be detected for temperatures below 90 °C can be explained. Essentially in the absence of external forces

the filler acts simply as additional chain "entanglement" sites. Below 90 °C the low frequency changes in the polymer matrix dynamics as a function of temperature can not be detected in the MHz-kHz frequency range of T_2 experiments. Therefore, at a filler fraction of 12.5 %, the addition of nanoparticles seems not to significantly decrease the T_2 values. Above 90 °C there is however, an abrupt slope change for both samples indicated this is the NMR T_g, and the T_2 and $d(T_2)/d(T)$ for neat sample is higher than that of the filled sample. This indicates that in both samples chain interactions and "entanglements" are being broken by the addition of energy to the system, giving the chains more molecular motion. The filled sample has slightly more "entanglements" that resist breaking more because of adsorption or interfacial bonding between chains and filler. More importantly, conventional mechanical percolation, which is only relevant upon stressing, or aggregation theories do not explain the observed differences in the dynamics via NMR of the neat and filled systems. .

a)

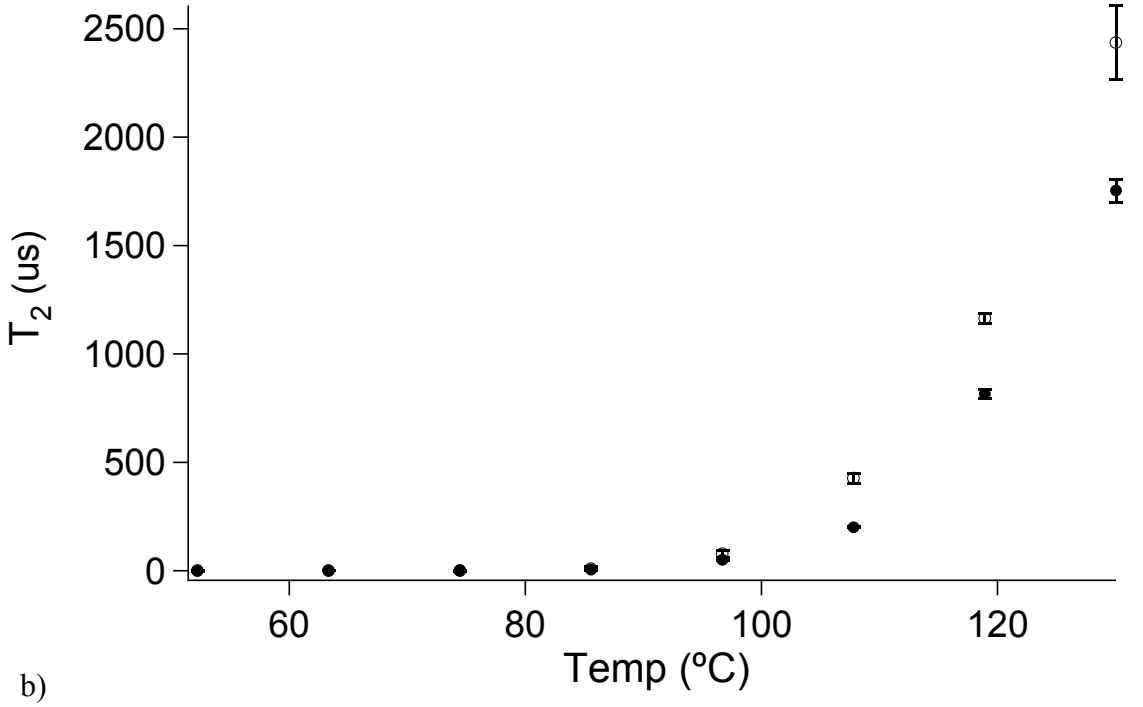

b)

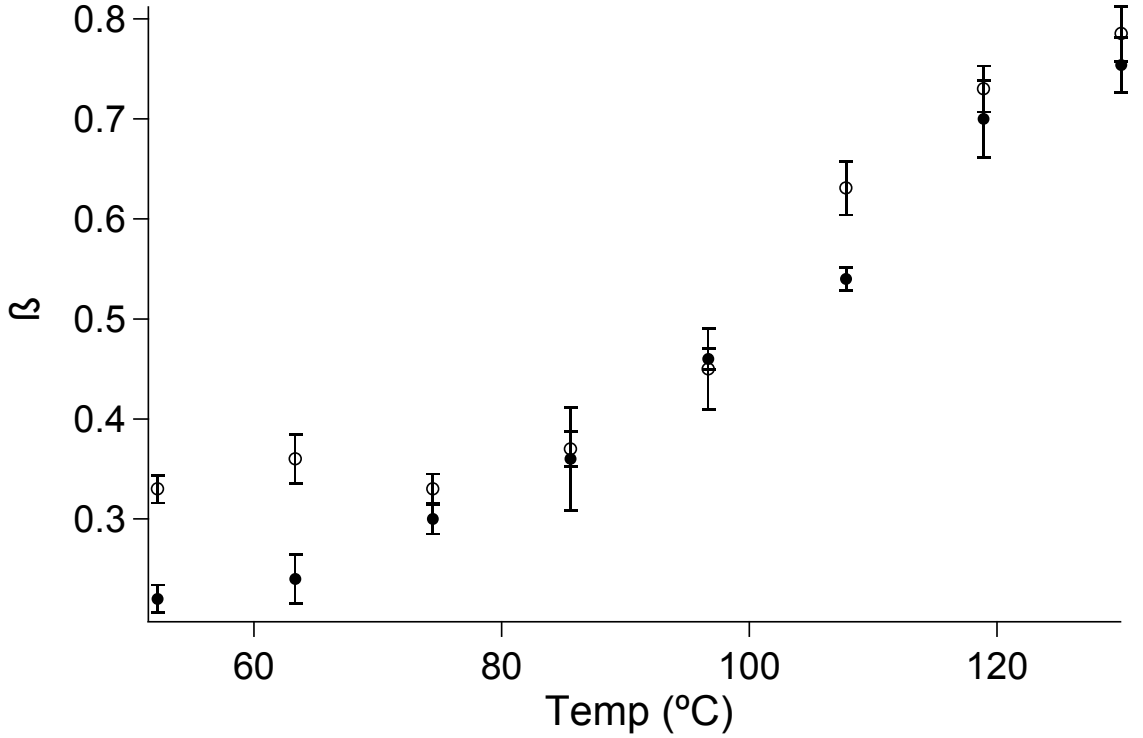

Figure 5.9. The T_2 and β values at various temperatures ranging from 45-130 °C were obtained using the KWW model with the constant offset and CMPG sequence. The error bars represent one standard deviation of 3 T_2 experiments 12.5 vol. % filled (●) Neat PVAc (○).

Another aspect to the T_2 data which must be considered is the effect of temperature on β. β for the filled sample is generally lower than that of the neat sample, because the additional entanglement sites cause the distribution of relaxation times to become more spread. In addition as the temperature rises the β for both samples approaches 1, characteristic of a single exponential relaxation. Both these observation support the claims that additional entanglements are causing a wider distribution of relaxations and that heating the sample breaks those entanglements. More interesting though, is the fact that the neat sample d(β)/d(T) is almost zero where the filled sample has a positive slope at temperatures below 80 °C. d(β)/d(T) of both samples is positive and slightly higher for the neat sample at temperatures above 80 °C. This result is because below 80 °C the nanoparticles impart additional stability to the polymer matrix whereas above 80 °C (~ $temp_{de\text{-}adsorption}$) de-adsorption from the filler begins to happen more readily. As a result the polymer dynamics of the filled sample are quickly pushed towards that of the neat sample, and is supported by similar rheological observations made at temperatures above 90 °C.[10-12]

What is meant by "entanglement" sites?

This seems to be a good point to briefly discuss what is meant by additional chain "entanglement" sites and its significance to the dynamics of a nano-filled polymeric system. As stated before the PVAc/silica nanocomposites was examined as though it was a filled elastomer, where free chains and the nature and density of chain entanglement sites controls the localized polymer dynamics and macroscopic mechanical properties. Therefore changes not only in localized dynamics but also for the observed macroscopic

properties of the nanocomposite are attributed to increasing the density of chain "entanglement" sites within the polymer matrix. This approximation of the change in polymer structure is accurate enough to describe the system of study; however, it is an immense simplification of the situation. The nanocomposite is composed of the innate intermolecular polymer chemical and topological interactions or "entanglements" seen in the neat sample, but also of nano-fillers which are not simple point entanglements between a few chains. The filler-matrix "entanglement" is characterized by of dozens of chains interacting with a particle through chemi- and physisorptive processes creating a bound polymer layer and an interphase orientated between bound and bulk polymer chains. This interphase is a most likely containing a nondescript gradient of chain mobilities in which the nature, strength, and number of "entanglements" or polymer topological constraints vary from the amorphous polymer in the neat sample.

Limitations of the KWW Model

A model rarely completely describes real phenomena. Therefore parameterization of the resulting data typically is a best-fit effort. During optimization of the parameters, unaccounted for factors and/or deviations from the model are incorporated into the parameters of the model. That seems to be the case here also. The KWW model assumes the population of exponential relaxers fits a single distribution.[41,45] The KWW model is empirically applied to describe a variety of very different relaxation processes, however using such a model without theoretical justification can lead to erroneous or even unrealistic results. A single KWW model may not be adequate to characterize more than one relaxation process. The T_2 and subsequent inverse Laplace transform of the T_2 data

suggest that, even for the neat sample, the data most likely correlates to an asymmetrical distribution of chain mobilities. The resulting asymmetrical chain mobility distribution corresponds to multiple relaxation processes, i.e α and β relaxation processes, for a large polydispersity of chain lengths. This is evident in the lineshapes in Figure 5.4. There is a mobile component at room temperature which leads to the observed superimposed lineshape because the relaxation time distribution consists of at least two well-separated peaks.

The narrow component seen in Figure 5.4, previously assigned to "sol"-like material may exists outside the actual spread of the main relaxation distribution as illustrated in the inset in Figure 5.10. This is supported by the offset parameter which suggests, excluding major baseline effects, that up to 10 % of the neat and filled samples have magnetization at the last data point taken on the T_2 curves. When this remaining magnetization was fit to an exponential function, it indicated that component had a T_2 characteristic decay time of 7 ms. Moreover, the filled sample further deviates from the KWW model as the interphase and polymer chains nearest the filler are fairly rigid and mostly likely exhibit non-exponential or even Gaussian-like T_2 decay which is usually associated with crystalline or glassy polymer content.[28]

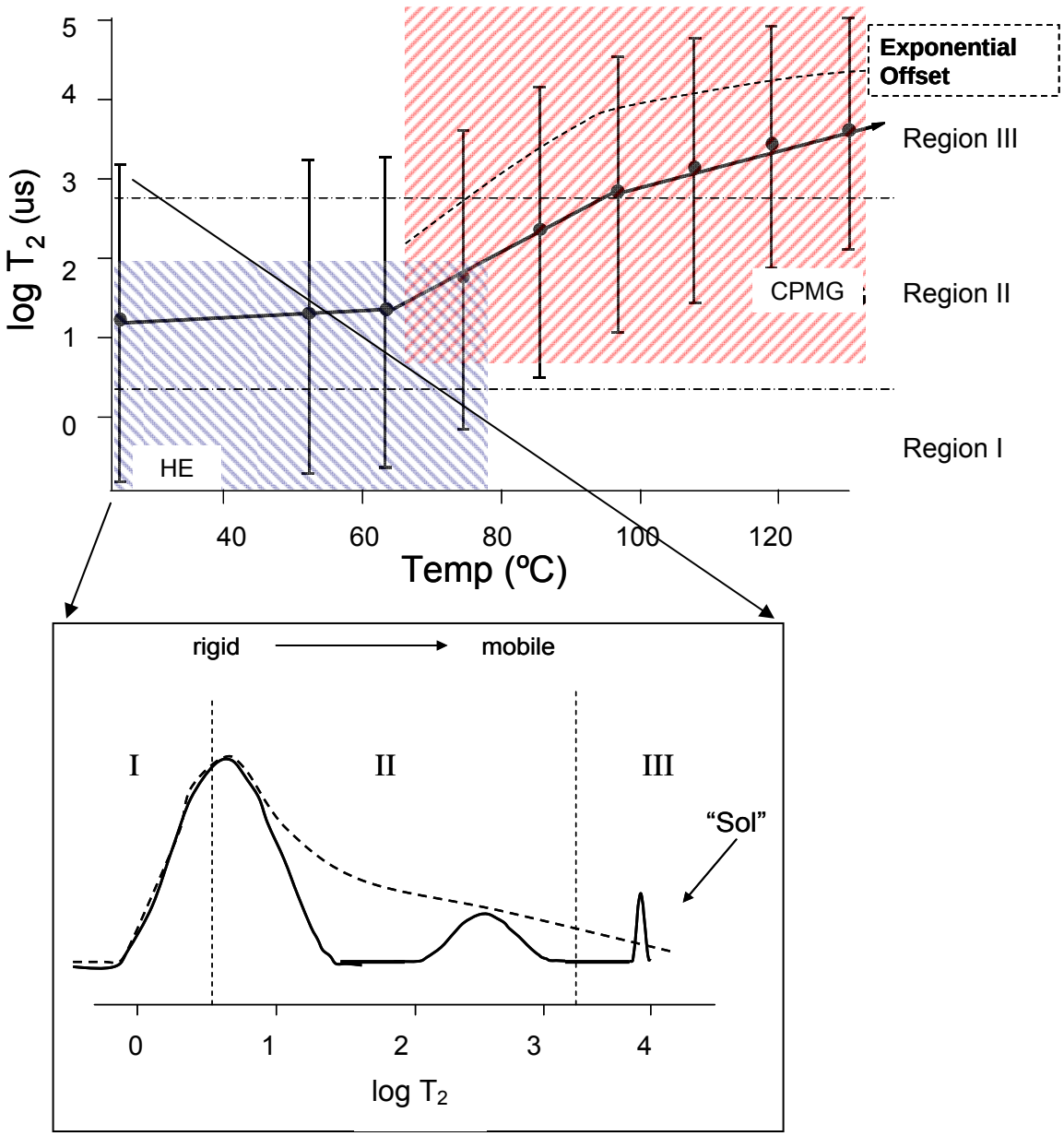

Figure 5.10. The T_2 values at various temperatures ranging from 45-130 °C. The dotted lines denote arbitrarily defined mobility region (Regions I, II, and III), and the inset below the T_2 versus temperature plot shows the proposed structure of the mobility distribution at room temperature based on the gathered data and published literature. The data points represent actual T_2 data for the neat PVAc sample, and the error bars represent the spread of the relaxation distribution based on the actual β and an asymmetrical Gaussian shape.

Limitation of the HE and CPMG Sequences

Figure 5.10 shows characteristic T_2 times versus temperature, where the points represent actual T_2 data for the neat PVAc sample, and the error bars represent the spread of the mobility distribution based on the actual β values and an asymmetrical Gaussian shape. Taking a slice in the temperature dimension at any one point would produce the mobility distribution for neat PVAc at that temperature, having the average T_2 time of the distribution centered at the marked point. In many ways Figure 5.10 summarizes the difficulties in analyzing the T_2 data. Recapping, the CMPG sequence uses a train of 180° inversion pulses to refocus magnetic field inhomogeneity effects arising from increased self-diffusion. This makes the CMPG sequence very effective at gathering T_2 decay information at higher temperatures, represented by the region in red. However, as a consequence of the train of 180° inversion pulses the CMPG sequence can not be used to detect the initial decay in faster relaxing material, i.e. crystals or glassy polymers. The Hahn-echo sequence on the other hand only utilizes one 180° inversion pulse, which is sufficient to refocus magnetic field inhomogeneity in polymers at lower temperatures near the T_g, represented by the region in blue. If a material relaxes with a single decay rate, it then becomes clear which sequence to use, however polymers, particularly amorphous materials, have been shown to have a wide relaxation distribution.[46] Consequently, as illustrated in Figure 5.10, parts of the relaxation distribution may lie outside the effective range of a particular sequence. In this case the signal from those regions can either be excluded from the decay, or for example, when a Hahn-echo sequence is used at higher temperatures on polymers appreciable dephasing occurs because of increased diffusion. This diffusion-related dephasing makes mobile

components decay faster, causing an overlapping of dipolar coupling and magnetic field inhomogeneity effects. This makes mobile chains appear as though they were rigid chains.

The dotted lines in Figure 5.10 and the inset below Figure 5.10 describe arbitrarily defined mobility regions, where region I includes the fastest decay components (the most rigid chains), while region II represents some intermediate relaxation ad mobility associated with the majority of the distribution and region III describes the slowest relaxing components with T_2 decays greater than ~ 3 ms (primarily the "sol" component). From this point on this chapter will refer to these "regions" described above to further discuss the T_2 results. The inset below the main plot in Figure 5.10 shows the most probable appearance of the mobility distribution of neat PVAc at room temperature. This is based on conclusions obtained from T_2 experiments and published literature, reflecting the z-projection of a slice in the temperature dimension at room temperature for the main plot in Figure 5.10.

CPMG with an Exponential Offset Data

Analyzing the data using the exponential offset essentially removes the slowest relaxing (mobile) components, accounting for the remaining ~ 10 % of the T_2 decay represented in region III. When treated that way, the T_2 data have a similar trend over the range of temperatures > 90 °C. T_2 values increase for both samples and are higher for the neat sample. The effect of temperature on β again shows a general increase with temperature particularly above 90 °C. However, below 90 °C unlike when processed with a constant offset the filled sample shows higher β values than the neat sample.

Initially this change was hard to understand, but utilizing Figure 5.10, removal of region III from the overall mobility distribution would weight the effect from regions I and II on the T_2 and β results. Supporting this is an order of magnitude decrease in T_2 and an increase in β for the neat sample when changing from a constant offset model to an exponential offset (corresponding to a narrower distribution that is shifted toward shorter T_2 values). The retarded motion of chains affected by the additional entanglements in the filled sample at lower temperatures (near T_g and below $temp_{de\text{-}adsorption}$) concentrate the proportion of chain in regions I and II compared to the neat sample, narrowing the distribution of mobilities in that region and increasing of the resulting β.

Hahn Echo Data

As stated before, a CPMG experiment loses information about the fastest relaxing material, or the relaxers in region I. To better illuminate the behavior of the neat and filled samples at the lower temperatures Hahn-echo results were analyzed. The T_2 value results again below 90 °C show no significant difference between the neat and filled samples. The filled sample shows β values higher than the neat samples much like the trend observed in the CPMG experiments analyzed with an exponential offset, supporting the claims made previously. This indicates at lower temperatures neglecting the effect of what is deemed the "sol" component the filler narrows a portion of the overall mobility distribution by concentrating the relaxers in regions I and II. Above 90 °C the Hahn-echo results become erratic and seemingly nonsensical because of reasons discussed above. To be clear, the results from the analysis of the CPMG experiments with an exponential offset and Hahn-echo experiments at low temperatures do not suggest the overall

mobility distribution is narrowing in the nanocomposite. Instead, the data show addition of the nanoparticle either causes a disproportional number of chains in the slow to intermediate mobility range to shift to shorter T_2 times or a greater shift in T_2 times for chains in a portion of the slow to intermediate mobility range. This would be manifested as a narrowing of the lower frequency components of the overall chain mobility distribution.

T_2 Inverse Laplace Transforms

The analysis of multi-component exponential decays can be difficult when utilizing any one particular exponential model especially when there is a wide distribution of unknown decay constants, decay constants with very similar values or appreciable noise or baseline effects. One method to resolve this is to extract the distribution of relaxer or exponential decays from the T_2 data using an inverse Laplace transform. Most inverse Laplace algorithms do this in a piecewise fashion, fitting a single exponential decay constant to a small user-defined portion of the T_2 decay. This component is subtracted from the overall decay, displayed by the inverse Laplace algorithm as area under a distribution curve, which correlates to the relative intensity of that decay component within the overall decay. This process then repeated over the complete range of T_2 data. Figure 5.11 (a) and (b) shows the inverse Laplace transform for T_2 experiments at various temperatures for the CMPG sequence at high temperatures and for the HE sequence at low temperatures, respectively. In general as the temperature is increased the peaks representing the T_2 distribution detected from the relaxation decay shift toward longer T_2 times. At lower temperatures (< 90 °C) the plots show what

appears to be two separate mobility distributions. The neat samples lower frequency relaxation peak seems to be slightly towards shorter relaxation times whereas the higer frequency relaxation peak seems to be slightly towards longer relaxation times. While both peaks have a larger spread than the filled sample. At 80 and 90 °C small additional peaks form at higher frequencies, again suggesting increased polymer matrix dynamics. More interestingly, above 90 °C the observed peaks for the neat sample are shifted to longer relaxation times than the filled sample and the filled sample show a larger spread in relaxation times. This supports the claim that as temperature is increased both samples shows increased polymer matrix dynamics as entanglements are being broken by the addition of energy to the system. Under these conditions the filled sample has slightly more entanglements that resist breaking, producing a more clear change in the center and spread of the relaxation distribution as seen in the inverse Laplace plots.

a)

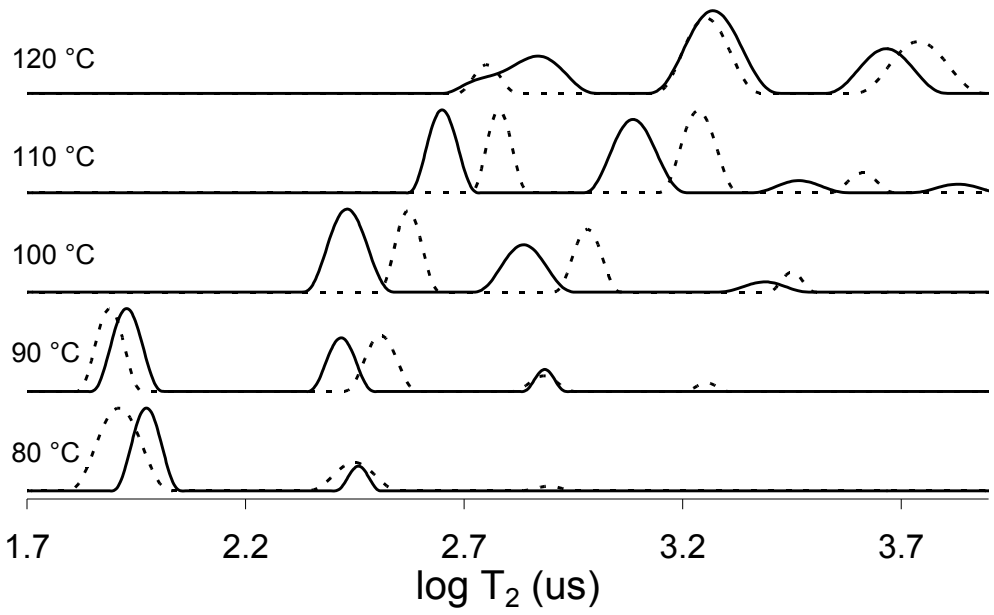

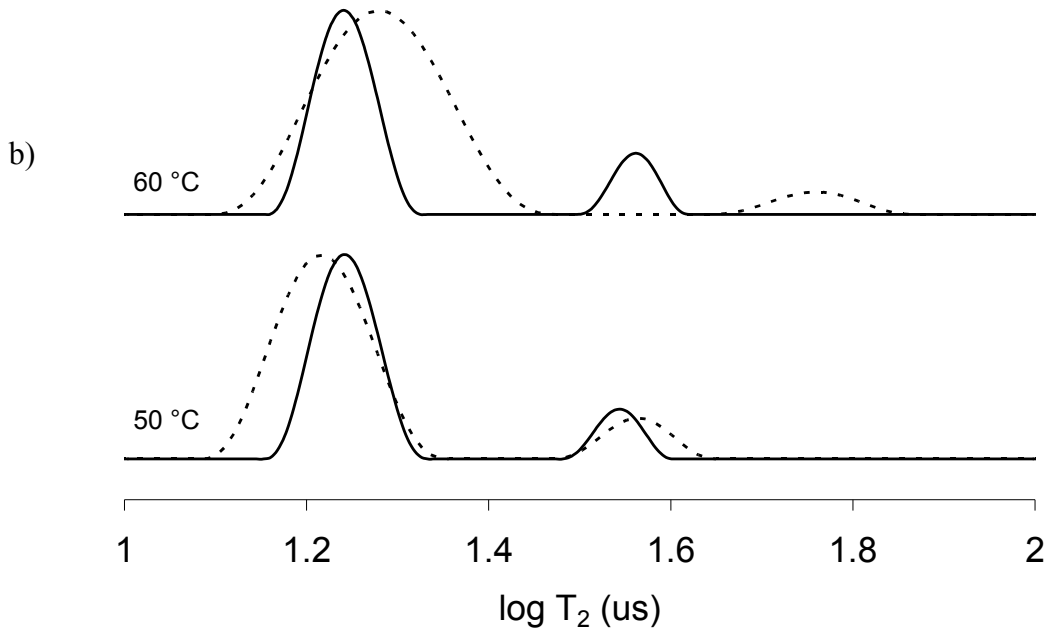

Figure 5.11. Distribution of spin-spin relaxation times produce via Laplace transformation T_2 experiments at various temperatures for (a) the CMPG sequence at high temperatures and (b) the HE low temperatures. PVAc filled with 12.5 vol. % of silica particles (solid line) Neat PVAc (dashed line).

5.4.5 2D Exchange Experiments

2D exchange experiments first conducted by Spiess and Schmidt-Rohr to study the slow chain dynamics of amorphous polymers above the T_g were repeated in this study at 55 °C to monitor motions of the side-group carbonyl in PVAc.[47,48] Figure 5.12 displays the 2D exchange sequence used. Magnetization is transfered to the carbonyl group by cross-polarization. After the first 90° pulse and incremented evolution time (t_1) serves as the basis for encoding the position of the carbonyl groups relative to the magnetic field in the first frequency dimension (ω_1). A second 90° pulse stores magnetization. During the mixing time (t_m) the carbonyl groups reorientate. A third 90° pulse recalls the magnetization, and the time at the end of the pulse sequence as the basis

for encoding the position of the carbonyl groups relative to the magnetic field in the second frequency dimension (ω_2). After 2D Fourier transform the position of the carbonyl groups before and after t_m are correlated in a 2D plot.

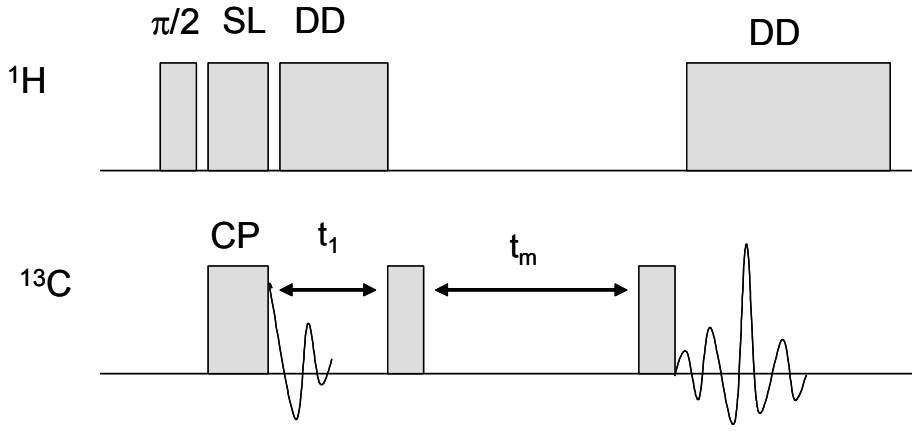

Figure 5.12. Pulse sequences for the measurement of molecular motion and dynamics in poly(vinyl acetate)/silica nanocomposites. π/2 and π denote 90° and 180° rf-pulses, respectively. 2D ^{13}C exchange sequence probes slow dynamics by monitoring the reorientation of the carbonyl group during a mixing time (t_m) with respect to B_o (SL = spin lock, CP = cross polarization and DD = decoupling).

Performing this experiment allows us to select a sub-ensemble of motion on the 1-10 kHz range and regain some of the chemical specificity lost in proton T_2 measurements. Carbonyl-group rotational reorientation after mixing times (t_m) of 1, 10, 20 and 100 ms, as seen in Figure 5.13 for the 10 ms mixing time, was tracked using 2D exchange experiments and analyzed with an autocorrelation function.

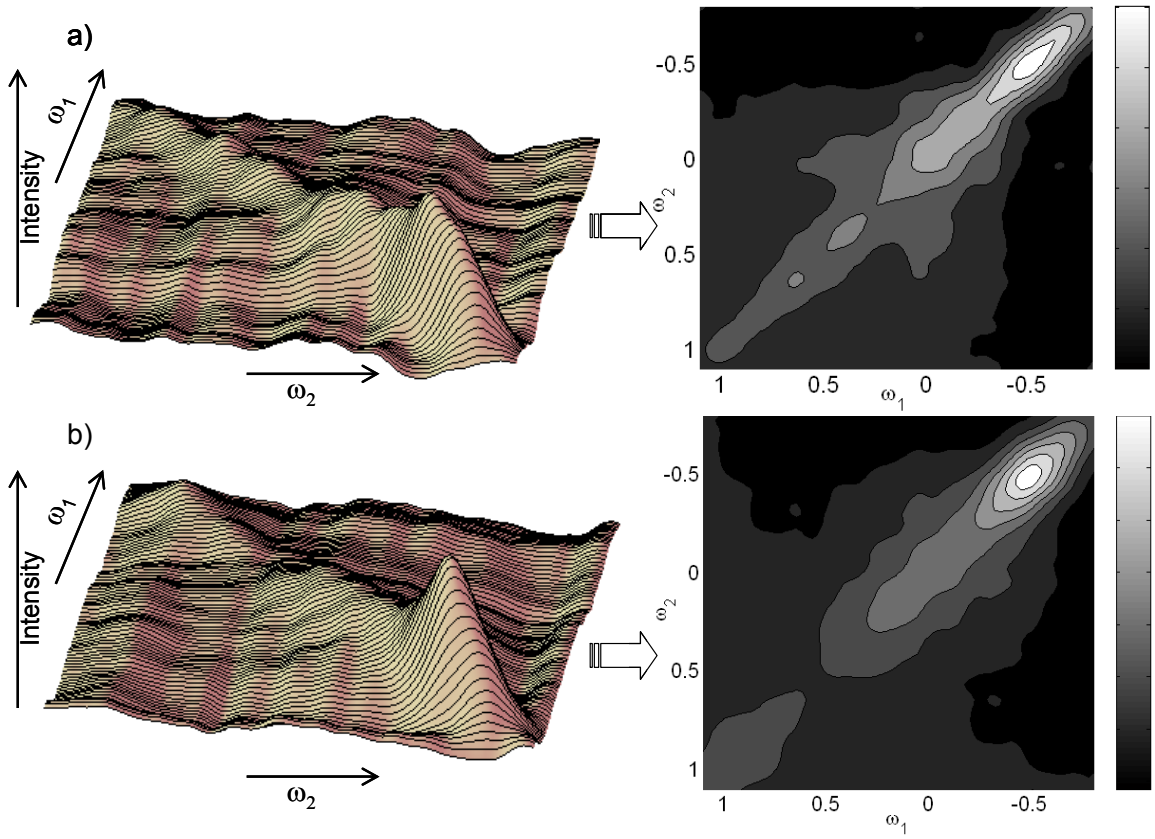

Figure 5.13. 2D 13C exchange spectra for (a) PVAc filled with 12.5 vol. % of silica particles (b) neat PVAc at 55 °C with a 10 ms mixing time. Intensity represents the probability of finding a polymer segment whose carbonyl-group resonates a frequency ω_1 and after tm that same segment resonating at frequency ω_2.

In the 2D ^{13}C exchange spectra, intensity along the diagonal plane (i.e. $\omega_1=\omega_2$) indicate no molecular reorientation has occurred during t_m, whereas off-diagonal intensity shows some segmental motion has taken place. Points along the correlation function were determined using Eq. 5.3, which correlates the probability of finding a polymer segment whose carbonyl-group resonates at a frequency (ω_1) and after t_m that same segment resonating at the same frequency (ω_2):

$$\langle \omega(0)\omega(t_m) \rangle = \sum_i \sum_j S_{ij} \omega_i \omega_j \qquad \text{Eq. 5.3}$$

where S_{ij} equals the normalized intensities seen in the exchange spectra, $\omega(0)$ is the frequency of a carbonyl-group in a polymer segment at the beginning of the experiment and $\omega(t_m)$ is the frequency of a carbonyl-group in the same polymer segment after the mixing time (t_m). This analysis along with the KWW model as seen in Figure 5.13 also revealed a broad distribution of correlation times for both the nanocomposite and the pure PVAc at a temperature slightly above T_g; however, while both are characterized by the same average correlation time of ~ 10 ms, the nanocomposite exhibits a wider distribution of correlation times with a β of 0.27 while the neat sample has β of 0.34. This result is consistent with the observed T_2 results. The double summation in Eq. 5.3 requires a flat surface baseline after the 2D Fourier transform, and depending on how the baseline was processed the integration gave various values. The error bars on the plot in Figure 5.14 represent the spread of these baseline effects. The results for the neat sample strongly agree with the results published in 1991 by Spiess, and further serve to validate the methodology and analysis used.[47,48]

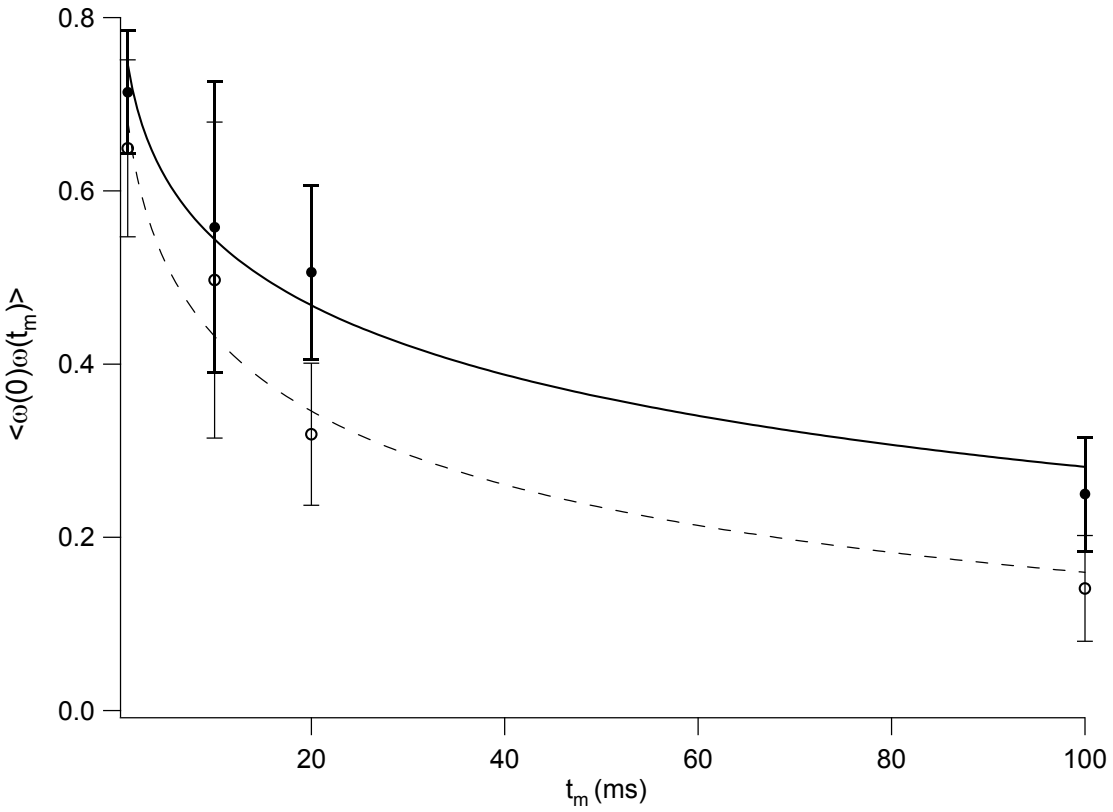

Figure 5.14. Correlation function for 2D exchange experiment at 55 °C for mixing time of 1, 10, 20, and 100 ms. PVAc filled with 12.5 vol. % of silica particles (●) Neat PVAc (○).

As seen in Figure 5.15, an inverse Laplace transformation of the correlation function produces a distribution function of the correlation times that graphically depicts the center and spread of the distribution. The population of chains maintaining a constant orientation during the mixing times is denoted by the integration of the curve left of the vertical lines (note the asymmetrical shape of the curve). The filled sample distribution is slightly wider and clearly asymmetrically shifted toward shorter correlation times, even though the center of mass for both peaks is approximately the same. This slower, wider distribution of molecular motions is due to the additional entanglements produced by the filler and further support the results and conclusions made for the T_2 experiments. An

every interesting result can be seen at the 100 ms mixing time. The population of chains remaining in the same orientation in the neat sample after 100 ms is ~ 3 % (area left of 100 ms). However, the filled sample has ~ 14 % of the population of chains remaining in the same orientation after 100 ms. This 10 % increase is almost certainty due the bound chains, the chains closest to the interface and/or in the interphase whose mobility can be considered reduced due chemical and topological interactions with the nanoparticles and bound polymer chains.

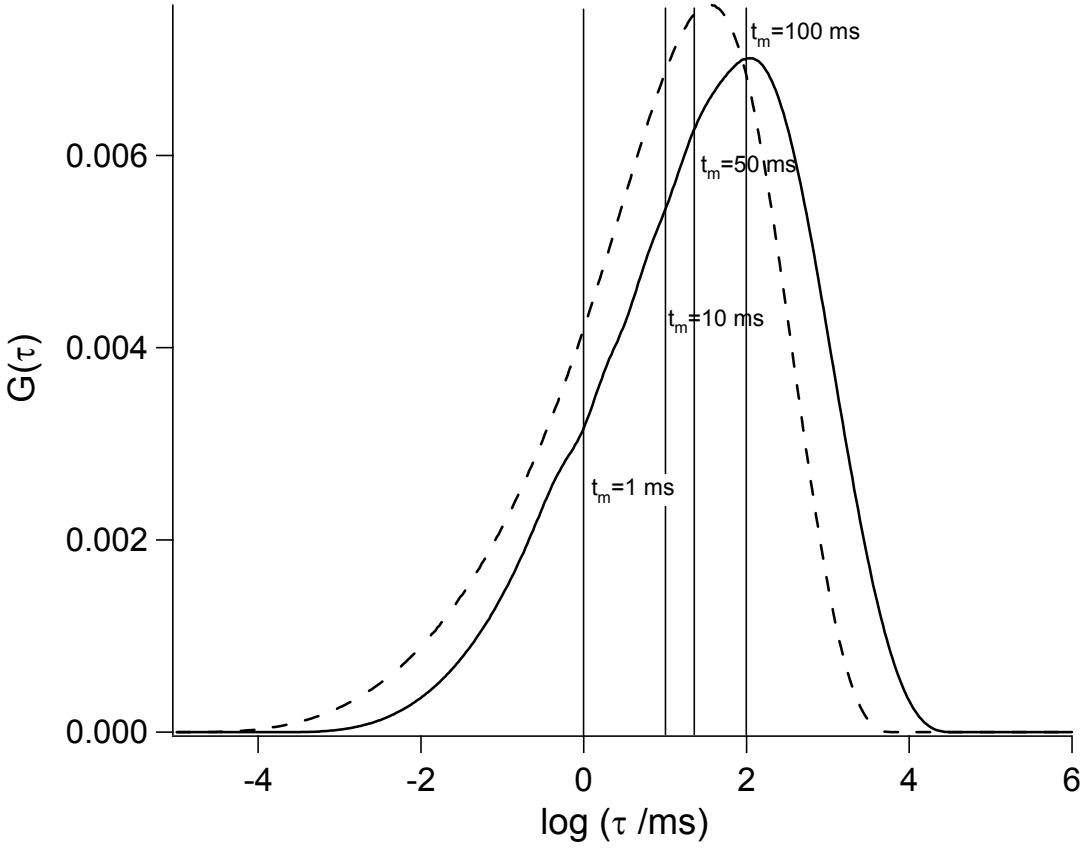

Figure 5.15. Distribution of correlation times produce via Laplace transformation of the KWW correlation function for 2D exchange experiment at 55 °C for mixing time of 1, 10, 20, and 100 ms. PVAc filled with 12.5 vol. % of silica particles (solid line) Neat PVAc (dashed line).

Similar information could be extracted from a centerband-only detection of exchange (CODEX) sequence. The sequence uses two short series of one-dimensional MAS spectra where each resolved chemical shift in the MAS spectrum can be used to determine the correlation function, correlation time, and motional amplitude of the selected resonance. The advantage of this sequence is the observation and characterization of slow segmental dynamics and reorientations while maintaining sensitivity and chemical shift resolution in a multi-dimensional sideband-free spectrum. However, the CODEX sequence does not produce a 2D synchronous plot, which not only produces an autocorrelation function but also can depicts the geometry of carbonyl-group reorientation over time via on- and off-diagonal intensity.

A major assertion made about the PVAc/silica nanocomposites is that the high surface area of the nanoparticles and interfacial interactions between the silica and the polymer changes the mechanism by which reinforcement is typically achieved in composite systems. The T_2 and 2D exchange experiments probe the overall relaxational behavior of the samples in the kHz-MHz range of frequencies and indicates that the molecular motions seen in the nanocomposite systems are in general slower and have a wider distribution. However, this description only provides limited information of how the structure of the neat sample differs from that of the nanocomposite. Another experiment is needed to probe the spatial heterogeneity of the systems to further indicate that the proposed structure in Figure 5. exists. One such experiment is a spin diffusion experiment.

5.4.6 Spin Diffusion Experiments

In this spin diffusion study, a filter based on an experiment conducted by Goldman and Shen selects what appears to be the most mobile polymer components, by analysis of the Bloch decay of the filled sample at 55 °C.[40,49] A Goldman-Shen sequence utilizes a filter in which magnetization of rigid material is allowed to attenuate between two 90° pulses separated by a filter time. During the mixing time (t_{mix}) the magnetization now stored in the mobile component of the polymer will diffusive throughout the sample. A t_{filter} of ~ 300 μs was chosen to allow the signal from the rigid chains to relax, while the remaining magnetization is left in the mobile region of the polymer sample. This magnetization is stored and recalled by a third 90° pulse after a mixing time has elapsed. The Goldman-Shen filter, as shown in Figure 5.16, can now be used to probe the full relaxation behavior of the mobile region of the polymer.[49,50] Also, during the mixing time, magnetization from the mobile chains will diffuse to the rigid chains until equilibrium is achieved; therefore by varying the mixing times the time to magnetization equilibrium can be determined and the distance between mobile and rigid components can be established.

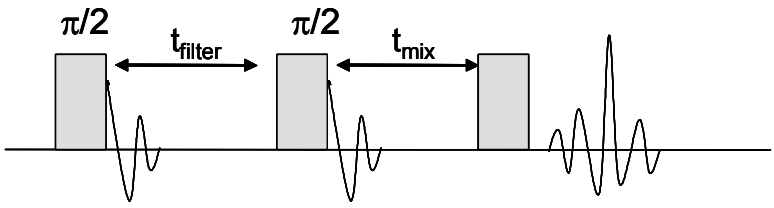

Figure 5.16. Pulse sequences for the measurement of molecular motion and dynamics in poly(vinyl acetate)/silica nanocomposites. π/2 and π denote 90° and 180° rf-pulses, respectively. The spin diffusion sequence selects mobile polymer chains, and measures the domain size as the magnetization equilibrates throughout the sample based on a pre-selected filter (t_{filter}).

An issue initially considered was what exactly was being probed in the spin diffusion experiments for the neat and filled sample. Later work was conducted by Spiess and co-workers, in which 4D-CP experiments were performed on PVAc. The 4D-CP sequence used measured the length and time scales associated with cooperatively rearranging regions of dynamic heterogeneity, composed of fast and slow relaxers at 55 °C.[42-44,51,52] The data showed clusters of rigid polymers segments were found to have a diameter of ~ 3 nm and persist on a time scale equal to the relaxation of the chain segments within them. These dynamic regions of fast and slow relaxers impart the non-exponential α-relaxation seen in an amorphous polymer and discussed above. Therefore a reasonable assumption in this study is that the signal attenuation in the resulting spin diffusion data was due to transfer of magnetization throughout the proton spin system of the matrix from a sub-ensemble of chains. At the beginning of the experiment the filter selects a sub-ensemble of mobile chains that are spatially transient over time in the neat samples. Though this is true when bulk sampling is taken the ration of mobile to rigid chains persist throughout the experiment. Essentially through an initial rate approximation measuring the effective size of mobile domains as defined by the filter is possible. Also, it is important to understand although we will assign a geometric diameter to the mobile and rigid regions in the neat sample the shape of these domains are undefined. As described by Spiess, these domains could be compact clusters forming an infinite combination of shapes or could be a continuous interpenetrating structure. However, we believe the filled sample on the other hand has more of a defined structure. The nanoparticles act as a point from which a gradient of chain mobilities is formed. The

filter in this case will select the chains whose motion is the least retarded, providing information about the filler-matrix structure in the nanocomposite.

Figure 5.17 shows the spin diffusion curves where the y-axis is the normalized intensity (I/I_o) of the mobile phase of the sample as a function of the square root of the mixing time for both the neat and filled samples at 55 °C. The two curves show different spin diffusion behavior. The neat sample shows a monotonic curve that suggests a plateau value is reached indicating a single initial fast decay process from mobile to rigid chains. An exact plateau value could not be obtained because useable data for the neat sample beyond t_m = 400 ms was not acquired for reasons stated in the experimental section. However for both data sets, an approximate plateau value was extracted by fitting an exponential function to the longest mixing times. The nanocomposite spin diffusion curve on the other hand appears to have a sigmoidal initial profile and shows a superposition of fast and slow decay processes, indicating three resolvable domain sizes characterized by mobile, rigid and intermediate chain mobilities.[53]

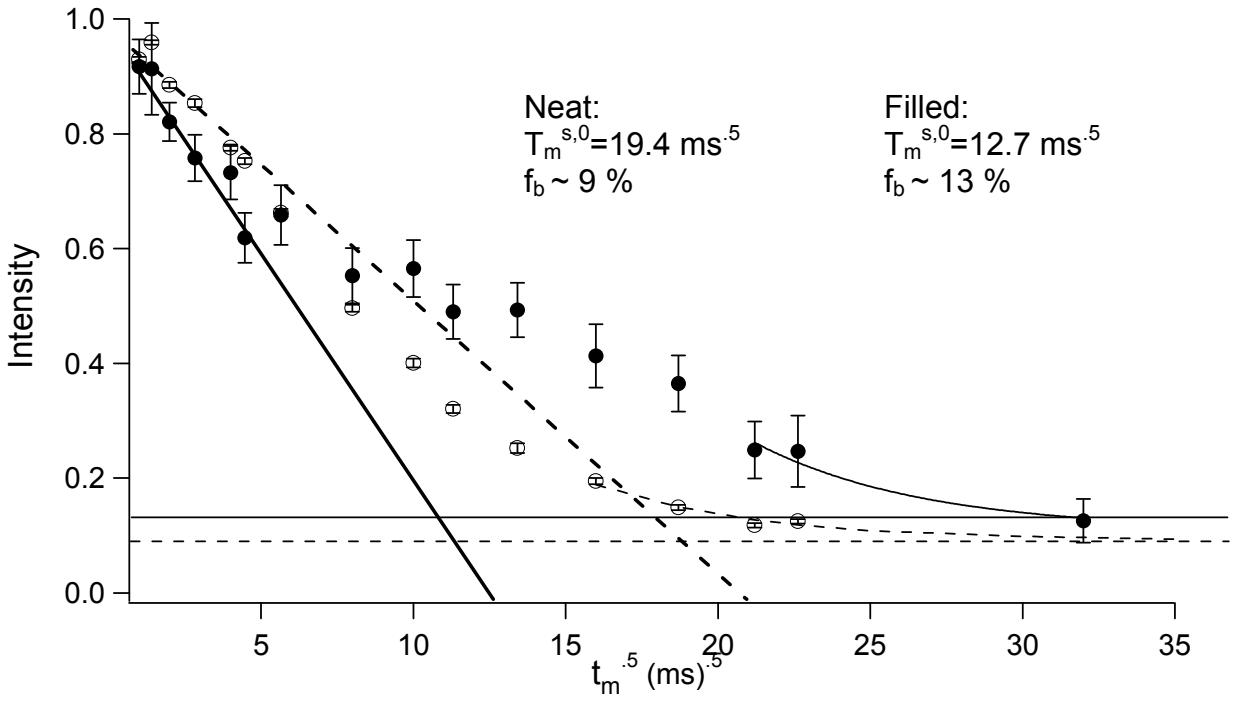

Figure 5.17. Spin diffusion curve plotted as normalized intensity of the mobile regions in the sample, as a function of square-root of the mixing time, $t_m^{½}$ at 55 °C. PVAc filled with 12.5 vol. % of silica particles (●) Neat PVAc (○).

The horizontal lines across Figure 5.17 are the plateau values corresponding to the ratio of protons in the mobile and rigid regions of the polymer. Although reported, the percent of mobile chains as determined by the plateau values in the neat sample is greater that the percent of mobile chains in the filled sample. This is not only counter intuitive, but in contrast with the mobile domain diameter determined by the initial rate approximations. This may be because the spin diffusion sequence and subsequent mathematical treatments were designed to probe systems with defined areas of mobile and rigid chain mobility that persist spatially over the mixing time like a polymeric co-block system. In the neat system not only are the regions of fast and slow mobilities of undefined shape but transient in space on a time scale shorter than that of the mixing

time. This alters the concentration-gradient driven sink-source spin diffusion occurring during the mixing time until equlibration. However, this effect should be minor on the results determined from the initial rate approximation because the initial slope is established within a few milliseconds of the experiment, roughly the relaxation time of the chains in the mobile regions. The diagonal lines use the initial rate approximation, where the extrapolated linear initial decay yields the x-intercept value, which is defined as the parameter $\sqrt{t_m}^{s,0}$ and is used to measure the diameter, d_{mobile}.

$$d_{mobile} = \frac{2\varepsilon}{\sqrt{\pi}} \sqrt{D_{eff} t_m^{s,0}} \qquad \text{Eq. 5.4}$$

where ε =3 for spherical, 2 for cylindrical and 1 for lamellar domains and $t_m^{s,0}$ is considered as a measurable quantity dependent on the magnetization exchange rate between the magnetization source phase (mobile chains) and sink phase (rigid chains).

D_{eff} is the effective spin diffusion coefficient and is calculated by dividing the geometric average by arithmetic average of D_{mobile} and D_{rigid} was obtained from a calibration curve prepared by Mellinger for mobile polymer chains, which is a function that relates spin diffusion coefficients to the $1/\pi T_2$ or full width at half-maximum of a ^1H linewidth.[54] The FWHM value for the mobile component for the filled and neat samples at 55 °C was ~1000 Hz; consequently the spin diffusion coefficient of the mobile chains in this system is defined as .24 nm^2/ms.

The spin diffusion coefficient for the rigid phase can be determined in several ways.[49,55-57] The approach used in this chapter considers the fact that even though the rigid regions in PVAc will have a different spin density and spin diffusion coefficient than other rigid polymer systems the differences will be moderate. This is attributed to the inherent structural similarities of most rigid polymer systems. Since the effective

spin diffusion coefficient is a ratio of averages for the square root of the coefficients, moderate error in the spin diffusion coefficient for the rigid phase will cause negligible inaccuracy when the domain sizes are determined. The spin diffusion coefficient of poly(methyl methacrylate) in the polystyrene-*co*-poly(methyl methacrylate) studied by Spiess is .8 nm^2/ms, and is the D_{rigid} used in this chapter.

In order to make this treatment more quantitative, a geometric model by which to formally describe the morphology of the nanocomposite system is proposed. The results obtained from Eq. 5.4 using an $\varepsilon = 3$ for polymeric blend systems assume a 3-D body-centered cubic array of spheres where one phase is contained in the spheres and the other phase exist in the space filling the unit cell.[55,56] In this hypothetical geometric model, whose general structure is depicted in Figure 5.18, the silica nanoparticles are assumed to be isotropically distributed (below percolation concentration and absent of silica particle network formation) throughout a matrix of PVAc forming a simple cubic skeleton. The rotational and translational motion of the polymeric region near the silica is restricted due to interactions with the nanoparticles. This forms a shell around the nanoparticles and is seen as the faster relaxing, slower interphase component. Consequently the chains in the space filling volume of the unit cell are composed of the faster diffusing and rotating, slower relaxing mobile component. Again it is important to stress this system actually has no real long-range order but this model describes the nanocomposite on average.

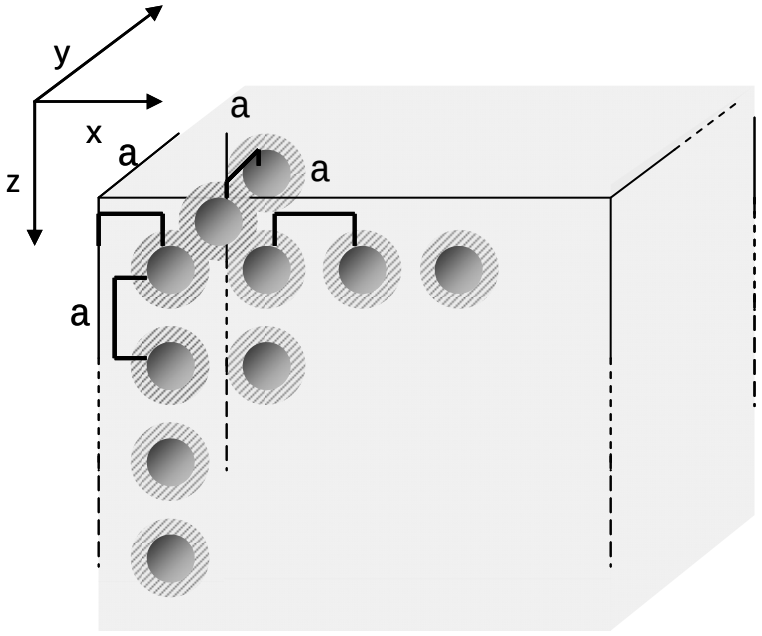

Figure 5.18. Space-filling representation of the PVAc matrix filled with 12.5 vol. % of silica particles that are isotropically distributed throughout the matrix forming a simple cubic skeleton with region of rigid polymer due to interactions a the interface of the silica and PVAc matrix characterized by light downward diagonal lines. Distance between edge of matrix and particles and in-between particles in x,y and z directions are equal, represented by **a**.

The spin diffusion experiments provide two parameters by which an effective diameter of the region of mobile chains can be determined. The first parameter $\sqrt{t_m}^{s,0}$ can provide an effective diameter of the mobile phase. The second parameter is the plateau value, which indicates the percent of rigid and/or bound chains in the sample. If the description of the nanocomposite morphology above is correct the plateau value should also correlate with the size of the shell around the silica.

The results in Table 5.1 show that for the neat sample, domains form between regions selected by the filter, $d_{mobile} \sim 34$ nm. The filled sample on the other hand formed two mobile domains: the smaller faster mobile domain with $d_{mobile} \sim 27$ nm is believed to be spatially static with respect to the mobile regions in the neat sample. This is because

the regions with mobile chains are defined or confined by the rigid shells that exist around the silica. The other domain of intermediate chain mobility perhaps represents polymer chains at the interphase between mobile and rigid regions with d_{inter} ~ 68 nm. However, the geometric representation of the nanocomposite morphology suggested above can not account for such a large interphasic region. Nothing in the model describes a situation where more than two mobility domains exist or domains exist that is larger than the spacing between particles. Therefore, the intermediate decay process, seen in Figure 5.17 for the filled sample, is more likely due to intermediate chain mobilities related to far-field interaction of the chains with the silica throughout the bulk of the sample. Essentially, the slower spin diffusion decay process results from chains whose mobility is altered via the cumulative effects of the "sphere of influence" of multiple nanoparticles, whose effect iterates throughout the sample.

Table 5.1. Calculated domain sizes for mobile regions in filled and neat samples obtained using a spin diffusion experiment, ε=3.

Samples	d_{mobile} *(nm)*	*%mobile*[e]	$Dia_{mobile\ by\ vol}$[f] *(nm)*	$Dia_{mobile\ by\ area}$[g] *(nm)*
Filled$_{@\ 55°C}$	27 ± 4[h], 68 ± 6[i]	13 ± 4	28	21
Neat$_{@\ 55°C}$	34 ± 4	9 ± 1		

Table 5.1 also shows the Dia_{mobile} calculated from the values of the percent mobile chains using volume and area arguments. This calculation was done by filling the space in a unit cell with a silica particle of the appropriate size, the appropriate amount of rigid and mobile polymer determined by percent mobile chains and the ratio of polymer to

[e] Percentage calculated from the plateau values of the spin diffusion curve of the filled and neat samples.
[f] Diameters calculated using the residual volume in a unit cube upon subtraction of the volume occupied by the nanoparticles and rigid polymer as defined by the plateau values.
[g] Diameters calculated using the residual area in a unit square upon subtraction of the area occupied by the nanoparticles and rigid polymer as defined by the plateau values.
[h] Diameters calculated from the initial fast decay in the spin diffusion curve of the filled sample.
[i] Diameters calculated from the slow decay in the spin diffusion curve of the filled sample.

silica. Assuming the morphology in Figure 5.18, a similar domain size of ~ 28 nm was calculated via the volume[j], supporting the results of the domain size as calculated from $\sqrt{t_m^{s,0}}$, while also validating the assumptions and geometric model above.

5.5 Conclusions

These experiments clearly show the power NMR has to investigate polymer dynamics. The T_2 data reveal that above T_g in the MHz range of motion, T_2 relaxation can be described with a KWW model, a distribution of exponential relaxations. Such data characterized the local molecular mobility of dangling ends, entangled chains, and chain interaction with the filler. The data clearly demonstrate that T_2 and β for the neat sample is higher than for the filled sample, suggesting the filler acts as additional chain entanglement sites. Also, as the temperature is increased these molecular motions break entanglements producing a more homogeneous relaxation behavior. A 2D exchange experiment showed that at temperatures slightly above T_g in the kHz range of motion, which was not detectable in the T_2 experiments, the neat sample has a higher β supporting the claim that the filler change the polymer dynamics of the system by acting as polymer entanglements. Lastly, the spin diffusion experiment suggests that there exists several regions of chain mobility, one of which is a shell of rigid polymer chains

---

[j] $Vol_{polymer} = Vol_{particle}\left(\frac{.875}{.125}\right)$ $\quad a = \sqrt[3]{Vol_{unit}} = \sqrt[3]{Vol_{particle} + Vol_{polymer}}$

$Vol_{rigid} = (\%rigid_{polymer})Vol_{polymer}$ $\quad r_{rigid} = \sqrt[3]{\left(\frac{3}{4\pi}\right)Vol_{rigid}}$

$Dia_{area} = \sqrt{2a^2} - (2r_{rigid} + 2r_{particle})$

$Dia_{vol} = 2\sqrt[3]{\left(\frac{3}{4\pi}\right)\left(a^3 - \left(\frac{4}{3\pi}\right)[r_{rigid} + r_{particle}]^3\right)}$

around the silica particle that have some far-field effect on more mobile chains outside the rigid region.

5.6 Future Work

The spin diffusion results on the nanocomposite only reflect the smallest distance between distinct mobile and rigid regions of the polymer matrix. Although the assumption is well based in logic and supported by other published work, it still assumes that the rigid region is bound to the nanoparticle. However, in the course of performing the spin diffusion experiments I attempted to use a novel pulse sequence to probe the length scale between the mobile polymer matrix and the nanoparticle itself. Figure 5.19 show the modified WISE spin diffusion experiment I propose to use. However, due to T_1 relaxation most of the signal is lost during the filter and mixing times. Moreover, the cross-polarization process is fairly inefficient since natural silicon has a low relative sensitivity. To circumvent this, the use of enriched silicon-29 nanoparticles could be used.

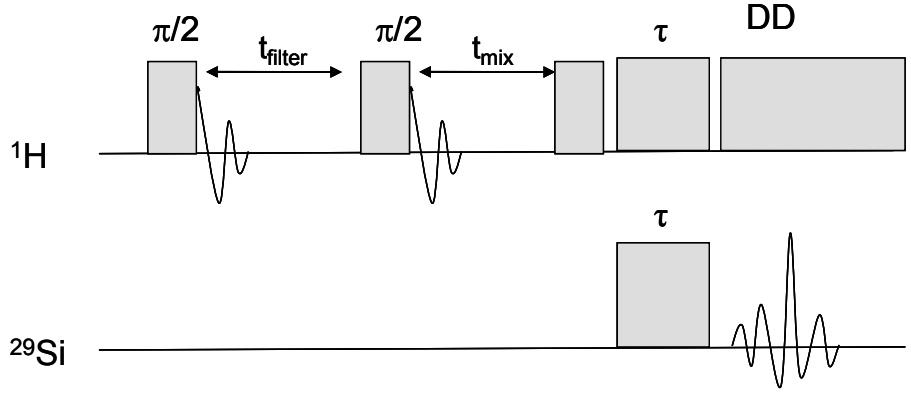

Figure 5.19. A modification of a WISE spin diffusion experiment which uses a filter to select mobile polymer chains, and measures the distance between the mobile region and the silica nanoparticle as the magnetization equilibrates throughout the sample and is cross polarized into the silica.

5.7 References

1. Ahmed, S.; Jones, F.; *Journal of Materials Science* **1990**, *25*, (12), 4933-4942.

2. Unal, U.; Mimaroglu, A.; *Journal of Reinforced Plastics and Composites* **2004**, *23*, (5), 461.

3. Liang, J.; *J. Appl. Pol. Sci.* **2002**, *83*, 1547-1555.

4. Heikens, D.; Hoen, N.; Barentsen, W.; Piet, P; Ladan, H.; *J. Polym. Sci. Polym. Symp.* **1978**, *62*, 309.

5. Cho, J.; Joshi, M.; Sun, C.; *Composites Science and Technology* **2006**, *66*, 1941-1952.

6. Gold, V.; Loening, K.; McNaught, A., *Compendium of Chemical Terminology: IUPAC Recommendations*. Blackwell Science Ltd: **1987**.

7. Zheng, Y.; Zheng, Y.; Ning, R.; *Materials Letters* **2003**, *57*, 2940-2944.

8. He, D.; Jiang, B.; *Journal of Applied Polymer Science* **1993**, *49*, 617-621.

9. Vassileva, E.; Friedrich, K.; *Journal of Applied Polymer Science,* **2003**, *89*, (14), 3774-3785.

10. Sternstein, S.; Ramorino, G.; Jiang, B.; Zhu, A.; *Rubber Chemistry and Technology* **2005**, *78*, (2), 258.

11. Sternstein, S.; Zhu, A.; *Macromolecules* **2002**, *35*, 7262-7273.

12. Sternstein, S.; Zhu, A.; *Composites Science and Technology* **2003**, *63*, 1113-1126.

13. Chazeau, L.; Brown, J.; Yanyo, L.; Sternstein, S.; *Polymer Composites* **2004**, *21*, (2), 202 - 222.

14. Wu, G.; Asai, S.; Sumita, M.; Hattori, T.; Higuchi, R.; Washiyama, J.; *Colloid. Polym. Sci.* **2000**, *278*, 220-228.

15. Vollenberg, P.; Heikens, D.; *Polymer* **1989**, *30*, 1656-1662.

16. Heiney, P.; Butera, R.; Mazur, S.; *J. Phys. Chem. B* **2000**, *104*, 8807-8821.

17. Wu, S.; *Polymer* **1988**, *29*, 2170-2173.

18. Komarneni, S.; *J. Mater. Chem.* **1992**, *2*, (12), 1219-1230.

19. Rong, M.; Zhang, M.; Shi, G.; Friedrich, K.; *Polym. Int.* **2004**, *53*, 176-183.

20. Rong, M.; Zhang, M.; Zheng, Y.; Zeng, H.; Friedrich, K.; *Polymer* **2000**, *42*, (7), 3301-3304.

21. Wu, C.; Zhang, M.; Rong, M.; Friedrich, K.; *Composites Science and Technology* **2002**, *62* 1327–1340.

22. Kalfus, J.; Jancar, J.; *Polymer* **2007**, *48*, 3935-3937.

23. Kalfus, J.; Jancar, J.; *Journal of Polymer Science: Part B: Polymer Physics* **2007**, *45*, 1380-1388.

24. Guth, E.; Gold, O.; *Phys. Rev.* **1938**, *53*, 322.

25. Hsich, H.; Hronas, M.; Hill, H.; Ambrose, R.; *Journal of Materials Science* **1983**, *19*, (9), 2997-3004.

26. Narayanan, R.; Zhu, A.; Ash, B.; Shofner, M.; Kumar, S.; Sternstein, S.; *Polymer* **2007**, *48*, 5734-5741.

27. Duer, M., *Solid State NMR Spectroscopy: Principles and Applications*. Blackwell Science: Malden, MA, **2002**.

28. Aliev, A.; Law, R.; *Nuclear Magnetic Resonance* **2003**, *32*, 238-292.

29. Blum, F.; Lin, W.; Porter, C.; *Colloid Polym. Sci.* **2003**, *281*, 197-202.

30. Lin, W.; Blum, F.; *Macromolecules* **1997**, *30*, 5331-5338.

31. Lin, W.; Blum, F.; *J. Am. Chem. Soc.* **2001**, *123*, 2032-2037.

32. Gambogit, J.; Blum, F.; *Macromolecules* **1992**, *25*, 4526-4534.

33. Brechet, Y.; Cavaille, J.; Gauthier, C.; *Advanced Engineering Materials* **2001**, *3*, (8), 571-577.

34. Shang, S.; Williams, J.; Söderholm, K. ; *Journal of Materials Science* **1995**, *30*, (17), 4323-4334.

35. Shang, S.; Williams, J.; Söderholm, K.; *Journal of Materials Science* **1992**, *27*, (18), 4949-4956.

36. Grohens, Y.; Brogly, M.; Labbe,C.; David, M.; Schultz, J.; *Langmuir,* **1998**, *14*, (11), 2929.

37. Keddie, J.; Jones, R.; Cory, R.; *Faraday Discuss.* **1994**, *98*, 219-230.

38. Ganapathy, S.; Chacko, V.; Bryant, R.;; *Macromolecules* **1986**, *19*, 1021-1029.

39. Souza, C.; Tavares, M.; *Journal of Applied Polymer Science* **1998**, *70*, 2457-2461.

40. Leisen, J.; Beckham, H.; Sharaf, M.; *Macromolecules* **2004**, *37*, 8028-8034.

41. Anderssen, R.; Husain, S.; Loy, R.; *Anziam J. 45 (E) pp, 2004* **2004**, *45*, (E), C800–C816.

42. Sillescu, H.; *Journal of Non-Crystalline Solids* **1999**, *243*, 81-108.

43. Tracht, U.; Feng, H.; Schmidt-Rohr, K.; Spiess, H.; *Phys. Rev. Lett.* **1998**, *81*, (13), 2727.

44. Matsuoka, S.; Quan, X.; *Macromolecules* **1991**, *24*, 2770-2779.

45. Apitz, D.; Johansen, P.; *Journal of Applied Physics* **2005**, *97*, 063507.

46. Alegria, A.; Goitiandia, L.; Colmenero, J.; *Polymer* **1996**, *37*, (14), 2915-2923.

47. Schmidt-Rohr, K.; Spiess, H.; *Phys. Rev. Lett.* **1991**, *66*, (23), 3020.

48. Schmidt-Rohr, K; Spiess, H. W., *Multidimensional Solid-State NMR and Polymers*. Academic Press: San Deigo, **1994**.

49. Nagapudi, K.; Leisen, J.; Beckham H.; Gibson, H.; *Macromolecules* **199**, *32*, 3025-3033.

50. Goldmen, M.; Shen, L.; *Phys. Rev.* **1966**, *144*, 321-331.

51. Tracht, U.; Heuer, A.; Spiess, H.; *Journal of Non-Crystalline Solids* **1998**, *235-237*, 27-33.

52. Tracht, U.; Wilhelm, M.; Heuer, A.; Spiess, H.; *Journal of Magnetic Resonance* **1999**, *140*, 460-470.

53. Stejskal, E.; Schaefer, J.; *Macromolecules* **1981**, *14*, 275.

54. Mellinger, F.; Wilhelm, M.; Spiess, H.; *Macromolecules* **1999**, *32*, 4686-4691.

55. VanderHart, D.; Earl, W.; *J. Magn. Reson.* **1981**, *44*, 361.

56. VanderHart, D.; *Solid State Nucl. Magn. Reson.* **1996**, *7*, 44-66.

57. Clauss, J.; Schmidt-Rohr, K.; Spiess, H.; *Acta Polymer.* **1993**, *44*, 1-17.

58. Hahn, E.L.; *Phys. Rev.* **1950**, *80*, 580.

59. Meiboom, S; Gill, D.; *Rev. Sci. Intr.* **1959**, *29*, 688.

60. Beckmann, P.; Dybowsk, C.; Journal of Magnetic Resonance **2000,** *146,* 379–380.

CHAPTER 6

Dynamics of Nanocomposites comprised of Poly(vinyl acetate)/Silica Nanoparticles Functionalized with Short PDMS Oligomers

6.1 Abstract

It has been shown that nuclear magnetic resonance of polymer nanocomposites can be applied to probe the molecular dynamics of the polymer chains in the composite matrix. Nanocomposites comprised of poly(vinyl acetate)/silica with short poly(dimethyl siloxane) oligomers (PVAc/silica-PDMS) tethered to the filler surface were made and studied to evaluate effects on the interface/interphase due to changes in the nanoparticle surface structure and chemistry. In addition to the additional reinforcement seen in dynamic mechanical analysis, T_2 data show clear evidence of reduced chain dynamics, probably due to polymer interactions with the filler and bound matrix polymer within the interphase. T_2 relaxation data were measured at temperatures between 45 and 130 °C and found to be stretched exponential in nature. At 90 °C, which is approximately 45 °C above the calorimetric T_g, the sample containing the silica nano-fillers had a wider distribution of T_2 relaxation times with a shorter characteristic T_2 relaxation time. As the experimental temperature is increased the width of the distributions for both the filled and neat samples narrows. The neat sample approaches a single exponential model fit much faster than the filled sample. The percent change in characteristic T_2 relaxation and the width of T_2 relaxation times (β) upon addition of the nano-filler to the neat PVAc increases with the PDMS surface treatment as compared to the untreated silica nanoparticles. With a 2D ^{13}C exchange NMR experiment at 50 °C, the correlation function of a selected sub-ensemble has been measured for motions on the 1 kHz range.

This experiment indicates both samples have a broad distribution of correlation times due to filler-matrix interactions, having the same characteristic correlation time. The filled sample shows a slightly broader distribution of correlation times than the neat sample.

6.2 Introduction

In Chapter 5, solid-state NMR was used to probe the interactions between PVAc and silica nanoparticles. The composite samples showed restricted dynamics, which were attributed to reduced local molecular mobility of chains inside the interface/interphase and additional entangled chains resulting from chain interactions with the filler. The spin diffusion experiments suggest the presence of several regions of chain mobility, one of which is an interphase or a shell of rigid polymer chains around the silica particle that have some far-field effect on more mobile chains outside the rigid region. This far-field effect in some combination with particle agglomeration shown with SAXS data was then used to explain the observed additional dynamic reinforcement, the Payne affect and subsequent modulus recovery upon lowering the strain amplitude. [1-4]

The size and nature of the interphase surrounding the filler is greatly affected by the filler surface chemistry and filler size, which in turn affects the bulk mechanical properties.[5-7] Sternstein et al. found changing the filler surface treatment could alter the storage and loss moduli of the composite and the relative rates of decrease in elastic modulus with increasing strain amplitude. Other than a nanoparticle with the native surface chemistry, three silane or siloxane surface treatments were examined, each having increasingly more silicone groups on the surface: dimethyldichlorosilane, hexamethyldisilazane, and short PDMS oligomers. In these cases, the interactions between the filler and matrix changes from hydrogen bonding to some combination of

physical adsorption and/or interpenetration of surface-tethered and matrix chains. Upon initial examination one might expect the relatively low miscibility of PDMS and PVAc to hinder interpenetration at the interface. However, dynamic mechanical data for the 12.5 vol. % composite show low-strain-amplitude modulus values that indicate the most reinforcement occurs with the particles having the PDMS chains on the surface and the lowest reinforcement for the dimethydichlorolsilane (hydrophobic) surface treatment, with the modulus for the composite composed of nanoparticles with native surface chemistry somewhere in between.[1-3] Sternstein attributes the viscoelastic behavior of the nanocomposite with particles having the PDMS chains on the surface with interpenetration of short surface-tethered and matrix chains due to a mechanism based on chain conformations that enable slippage at the interface.[2,3]

The mechanism by which additional reinforcement is imparted to a composite composed of filler with an oligomeric brush surface treatment is mostly through interpenetration of surface-tethered and matrix chains. The filler-matrix interface immobilizes the matrix chains via true chain entanglements. Therefore, when stress is applied to this type of composite material (above some minimal filler fraction), stress is concentrated at regions near the filler and dissipated over its entire deformation zone.[8-11] Though not heavily discussed in Chapter 5, the strength or adhesive capability of the filler-matrix interaction determines the relative amount of stress that the composite can dissipate before interfacial failure occurs. This damping effect directly correlates to the observed increase in elastic modulus seen in the nanocomposites relative to the neat material; however upon interfacial failure the elastic modulus will quickly approach that of the neat material (when above T_g). The entanglements located at the interface and

within the interphase not only act to increase the modulus and toughen the material but also influence the far-field mobility of other chains with a greater intensity than surface filler-matrix interactions based on adsorption solely promoted by secondary forces. The interface/interphase is dominated by the adhesion between chains on the filler and polymer in the matrix, and in general the adhesive force for interpenetrated interfacial systems can be classified in a combination of three possible interactions (similar to those dominating polymer-polymer interfaces) which adsorb stresses at the interface.

The stresses applied to composites where the interface is dominated by interpenetration of surface-tethered and matrix chains can be dissipated by (i) van der Waals or other secondary bonding such as hydrogen bonding between the filler and matrix across the interface, (ii) those chains from the matrix and tethered to the filler which cross the interface and are coupled by physical entanglements, and (iii) those matrix chains that cross the interface and are coupled by enthalpic interactions with the tethered chain at the interface.[12] The mechanism of interfacial interaction, the failure mechanism of the interface, and the amount of stress dissipation before interfacial failure is dictated by polymer-polymer entanglement, much like the interface of two polymer layers. **Error! Reference source not found.**.1 shows the major pathways for polymer-polymer delamination: (i) chain pull-out, (ii) chain scission, and (iii) craze formation and failure.[12,13]

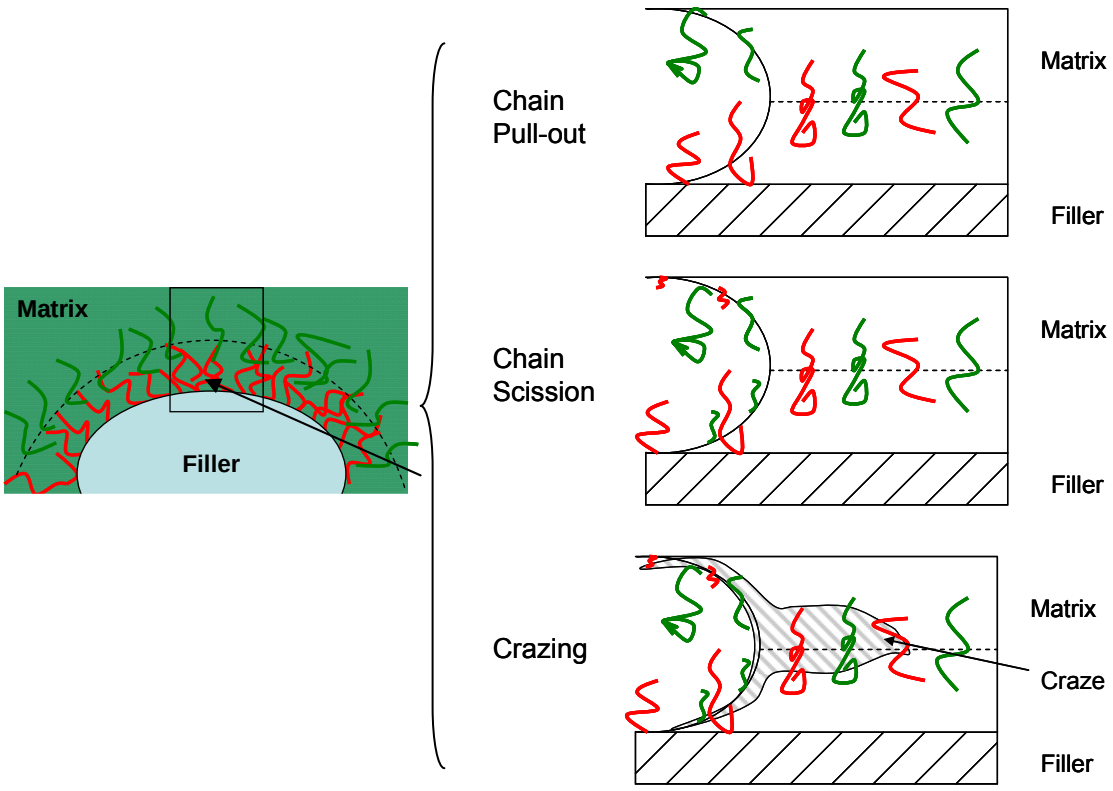

Figure 6.1. Failure mechanisms at the filler-matrix interface and interphase.

The factors dominating the behavior of the filler-matrix interface for a filler whose surface is modified with tethered polymer chains include: (1) the length of the polymer segments that are interacting (whether they are long enough to entangle or $N>N_e$, where N_e is the entanglement degree of polymerization), (2) the surface density of the tethered polymer chains on the filler, (3) the breakage strength or fracture energy (G_o) of the tethered polymer chains, (4) a thermodynamic mixing term (χ) describing the compatibility of the tether polymer on the filler and polymer in matrix and (5) the propensity of crazing ahead of a propagating crack.[12,13] Whereas adsorption and desorption controls the interfacial failure mechanism in a composite composed of untreated silica filler or silica filler with small surface-modifying moieties.

Chain pull-out of the tether chains on the filler is linked to the interfacial toughness of composite material whose interphase is dominated by interpenetration of surface-tethered and matrix chains. Most models define a stress threshold above which the rate of failure by chain pull-out increases. This threshold is defined as the fracture energy, G_o, of the interface and can be expressed by the following relationship:

$$G_o = C\sigma N^2 \qquad \text{Eq. 6.1}$$

where σ is the surface density of tethered chains , N is the degree of polymerization of the tethered polymer chains and C is a constant that includes a description of the type and energetics associated with interaction between the polymer in the matrix and the polymer on the filler.[12-15]

Chain scission, on the other hand, relies on the fracture of the covalent bonds making up the polymer chains on the surface of the filler. This failure mechanism is particularly prevalent when the polymer chains on the filler are long and the interactions between polymer chains at the interface/interphase are sufficiently large. Again fracture energy, G_o, is also associated with this failure mechanism and can be expressed by another relationship:

$$G_o \approx \sigma f_b \qquad \text{Eq. 6.2}$$

where σ is the surface density of tethered chains and f_b is the force required to break one bond along the backbone of the tethered polymer on the filler.[9,11-13,15]

If the interface undergoes significant plastic deformation a craze is formed, whose shape and size is determined by the load-bearing capacity of the polymer chains in the interphase. Upon further deformation in the interphase the polymer chains are stretched, increasing the stress at the crack tip and increasing the craze width. Once the craze is large enough due to deformation, it can fail by either chain pull-out or chain scission.

Models show failure due to crazing is related to the square of f_b, the force required to break one bond along the backbone of the tethered polymer on the filler:[9,11-13,15]

$$G_o \approx (\sigma f_b)^2 \qquad \text{Eq. 6.3}$$

Homogeneous dispersion of filler within the matrix is also an important issue when analyzing the effect of nano-filler in a composite. The increased filler–filler interactions because of the high surface area of the filler can lead to particle aggregation. In many cases, formation of larger clusters of nanoparticles because of this increased filler-filler interaction can be observed leading to material failure when subjected to stress. To increase dispersion of silica particles particularly in a hydrophobic environment of a polymer matrix, the surface chemistry of the nanoparticle is often modified. The use of small hydrophobic moieties as surface treatment to promote dispersion and adsorption of the polymer matrix onto the surface of the nanoparticle is commonplace.[16] While grafting polymerization or grafting schemes, using either "from" or "to" methodology, are also used to modify the hydrophobicity of fillers.[16,17] As a result, the filler-matrix miscibility is increased, and the filler-matrix interactions are consequently modified through the entanglement between the grafted polymer and the polymer matrix. The last effect is what I would like to probe in this chapter.

For example, a tougher poly(propylene) (PP) was formulated by dispersing nano-silica within the PP matrix by blending in a twin screw extruder. The filled PP showed stiffening, strengthening and toughening effects at a rather low filler content. Samples were compounded with untreated silica or silica modified with PP oligomers by graft polymerization initiated by irradiation. The molded parts formed from the PP

nanocomposite with the untreated silica failed by brittle cleavage while the composite with the surface-treated filler showed only plastic yielding.[11,18]

In this chapter, the chain dynamics in PVAc/silica-PDMS nanocomposites were examined with solid-state NMR in an almost identical fashion as in Chapter 5. Nanocomposites containing 12.5 vol. % nano-filler with PDMS surface treatments were studied with ^{1}H T_2 relaxation measurements and 2D ^{13}C exchange experiments.

6.3 Experimental Section

6.3.1 Materials

Amorphous PVAc (purchased from Polysciences) with a weight-average molecular weight of 90 kg/mol was used. The sample showed a T_g of ~ 42 °C measure by DSC. The polymer was obtained from Aldrich. The silica nano-filler was TS-720 fumed silica with a dimethyl siloxane surface treatment which was obtained from Cabot. Two samples were prepared: one sample of neat PVAc, the other contained 12.5% by weight of fumed silica with PDMS surface treatment with a specific surface area of approximately 115 meters squared per gram.

6.3.2 Instrumentation

Differential scanning calorimetry was performed on a Seiko Instruments DSC 220C under nitrogen purge on samples weighing 10 – 15 mg sealed in aluminum pans heated at a rate of 10 °C/min. Thermogravimetric analysis were performed on a Seiko Instruments TG/DTA 320 under nitrogen purge on samples weighing 10 – 15 mg in aluminum or platinum pans heated at a rate of 10 °C/min.

Dynamic light scattering in acetone was conducted with a Wyatt Technologies DAWN EOS light scattering detector equipped with a quasielastic light scattering autocorrelator.

Solid-State NMR Measurements

The nanoparticle NMR samples were prepared by loading them into 4-mm cylindrical ceramic MAS rotors. Repetitive steps of packing sample into the rotor were done to fully compress and load the maximum amount of sample. Solid-state NMR measurements were carried out on a Bruker DSX-300 spectrometer in a Bruker double-resonance MAS probehead at spinning speeds of 2 or 10 kHz. 128 scans were collected for ^{1}H spectra. ^{13}C and ^{29}Si spectra were gathered 5K scans with 10 s repetition delay. Both DP and CP experiments were performed with CP spectra having a 1 ms contact time.

The NMR samples were prepared as in Chapter 5. The ^{1}H T_2 measurements and 2D ^{13}C exchange experiments were conducted as in Chapter 5.

6.4 Results and Discussion

As stated before, the purpose of this chapter is to repeat the investigation of the interphase of the filler-matrix when the filler has been modified with a polymer brush to enhance dispersion and interfacial interaction. Information about the nanoparticle and the structure of the surface modification is needed first to make any appreciable conclusions from the NMR data of the composite. The silica nano-filler was TS-720 fumed silica with PDMS surface treatment obtained from Cabot. The manufacturer lists the specific

surface area obtained from nitrogen adsorption and BET analysis as 115 m^2/g, which corresponds to a particle diameter of ~ 20 nm.

The major particle radius distribution for the silica nanoparticles with PDMS surface treatment was measured with dynamic light scattering (DLS) and ranges from 49 to 306 nm with the peak maximum at 111 nm (SAXS data for the 2.5 vol. % PVAc/silica-PDMS composite suggests the radius for smallest of particle cluster in the matrix to be 70 nm). [4] Two other peaks are present in the overall particle radius distribution, one representing a single particle with a mean radius of 4 nm (or a particle diameter of 8 nm) and the other corresponding to larger aggregates with a hydrodynamic radius around 5430 nm. Both the SAXS data and DLS show not only that the nanoparticle with PDMS surface treatment itself is slightly smaller (also supported by nitrogen adsorption and BET analysis performed by the manufacturer) but it also forms smaller particle clusters than the silica with no surface treatment used in Chapter 5. This would indicate a better dispersive capability which is reflected in the material's increased reinforcement and mechanical properties of the nanocomposite.[4]

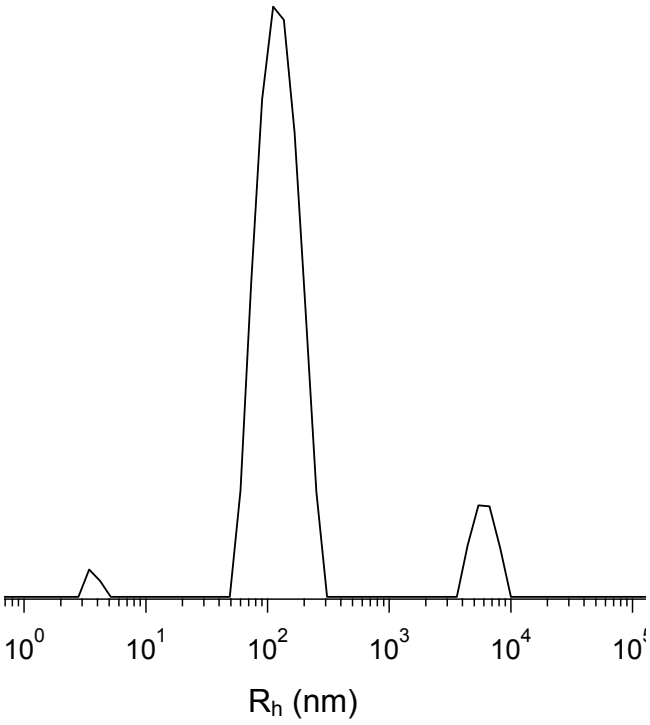

Figure 6.2. Hydrodynamic radius distribution of silica-PDMS nanoparticles and their aggregates after dispersion and sonication in dilute acetone solution at 25 °C from dynamic light scattering.

^{1}H and ^{29}Si NMR spectra were taken to determine the chemical structure of the silica surface. CAB-O-SIL© TS-720 fumed silica is described by Cabot as "high-purity silica which has been treated with a dimethyl silicone fluid". Based the NMR data, more than likely the surface treatment was performed by creating a mixture of untreated silica particles with a PDMS fluid either neat or in a dispersive solvent, and the suspension then was either heated or exposed to a basic or acidic catalytic group to cause depolymerization of the PDMS chains. The resulting silanolate group can then react with the –SiOH functionality on the surface of the nanoparticle.

The ^{1}H NMR spectrum obtained for the silica with PDMS surface treatment is shown as Figure 6.2 (a). The spectrum shows a peak at ~ .2-.08 ppm which corresponds

to the chemical shift of the methyl protons attached to the silicon atoms along the PDMS backbone. The fairly narrow resonance at ~ 2.2 ppm is attributable to –SiOH groups on the surface of the nanoparticle.[19] Typically this peak is seen as a broad resonance ranging from 2-5 ppm. Bronnimann et al. performed a study on the dehydration of a silica gel surface. Using high-resolution ^{1}H NMR, spectra of silica gel samples at different stages of hydration were collected to resolve the effect of moisture on the NMR signal resulting from surface –SiOH groups. They identified three resolvable peaks and attributed them to physisorbed water at 3.5 ppm, hydrogen-bonded silanol groups at 3.0 ppm and isolated silanol groups.[20,21] The isolated silanol resonance was detected upon evacuation of the sample at 500 °C leaving only a relatively sharp peak at ~ 1.7-2.1 ppm. The peak at ~ 2.2 ppm in Figure 6.2 (a) seems to indicate a major proportion of the residual silanol groups on the surface of the nanoparticle are isolated. Therefore, the PDMS surface treatment makes the nanoparticle surface hydrophobic and prevents appreciable adsorption of moisture.

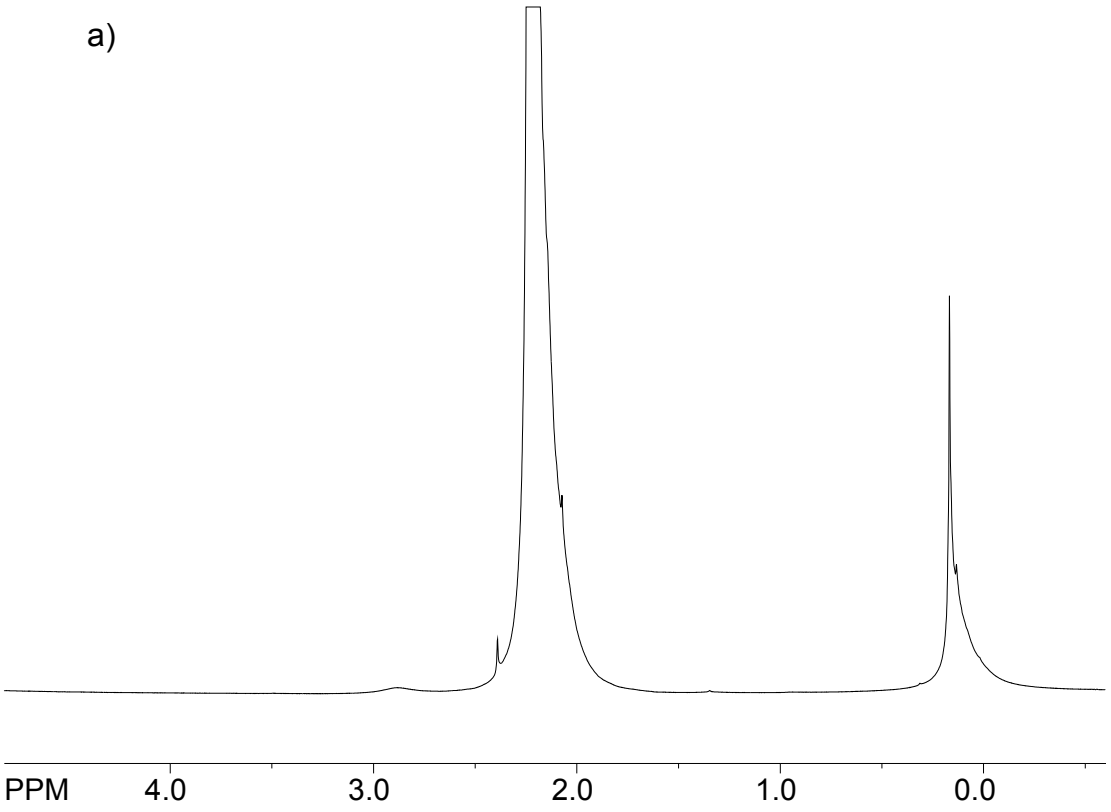
a)
PPM
4.0
3.0
2.0
1.0
0.0

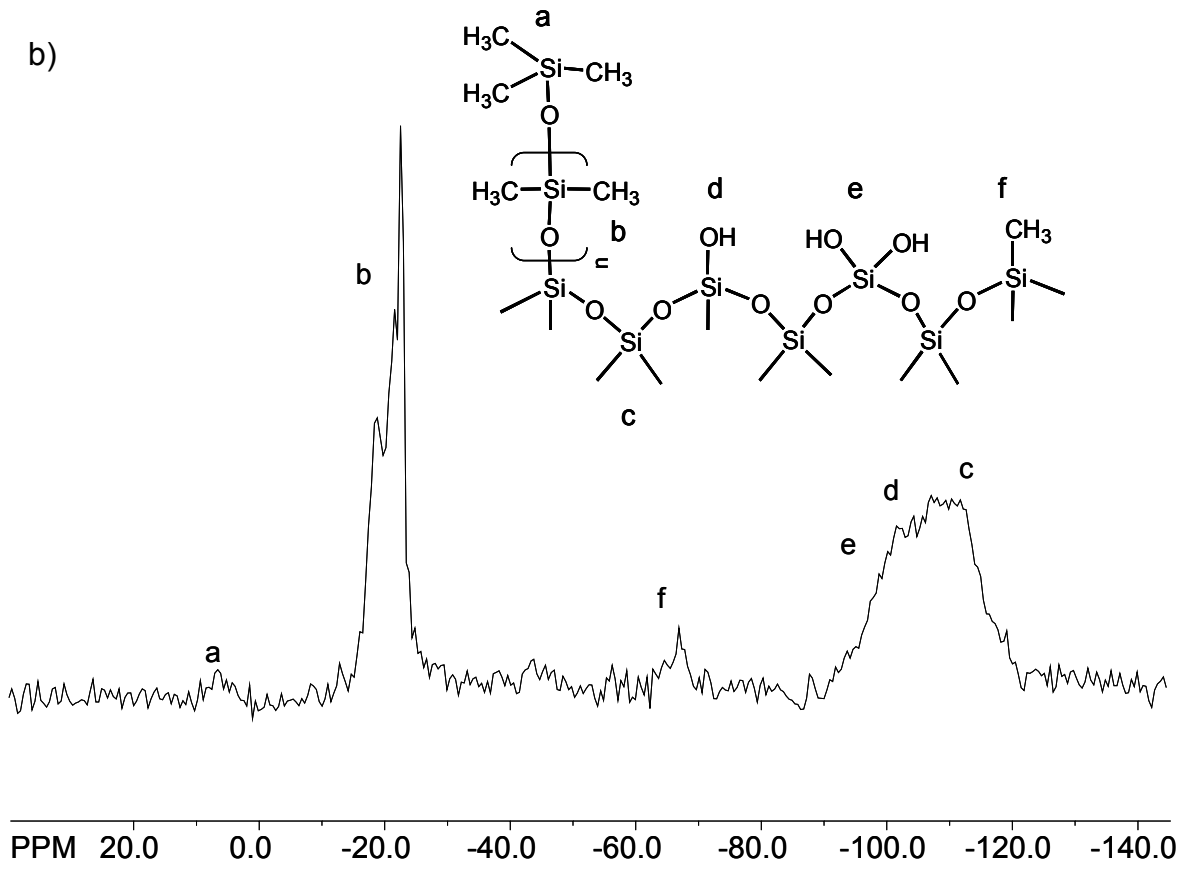

Figure 6.3. ^{1}H MAS at 2 kHz (a) and ^{29}Si CP MAS 10 kHz (b) solid-state spectra for TS-720 nanoparticles at room temperature.

The ^{29}Si NMR spectrum seen in Figure 6.3 (b) shows a narrow resonance at -22.2 ppm belonging to the silicon in the dimethyl siloxane groups along the backbone of the surface-tethered PDMS. The broad resonance at -110 ppm, actually is composed of three overlapping peaks centered at -90, -100 and -110 ppm.[22-24] The resonance at -90 and -100 ppm represents the residual surface D group silicon (silicon atoms with two siloxane bonds and two hydroxyl groups) and M group silicon (silicon with three siloxane bonds and one hydroxyl group) respectively. The resonance at -110 ppm can be attributed to the internal Q group silicon (silicon atoms with four siloxane bonds), though the relative

peak intensity represented in the convoluted peak may be misleading as this was a cross polarization experiment. Magnetization transfer efficiency decreases as the distance between protons and silicon atoms are increased; therefore the silicon toward the center of the particle will not produce much peak intensity. The two remaining resonances at 6.8 and -65 ppm corresponds to the trimethylsilyl end groups on the PDMS chains and to surface silicon atoms with three siloxane bonds and one methyl group. This suggests the dimethyl silicone fluid used in the surface treatment did indeed contain trimethylsilyl end groups.

6.4.1 Thermal Analysis

The silica nanoparticles with PDMS surface treatment were characterized by TGA analyses under a N_2 atmosphere. Decomposition of the siloxane backbone was observed in the temperature range 400 - 600 °C. Also, note that no other weight loss occurs indicating the nanoparticle does not readily retain solvent or adsorb water, supported by the lack of a broad silanol peak in Figure 6.2 (a). Using TGA it was determined that the nanoparticle is ~ 10 % by mass PDMS, and by using the quoted particle diameter and specific surface area the amount of PDMS on the surface of one nanoparticle is ~ 9900 repeat units.[k]

[k] $RU\ /\ particle = SA\left(\frac{1}{specificSA}\right)\left(\frac{1}{silica:PDMS}\right)\left(\frac{1}{Mass_{RU}}\right)(N_A)$, where *silica:PDMS* is the ratio by weight of silica to PDMS determined by TGA, *SA* is the surface area of one particle with a diameter of 20 nm, Mass = 74 g/mol and *specific SA* = 115 m^2/g.

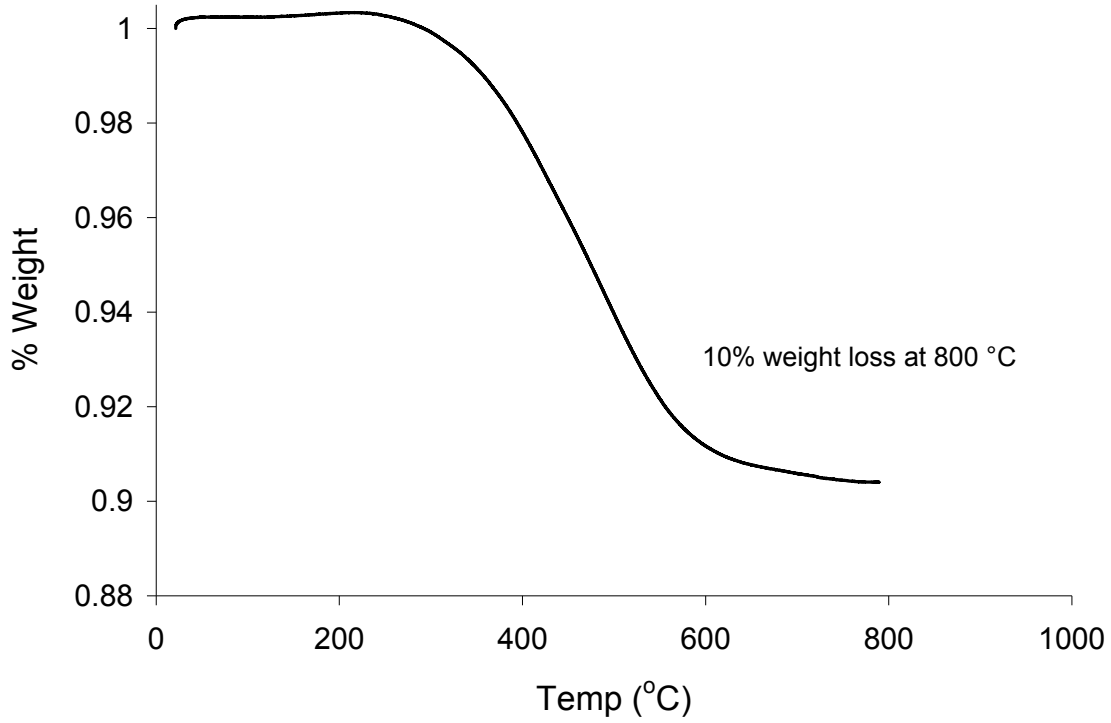

Figure 6.4. Thermogram (heating rate, 10 °C/min) for TS-720 nanoparticles that contain PDMS on their surface.

Figure 6.5 shows the DSC thermograms for neat PVAc and PVAc/silica-PDMS nanocomposite. The glass transition temperatures observed showed a slightly higher T_g for the nanocomposite, and is ~ 4 °C higher than the T_g for the neat sample which displayed a T_g at 43 °C. The increase is small, however the change in transition temperature suggests some change in the mobility of the bulk sample due to addition of the nanoparticles. Compared to the glass transition temperature shift in the nanocomposite using the silica with native surface chemistry, this composite showed a larger change. This follows the published DMA data, which showed the nanoparticle with the PDMS surface treatment increased the storage and loss moduli much more than the untreated silica.[1-3]

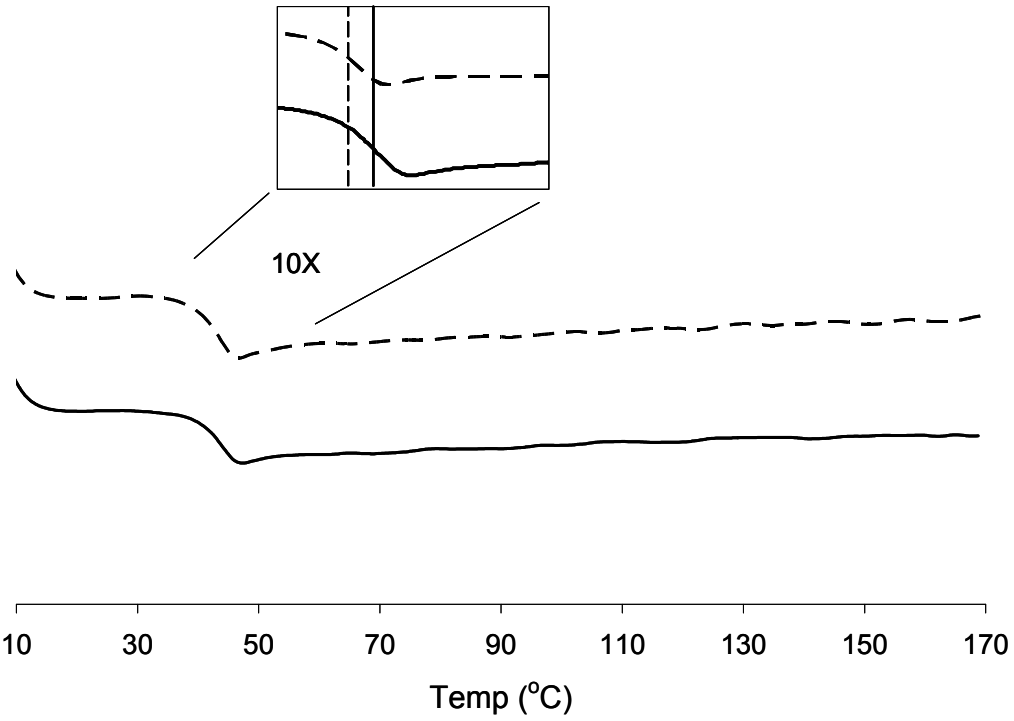

Figure 6.5. DSC thermograms (second heating, 10°C/min) for neat PVAc (dotted line) and PVAc/silica-PDMS nanocomposite (solid line).

6.4.2 ^{1}H Spectra and Bloch Decay Experiments

Figure 6.6 shows a series of ^{1}H solid-state NMR spectra for both the neat PVAc and PVAc/silica-PDMS nanocomposite. The spectra in Figure 6.6 are fairly symmetric line-shapes, seemingly described by Gaussian or Lorentzian functions. The first observation of note is the lineshape of the neat sample at room temperature. Chapter 5 goes into some detail about the appearance of the neat sample at low temperatures. The spectrum of the neat PVAc shows the superposition of at least two but what appears as the convolution of multiple peaks, with the broad components dominating the lineshape. The presence of a narrow component in Figure 6.6 (a) and (c) at room temperature seemed counterintuitive Figure 6.6 (c) overlays the neat and filled PVAc spectra for

comparison in a stacked fashion for 4 temperatures to show lineshape/width differences. When visibly dissimilar the neat sample is denoted by a red arrow). The narrower lineshape components suggest there is a fairly mobile component in the PVAc present at ~ 20 °C below the glass transition temperature. The narrow component begins to dominate the lineshape with an increase in temperature. This indicates overall chain mobility increases as the polymer structure goes from a glass to a rubber. Upon cooling from 130 °C to room temperature, the narrow component re-appears with the same relative intensity and linewidth. The re-appearance of this peak excludes solvent or moisture as the source of the narrow component at low temperatures. In Chapter 5, using 2D heteronuclear WISE NMR to probe the molecular dynamics of individual chemical groups, it was concluded that most likely the narrow component originated from smaller oligomeric "sol"-like polymer chains. The data here further support this as the neat PVAc was synthesized by a different manufacturer, yet exhibits the same ^{1}H lineshapes, indicating that it is not a sample-related issue. Instead, it is indicative of PVAc synthesized by free radical polymerization with similar molecular weight profiles.

a)

Neat PVAc

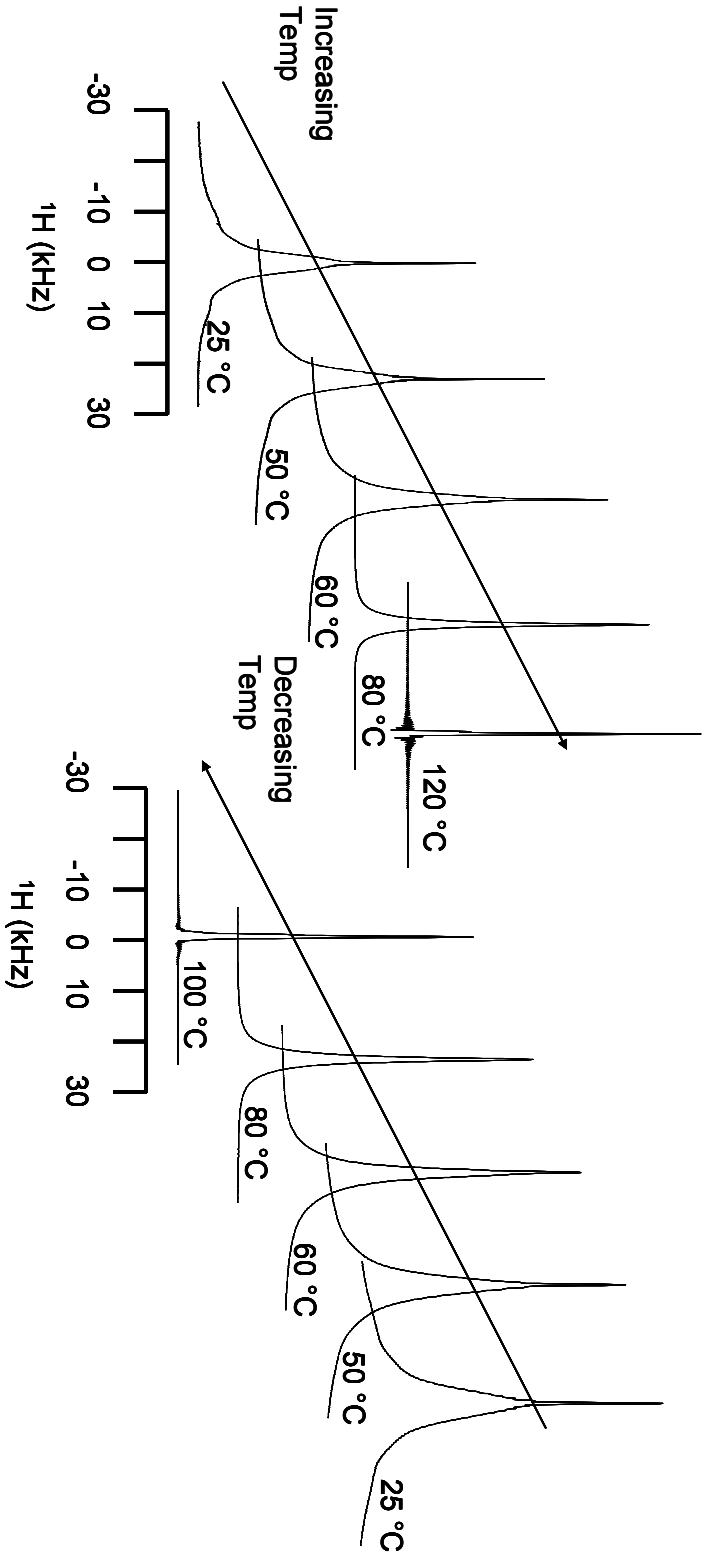
Increasing Temp
25 °C
50 °C
60 °C
80 °C
120 °C
Decreasing Temp
100 °C
80 °C
60 °C
50 °C
25 °C
-30 -10 0 10 30
1H (kHz)
-30 -10 0 10 30
1H (kHz)

b)

PVAc/silica-PDMS
Nanocomposite

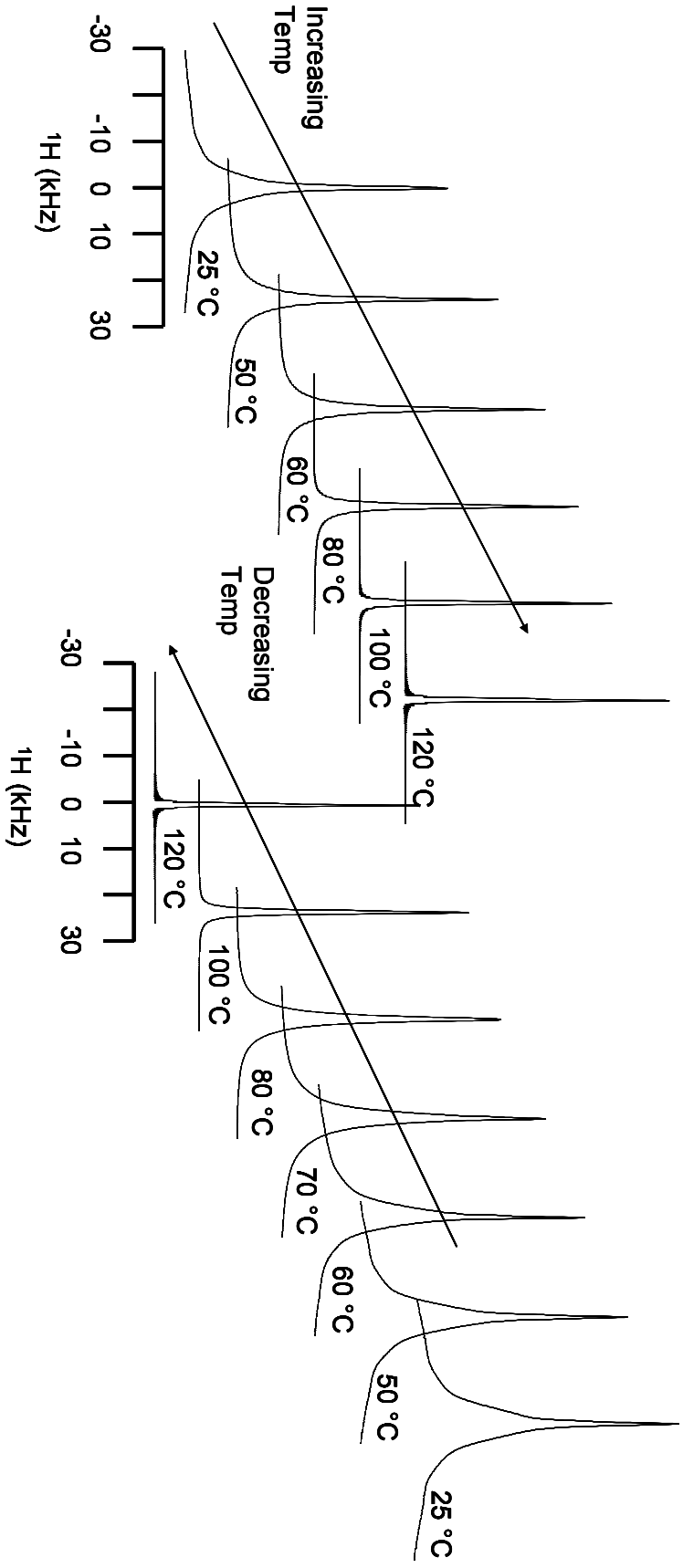

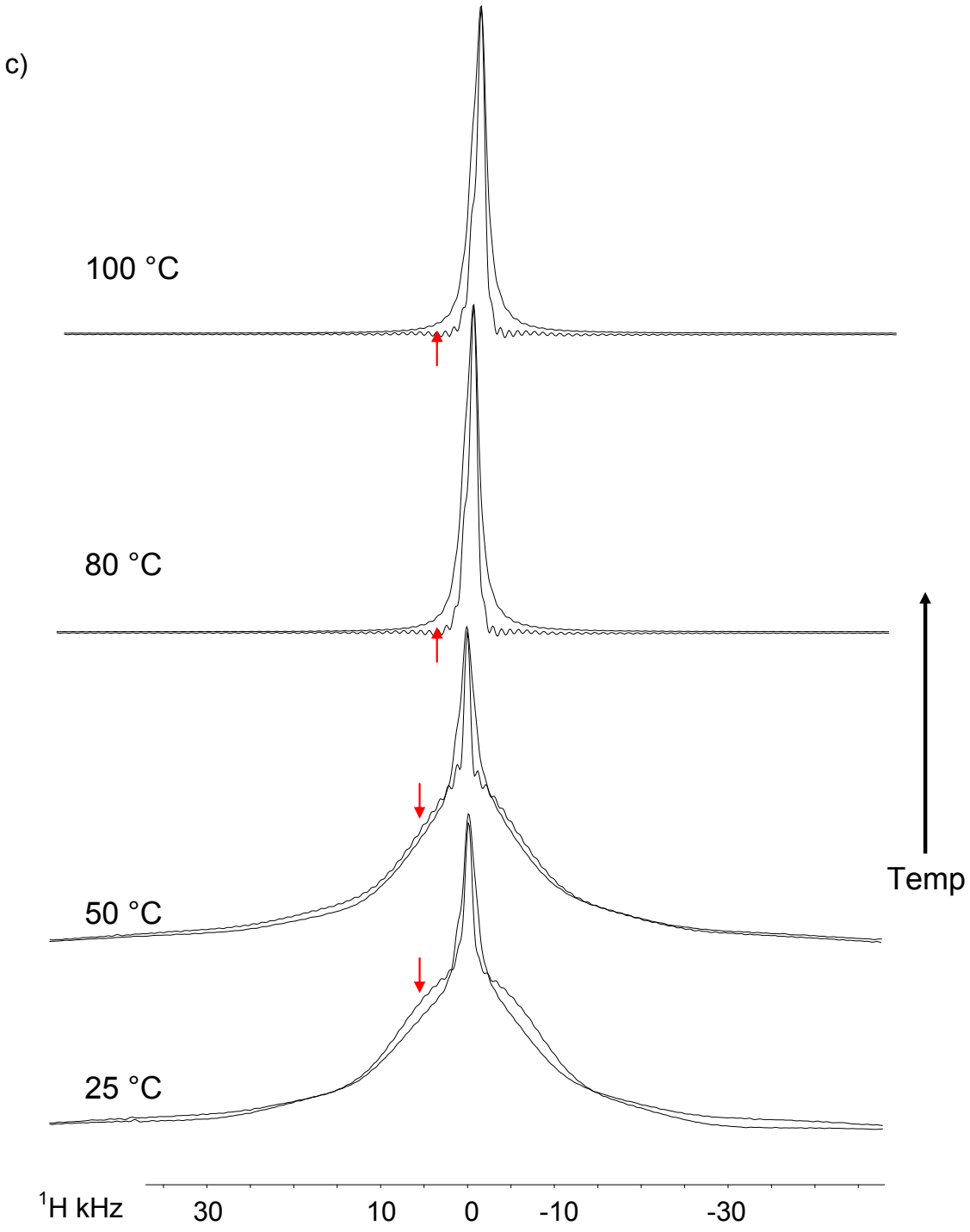

Figure 6.6. ^{1}H spectra for (a) neat PVAc and (b) PVAc/silica-PDMS nanocomposite at various temperatures. (c) Stacked spectra of the neat PVAc (denoted by a red arrow) and PVAc/silica-PDMS nanocomposite.

More important is the appearance of the spectra of the filled composite. Unlike the lineshape for the composite composed of filler with no surface treatment, the spectra at room temperature in Figure 6.6 (c) show an overall linewidth that is very similar for both filled and neat samples. Also, the narrowest component of the peak is wider for the filled sample than for the neat sample whereas the narrowest component for the composite with filler having no surface treatment and the neat PVAc were the same. This may suggest that the PDMS surface treatment reduces the mobility of this "sol"-like polymer component more efficiently than the silica with no surface treatment.

For both neat and filled samples as temperature is increased the lineshape narrows. At temperatures below or near T_g, the lineshape/width for the filled and neat spectra are almost identical except for the width of the narrowest component. The progression to a completely narrow lineshape/width requires higher temperature to initiate and achieve for the filled sample. More importantly, though both filled and neat spectra show narrow lineshapes at 100 °C, unlike the composite filled with untreated nanoparticle the linewidths of the two samples are notably different. This suggests that there is some mechanism in the filled sample that significantly increases the portion of rigid chains at temperatures above 50 °C. This same mechanism seems to also be more robust with respect to temperature as its effects are clearly still present at 100 °C.

6.3.3 Spin-Spin Relaxation Experiments

In Chapter 5 the use of Hahn echo (HE) and Carr-Purcell-Meiboom-Gill (CPMG) sequences were described to probe various regions of the chain mobility distribution.[25-27] Though there will be differences in the results depending on the sequence and data

processing procedure used, this chapter will only use the CPMG sequence and analyze the data with the KWW model with a constant offset.

Figure 5.7 shows typical spin-echo decay curves for the neat and filled samples. The curves clearly illustrate the stretched exponential character of the decay.

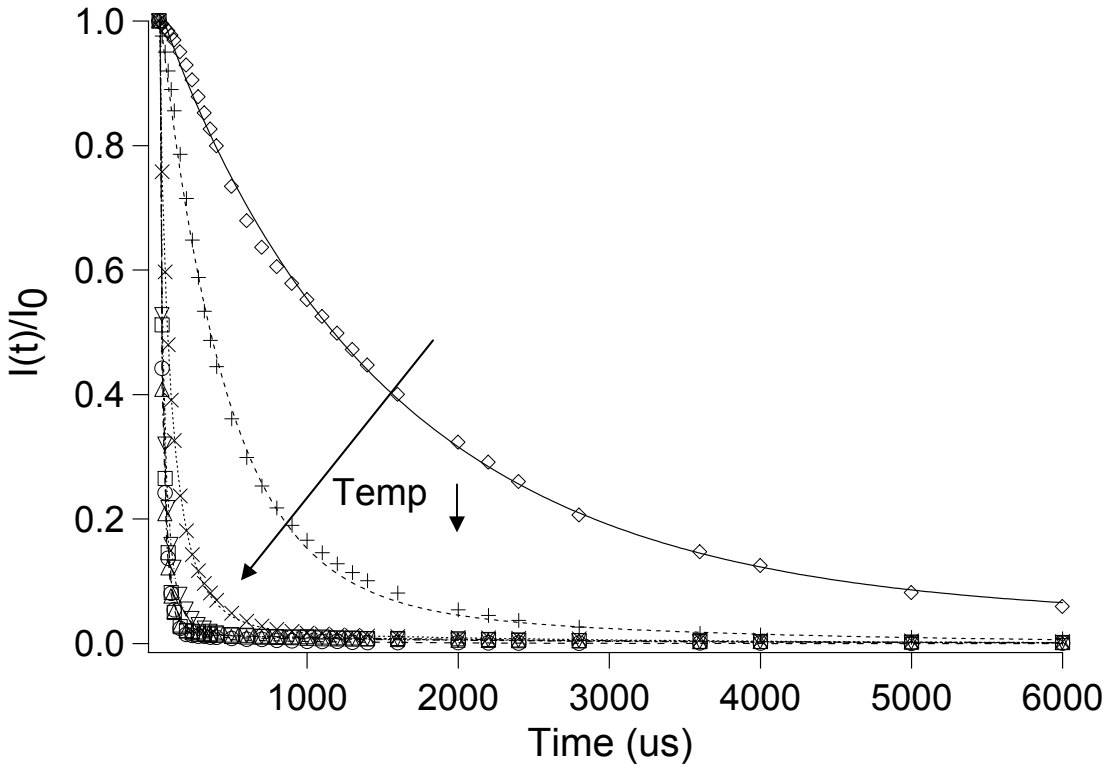

Figure 6.7. Plot of CPMG spin-echo decay for various temperatures for the neat sample. The decays are fitted to a KWW decay function as described in the text.

The values for the charactierstic T_2 relaxation times, which describe the center of the chain mobility distribution, and β values, which describe the spread of the chain mobility distribution from the KWW fit,[28] are plotted in Figure 6.8 as a function of temperature. At temperatures between ~50 and 90 °C the characteristic T_2 value of the both the neat and filled sample are very similar and < 20 μs.

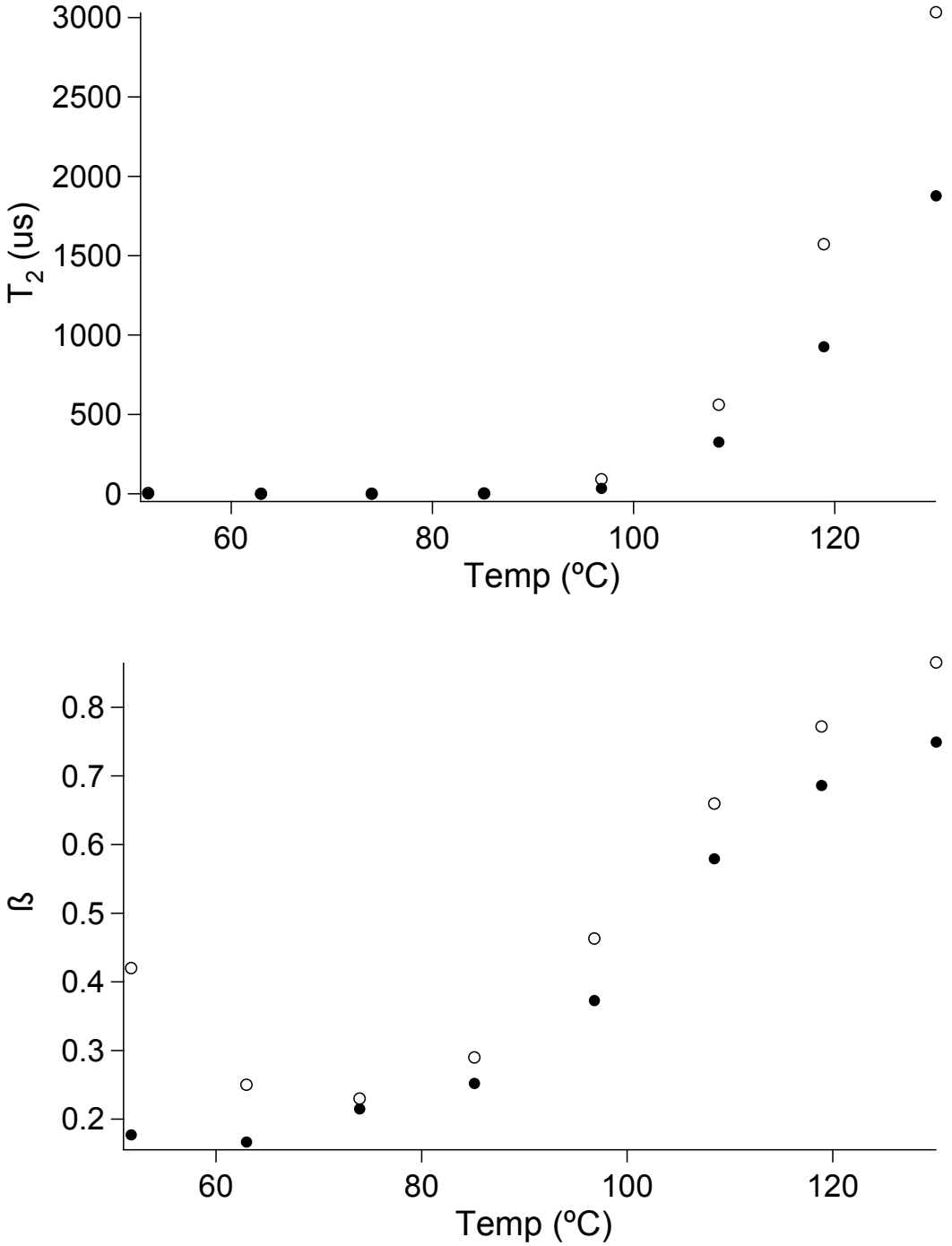

Figure 6.8. The T_2 and β values at various temperatures ranging from 50-130 °C were obtained using the KWW model with the constant offset and CPMG sequence. PVAc/silica-PDMS nanocomposite (●) Neat PVAc (○).

Above 90 °C the neat sample displays T_2 values greater than that of the filled sample suggesting that within the probed frequency range the neat sample has a greater average chain mobility with respect to the filled sample. As the temperature is increased to 130 °C the difference in the T_2 values for the neat and filled samples increases until at ~ 130 °C, the neat sample shows a T_2 value of almost double that of the filled sample. This identical behavior was observed in the composite having filler with no surface treatment and again indicates that in both samples chain entanglements are being broken by the addition of energy to the system, giving rise to more molecular motion. Therefore, the filled sample has more entanglements that resist breaking because of interfacial bonding between chains and filler.

Above 50 °C the β values for the neat sample are higher than that of the filled sample, suggesting the neat sample has a narrower distribution of the chain mobilities over all the studied temperatures. As the temperature is increased to 130 °C, β also increases, approaching 1. Like the composite having filler with no surface treatment this increase in β represents the breaking of chain entanglements, de-adsorption of the matrix from the filler and the subsequent narrowing of the distribution of the chain mobilities. However unlike the composite with filler with no surface treatment, the β values for the neat and filled samples seem to diverge due to a much lower d(β)/d(T) for the filled sample. This indicates that de-adsorption from the filler happens more readily in the untreated filled nanocomposite sample, while also suggesting the composite with a PDMS surface treatment seems to be more effective at higher temperatures. Essentially, the interaction at the interface is more robust with respect to temperature in the composite with a PDMS surface treatment. The differences in the appearance of the ^{1}H NMR

spectra at high temperatures seem to support this conclusion. Considering, the linewidths for the filled and neat samples with no surface treatment at 100 °C are the same. Whereas the linewidths for the filled sample with PDMS surface treatment is greater than that of the neat sample at 100 °C.

Qualitative correlations can be made between the changes in relaxation times and the morphological changes that occur upon blending the matrix polymer with the filler. To evaluate the difference in the surface treatment, the percent change between the neat sample and the filled composite was calculated for both fitting parameters, T_2 and β, for both the filler with the native surface chemistry and PDMS surface treatmen. (see Figure 6.9) Figure 6.9 shows that the composite with the PDMS surface treatment showed a 4- and 8-fold increase in the percent change for the T_2 and β values, respectively. Through chain interpenetration, the PDMS surface treatment reduces the degrees of motional freedom in the matrix polymer chains, and as a result the spin-spin relaxation experiments show a large decrease in relaxation times and a much wider distribution for the PVAc/silica-PDMS nanocomposite with respect to the neat sample.

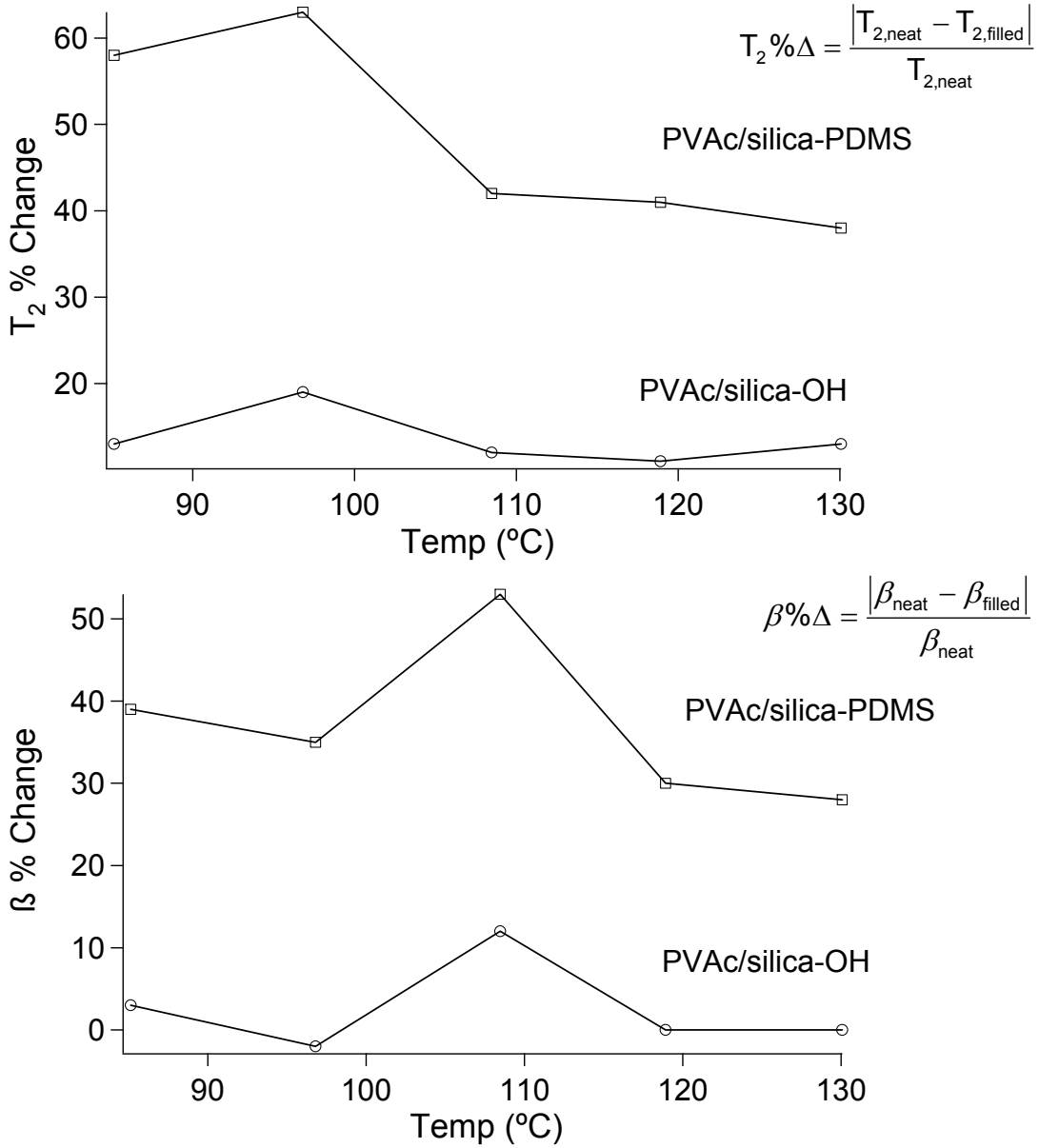

Figure 6.9. The percent change in T_2 and β values when filler is added to were neat PVAc at various temperatures from 50-130 °C. The values were obtained using the KWW model with constant offset to fit data collected using a CPMG sequence. PVAc/silica-PDMS (□) PVAc/silica-OH(○).

6.4.3 2D Exchange Experiments

2D ^{13}C exchange experiments to study the slow chain dynamics of amorphous polymers above the T_g were repeated in this chapter at 50 °C to monitor motions of the

side-group carbonyl in PVAc.[29-31] For comparison purposes I would have like to run this experiment at 55 °C as done in Chapter 5, as a small change in temperature can impart very different slow chain dynamics. However, the major drawback to this type of 2D exchange sequence is the amount of signal lost and the artifacts created due to T_1 relaxation during t_m. At 55 °C I could not get efficient cross polarization conditions to extract useful data for this particular nanocomposite system.

Carbonyl-group rotational reorientation after mixing times of 1, 10, 20, 50 and 100 ms was tracked using 2D exchange experiments and analyzed with an autocorrelation function. The autocorrelation function shown in Figure 6.0 was described by a KWW model, fitting a characteristic correlation time and the width of the distribution of correlation times (β). Both the filled and neat samples showed the same average correlation time of ~ 10 ms, the nanocomposite exhibits a slightly wider distribution of correlation times with a β of 0.25 while the neat sample exhibited a β of 0.29. Though an error calculation was not performed this difference in β most likely is not statistically significant.

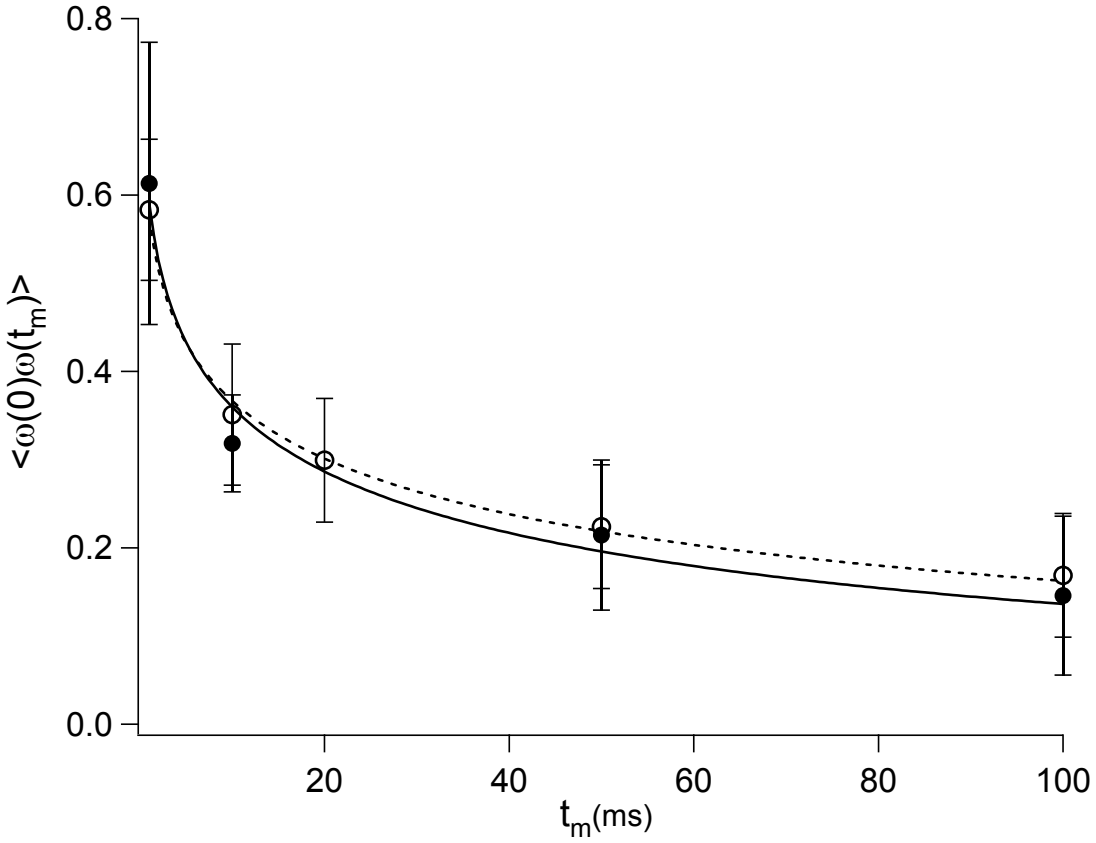

Figure 6.10. Correlation function for 2D exchange experiment at 50 °C for mixing time of 1, 10, 20, 50 and 100 ms. PVAc filled with 12.5 vol. % of silica particles (●) Neat PVAc (○).

Figure 6.11 shows the inverse Laplace transform of the correlation functions in Figure 6.10. Unlike the distribution seen with the nanocomposite of the untreated silica at 55 °C, the filled sample shows a re-orientation distribution that is not asymmetrically shifted but only may be wider than the neat sample. As expected the wider distribution of molecular motions in the filled sample is due to the additional "entanglements" produced by the filler. The fact the distribution did not asymmetrically shift can either be due to the further reduced dynamics of the system because of the change in experimental temperature or the surface treatment on the filler. Though I can not be certain, the ^{1}H spectra at 50 °C show no appreciable difference in the lineshape/width for the neat and

filled samples. The 2D exchange results seemingly support this observation, indicating the filler with PDMS surface treatment does not modify the dynamic of the polymer matrix at low temperatures nearly as much as the filler with no surface treatment. This conclusion is important as this may affect the choice of filler for an application and subsequent mechanical performance.

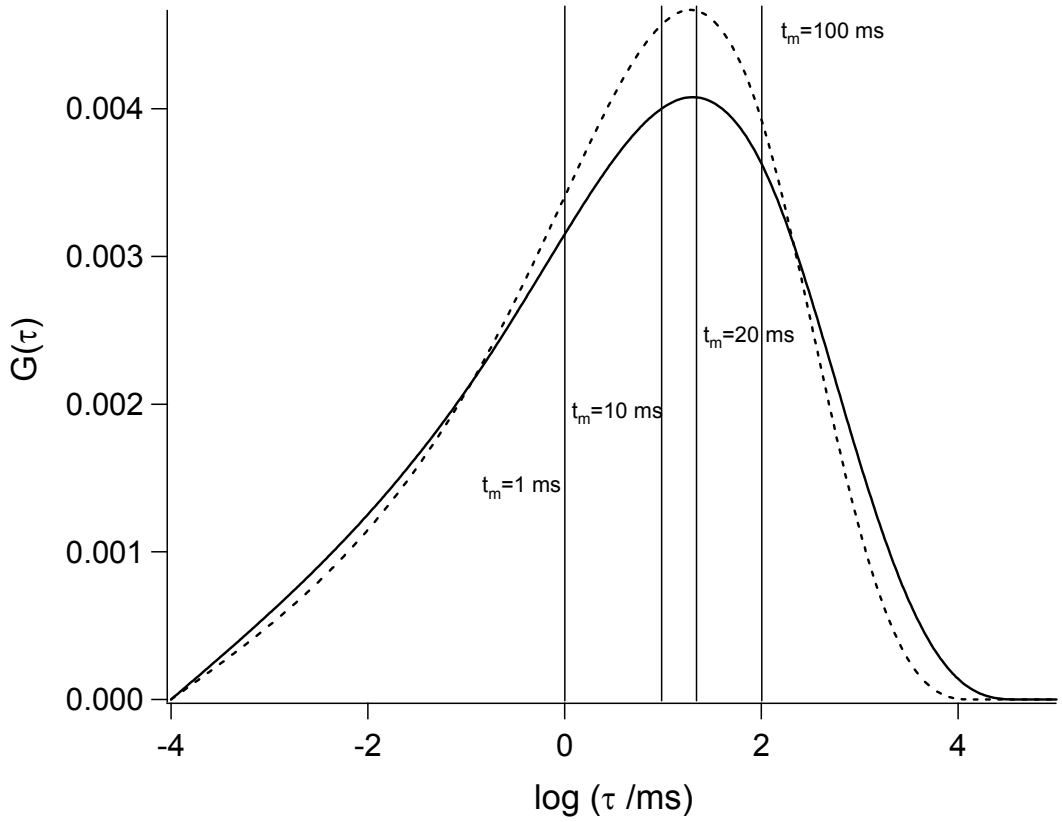

Figure 6.11. Distribution of correlation times produced via Laplace transformation of the KWW correlation function for 2D exchange experiment at 50°C for mixing time of 1, 10, 20, and 100 ms. PVAc filled with 12.5 vol. % of silica-PDMS particles (solid line) Neat PVAc (dashed line).

6.5 Conclusions

The T_2 data reveal that above T_g in the MHz range of motion, T_2 relaxation can be described with a KWW model. At 90 °C, which is approximately 45 °C above T_g, the

sample containing the silica nano-fillers had a wider distribution of T_2 relaxation times with a shorter characteristic T_2 relaxation time. When comparing the filled composite to the neat PVAc, the composite of the silica with the PDMS surface treatment shows a larger effect on T_2 and β over the same range of temperatures. A 2D exchange experiment showed that at temperatures slightly above T_g in the kHz range of motion, which was not detectable in the T_2 experiments, the neat sample has a higher β supporting the claim that the filler changes the polymer dynamics of the system by acting as polymer entanglements.

6.6 References

1. Sternstein, S.; Ramorino, G.; Jiang, B.; Zhu, A.; *Rubber Chemistry and Technology* **2005**, *78*, (2), 258.

2. Sternstein, S.; Zhu, A.; *Macromolecules* **2002**, *35*, 7262-7273.

3. Sternstein, S.; Zhu, A.; *Composites Science and Technology* **2003**, *63*, 1113-1126.

4. Narayanan, R.; Zhu, A.; Ash, B.; Shofner, M.; Kumar, S.; Sternstein, S.; *Polymer* **2007**, *48*, 5734-5741.

5. Ahmed, S.; Jones, F.; *Journal of Materials Science* **1990**, *25*, (12), 4933-4942.

6. Komarneni, S.; *J. Mater. Chem.* **1992**, *2*, (12), 1219-1230.

7. Jordan, J.; Jacob, K.; Tannenbaum, R.; Sharaf, M.; Jasiuk, I.; *Materials Science and Engineering* **2005**, *A 393*, 1-11.

8. Sides, S.; Grest, G.; Stevens, M.; *Physical Review E* **2001**, *64*, 050802 (R).

9. Rong, M.; Zhang, M.; Shi, G.; Friedrich, K.; *Polym. Int.* **2004**, *53*, 176-183.

10. Rong, M.; Zhang, M.; Shi, G.; Friedrich, K.; *Journal of Materials Science Letters* **2000**, *19*, 1159-1161.

11. Rong, M.; Zhang, M.; Shi, G.; Friedrich, K.; *Tribology International* **2003**, *36*, 697-707.

12. Brown, H.; *Ann. Rev. Mater. Sci.* **1991**, *21*, 463-489.

13. Raghava, R.; Smith, R.; *Journal of Polymer Science: Part B: Polymer Physics* **1989**, *27*, 2525-2551.

14. Washiyama, J.; Kramer, E.; Creton, C.; Hui, C.; *Macromolecules* **1994**, *27*, 2019-2024.

15. Kramer, E.; Norton, L.; Yan Sha, C.; Hui, C.; *Faraday Discuss.* **1994**, *98*, 31-46.

16. Currie, E.; Norde, W.; Stuart, M.; *Advances in Colloid and Interface Science* 2003 *100 –102* 205–265.

17. Zhao, B.; Brittain, W.; *Prog. Polym. Sci.* **2000**, *25*, 677–710.

18. Wu, C.; Zhang, M.; Rong, M.; Friedrich, K.; *Composites Science and Technology* **2005**, *65*, 635–645.

19. Hartmeyer, G.; Marichal, C.; Lebeau, B.; Rigolet, S.; Caullet, P.; Hernandez, J.; *J. Phys. Chem. C* **2007**, *111*, 9066-9071.

20. Bronnimann, C.; Zeigler, R.; Maciel, G.; *J. Am. Chem. Soc.* **1988**, *110*, (7), 2023.

21. Kinney, D.; Chuang, I.; Maciel, G.; *J. Am. Chem. Soc.* **1993**, *115*, 6786-6794.

22. Litvinov, V.; Barthel, H.; Weis, J; *Macromolecules* **2002**, *35*, 4356-4364.

23. Maher, J.; Cooper, N.; *J. Am. Chem. Soc.* **1980**, *102*, 7606-7607.

24. Sindorf, D.; Maciel, G.; *J. Am. Chem. Soc.* **1981**, *103*, 4263-4265.

25. Aliev, A.; Law, R.; *Nuclear Magnetic Resonance* **2003**, *32*, 238-291.

26. Meiboom, S; Gill, D.; *Rev. Sci. Intr.* **1959**, *29*, 688.

27. Hahn, E.L.; *Phys. Rev.* **1950**, *80*, 580.

28. Anderssen, R.; Husain, S.; Loy, R.; *ANZIAM J.* 2004, *4*, (E), C800–C816.

29. Schmidt-Rohr, K.; Spiess, H.; *Phys. Rev. Lett.* **1991**, *66*, (23), 3020.

30. Schmidt-Rohr, K.; Spiess, H.; *Macromolecules* **1992**, *25*, 3273-3277.

31. Schmidt-Rohr, K; Spiess, H. W., *Multidimensional Solid-State NMR and Polymers*. Academic Press: San Deigo, **1994**.

CHAPTER 7

Dynamics of Nanocomposites comprised of Poly(vinyl acetate)/Silica Nanoparticles with PDMS Tethers or Loops

7.1 Abstract

SiO_2 nanoparticles with poly(dimethyl siloxane) surface-tethered or looped structures were synthesized by surface grafting commercially available mono-terminated and telechelic PDMS oligomers. This was achieved by first modifying the silica with triethyloxysilane to convert surface-present silanol groups to hydrosilane functionality. The terminal carbinol groups on the PDMS oligomeric precursors were covalently attached, forming a polymer brush-like structure via the newly converted Si-H groups at the surface of the silica, using a platinum-catalyzed O-silylation coupling reaction. The structure of the PDMS brush layer at the surface of the silica was studied by means of TGA, ^1H MAS NMR and T_2 relaxation experiments. While NMR confirms the presence and covalent attachment of PDMS on both the nano-filler modified with loops and tethers, TGA suggests that the amount of PDMS on the surface of one nanoparticle modified with loops is ~ 41 chains or $1.81*10^{18}$ chains/m^2 of particle and with tethers is ~ 5 chains or $2.20*10^{15}$ chains/m^2 of particle. T_2 relaxation experiments on the nanoparticles suggest that the structure on the nano-filler modified with loops indeed has both end groups attached to the surface of the particle. The T_2 relaxation data also indicate the nano-filler modified with tethers has much more overall chain mobility and only one end group attached to the surface of the particle. Nanocomposites comprised of poly(vinyl acetate)/silica with short PDMS oligomers in a loop or linear tethered

conformation were made and studied to evaluate the changes in the composite interface/interphase due to changes in the topological structure of the surface treatment. T_2 relaxation data were measured at temperatures between 45 and 120 °C and found to be stretched exponential in nature.

7.2 Introduction

Grafting or tethering polymer chains, either covalently or non-covalently to solid supports or at interfaces is a widely used route to tailoring surface properties, adhesion properties or compatibilizing interfaces.[1] The development of chemical microsensors for a host of applications has initiated a great deal of research in the control growth of thin-films onto solid supports. To be useful as a sensor the organic layer attached to the substrate must have well-defined structures exhibiting uniformity, stability, and reproducibility. Using self-assembled monolayers in which the head groups have silane functionality and the tail groups have vinyl functionality, covalent attachment of polymers through catalytic hydrosilylation reactions were achieved. Yang grafted poly(methylhydrosiloxane) (PMHS) oligomers or PMHS derivatives that incorporate molecular recognition sites onto the solid surfaces covered with vinyl-terminated SAMs using hexachloroplatinate(IV) hexahydrate. He was actually able to fabricate sensors to could detect *o*-nitrotoluene (TNT) at parts per billion concentrations.[2]

Another sensing application uses gold nanoparticles functionalized with oligonucleotides. A DNA array detection method was then developed using the binding of the gold nanoparticles functionalized with oligonucleotides with target nucleotides. The binding events localize the gold nanoparticles within silver electrodes on a micro-

fluidic chip bridging the gap between electrodes. This leads to an increase in conductivity, and it was reported that this system could detect DNA at concentrations as low as 500 femtomolar.[3]

To increase an inorganic material ability to disperse in hydrophobic environments often polymer is attached to the surface to modify its hydrophobicity. Monodispersed polystyrene/silica composite particles were synthesized via *in-situ* emulsion polymerization of styrene. The silica nanoparticles were first modified with oleic acid through reaction of the carboxylic acid group and the silanol functionality on the silica. The modified particles were then added to styrene monomer and the reaction latex encapsulating the silica in PS.[4]

The majority of published literature is related to the tethering of linear conformations or encapsulation of a solid support. However, I believe grafting polymer loops to the surface would further alter the surface, adhesion or interfacial properties of a substrate. To begin to understand the potential of these looped structures I first looked a work conduct by Dadmun et al. They investigated the role of copolymer architecture on compatibilizing polymer layers. Specifically his group made a series of styrene and methyl methacrylate copolymers with varying architectures to compatibilize a polystyrene/poly(methyl methacrylate) interface.[5] Using anionic polymerization to synthesize PS-*b*-PMMA, a diblock, triblock, pentablock, heptablock copolymer and a random copolymer with similar molecular weights and comonomer fractions were prepared. The interface of the PS and PMMA polymer layer was saturated by the co-block materials, and interfacial fracture toughness was investigated using an asymmetric double cantilever beam. It was found that increasing the number of blocks strengthens

the PS/PMMA interface. When block segments had a molecular weight greater than ~ 21 kg/mol (a minimal block length needed for entanglement $N>N_e$) each block extended sufficiently enough into the polymer layer to cause anchoring. This anchoring was compared to stitching of the polymer layers together. As the number of blocks increase, the number of times the copolymer crosses the interface increases, increasing the number of stitches along the interface.[5-7] The loop formations, as seen in Figure 7.1, in the given polymer layers entangle with the homopolymer and their connectivity along the interface creates a mechanism by which stress can be transferred and distributed over the entire interfacial area. Specifically, when the number of blocks were increased from a diblock (similar to a linear tether) to a triblock (forming a loop at the interface) the fracture toughness of the PS/PMMA interface increased from 30 to 40 J/m^2.[5]

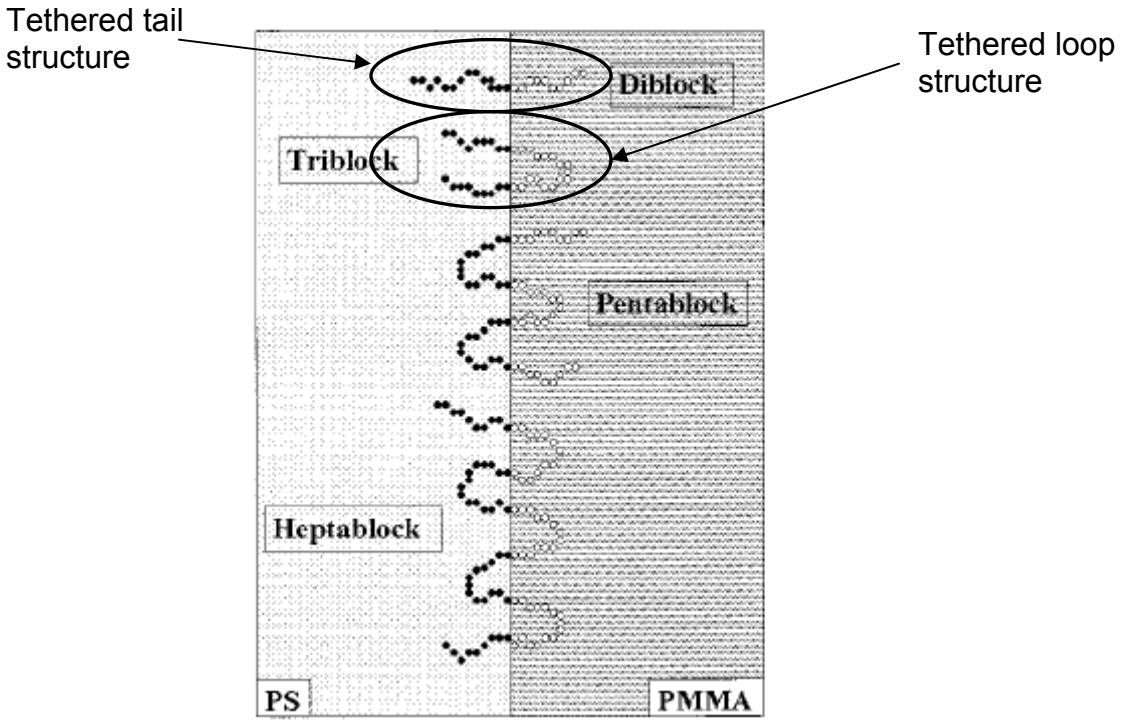

Figure 7.1. Illustration depicting the multiblock copolymers at the polymer layer interface. [Reprinted with permission from Eastwood, E.; Dadmun, M. Macromolecules **2002**, 35, 5069-5077. Copyright © 2002 American Chemical Society.]

Most work involving the synthesis and characterization of polymer brush layers on surfaces and at interfaces revolve around tethering linear polymers to create tail conformations at the surface. However, the formation and subsequent application of loop conformations at surfaces and interfaces can be advantageous, as they exhibit enhanced and novel interfacial properties relative to those tethered chains in linear tail conformations. Monte Carlo simulations done by both Dadum and Balazs support the experimental results above on multi-block copolymer interfacial compatibilizers and demonstrated that, given a block segment extended sufficiently enough into the polymer layer the number of "stitches" determined the ability of the copolymer to improve interfacial adhesion. Whether failure occurs by chain scission or pull-out, the loop conformations that extended into each polymer layer for the multi-block system greatly increased interfacial adhesion as compared to the di-block system, which again represents a tail conformation at the interface.[8-10] Irvine et al. conducted self-consistent mean-field treatments of grafted linear and star polymers at an impenetrable surface. They suggest grafted star polymers may display advanced resistivity to cell and protein adhesion, attributing this to increased surface coverage compared to the linear polymers and consistent with of multiple end groups localized at the surface forming looped structures.[11] Shull, on the other hand, obtained numerical solutions from a set of self-consistent-field equations describing telechelic polymers whose end groups adsorbed onto a substrate, again forming a loop. He found that an adsorbed polymer layer of loops had an enhanced tendency for autophobic wetting, the property of a liquid being unable to spread upon its own adsorbed monolayer.[12] Some preliminary work conducted in our

laboratory show cyclic polymers (PDMS) resisted surface leaching more than linear polymers (PDMS) of the same chemical identity and molecular weight from an incompatible polymer matirx (PS).

Litvinov et al. examined at the structure of a grafted layer of PDMS on silica particles. Though their intention was not to form looped structures at the surface, they found using ^{1}H and ^{29}Si NMR spectroscopy the grafted PDMS had a reduced relative amount of chain ends. This indicated that a considerable proportion of the grafted PDMS formed loops. The grafted PDMS layer was applied by mixing with a PDMS rubber facilitating adsorption, they then prepared two samples. The first sample followed adsorption with thermal heating to cause covalent attachment. The other sample was washed to remove the bound PDMS. DSC and proton NMR T_2 relaxation experiments were used to determine grafting density, the mobility and structure of the grafted chains.[13]

In this chapter, a synthetic route to attach PDMS chains in either a tail conformation or loop conformation was investigated. The idea being that loop conformations will increase interfacial reinforcement of the nanoparticle with the polymer matrix, increasing the resulting reinforcement. Chain dynamics in PVAc/silica nanocomposites were examined with solid-state NMR in an almost identical fashion as in Chapter 5. Nanocomposites containing nano-filler modified with looped and linear PDMS surface treatments were studied with ^{1}H T_2 relaxation measurements.

7.3 Experimental Section

7.3.1 Materials

All reagents were used as received. Monocarbinol-terminated PDMS (M_n ~ 5,500 g/mol, 100 cst) and dicarbinol-terminated PDMS (M_n ~ 5,500 g/mol, 110-140 cst) were purchased from Gelest. Hydrogen hexachloroplatinate(IV) hexahydrate (≥ 37.50% as Pt), hydrochloric acid (ACS reagent, 37%), dioxane (anhydrous, 99.9%), toluene (anhydrous, 99.9%), diethyl ether (HPLC grade, 99.8%) and tetrahydrofuran (HPLC grade, 99.8%) were purchased from Aldrich. Triethyloxysilane (98%) was purchased from Alfa Aesar.

Amorphous PVAc (purchased from Polysciences) with a weight-average molecular weight of 90 kg/mol was used. The sample showed a T_g of ~ 42 °C measure by DSC. The polymer was obtained from Aldrich. The silica nano-filler was MP-5 fumed silica which was obtained from Cabot and modified by the following procedure. Two samples were prepared: one sample of PVAc blended with 12.5 % by weight of fumed silica with tethered PDMS and the other contained 12.5 % by weight of fumed silica with looped PDMS having a specific surface area of approximately 200 m^2/g.

7.3.2 Instrumentation

Thermogravimetric analysis was performed on a Seiko Instruments TG/DTA 320 under nitrogen purge on samples weighing 10 – 15 mg in aluminum or platinum pans heated at a rate of 10 °C/min.

Solid-State NMR Measurements

The nanoparticle NMR samples were prepared by loading them into 4-mm cylindrical ceramic MAS rotors. Repetitive steps of packing sample into the rotor were done to fully compress and load the maximum amount of sample. Solid-state NMR

measurements were carried out on a Bruker DSX-300 spectrometer in a Bruker double-resonance MAS probehead at spinning speeds of 2 kHz. 128 scans were collected for ^{1}H spectra and ^{1}H T_2 measurements. ^{1}H T_2 measurements were conducted on swollen gel samples where a filled rotor was saturated with chloroform-*d* for 2 hours to equilibrate. ^{29}Si spectra were gathered by collecting 5K scans with 10 s repetition delay. Both DP and CP experiments were performed with CP spectra having a 1 ms contact time.

The NMR samples were prepared as in Chapter 5. The ^{1}H T_2 measurements were conducted as in Chapter 5.

7.3.3 Synthesis

Glassware was dried at 120 °C overnight. Round-bottom flasks with stir bars were sealed with rubber septa and cooled while evacuating and then backfilling with dry N_2.

Silanization of the Silica Nanoparticles.[14,15,21]

In a 250-mL flask with magnetic stir bar and condenser under positive nitrogen pressure, a septum was removed and 5 g of silica nanoparticles, which had been dried at 110 °C in a vacuum overnight, was transferred to the flask using a spatula. The flask was then evacuated and anhydrous dioxane (100 mL) was charged by cannula. After allowing a minimum amount of time for the nanoparticles to suspend (typically ~ 5 min), 7 ml of a 2.3 M aqueous solution of HCl was added with a syringe, and the mixture was stirred while heating to 80 °C. After allowing the temperature to stabilize, 45 ml of a .5 M solution of triethyloxysilane in THF was added with a syringe over 20 min. The solution was refluxed and stirred for another 1 hour. The particles were separated from the reaction mixture using a centrifuge at 3000 rpm for 40 min, then re-suspended in a 20:80

distilled water/THF solution. The particles were again separated from solvent using the centrifuge as before. This step was repeated, re-suspending the particles in pure THF and the diethyl ether. The particles were then washed with THF in a Soxhlet extractor for 2 hours before drying them in at 110 °C in a vacuum overnight.

Functionalization of the Silanized Silica Nanoparticles with PDMS Tethers or Loops.

In a 100-mL flask with magnetic stir bar and condenser under positive nitrogen pressure, a septum was removed and silanized silica nanoparticles (.8 g) were transferred to the flask using a spatula. The flask was then evacuated and anhydrous toluene (30 mL) was charged by cannula. After allowing a minimum amount of time for the nanoparticles to fully suspend (typically ~ 5 min), 2.5 ml of a .0035 M solution of hexachloroplatinate(IV) hexahydrate in THF was added with a syringe, and the mixture was stirred, while heating to reflux.[16] For tethers: Monocarbinol-terminated PDMS (.0004 mmol, 1 g) was dissolved in 8 ml of anhydrous toluene and added over 2 hours. For loops: Dicarbinol-terminated PDMS (.0002 mmol, .5 g) was dissolved in 8 ml of anhydrous toluene was added over 10 hours. The reaction mixture was refluxed for 8 more hours and allowed to cool. The particles were separated from the reaction mixture using a centrifuge at 3000 rpm for 40 min, then re-suspended in a 20:80 distilled water/THF solution. The particles were again separated from solvent using the centrifuge as before. The step was repeated, re-suspending the particles in chloroform and then diethyl ether. The particles were then washed with THF in a Soxhlet extractor for 2 hours before drying them at 60 °C under vacuum overnight (~ 80 % yield).

7.4 Results and Discussion

Of the numerous methods for covalently attaching a functionalized oligomer to a silica surface, in this chapter I will explore the synthesis of a bonded phase via O-silylation of polymer chains with terminal carbinol groups on a hydrosilane-containing silica support. The α-mono-carbinol and α,ω-di-carbinol PDMS used is commercially available and is similar to the material used in Chapter 4 to create the ionic-reactive PDMS moiety. The above proposed synthetic route seemed particularly attractive because of the availability of the precursor, my familiarity with hydrosilylation reactions and the fact that once modified to a hydrosilane-containing silica nanoparticle the surface modifying procedure requires only a single step. Scheme 7.1 and Scheme 7.2 depict the synthetic routes selected to form PDMS loops and tethers on the surface of a silica nanoparticle.

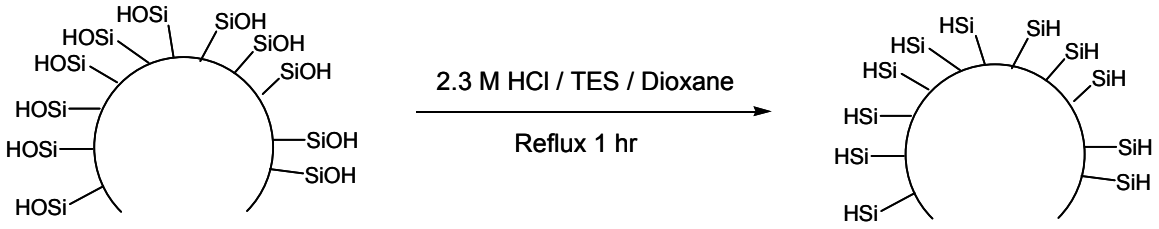

Scheme 7.1. Acid-catalyzed hydrosilanization of silica nanoparticles with triethyloxysilane (TES).

As shown in the Scheme 7.1 the silanol groups present on the surface of the silica are converted to hydrosilane groups by acid-catalyzed silanization with triethyloxysilane (TES).[14,15] The use of an aprotic solvent such as dioxane is important to avoid a competitive silanol esterification reaction. Figure 7.1 shows IR spectra collected by

diffusive reflectance of the hydrosilane modified silica, which had been washed in a Soxhlet extractor with THF for 2 hours to remove residual TES. The Si-H stretching band at ~ 2260 cm^{-1} is clearly present in the silica with hydrosilane surface treatment. The IR spectra of the unmodified silica nanoparticle[1] which was used as a precursor in the hydrosilanization reaction is also included in Figure 7.1 as a control to definitely show that the surface chemistry of the nanoparticle has been modified.

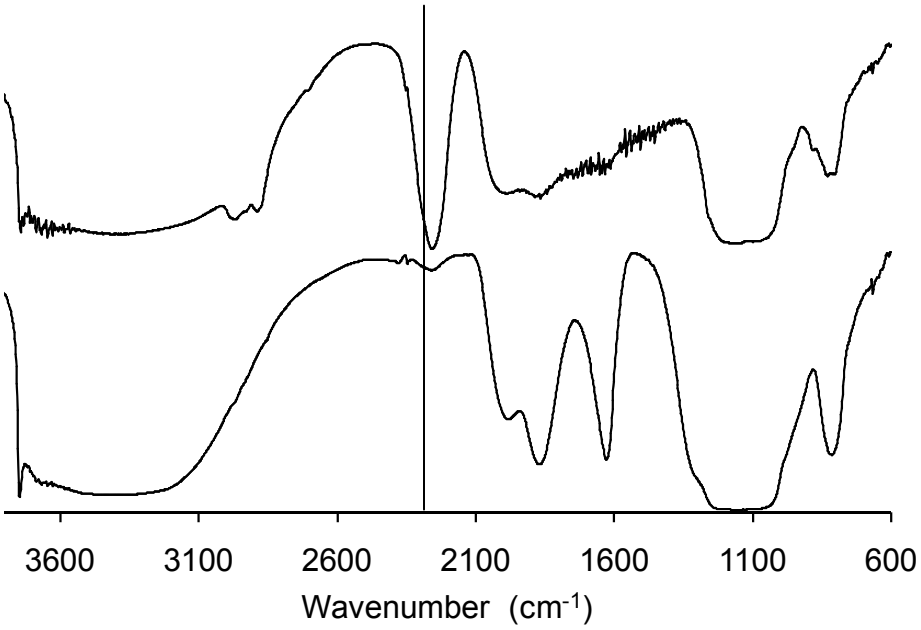

Figure 7.2. Diffusive IR spectra taken of the hydrosilane derivative of the silica nanoparticle after exposure to TES (top) and the unmodified silica (bottom).

Another aspect to be considered in these spectra is the absorption band at ~ 3200-3800 cm^{-1} due to free isolated and hydrogen-bonded hydroxyl groups. The O-H stretching of the silanols is still present in both the unmodified silica precursor and

[1] The silica nanoparticles used are the MP-5 fumed silica with no surface treatment obtained from Cabot. The manufacture list the specific surface area obtained from nitrogen adsorption and BET analysis as 200 m^2/g, which corresponds to a particle diameter of ~27 nm.

hydrosilane modified silica product. This indicates a considerable number of silanol sites remain unmodified on the surface of the silica product.

GPC on the PDMS precursors indicate that the molecular weight of both mono-terminated and telechelic PDMS oligomers is $M_n \sim 5.5$ kg/mol. This corresponds to ~ 60 repeat units of dimethylsiloxy groups, and because the terminal carbinol functionality contains oxyethylene spacers is actually ~ 90 mol % of the chain.

In scheme 7.2, carefully chosen polymer architectures were used and the route is specifically designed to produce only either loops or tethers on the surface of a solid support. Fixation of the reactive oligomers is performed by an O-silylation reaction between the hydrosilane groups on the surface of the nanoparticle and the terminal hydroxyl groups on the PDMS under reflux conditions with a catalyst. The platinum catalyst used was the so called Speier's catalyst, dihydrogen hexachloroplatinate (IV) hexahydrate.[16] The α-mono-carbinol terminated PDMS only has one reactive site which is located at the terminal end of the polymer chain. Excluding some unexpected reaction, this reactive oligomer whose other terminal end is a butyl group should produce a polymer brush-like structure on the surface of the silica nanoparticle. The α,ω-di-carbinol PDMS is telechelic in nature, having reactive functionality at either terminal end of the polymer chain. This precursor could possibly form a tethered tail conformation with a terminal carbinol group exposed or interconnect particles forming a network, but because of the carefully chosen reaction conditions more likely will form loops on the surface. To selectively facilitate loop formation the reaction was run under pseudo-dilution,[17] where the PDMS precursor was added very slowly over a 10 hour period and the final concentration was well below the overlap concentration of the PDMS. This was

done not only to limit interparticle network formation but also to ensure the available hydride sites on any one nanoparticle are not fully occupied before both ends of a telechelic PDMS chain can find the surface.

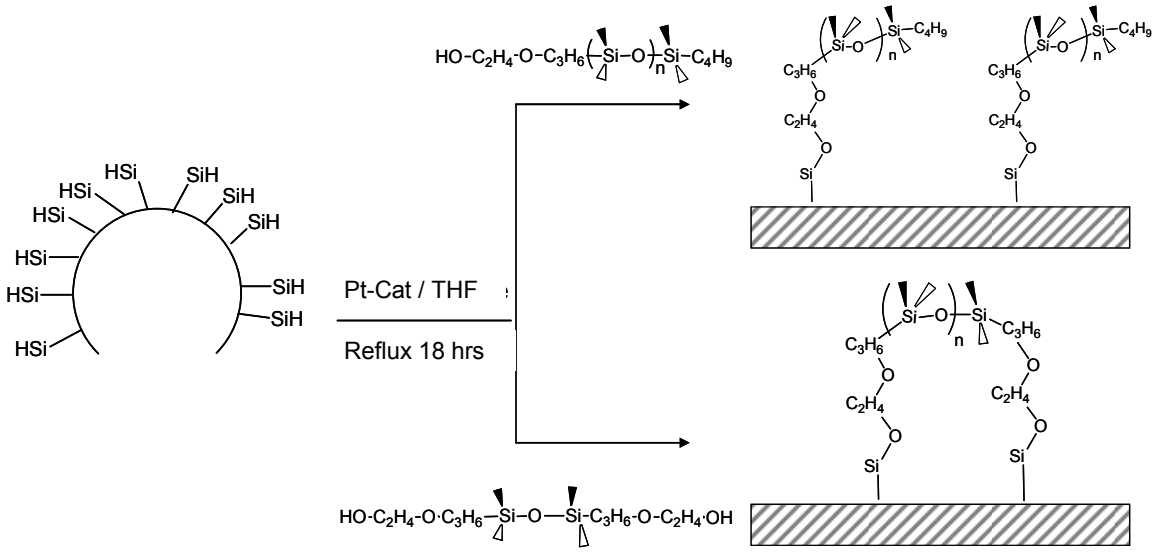

Scheme 7.2. Functionalization of the hydrosilane derivative of the silica nanoparticle via dehydrogenative coupling of the carbinol end group on commercially available α,ω-di- and α-mono-functionalized PDMS oligomers.

Both nanoparticle products were again washed in a Soxhlet extractor with THF for 2 hours to remove residual PDMS. Therefore any detectable PDMS should be attached to the particle surface. NMR of a sample of silica nanoparticle with adsorbed carbinol terminated-PDMS was used to ensure the washing procedure was sufficient to remove any residual PDMS, and is shown in Figure 7.3. One of the easiest spectroscopic techniques to verify fixation of the PDMS oligomers and their topology on the surface is to use 1H MAS NMR. The spectra shown in Figure 7.4 and Figure 7.5 are of silica nanoparticles swollen in deuterated chloroform (to increase chain mobility) and spun at 2 kHz with the intention of gaining sufficient chemical shift resolution to indentify end

groups and detect NMR resonance shifts in the methylene group in the oxyethylene spacers adjacent to the hydroxyl groups upon reaction.

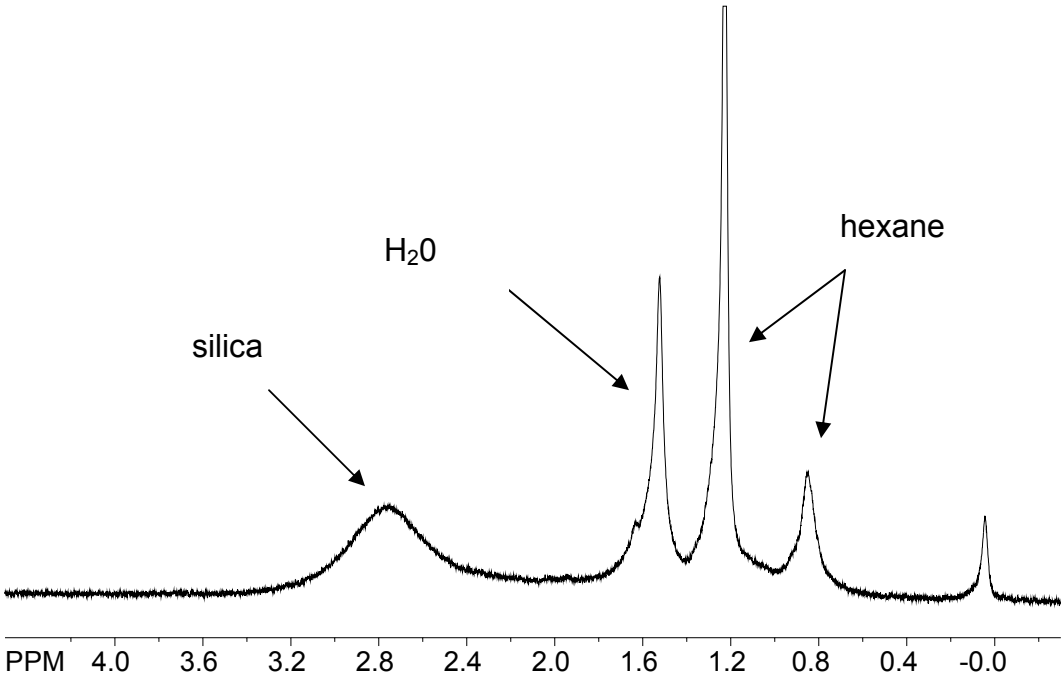

Figure 7.3. ^{1}H NMR MAS spectra of the nanoparticle in cholorform-*d* at 2 kHz after α-mono-carbinol PDMS oligomer was adsorbed onto the surface. The PDMS was then removed as described in the experimental section, by suspension of the nanoparticles in THF/H_2O, chloroform and then diethyl ether. This step was followed by washing in a Soxhlet extractor with THF for 2 hours.

The 1H NMR MAS spectrum obtained for the silica modified with PDMS tethers is shown in Figure 7.4 along with the solution spectrum of the of α-mono-carbinol PDMS oligomer which is stacked beneath. Both spectra show a peak at ~ -.2-.3 ppm which corresponds to the chemical shift of the methyl protons attached to the silicon atoms along the PDMS backbone, indicating that fixation did indeed occur. In the solution spectrum of the α-mono-carbinol PDMS oligomer there are three other chemical shifts of note, the chemical shift of the protons on the α carbon to the hydroxyl at 3.65 ppm, the

hydroxyl proton at 2.2 ppm and the terminal methyl located on the butyl end group at .8 ppm. The terminal methyl resonance is clearly seen in the ^{1}H NMR MAS spectra of the nanoparticle gel in Figure 7.4. However, detecting a change in chemical shift for the methylene spacer adjacent to the hydroxyl group or the disappearance of the hydroxyl proton is very difficult because of the line-broadening and overlapping signals particularly at ~ 2.4-4.7 ppm due to a fairly broad resonance, which is attributable to hydrogen bonded –SiOH groups on the surface of the nanoparticle.[18-20]

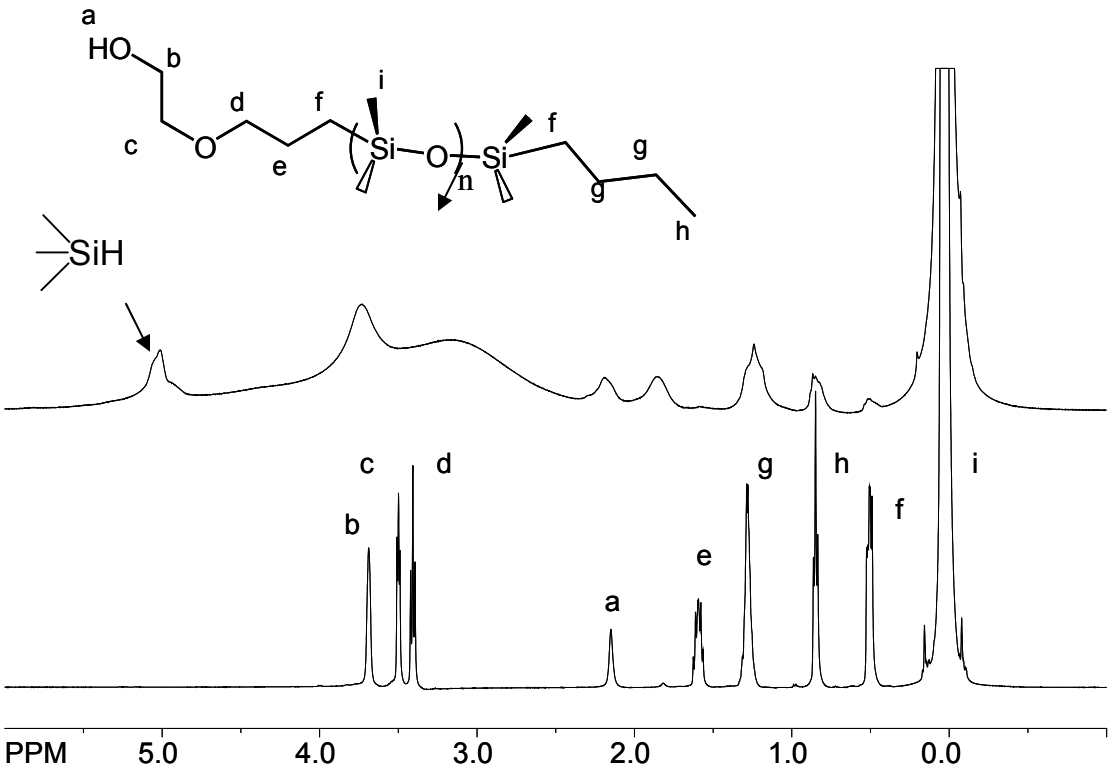

Figure 7.4. ^{1}H NMR MAS spectra of the nanoparticle gel swollen in chloroform-*d* at 2 kHz (top) and the solution spectra of α-mono-carbinol PDMS oligomer used to functionalize the surface of the nanoparticle (bottom).

The ^{1}H NMR MAS spectrum obtained for the silica modified with PDMS loops is shown in Figure 7.5 along with the solution spectrum of the of α,ω-di-carbinol PDMS oligomer which is stacked beneath. Again both spectra show a peak at ~ -.2-.3 ppm which corresponds to the chemical shift of the methyl protons attached to the silicon atoms along the PDMS backbone, indicating that fixation occurred. In the solution spectrum of the α,ω-di-carbinol PDMS oligomer there are two additional chemical shifts of note, the chemical shift of the protons on the α carbon to the hydroxyl group at 3.65 ppm, and a broad resonance for the hydroxyl proton at 2.1 ppm, as seen in the inset in Figure 7.5. Again the complete disappearance of the peak representing the hydroxyl proton and/or a change in chemical shift for the protons on α carbon would indicate not only fixation but also the formation of loops. However, the same issues in reading the ^{1}H NMR MAS spectrum of the nanoparticle with tethers also prevent definitive conformation that loops exist on the surface.

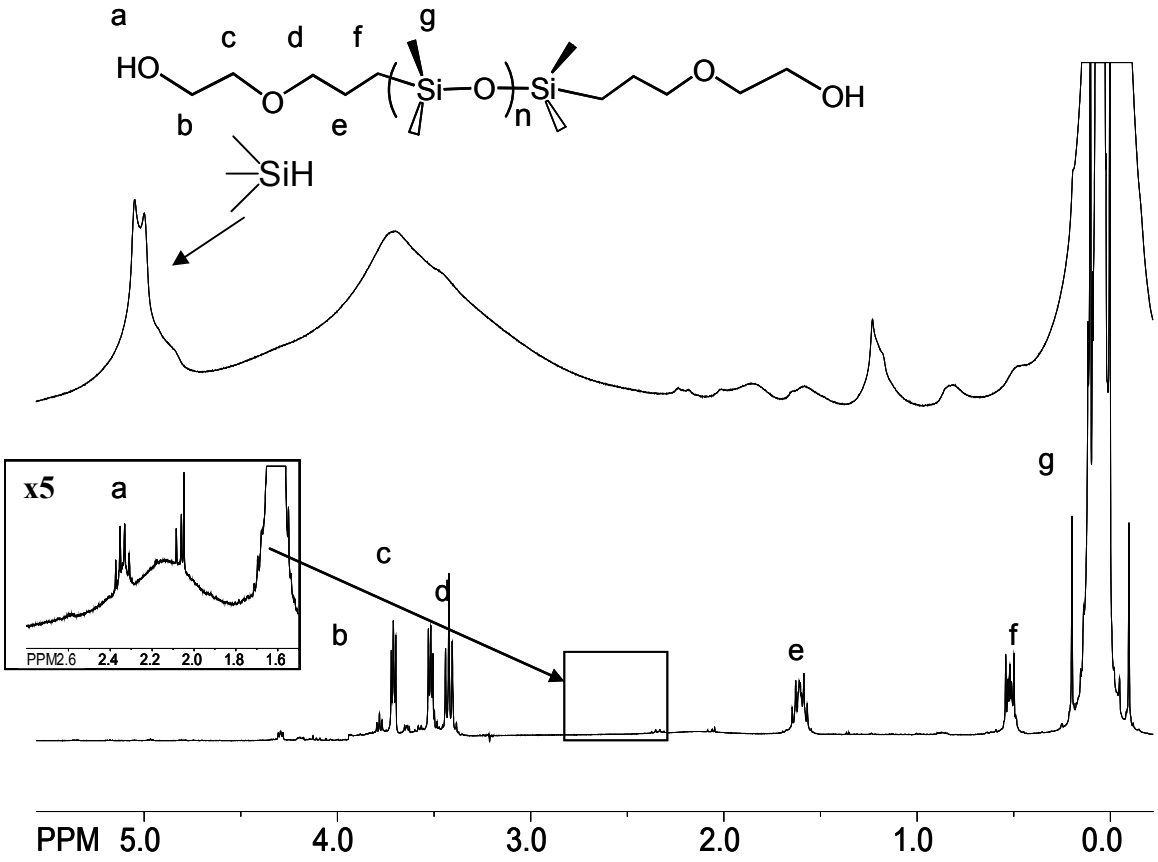

Figure 7.5. ^{1}H NMR MAS spectra of the nanoparticle gel swollen in chloroform-*d* at 2 kHz (top) and the solution spectra of α,ω-di-carbinol PDMS oligomer used to functionalize the surface of the nanoparticle (bottom). The inset shows an enlarged of the region of the solution spectra depicting a broad hydroxyl resonance which integrated to match the relative proper proportion of protons in the linker group.

Silica nanoparticles with either loops or tethers were characterized by the TGA analyses under a N_2 atmosphere to determine the grafting density as seen in Figure 7.6. Using TGA it was determined that the nanoparticle modified with loops is ~ 3.2 % by mass PDMS (silica:PDMS = 30.25 g of silica per 1 g of PDMS) and the nanoparticle with modified tethers is ~ .40 % by mass PDMS (silica:PDMS = 249 g of silica per 1 g of PDMS). Using the quoted particle diameter and specific surface area above, the amount of PDMS on the surface of one nanoparticle modified with loops is ~ 41 chains or

$1.81*10^{18}$ chains/m^2 of particle and with tethers is ~ 5 chains or $2.20*10^{15}$ chains/m^2 of particle.[m]

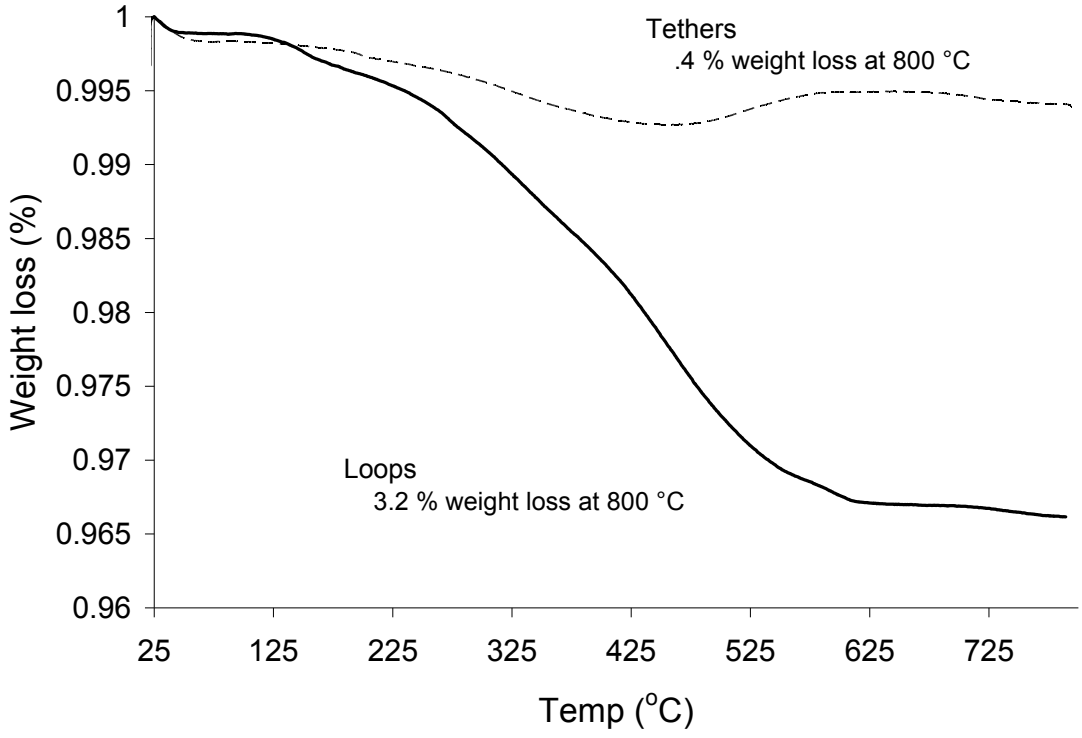

Figure 7.6. Thermograms (heating rate, 10 °C/min) on silica nanoparticles functionalized with α-mono-carbinol (dotted line) and α,ω-di-carbinol (solid line) PDMS oligomers.

To extract more information about the grafted PDMS on the surface of the silica, I used ^1H T_2 relaxation experiments. Spin-spin relaxation is very sensitive to chain dynamics, as the relaxation process is directly related to amount of dipole-dipole interactions between proton spins and the averaging of these interactions due to molecular mobility. By swelling the nanoparticle in chloroform-*d* and forming a gel the

[m] $chains/particle = SA\left(\frac{1}{specificSA}\right)\left(\frac{1}{silica:PDMS}\right)\left(\frac{1}{M_n}\right)(N_A)$, where *silica:PDMS* is the ratio by weight of silica to PDMS determined by TGA, *SA* is the surface area of one particle with a diameter of 27 nm, M_n = 5.5 kg/mol and *specific SA* = 200 m^2/g.

difference in the mobility of chains bound to the silica and chains in the swollen portion of the gel can be significant.[13] The proportion of signal arising from each can be used to determine the relative portion of bound PDMS protons (protons near the silica surface) and PDMS protons in the solvated regions of the gel. Also, that information along with the characteristic T_2 values, which describe the degree of chain mobility (short T_2 are linked to rigid material and long T_2 linked to mobile material), can be used to infer information on grafting density, the length of the swollen tethered polymer chain and the interaction the tethered polymer chain has with the surrounding solvent.

The decay of the transverse magnetization of two silica samples is shown in Figure 7.7. The gel samples were spun at 2 kHz and a CPMG sequence was used to reduce line broadening. The particular resonance of interest is the signal at -.2-.3 ppm which corresponds to the chemical shift of the methyl protons attached to the silicon atoms along the PDMS backbone. Because the curves indicate two decay processes, the T_2 decay was fit to a double exponential model, where the faster decaying component is attributed to bound PDMS chain protons and the slower decaying component the PDMS protons in the solvated regions of the gel.

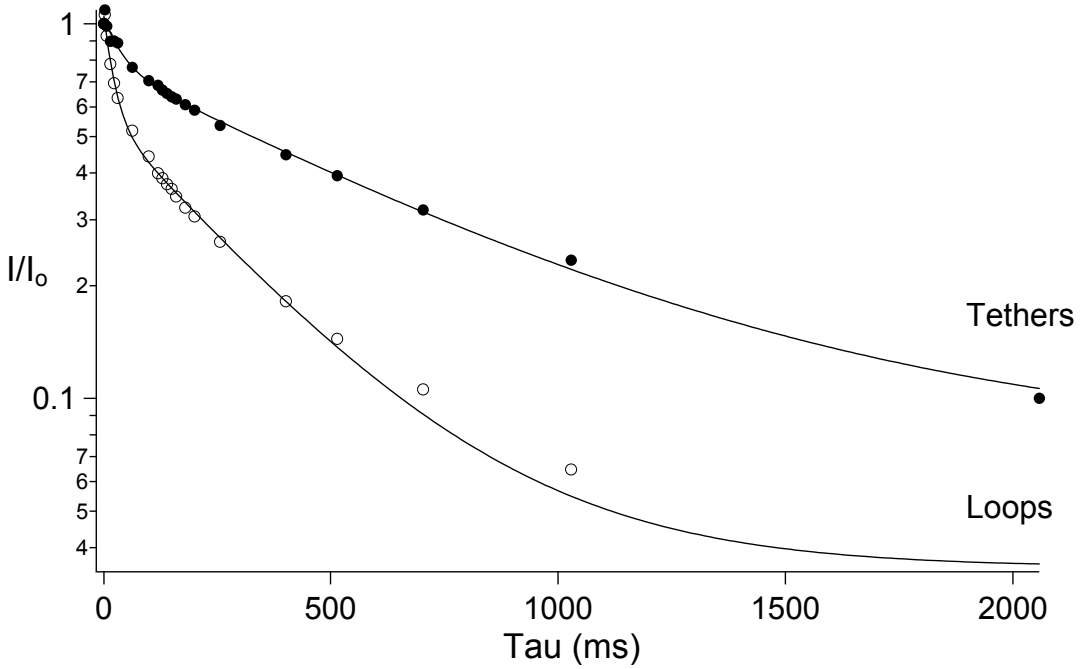

Figure 7.7. Spin-spin relaxation of the methyl protons at ~ 0 ppm on the backbone of the PDMS oligomers attached to the nanoparticle surface for the tethered (●) and looped (○) topologies, where the fitted lines correspond to a double exponential model. The nanoparticles were swollen as a gel in chloroform-*d*.

Figure 7.7 shows a much faster decay for the nanoparticle with loops over the entire decay curve indicating that the polymer chains on that sample are more rigid. This is most likely because local chain mobility is greatly reduced because of strongly hindered motions due to chain anchoring to the silica surface and adsorptive interaction of PDMS monomer units with the silica surface. Because the samples were first washed in a Soxhlet extractor the anchoring is at least in part, if not completely due to covalent bonding resulting from an O-silylation reaction. Also, the curve clearly shows the faster decaying component of the spin relaxation for the nanoparticle with modified loops is a greater proportion of the decay curve. These two qualitative observations of the decay behavior indicate the nanoparticle with loops contain PDMS with much reduced dynamics. This slower chain motion is even observed in the swollen PDMS chain

segments, which are located between attachments, and perhaps due to a difference in chain configuration and/or a particularly high grafting density.

Table 7.1 lists the T_2 results from spin-spin relaxation of the methyl protons on the backbone of the PDMS oligomers the nanoparticles modified with surface tethers or loops. The T_{2a} value corresponds to the relaxation component with the shortest decay times, representing the bound polymer segments and is 33 and 22 ms for the nanoparticle modified with tethers and loops, respectively. The nanoparticle with loops has a shorter T_2 value for the bound polymer segments (T_{2a}). Though the difference is small, the calculated standard deviation and the appearance of the initial decay process seen in Figure 7.7 suggest that it is a statistically significant difference. The difference could be due to additional reduction in dynamics in repeat units near the silica surface because of the loop configuration. However, I suspect the difference could also can be attributed to a large difference in grafting density, which was determined earlier by TGA. The parameter W_a is a fitting parameter describing the weight or proportion of protons corresponding to the component with the shortest decay times (T_{2a}). ~ 30 % of the PDMS protons on the nanoparticle modified with tethers is associated with the bound PDMS monomer units while the percentage increases to ~ 50 % for the nanoparticle modified with loops, serving as further proof of a loop versus tether configuration.

Table 7.1. T_2 results from spin-spin relaxation of the methyl protons on the backbone of the PDMS oligomers. The statistical data results from three trials.

		W_a	T_{2a} (ms)	W_b	T_{2b} (ms)
Tethers	**Avg.**	0.29	33	0.69	623
	Std. Dev.	*0.04*	*6.9*	*0.04*	*28*
Loops	**Avg.**	0.50	22	0.53	320
	Std. Dev.	*0.02*	*0.51*	*0.01*	*9*

The T_{2b} value is the relaxation component with the longest decay times, representing the mobile polymer segments associated with swollen polymer and is 623 and 320 ms for the nanoparticle modified with tethers and loops, respectively. The amplitude of chain motion in the nanoparticle modified with loops is also half that of the sample with surface tethers. The magnitude of the difference is such that it indicates the mobile polymer segments in the region outside the particle/PDMS interface has less degrees of freedom for the looped material, which would have resulted from attachment at both ends of the PDMS oligomer.

T_2 relaxation experiments were then conducted on the composites of these nanoparticles in PVAc and were intended to probe the dynamics of the composite system, particularly at the interface/interphase. Figure 7.8 show the T_2 and β values as a function of temperature using the CPMG sequence and analyzed KWW model with the constant offset. Both parameters can be used to elude information about the molecular motion of the PVAc matrix in the nanocomposite composed of nanoparticles modified with PDMS loops and tethers. At 50, 90, 100 and 110 °C, the sample containing the silica nano-fillers with loops had a wider distribution of correlation times. The T_2 data show that from 50 °C to near 120 °C the characteristic relaxation time for both composite samples increase, eventually showing the nanocomposite composed of silica nano-fillers modified with PDMS loops having the longer T_2 times. This indicates that the polymer chains in the PVAc matrix over that temperature range in that composite are more mobile. This seems counter-intuitive and along with the observed β values suggest the T_2 results in Figure 7.7 inaccuracy reflect the dynamics of the systems.

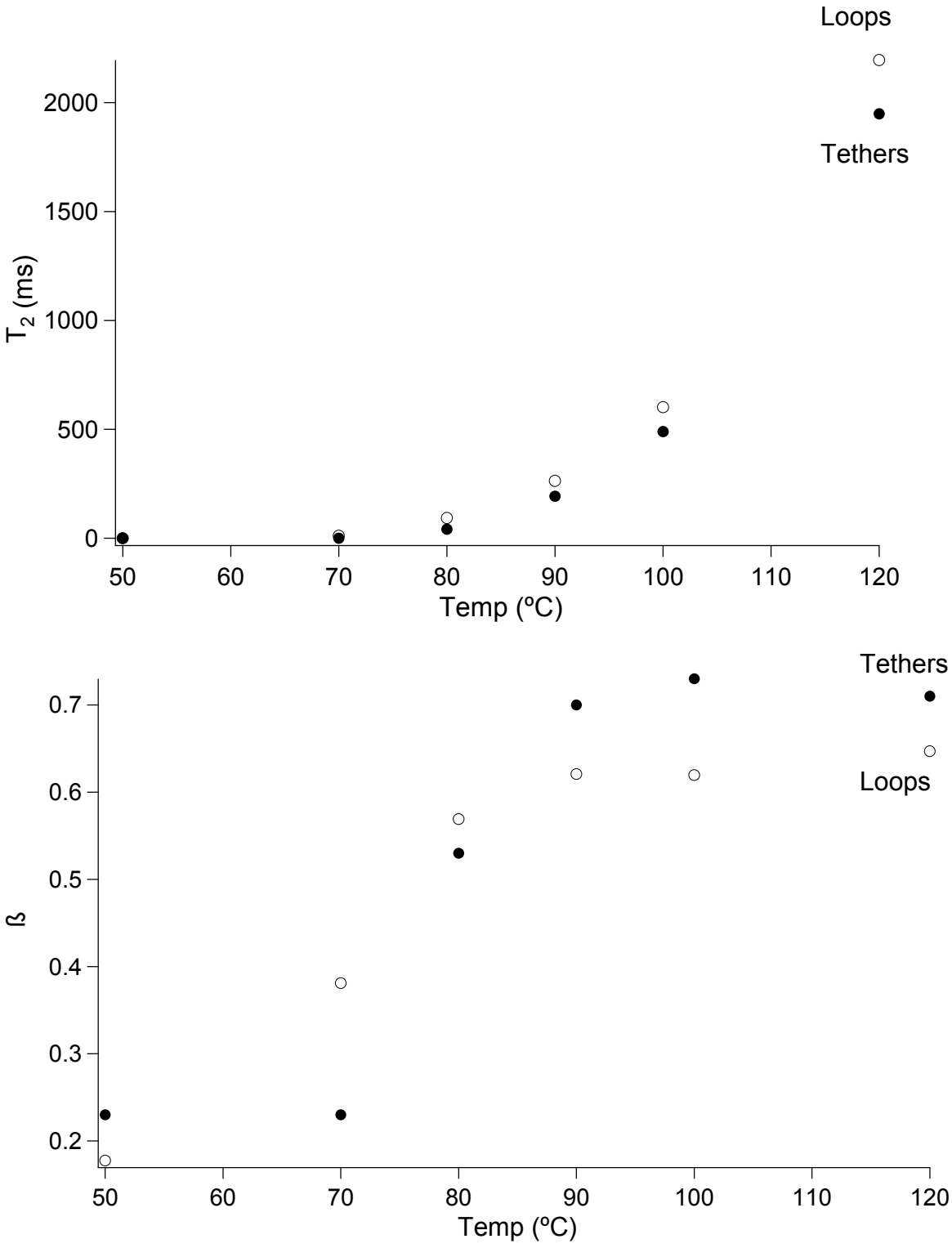

Figure 7.8. The T_2 and β values at various temperatures ranging from 50-120 °C were obtained using the KWW model with the constant offset and HE sequence. PVAc/Silica tethered PDMS (●) PVAc/Silica-looped PDMS (○)

Though highly unlikely that a systemic error occurred, multiple samples were not prepared, TGA on the composite was not run to verify the composite were indeed 12 wt. % and repeated T_2 experiments were not conducted to verify the accuracy or precision of the results. There are multiple factors that could have affected the system and give rise to the results above. First, the TGA data on the nanoparticles suggest a relatively low amount of PDMS was grafted onto either nanoparticle samples and a large discrepancy in the grafting density for the nano-filler modified with loops and tethers. Also, optimally the nanoparticle modified with loops should be twice as large as the tethers. Control of the length of the PDMS on the particle and the grafting density is important, as adhesive work and subsequent interfacial failure mechanisms are strongly related to both those parameters. The residual hydrosilane content on the surface of the nanoparticle also may change the system. If the residual hydrosilane content is too high it may dominate the surface properties of the nanoparticles in the composite, this would mask or convolute the effect of either loops or tethers on the nanocomposite polymer dynamics.

7.5 Conclusions

The T_2 relaxation is very sensitive to chain mobility and dynamics, and can be used to determine information on a system of swollen nanoparticles. The result can be used to extract quantitative and qualitative measures of grafting density, the length of tethered chains and their topology on the surface. Studying T_2 relaxation provides an advantage to simple FTIR or 1D NMR spectroscopy because it does not require positive identification of low intensity end group signals which can be obscured by other overlapping resonances, making them difficult to integrate. The results show PDMS is

attached to the surface of the silica and indeed has the intended loop or tethered conformations.

7.6 References

1. Zhao, B.; Brittain, W.; *Prog. Polym. Sci.* **2000**, *25*, 677-710.

2. Yang, X.; Shi, J. Johnson, S.; Swanson, B.; *Langmuir* **1998**, *14*, (7), 1505-1507.

3. Park, S.; Taton, A.; Mirkin, C.; *Science* **2002**, *295*, 1053.

4. Ding, X.; Zhao, J.; Liu, Y.; Zhang, H.; Wang, Z.; *Materials Letters* **2004**, *58*, 3126-3130.

5. Eastwood, E.; Dadmun, M.; *Macromolecules* **2002**, *35*, 5069-5077.

6. Huang, Z.; Alonzo, J.; Liu, M.; Dadmun, M.; *Macromolecules* **2006**, *39*, 8434-8439.

7. Huang, Z.; Alonzo, J.; Liu, M.; Dadmun, M.; *Macromolecules* **2008**, *41*, 1745-1752.

8. Dadmun, M.; *Macromolecules* **1996**, *29*, 3868-3874.

9. Dadmun, M.; *Macromolecules* **2000**, *33*, 9122-9125.

10. Balazs, A.; Gersappe, D.; Harm, P.; Irvine, D.; *Macromolecules* **1994**, *27*, 720-724.

11. Irvine, D.; Mayes, A.; *Macromolecules* **1996**, *29*, 6037-6043.

12. Shull, K.; *Faraday Discuss.* **1994**, *98*, 203-217.

13. Litvinov, V.; Barthel, H.; Weis, J; *Macromolecules* **2002**, *35*, 4356-4364.

14. Ketelson, H.; Brook, M.; Pelton, R.; *Chem. Mater.* **1995**, *7*, 1376-1383.

15. Krasnoslobodtsev, A.; Smirnov, S.; *Langmuir* **2002**, *18*, 3181-3184.

16. Zhang, C.; Laine, R.;; *J. Am. Chem. Soc.* **2000**, *122*, 6979-6988.

17. Huang, Z.; Haining, J.; Mays, J.; Dadmun, M.; *Macromolecules* **2008**, *41*, 1009-1018.

18. Hartmeyer, G.; Marichal, C.; Lebeau, B.; Rigolet, S.; Caullet, P.; Hernandez, J.; *J. Phys. Chem. C* **2007**, *111*, 9066-9071.

19. Kinney, D.; Chuang, I.; Maciel, G.; *J. Am. Chem. Soc.* **1993**, *115*, 6786-6794.

20. Bronnimann, C.; Zeigler, R.; Maciel, G.; *J. Am. Chem. Soc.* **1988**, *110*, (7), 2023.

21. Sandoval J.; Pesek, J.; *Anal. Chem.* **1991**, *63*, 2634-2641.

Appendix A

PDMS Sample	Experimental M_n (g/mol)	Viscosity (cSt)	Manufacturers M_n/M_w (g/mol)		GPC				LS	MALDI	NMR
					PDMS Broad Std[1]		PS Narrow Std [2]				
					M_n (g/mol)	M_w (g/mol)	M_n (g/mol)	M_w (g/mol)	M_w (g/mol)	M_n (g/mol)	M_n (g/mol)
Gelest DMS-S15	1500	45-85	2000-3000		460	4500	4000	7000		1297	2600
Gelest DMS-S21	4200	90-120	4200		1100	8100	6500	11100			
Gelest DMS-S27	18000	700-800	18000		12700	33000	16100	38400			26000
Gelest DMS-S31		1000	26000		10300	34100	18800	42800			
Gelest DMS-S35	35000	5000	49000		35400	66100	47100	89700	74300		56000
Gelest DMS-S42	45000	18000	77000		63100	97200	76700	141000			
Aldrich PMDS Std 1			13700	38900			16600	49700			
Aldrich PMDS Std 2			46000	92400			56000	124000			
Aldrich PMDS Std 3			106000	182000			114000	218000			

Table A.1. Molecular weights of Gelest linear PDMS precursors.

[1]Molecular weights determined by GPC using a relative calibration curve of the 3 broad Aldrich PDMS standards on the Hr 1,3, and 4 column setup.

[2]Molecular weights determined by GPC using a universal calibration curve of 6 narrow PS standards on the Hr 1,3, and 4 column setup, k=0.00421 ml/g and α=0.83.

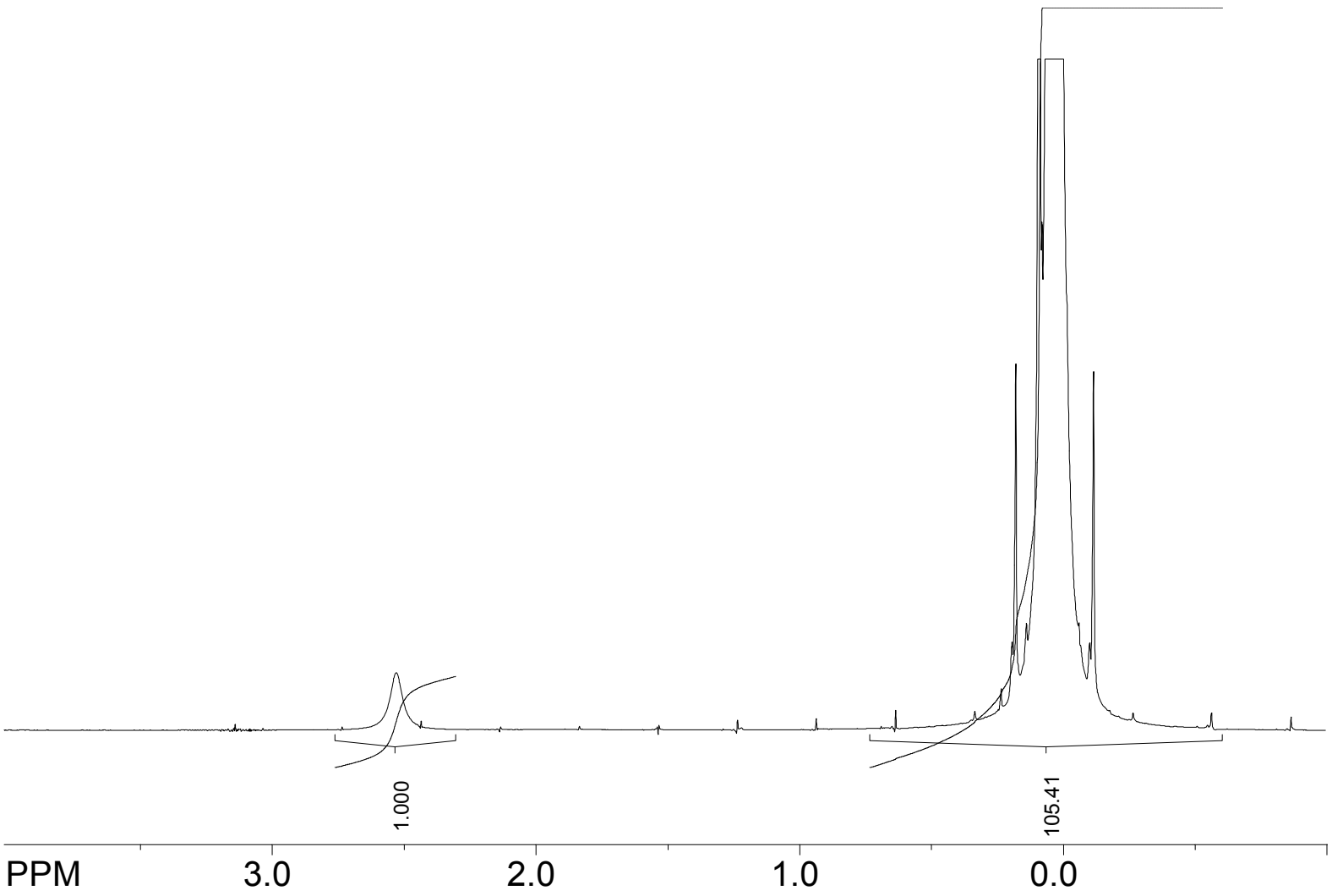

Figure A.1. ^{1}H NMR spectrum of S15 PDMS precursor

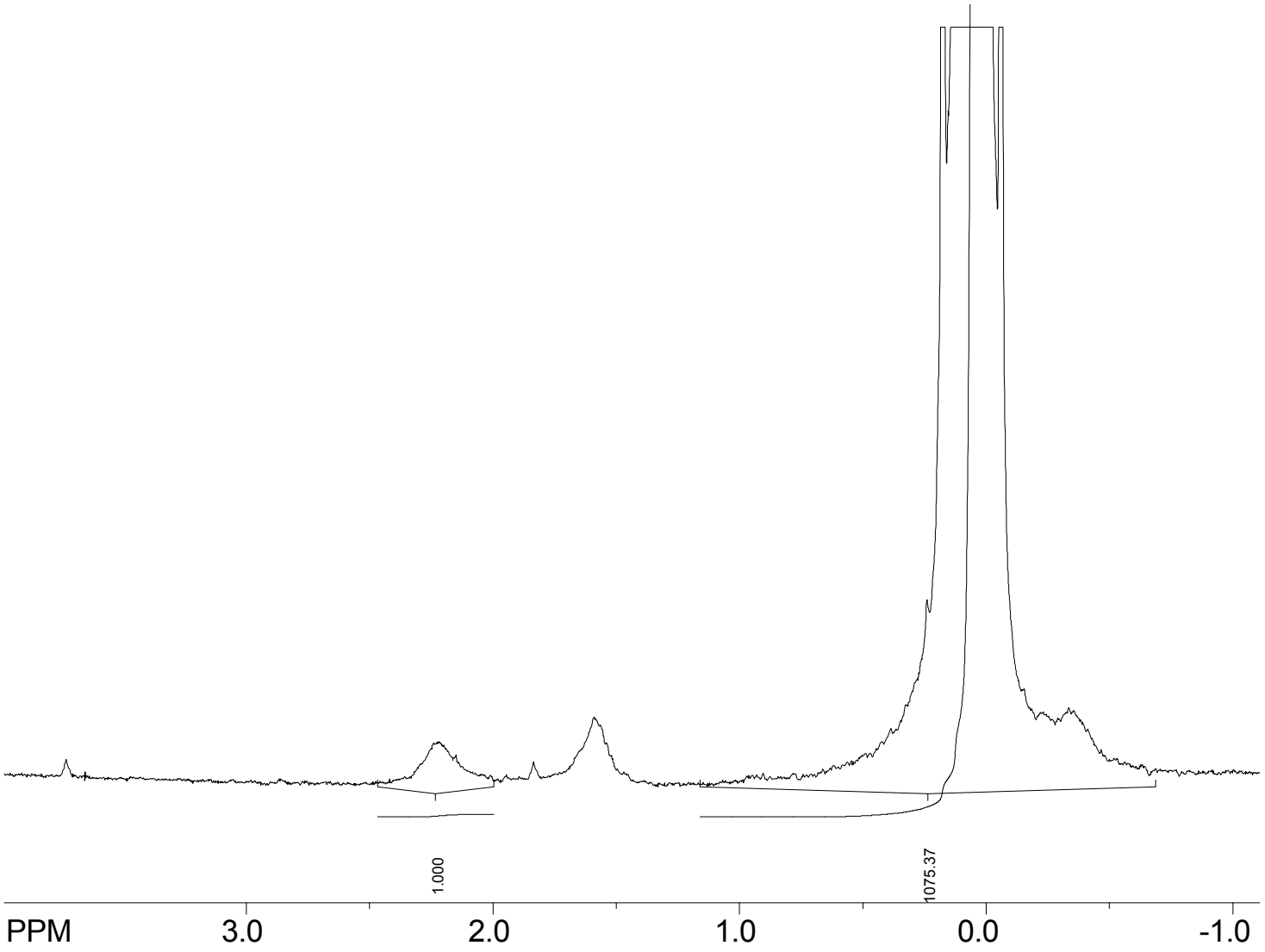

Figure A.4. ^{1}H NMR spectrum of S27 PDMS precursor

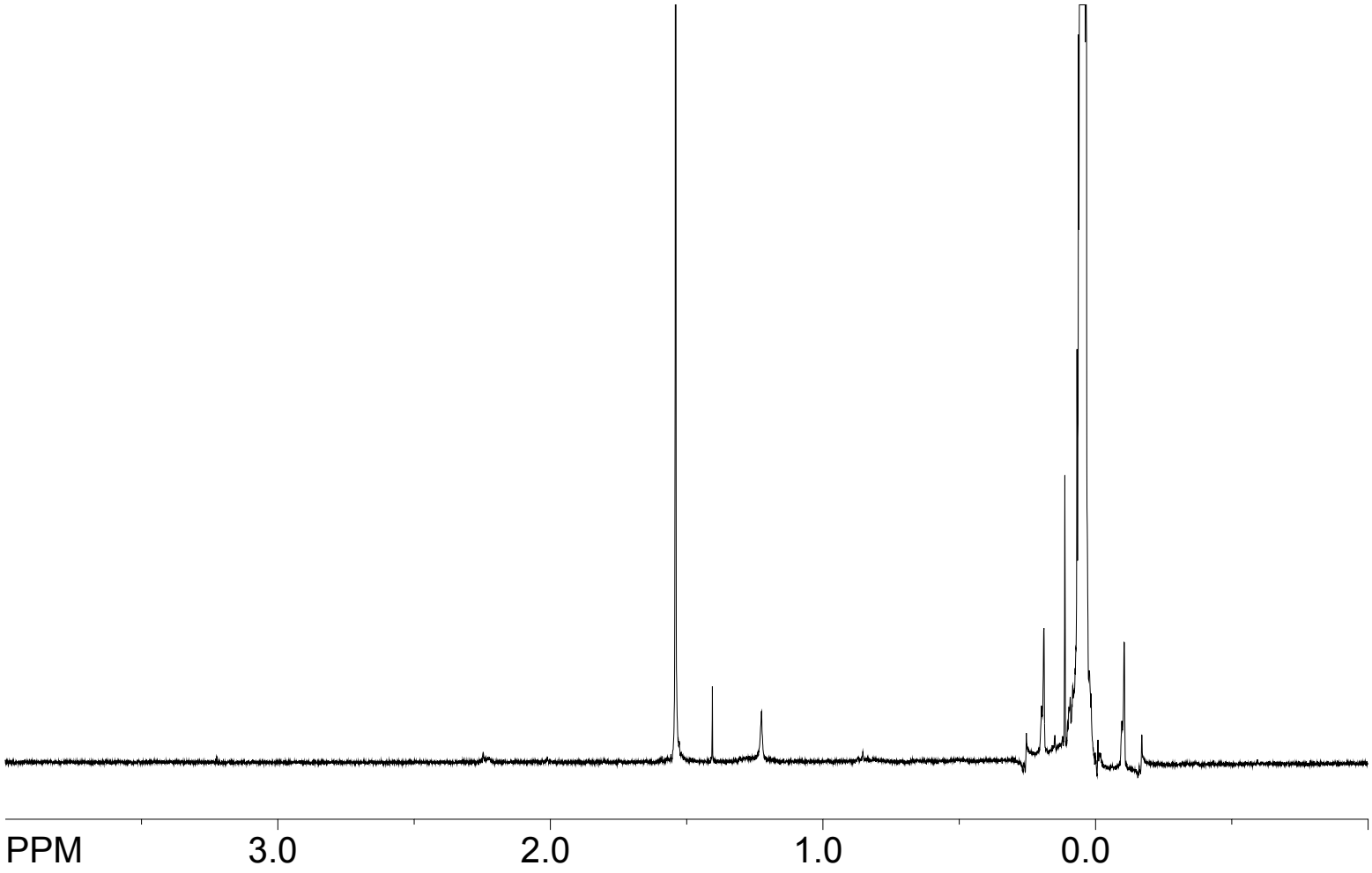

Figure A.7. ^{1}H NMR spectrum of S15 PDMS resin quenched at 15 min

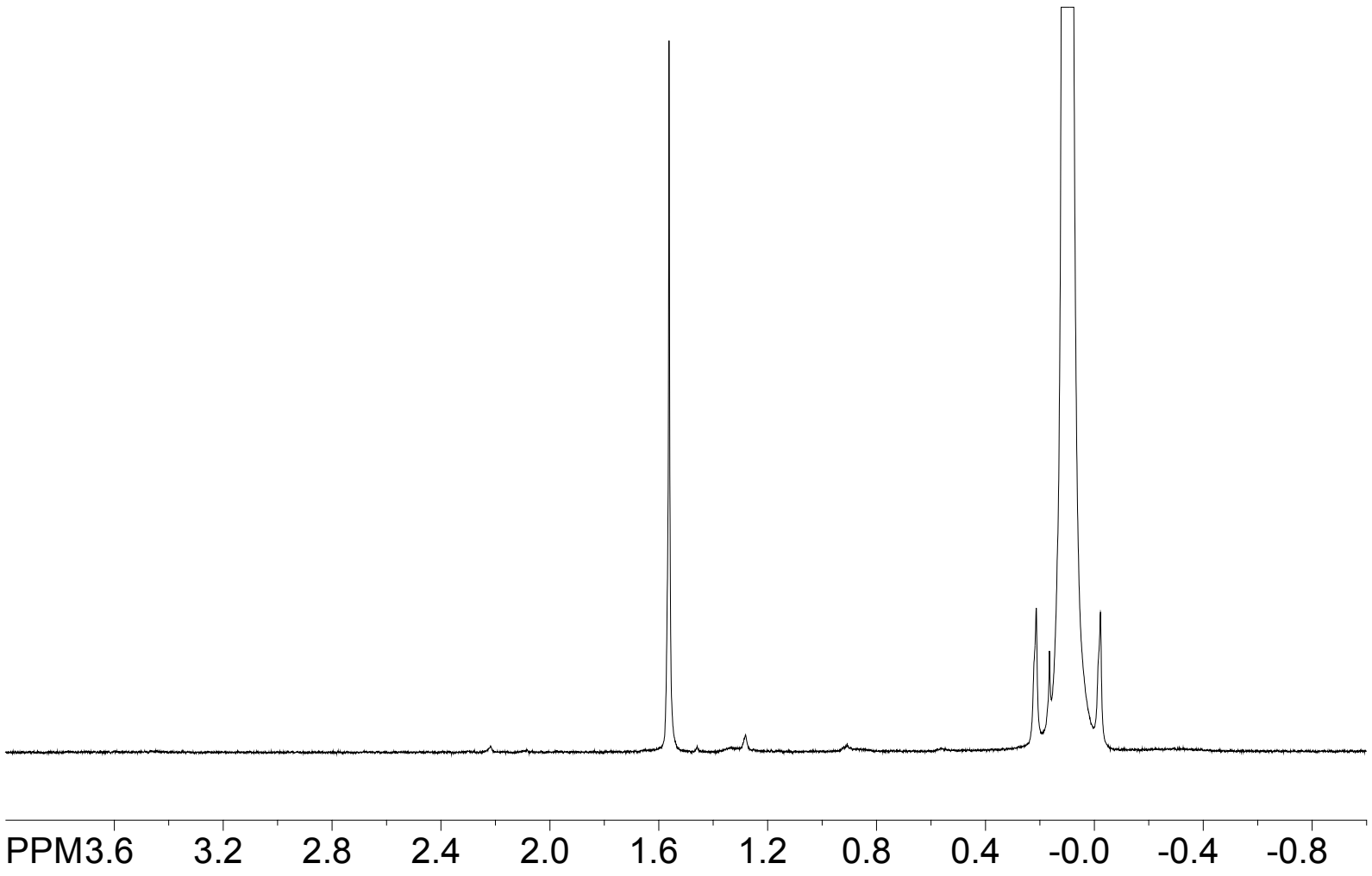

Figure A.8. ^{1}H NMR spectrum of S15 PDMS resin quenched at 30 min

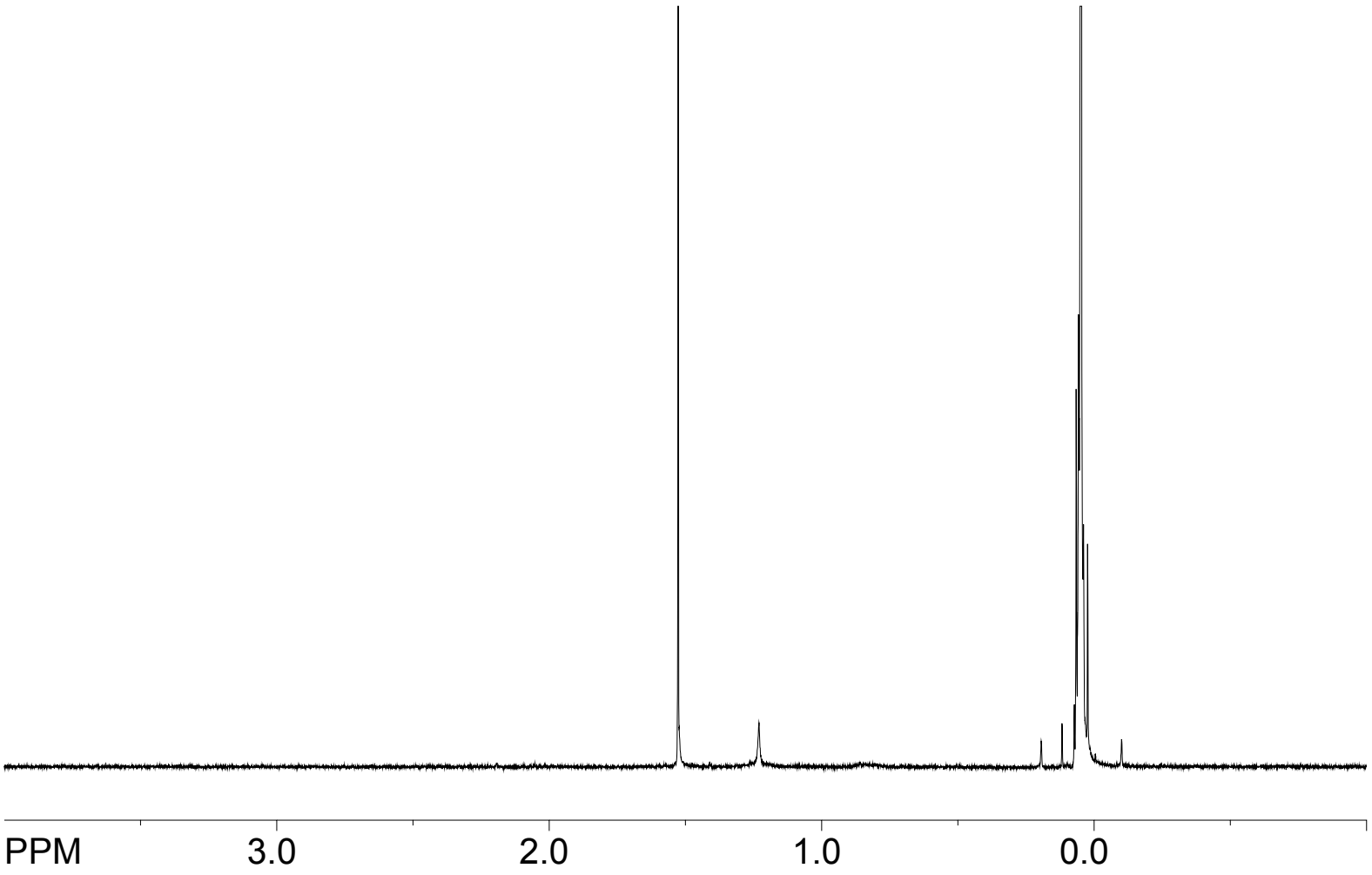

Figure A.9. ^{1}H NMR spectrum of S27 PDMS resin quenched at 5 min

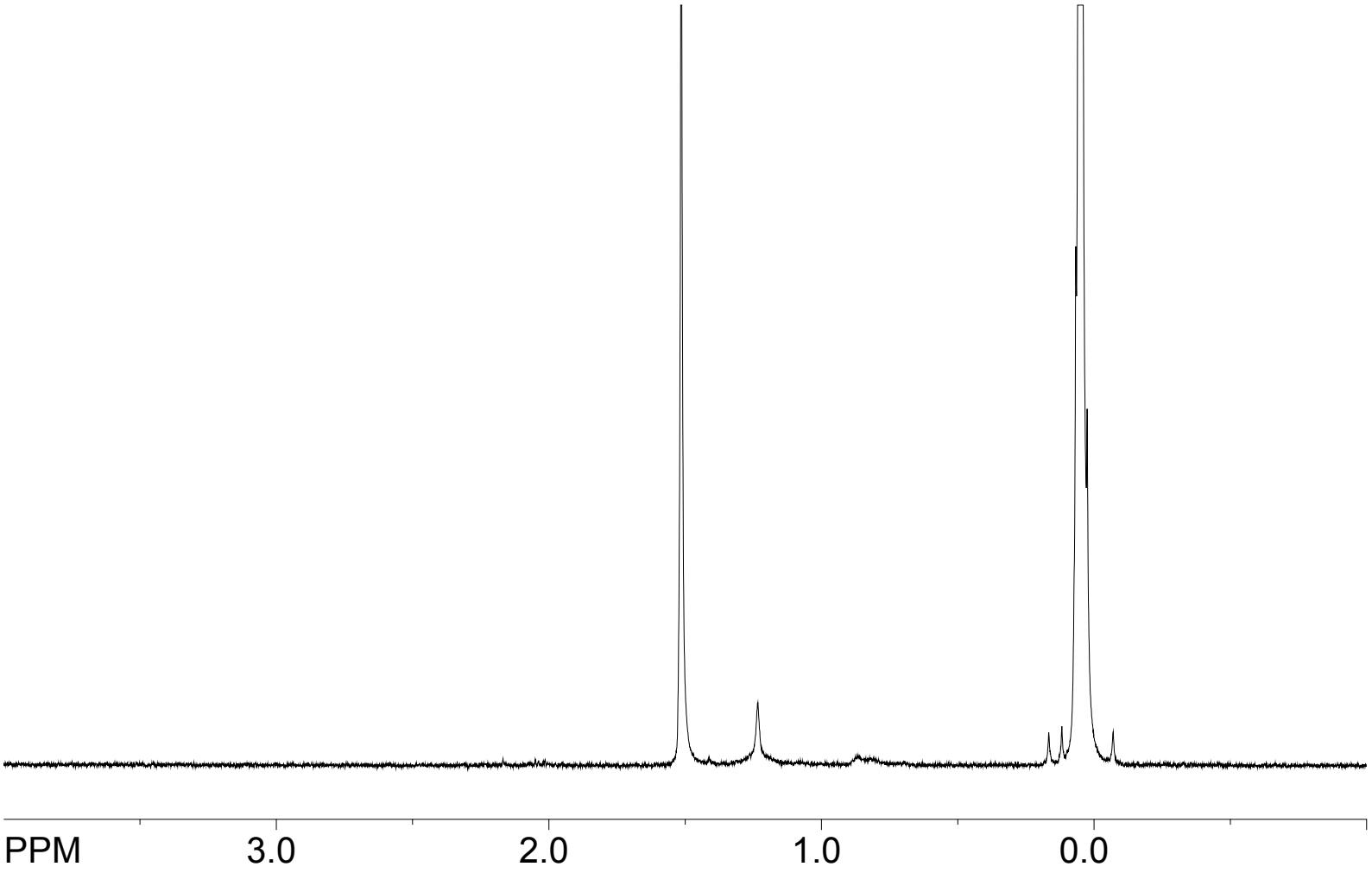

Figure A.10. ^{1}H NMR spectrum of S27 PDMS resin quenched at 15 min

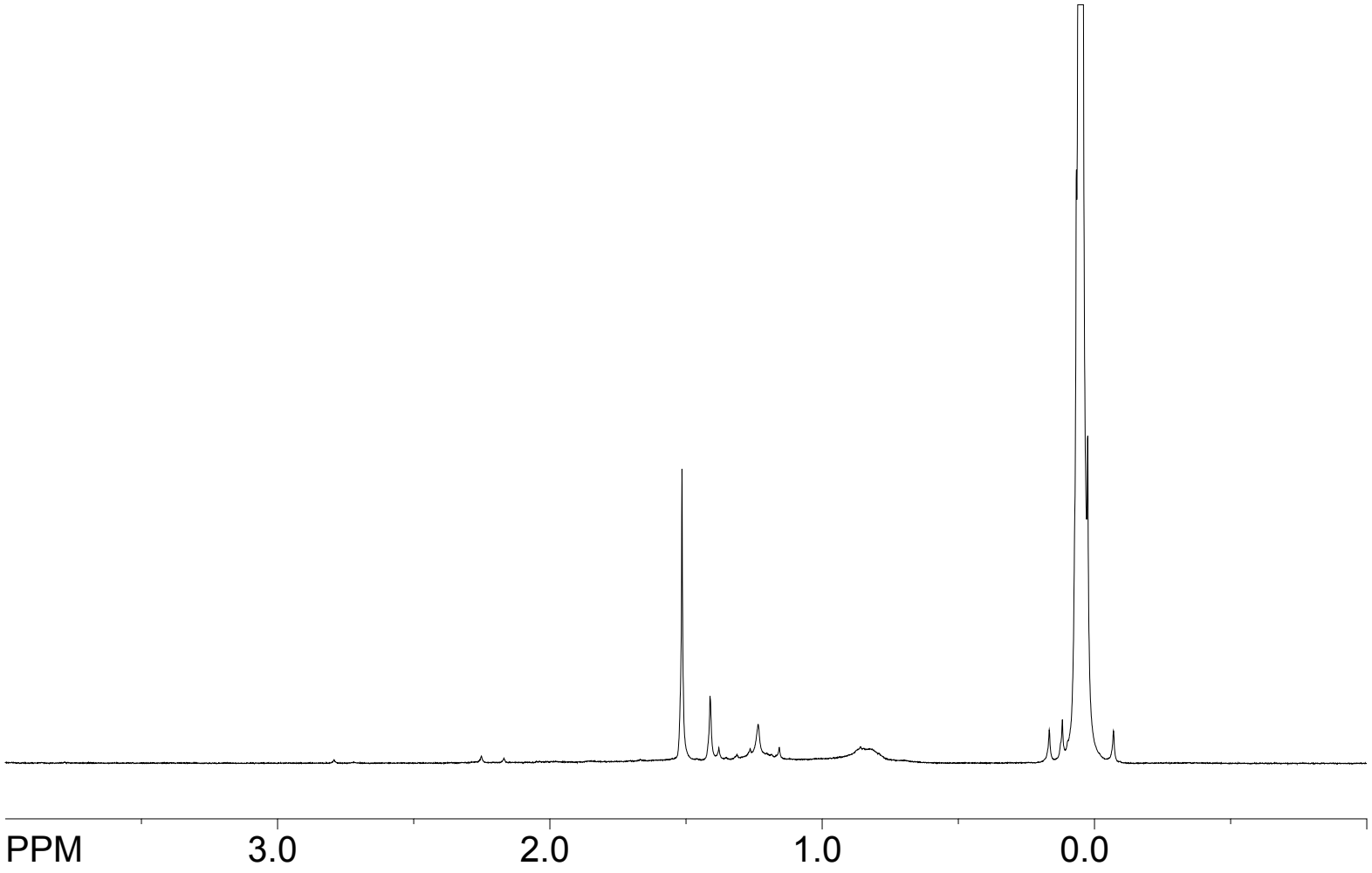

Figure A.11. ^{1}H NMR spectrum of S21 PDMS resin quenched at 30 min

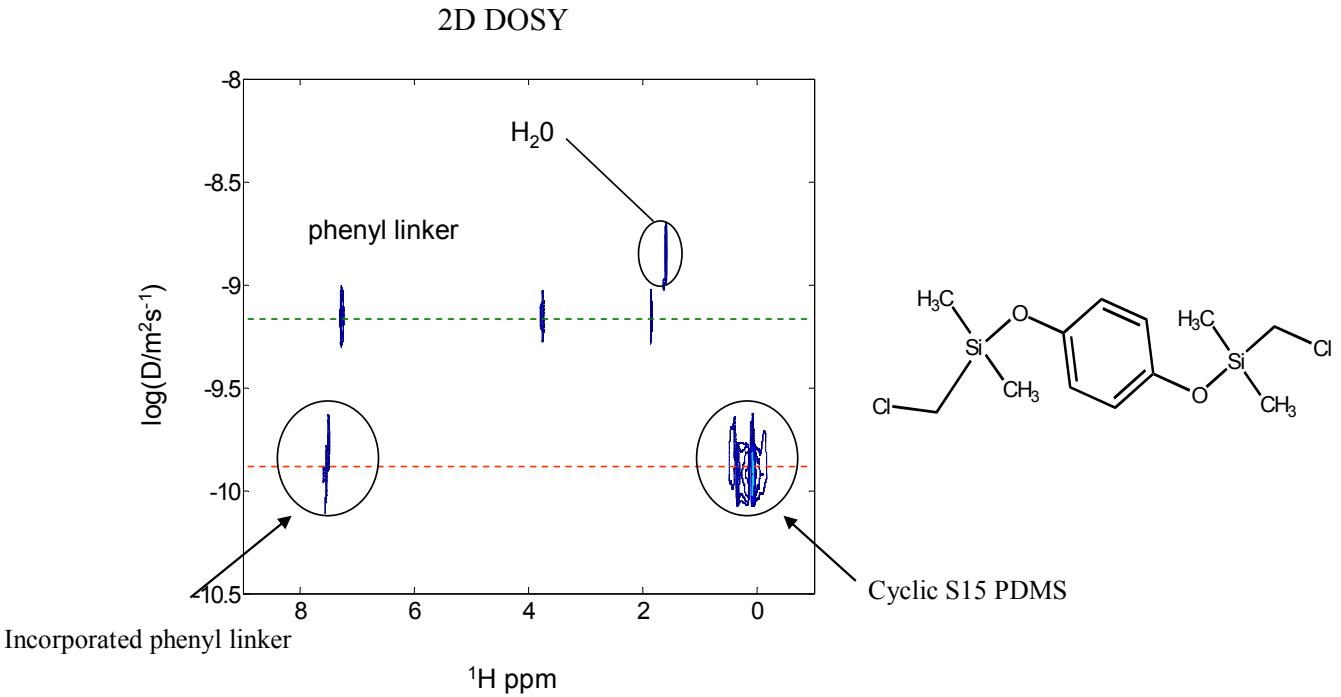

Figure A.12. ^{1}H 2D-DOSY NMR spectrum of S15 PDMS quenched with bis-phenyl linker

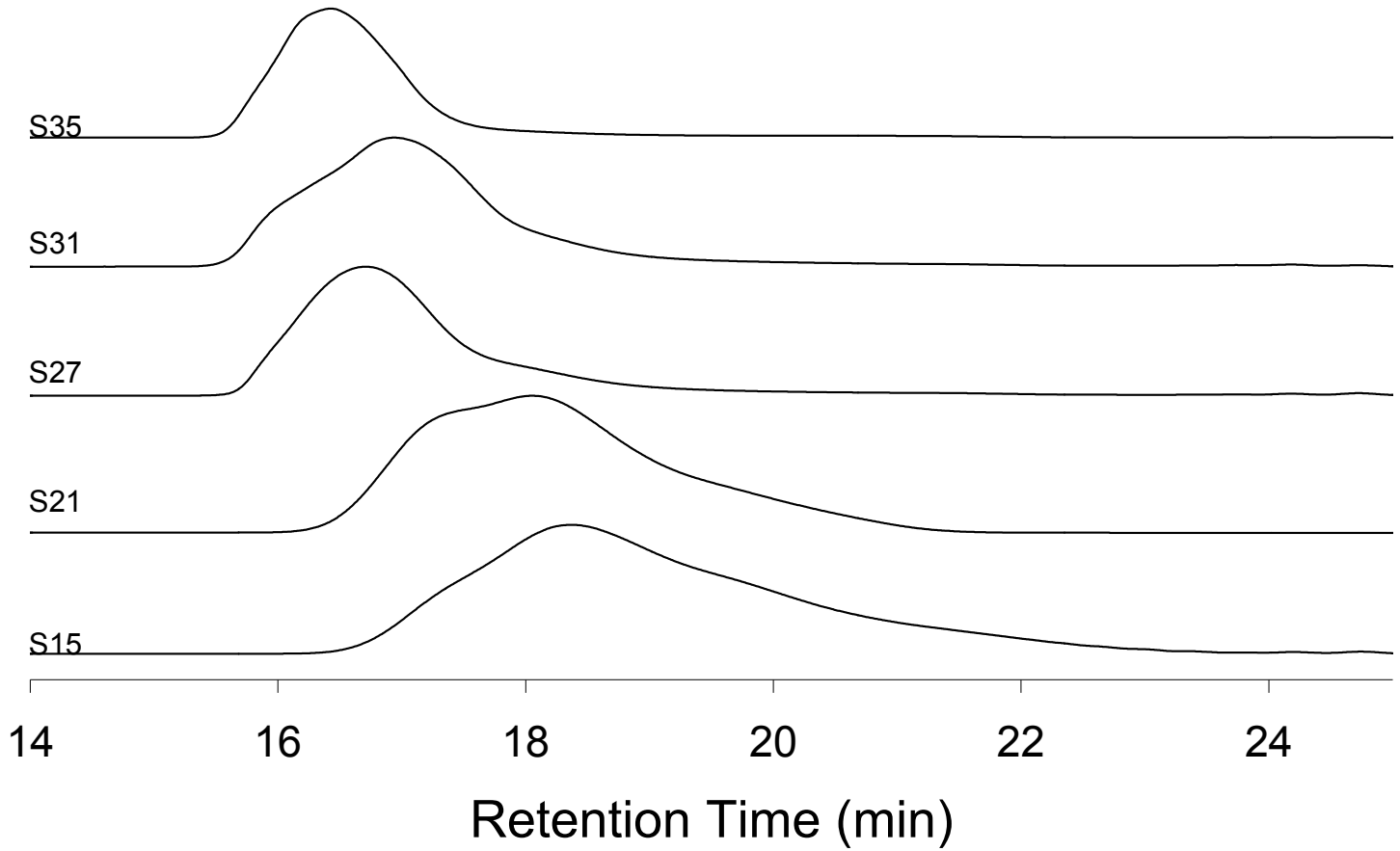

Figure A.13. GPC chromatographs of linear PDMS precursors on the Hr 0.5, 1, and 3 column setup

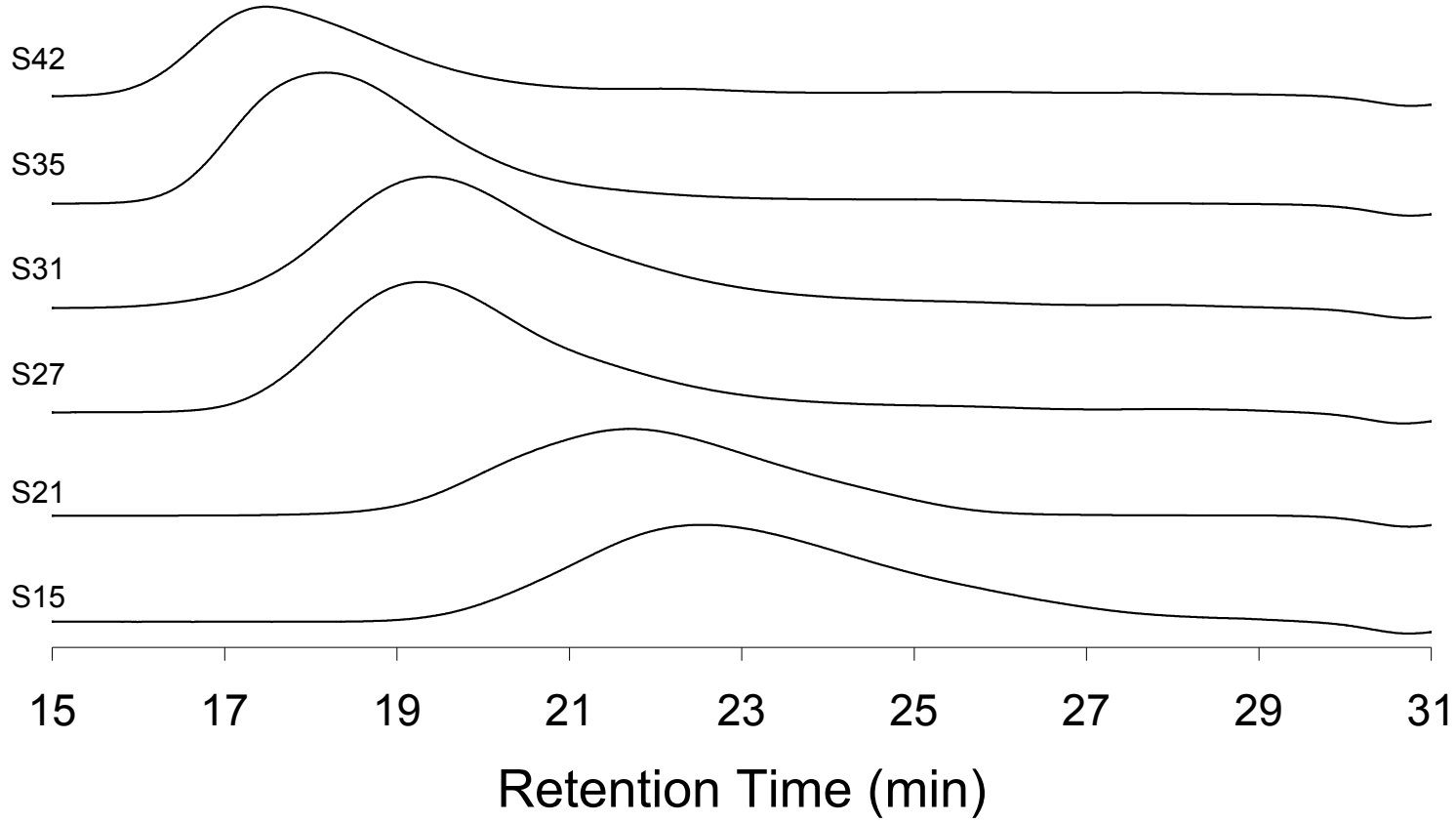

Figure A.14. GPC chromatographs of linear PDMS precursors on the Hr 1, 3, and 4 column setup

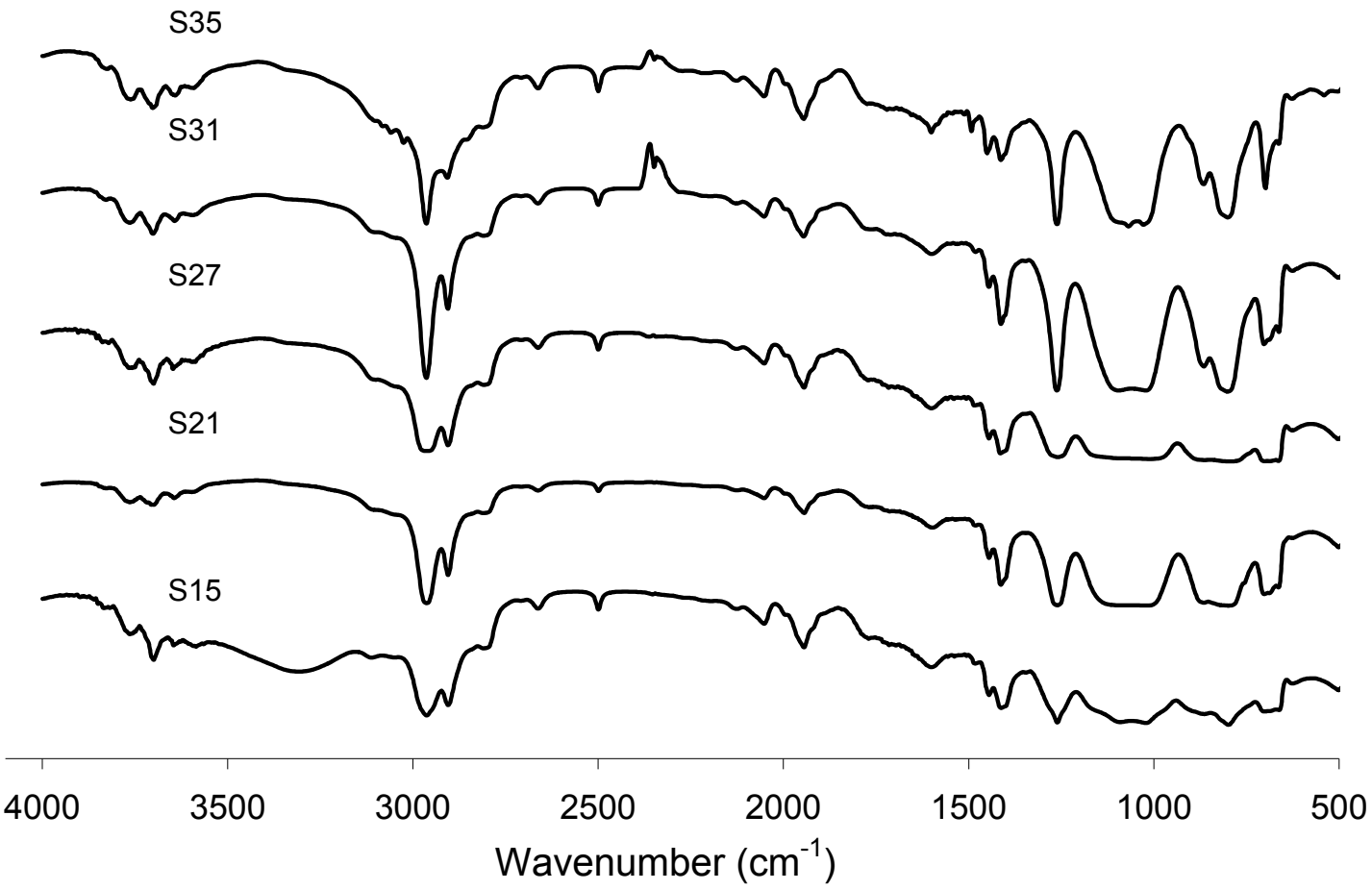

Figure A.15. IR spectra of linear PDMS precursors

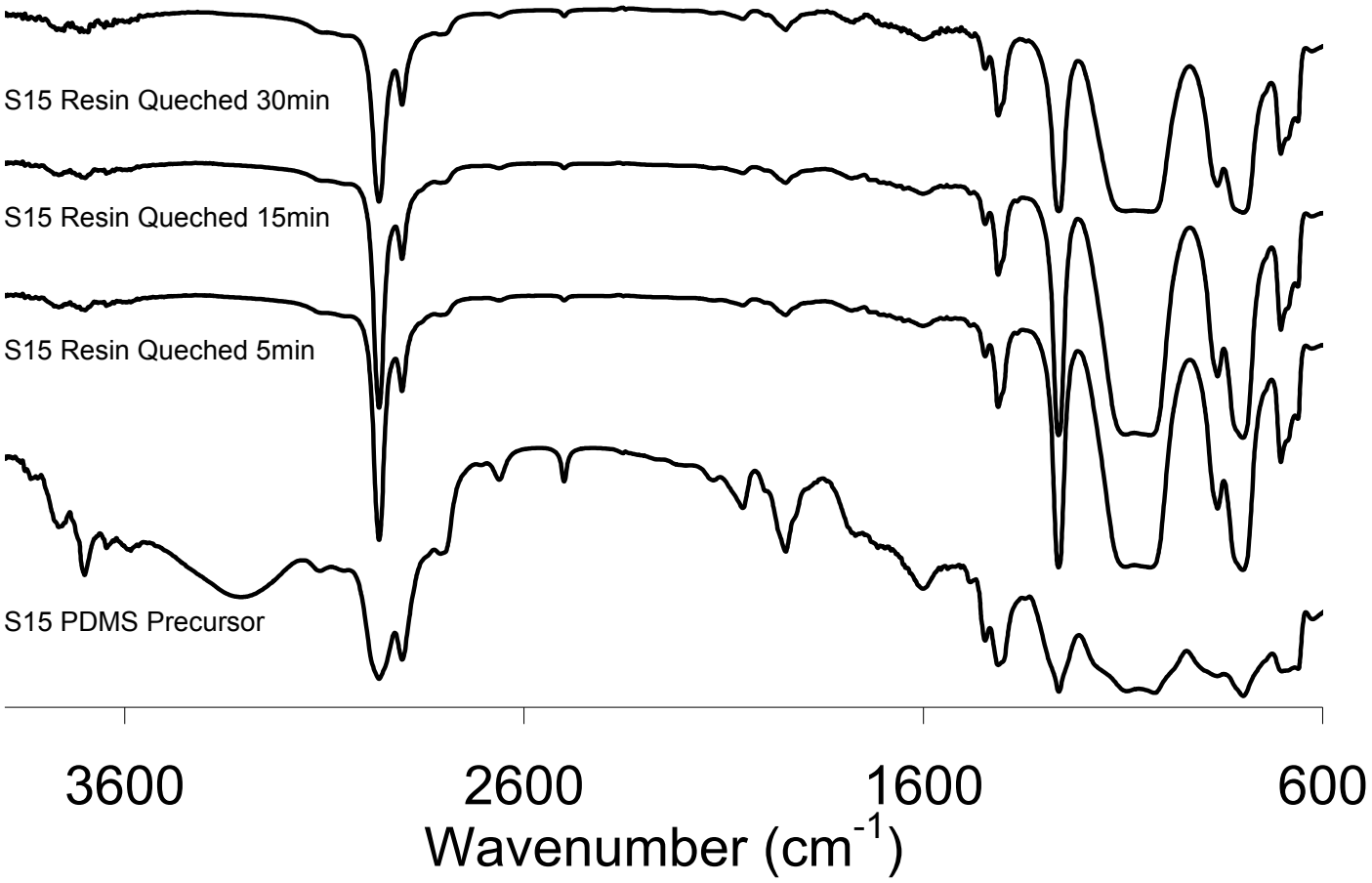

Figure A.16. IR spectra of cyclic PDMS product

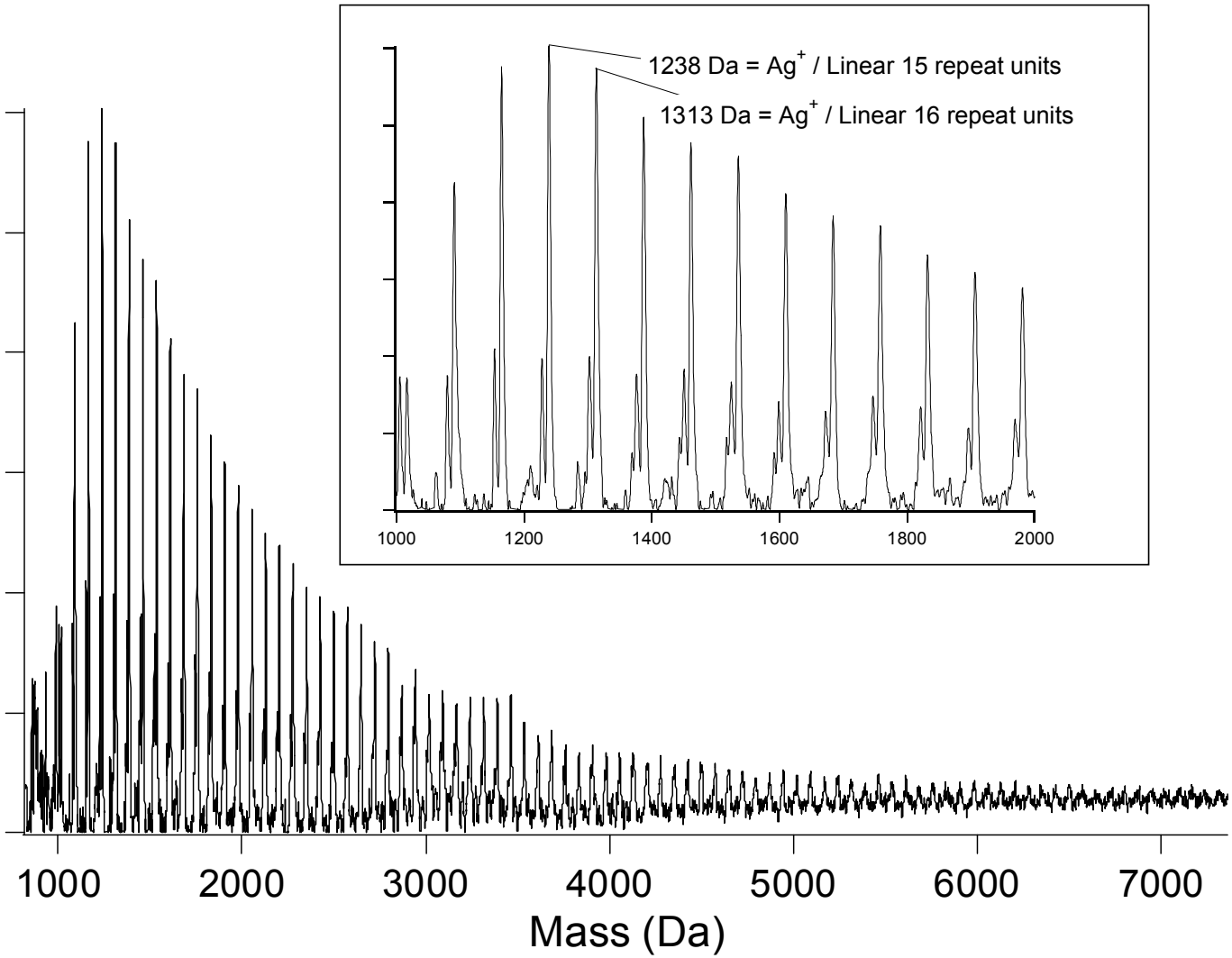

Figure A.17. MALDI spectra of linear S15 PDMS precursor

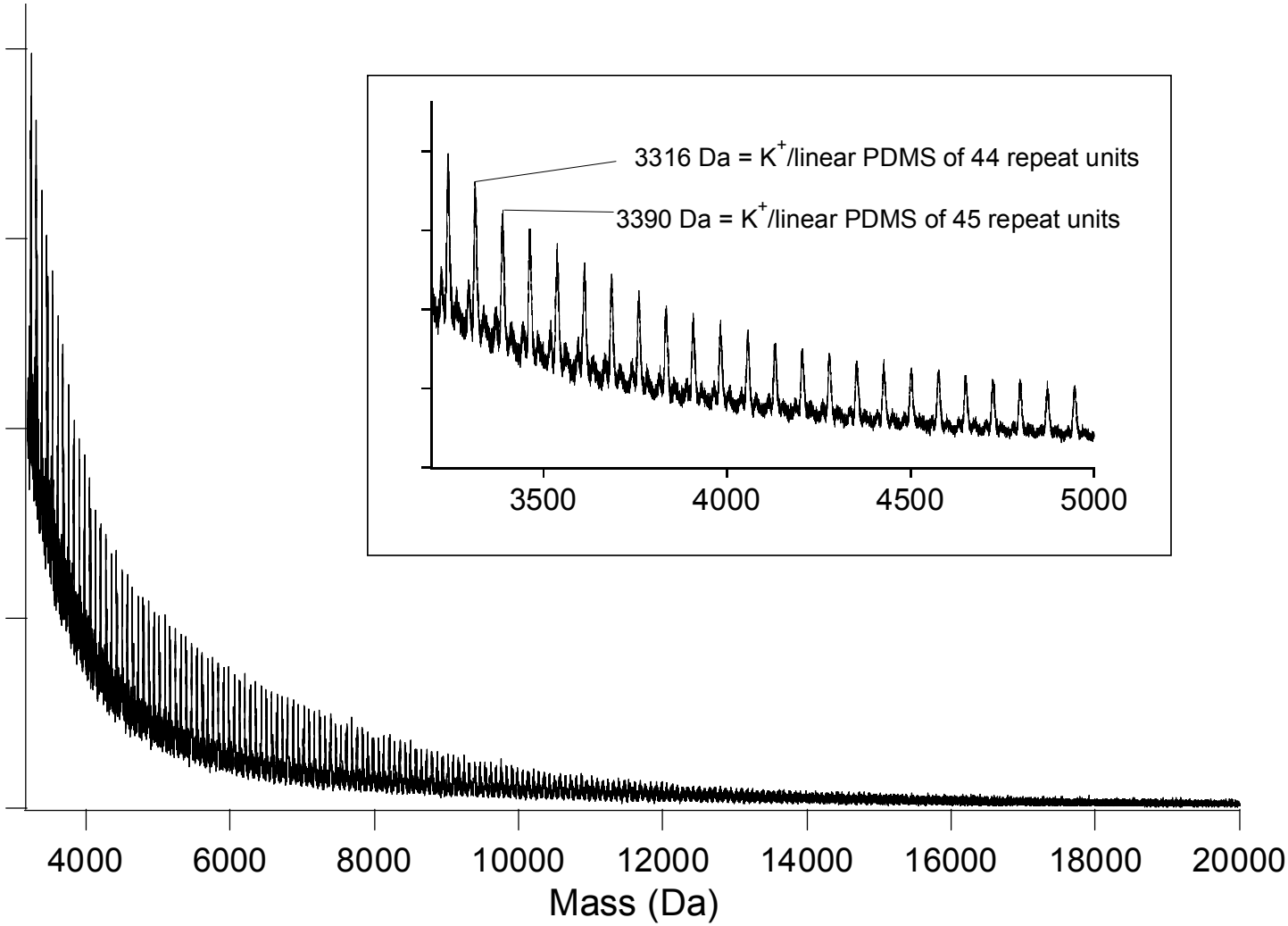

Figure A.18. MALDI spectra of linear S27 PDMS precursor

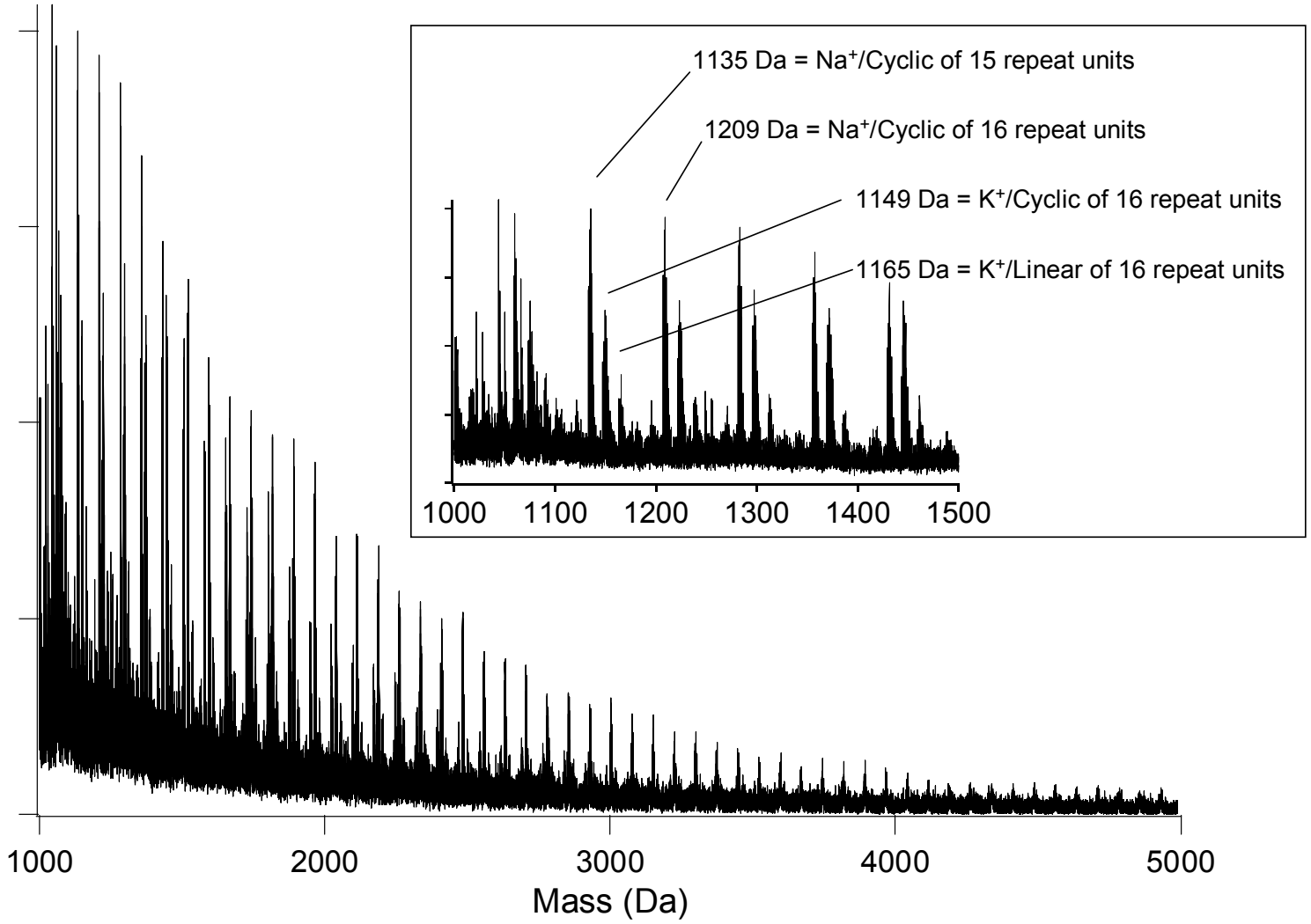

Figure A.19. MALDI spectra of methanol quenched cyclic product after 2 min for the S15 PDMS precursor

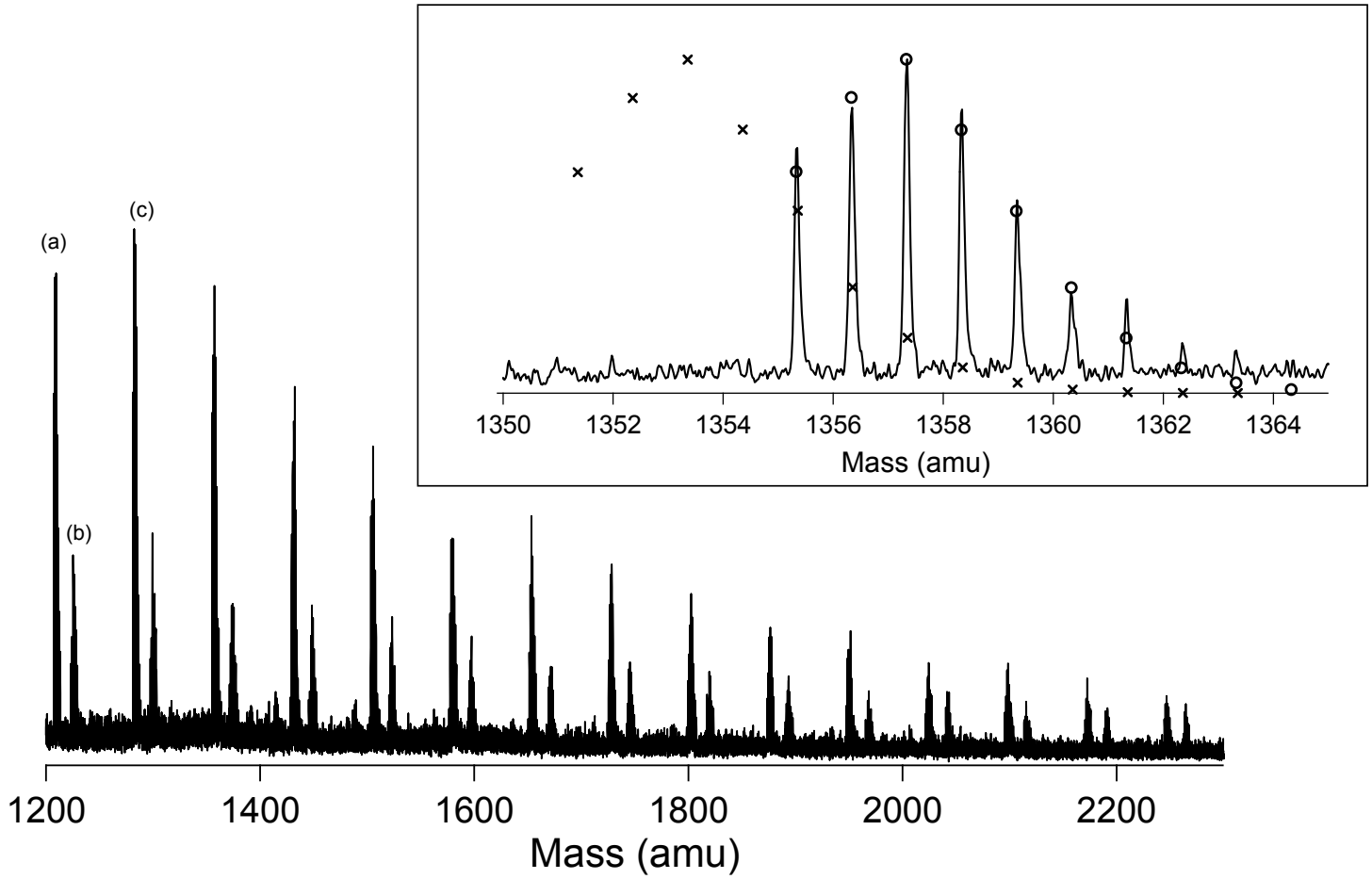

Figure A.20. MALDI-ToF spectrum of the methanol quenched product (above overlap concentration) trapped at 5 min after deprotonation of α,ω-dihydroxy-PDMS (M_n ~35 kg/mol, 5000 cSt). (a) 1281 amu = Na^+/cyclic PDMS of 17 repeat units, (b) 1299 amu = Na^+/linear PDMS of 17 repeat units, (c) 1355 amu = Na^+/cyclic PDMS of 18 repeat units. The inset is of a zoom view of the isotope multiplets from the sodium cationized cyclic PDMS at 1355 amu. The (x) represent the simulated isotropic distribution of linear H^+/PDMS, where (o) represents the simulated isotropic distribution of cyclic Na^+/PDMS.

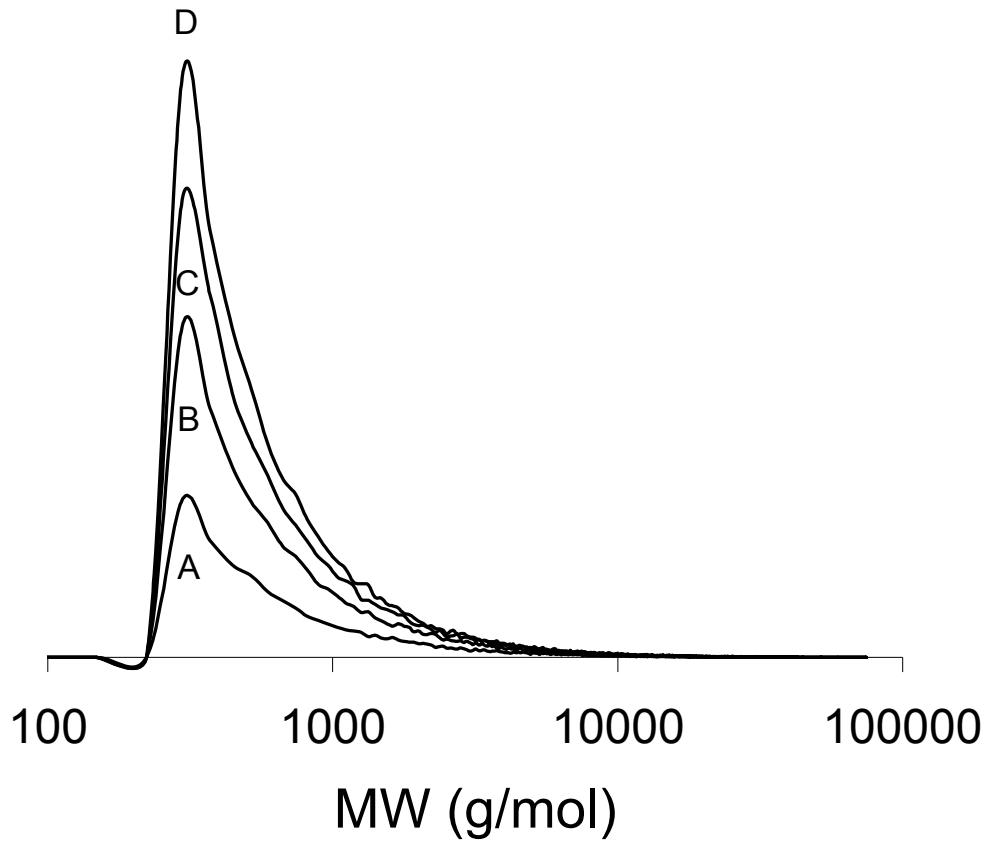

Figure A.21. Simulated cyclic distributions of a fictional distribution centered at 50 kg/mol linear precursor with a PDI=1.1 after (A) 5, (B) 10, (C) 15 and (D) 25 cyclization iterations.

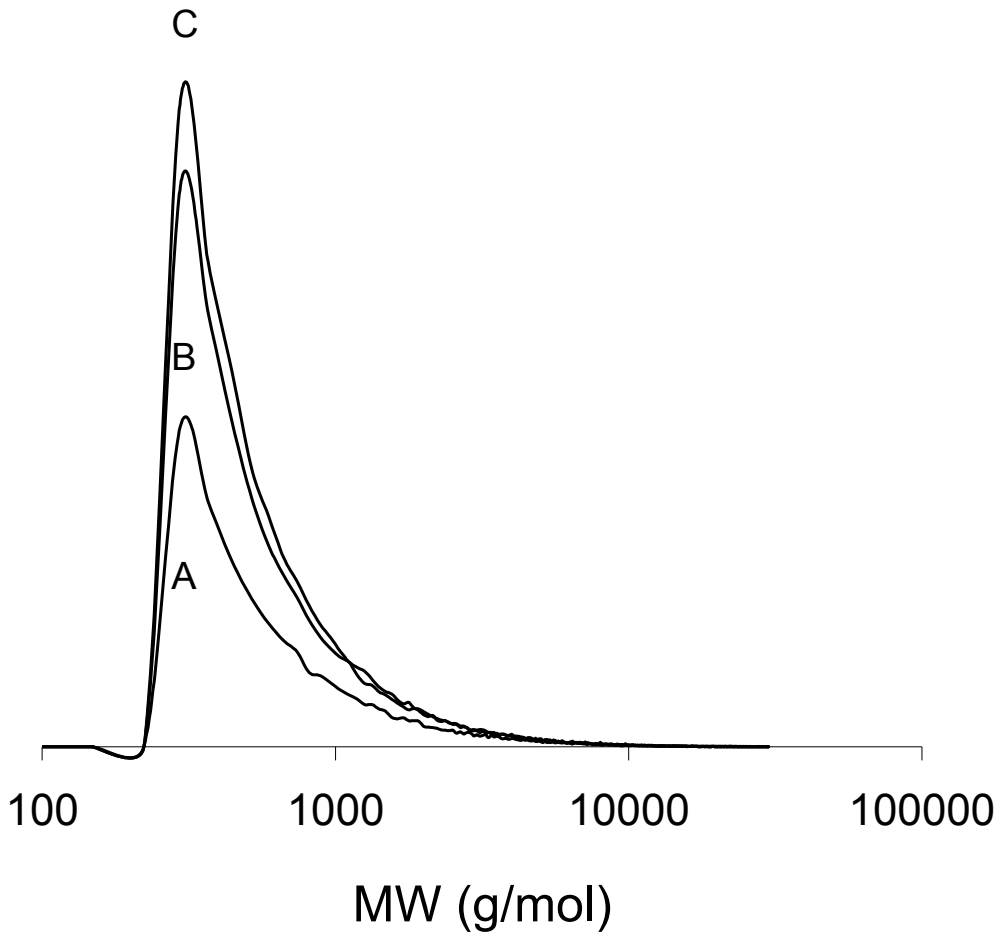

Figure A.22. Simulated cyclic distributions of a S27 linear precursor after (A) 2, (B) 5 and (C) 10 cyclization iterations.

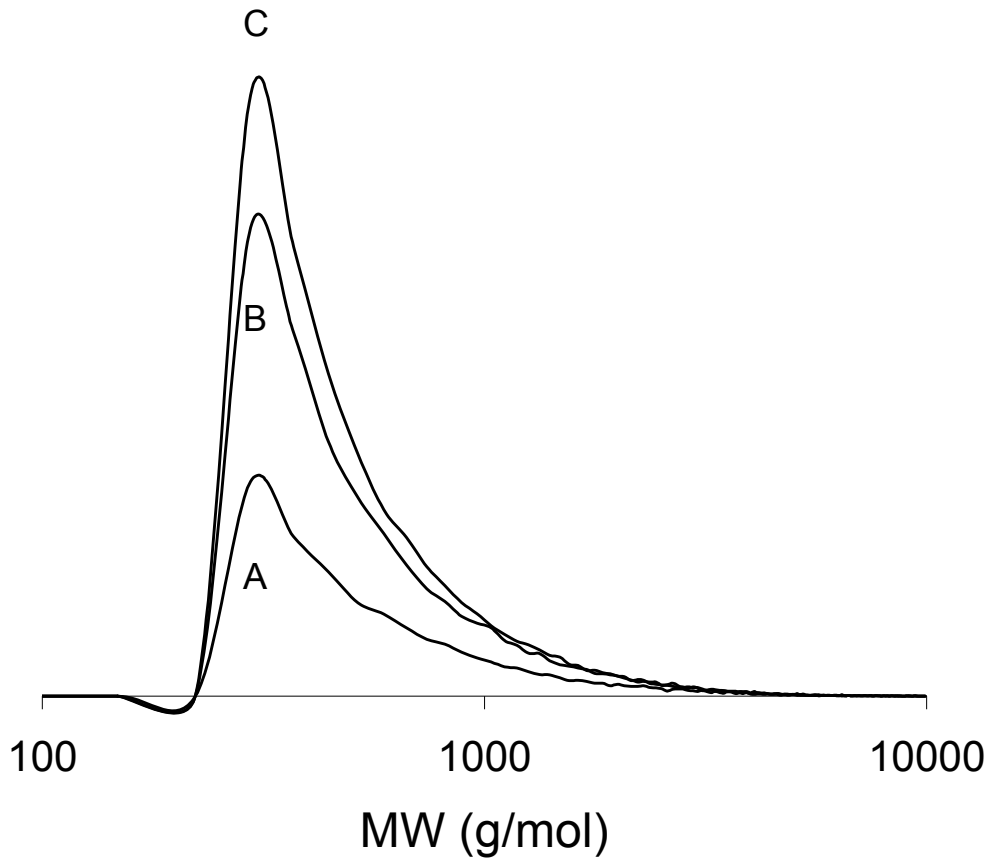

Figure A.23. Simulated cyclic distributions of a S15 linear precursor after (A) 2, (B) 5 and (C) 10 cyclization iterations.

```
% Macro: Runs multiple simulations of multiple cyclization iteration or
% events for PDMS from a list

format short e;
v_list=zeros(1,7);

%Data Entry
Mn=input('Number Average Molecular Weight (g/mol):  ');
PDI=input('PDI (g/mol):  ');
range=input('Range at least 100,000 (g/mol):  ');
PoP=input('Population Size 10000-50000:  ');
Exc=input('Smallest Cyclic Size recovered:  ');
Exc_2 =input('Smallest Large Cyclic Size:  ');
Exl=input('Smallest Linear Size recovered:  ');

disp('Enter 7 Cyclization Iterations');
for t =1 : 7
   It=input('Number of Cyclization Iterations:  ');
   v_list(t) = It;
end

%Create result arrays
l_Results=zeros(2,7);
c_Results=zeros(4,7);
Result=zeros(1,2);
ov_lDis = distr(Mn, PDI, range,PoP);
fv_cDis =  zeros(7,size(ov_lDis,2));

%Iterations
for r = 1 : 7

    cycle = 0;
    Start=0;
    Finish=0;
    Thread=0;

    % fills dis a structure with DP_l and topology
    % fills vDis a vector with Gaussian MW distrubtuion of Linear
    vDis_l = ov_lDis;
    vDis_c = zeros(1,size(vDis_l,2));

    %Initial Yield Calculation of Linear material
  for i = 1 : size(vDis_l,2)
      Start = Start + i * vDis_l(i);
  end

  for b = 1 : v_list(r)

    %Cyclization
    for i = 5 : size(vDis_l,2)
    count = vDis_l(i);
    vProb = cyclize(i);

      for j = 1 : count
          cycle = 0;
          a = 0;
          while a == 0
              a = round(size(vProb,2) * rand(1));
          end
          cycle = vProb(a);
          if  vDis_l(i) > 0
              vDis_l(i) = vDis_l(i) - 1;
              if i ~= cycle
                  vDis_l(i-cycle) = vDis_l(i-cycle) + 1;
              end
              vDis_c(cycle) = vDis_c(cycle) + 1;
          end
       end
    end
  end

Result=Cal_Dis(vDis_l,'L',Exl);
l_Results(1,r) = Result(1,1);
l_Results(2,r) = Result(1,2);
Result=Cal_Dis(vDis_c,'C',Exc);
c_Results(1,r) = Result(1,1);
c_Results(2,r) = Result(1,2);
%Final Yield Calculation of Cyclic Product
   for i = Exc : size(vDis_c,2)
       Finish = Finish + i * vDis_c(i);
   end
 %Final Yield Calculation of Cyclic Product
   for i = Exc_2 : size(vDis_c,2)
       Thread = Thread + i * vDis_c(i);
   end
c_Results(3,r) = Finish/Start;
c_Results(4,r) = Thread/Start;
fv_cDis(r,:) = vDis_c;

end
```

Program A.1. Runs multiple simulations of multiple cyclization iterations or events for PDMS from a user defined list

```
function out=distr(Mn,PDI,size,num)
% Creates and Plots MW distribution of linear PDMS based on Mn and PDI
sigma = Mn * (PDI-1)^(1/2);
pop = zeros(1,size);
a = 1/ (sigma*sqrt(pi*2));

 %fill pop
 for i =  92 : 74 : size
      pop(i) = a *exp( -(i-Mn)^2/(2*sigma)^2);
 end

 pop = pop / sum(pop);
 pop = num * pop;
 pop = floor(pop);
 semilogx(pop);
 xlabel('(g/mol)');
 out1 = struct('DP_I',{});

 count = 1;
 for i =  1 : size
   if pop(i) > .1
      out1(count).DP_I = pop(i);
      count = count+1;
   end

end
out = [out1.DP_I];
```

Program A.2. Function that creates and plots MW distribution of linear PDMS based on M_n and PDI using a Gaussian function

```
function out=cyclize_K(size,C)
% Randomly cyclizes a PDMS chain of size based on end-to-end kinetics with
% as function kinetic slope K = C * log(N)
count = 1;
count_1=4;
pop = zeros(1,size);
A =10;

if -C > 1
    A = 1;
end

 %fill pop
 times(1) = 0;
  for i =  4 : size
       times(i) = ceil( A*(10^(C*log10(count_1)+9.7432) / 10^(C*log10(size)+9.7432))  );
       count_1 = count_1 + 1;
  end

 pop_size = sum(times);
 pop = zeros(1,pop_size);


 %fill pop
 for i = 4 : size
    for j = 1 : times(i)
        pop(count) = i;
        count = count + 1 ;
    end
 end



 out = pop;
```

Program A.4. Function that randomly cyclizes a PDMS chain of size, based on end-to-end kinetics as described by the function kinetic slope K = C * log(N)

Determining calibration constants k_{RI} and k_{UV} with 1.5 kg/mol naphthalene end-labeled cyclic and linear product mixture:

$$\left(\frac{N_{RU}}{N_{END}}\right)_{NMR} c = \left(\frac{N_{RU}}{N_{END}}\right)_{GPC}$$

NMR on the 1.5 kg/mol labeled sample will determine the ratio of end groups to PDMS repeat units. Though the ratio of end groups to repeat units in the GPC is the same as determined by NMR, the absolute value of end groups and repeat unit eluting from the column is undetermined (depends on the injection volume and concentration). c is a scaling constant that relates the ratio of end group and repeat unit to the absolute number of end groups and repeat units eluting from the column.

$$\therefore N_{RU_{GPC}} = N_{RU_{NMR}} c \text{ and } N_{END_{GPC}} = N_{END_{NMR}} c$$

$$k_{RI} = \frac{A_{RI_{5kg/mol}}}{N_{RU_{GPC1.5kg/mol}}} \qquad k_{UV} = \frac{A_{UV_{5kg/mol}}}{N_{END_{GPC1.5kg/mol}}}$$

$$k_{RI} = k_{RI} c = \frac{A_{RI_{5kg/mol}}}{N_{RU_{NMR1.5kg/mol}}} \qquad k_{UV} = k_{UV} c = \frac{A_{UV_{5kg/mol}}}{N_{UV_{NMR1.5kg/mol}}}$$

Determining M_n, PDI and % cyclic on other molecular weights:

RI

$$I_{RI_i} = k_{RI} N_{L+C_i} M_{L+C_i}$$

$$\frac{I_{RI_i}}{k_{RI}} = N_{L+C_i} M_{L+C_i}$$

$$\sum \frac{I_{RI_i}}{k_{RI}} = \sum N_{L+C_i} M_{L+C_i} = \sum RU_{L+C_i}$$

$$\sum \frac{I_{RI_i}}{k_{RI} M_{L+C_i}} = \sum N_{L+C_i}$$

UV-Vis

$$I_{UV_i} = k_{RI} N_{END_i}$$

$$\frac{I_{UV_i}}{k_{UV}} = N_{END_i}$$

M_{Li} can be determined from the calibration curve and the retention times

$$\therefore \frac{I_{UV_i} M_{L_i}}{2k_{UV}} = N_{L_i} M_{L_i}$$

$$\sum \frac{I_{UV_i} M_{L_i}}{2k_{UV}} = \sum N_{L_i} M_{L_i} = \sum RU_{L_i}$$

$$\sum \frac{I_{UV_i}}{2k_{UV}} = \sum N_{L_i}$$

% cyclic yield:

$$\% \text{ cyclic} = 1 - \frac{\sum RU_{L_i}}{\sum RU_{L+C_i}}$$

M_n and PDI:

$$N_{C_i} = N_{L+C_i} - N_{L_i}$$

$M_{C\,i}$ can be determined from the calibration curve and the retention times

$$M_{n_C} = \frac{\sum N_{c_i} M_{C_i}}{\sum N_{C_i}}$$

$$M_{n_L} = \frac{\sum RU_L}{\sum N_{L_i}}$$

Calculation A.1. Topologically-resolved GPC dual detection of end-labeled naphthalene linear PDMS/cyclic PDMS product mixture resulting from cyclodepolymerization of PDMS linear precursors